" STUDIES OF LOW LATITUDE IONOSPHERE "

Ph.D. THESIS

by

HARISH CHANDRA

submitted to

GUJARAT UNIVERSITY

*

DECEMBER 1969

PHYSICAL RESEARCH LABORATORY
AHMEDABAD
INDIA

DEDICATED IN THE MEMORY OF

"BAPU"

THE FATHER OF NATION

IN HIS BIRTH

CENTENARY YEAR.

*

PREFACE

With the establishment of a Rocket Launching Station at Thumba, very near to the magnetic equator (0.6°S dip), ionospheric drift recordings were started at Thumba by the Aeronomy Group of the Physical Research Laboratory. A drift recorder employing closely spaced antennas was installed in January 1964. The horizontal drift and the parameters of the irregularities in the electrojet height and in the F-region heights for the daytime hours in the years 1964-65 were studied and have been described by Mr. M.R. Deshpande in his Ph.D. thesis.

To study other features of the equatorial ionosphere, an automatic ionospheric recorder, model C4, kindly made available by the WPC branch of the Government of India, was installed in October 1964.

Additional aerials were set up in May '67 to study the ground diffraction patterns at Thumba which are highly field-aligned and elongated along N-S. The drift observations were extended to nighttime from January 1967.

The present thesis comprises (1) a detailed study of the drift motion and the probable sizes of the irregularities in the ionosphere over Thumba during the period 1964-67, and (2) some general features of the equatorial ionosphere at Thumba and at other equatorial stations. The Thesis has been divided into three sections.

SECTION - I

The first section is introductory and describes briefly the geomagnetic field, dynamo theory, electrojet, electro-magnetic drifts and other properties of the equatorial ionosphere.

SECTION - II

This section deals with the drift measurement at Thumba and is sub-divided into seven chapters.

1) A brief introduction to the subject and some methods to determine winds and drifts at the ionospheric heights,

2) The experimental set-up used at Thumba,

3) The fading of the radio waves and their characteristics at Thumba,

4) The results of the apparent drift calculations for the period 1964-67 using simple time delay method. This is followed by a latitudinal survey,

5) Correlation methods and the results of the steady and random components of drift, and size and shape of the irregularities at Thumba in the years 1964 and 1967.

6) Effect of magnetic activity on the various parameters of drift and anisotropy at Thumba.

7) Comparison of the results at Thumba with those at other stations.

SECTION - III

Other features of the equatorial ionosphere are discussed in the third section of the thesis which is sub-divided into four chapters.

1) Results of ionospheric sounding at Thumba during the period January 1965 to December 1967 and then comparison with the data obtained at Kodaikanal and Trivandrum (Manual Ionosonde).
2) Electron density distribution with height at Thumba.
3) Characteristics of spread-F at Thumba.
4) Solar cycle and seasonal variations of spread-F at other equatorial stations.

The author was resident research scholar in-charge of the Ionospheric Station at Thumba from May 1965 to December 1967. Regular vertical ionospheric soundings and all the drift observations during this period were taken by the author.

The entire reduction and analysis of the drift records for the period 1965-67 as well as the consolidation of all the available drift data were done by the author at Ahmedabad. The world wide study of equatorial spread-F is based on the data published by the respective observatories, while the spread-F study at Thumba is based on the data reduced and classified by the author directly from the ionograms.

R G Rastogi 29/12/69
R.G. RASTOGI
PROFESSOR-in-CHARGE.

Harish Chandra
HARISH CHANDRA
AUTHOR

ACKNOWLEDGEMENTS

I express my gratitude to Professor R.G. Rastogi for the keen guidance throughout the course of the research work and to Professor K.R. Ramanathan for his valuable advice.

Thanks are due to Dr. M.R. Deshpande for the unstinting help in the initial stages of my work at Thumba, to Mr. K.J. John for the assistance towards the maintenance of the ionosonde and other ionospheric equipments at Thumba and to Mrs. S. Jani for computational assistance.

Thanks are also due to all other members of our Group for their continued cooperation and to the staff of the PRL computer section for the data processing with the IBM 1620 Computer.

Finally, thanks are due to Professor V.A. Sarabhai, Chairman, Indian Space Research Organisation, for the facilities provided to the Ionospheric Observatory at the Rocket Range and to the Ministry of Education, Government of India, for the award of a research scholarship.

******

C O N T E N T S

contd...(ii)

contd....(iii)

SECTION - I

INTRODUCTION

CHAPTER - 1

Brief description of geomagnetism and ionospheric phenomena near the magnetic equator

CHAPTER I.1

BRIEF DESCRIPTION OF GEOMAGNETISM AND IONOSPHERIC PHENOMENA NEAR THE MAGNETIC EQUATOR

I.1.1. Earth's magnetic field

The geomagnetic field intensity (F) at a point is generally described by its components; (1) Northward component (x), (2) Eastward component (y) and (3) vertically downward component ( ). The parameters which are usually measured to describe the geomagnetic field are:

1. Magnetic declination $D = \tan^{-1} \frac{Y}{X}$
2. Magnetic inclination $I = \tan^{-1} \frac{Z}{H}$
3. Horizontal component $H = \sqrt{X^2 + Y^2}$

and 4. Vertical component $V = Z$

To a first approximation, the earth's main field resembles that of a magnetic dipole located at the centre of the earth having its axis at an angle 11.7° to the axis of earth's rotation. The dipole axis intersects the earth's surface at points 73.3°N, 69.0°W and 78.3°S, 11.0°E and are called geomagnetic poles. A geomagnetic coordinate system based on the geomagnetic poles has been defined. The angular distance θ_m measured at the centre of earth from the geomagnetic North pole is called the geomagnetic co-latitude. Geomagnetic latitude ϕ_m in this system is given by $\phi_m = 90^{\circ} - \theta_m$. Geomagnetic longitude λ_m is measured

Eastward from the particular geomagnetic meridian which contains the geographic south pole. The geomagnetic co-latitude and longitude are related to the geographic co-latitude (θ) and longitude (λ) by the relations:

$$\cos\theta_m = \cos\theta_p \cos\theta + \sin\theta_p \sin\theta \cos(\lambda - \lambda_p)$$

$$\sin\lambda_m = \frac{\sin\theta}{\sin\theta_m} \sin(\lambda - \lambda_p) \qquad \ldots\ldots(1)$$

where $\theta_p = 11.7^\circ$ and $\lambda_p = 69^\circ$.

Geomagnetic equator is defined as the locus of points where $\theta_m = 90^\circ$. These are the points where the vertical component V or inclination I is zero as estimated from dipole approximation. The inclination at a point is described by the relation:

$$\tan I = \frac{Z}{H} = 2 \tan \phi_m \qquad \ldots\ldots(2)$$

The magnetic poles or dip poles are the points where magnetic intensity is observed to be vertical and they differ in location from the geomagnetic poles because the latter are chosen so as to give the best representation of the earth's main field as a whole. The observed values of inclination at a point may differ from that calculated due to dipole at regions where the field departs from that expected of the approximate dipole field. Hence

a similar latitude can be described on the basis of observed inclination at a place (instead of the inclination due to the dipole field) and is mentioned as magnetic latitude or dip latitude pf the place. Magnetic or dip equator is therefore defined as the locus of points where observed inclination is zero or where magnetic field intensity is horizontal and differs somewhat from the geomagnetic equator.

Even though the earth's magnetic field is horizontal at any point on the magnetic equator, the intensity of the field varies considerably with longitude such that H = .39 Gauss at Thumba and only .29 Gauss at Huancayo. To account for these longitudinal effects, a better approximation of the earth's magnetic field to a dipole field is obtained when the dipole is displaced from the centre of earth. Bartels (1936) found from the analyses of data for the year 1922 that the eccentric dipole is displaced by 342 km towards the point 6.5 N^{o} lat. and 161.8^{o} long.

Parkinson and Cleary (1958) found that the centre of the eccentric dipole in 1955 was displaced by about 436 km from the centre of earth towards the point 15.6^{o}N, 159.9^{o}E. Cain et al (1965) have drawn maps of the computed components of magnetic field in the year 1965. In the equatorial region maximum in H was observed at a point

about $12^{o}N$, $95^{o}E$ with a value .413 Gauss while a minima was found to occur at a point about $5^{o}N$, $55^{o}W$ with a value of H less than .27 Gauss.

I.1.2. Magnetic field variations - Dynamo theory

The geomagnetic field at any place is found to undergo very slow changes of the period of few years, which are known as secular variations. There are regular variations which are related to the solar and the lunar day. The quiet day solar component (S_q) and a smaller lunar daily component (L) are supposed to be caused by the current systems in the upper atmosphere. There are occassional large perturbations in the magnetic field which are associated with the disturbances in the sun.

Regular diurnal variations of the compass needle were discovered in the eighteenth centry by Grahm (1722). Belfour Stewart (1882) ascribed these magnetic variations due to currents in the region now known as ionosphere. He also indicated that these currents could be driven by electric fields induced by the motion of the air across the earth's magnetic field lines. This idea has become known as the dynamo theory because the moving atmosphere is something like the armature of a dynamo, the earth is a magnet and the conducting atmosphere is the windings.

Schuster (1889) studied the geomagnetic daily variation field on a world wide scope by the method of spherical harmonics and estimated the current system responsible for the geomagnetic variations and concluded that the location of the equivalent current system to be mainly external (overhead). The presence of the ionised region in upper atmosphere was further implied by Marconi's high frequency trans-atlantic communication in 1901, but the direct evidences of an ionised region (ionosphere) were made only in 1925 by Appleton and Barnett, and Breit and Tuve independently.

Stewart's idea was put into a quantitative form by Schuster (1908) who demonstrated that upper atmospheric currents could be explained by tidal air motions similar to those observed at grouhd level. He also suggested that the required large electric conductivity of the upper atmosphere must be produced by solar ultraviolet radiations.

Chapman (1913, 1919) developed a dynamo theory suitable for both the solar and the lunar daily variations and concluded that the conductivity must be greater by a factor of 10 than that estimated by Schuster.

Pederson (1927) drew attention to the anisotropy of the electric conductivity due to the presence of the magnetic field which results in the reduction of the con-

ductivity. Early calculations on this basis showed the conductivity in the ionosphere much less than that required to explain the magnetic field variations based on dynamo theory.

Studies of the atmospheric oscillations by Talyor (1936), Pekris (1937) and Wilkes (1949) indicated that the speed of the tidal motion could be expected to increase with the inverse square root of the air density. Thus the upper atmosphere oscillations might be much larger than those at ground. In spite of this increase in tidal amplitude with height, the conductivity of ionosphere fell short by a factor of 5 to 10 to that adequate to explain the dynamo theory.

Cowling (1933) considered the effect of the Hall currents and subsequent polarization of the medium and concluded that the conductivity increased from Pederson value to that obtained in the absence of the magnetic field. Martyn (1948) suggested that this effect might be responsible for the high conductivity required to explain the dynamo theory. Cowling and Borger (1948) showed that the Martyn's suggestion would be invalid except near the magnetic equator because the polarization would leak out at other latitudes.

Existence of an abnormally large daily variation of the horizontal component of earth's magnetic field was

brought to light in 1922 when a geomagnetic observatory was established near the magnetic equator at Huancayo (Peru). McNish (1937) ascribed this abnormal range in H due to locally concentrated electric currents in the upper atmosphere flowing eastward above the magnetic equator.

It was first shown by Egedal (1947) that the abnormal daily range of H are observed at stations situated within a narrow zone near the magnetic equator. Martyn (1949) attributed these enhancements due to increased conductivity near the equator during the daytime because of the inhibition of the Hall currents due to the polarization of the medium.

This high concentration of electric current flowing from West to East in a narrow belt flanking the dip equator on the sunlit hemisphere was named equatorial electrojet by Chapman (1951).

The effect of Hall polarization on the conductivity of ionosphere at all latitudes was studied by Hirono (1950, 1952 & 1953), Maeda (1951), Baker and Martyn (1953) and many others. They showed that over the whole earth the effective conductivity appears to be greater than the Pederson conductivity by a factor of at least 6 and is further increased by a factor of 2 to 5 near the

magnetic equator. This explains the observed geomagnetic variations on ground as well as the anomalous variations near the equator.

I.1.3. Electrical conductivities in upper atmosphere

Considering the ionosphere as an infinite, lightly ionized gas in which there are n_r changed particles of the r^{th} type in a unit volume, where r = e plus or minus for the electrons, positive ions and the negative ions respectively, if a particle of r^{th} type has charge e, mass m_r, collision frequency $\omega_r = e_r B/m_r$, B being the intensity of the magnetic field in the medium, the conductivity of the medium is then given by the sum of following components.

(1) Direct or longitudinal conductivity (σ_0)

When an electric field is parallel to the magnetic field, the conductivity along the electric field is called longitudinal conductivity. This is independent of the magnetic field and is given by

$$\sigma_0 = \sum_r \frac{n_r e_r^2}{m_r \nu_r} \qquad \ldots(1)$$

(2) Pederson conductivity (σ_1)

When an electric field is perpendicular to the magnetic field, the conductivity along the electric field

is called Pederson conductivity and is given by

$$\sigma_1 = \sum_r \frac{n_r \nu_r e_r^2}{m_r(\nu_r^2 + \omega_r^2)} \qquad \ldots(2)$$

(3) Hall conductivity (σ_2)

In cases of crossed electric and magnetic field, the conductivity perpendicular to both the electric and the magnetic fields, called Hall conductivity, is given by

$$\sigma_2 = -\sum_r \frac{n_r \omega_r e_r^2}{m_r(\nu_r^2 + \omega_r^2)} \qquad \ldots(3)$$

(4) Cowling conductivity (σ_3)

When the medium is bounded in the direction of Hall current, flow of this current results in polarization and the polarization field inhibits the Hall current.

If E is the applied electric field perpendicular to the magnetic field and E_p is the polarization field then for complete inhibition of Hall current

$$\sigma_2 E = \sigma_1 E_p$$

hence $E_p = \frac{\sigma_2}{\sigma_1} E$

This polarization field results in additional current density along the original electric field E. The total current along E being $\sigma_1 E + \sigma_2 E_p$

$$= \left(\sigma_1 + \frac{\sigma_2^2}{\sigma_1}\right) E$$

$= \sigma_3 E.$

Cowling conductivity σ_3 is thus higher than the Pederson conductivity σ_1. The increase in the conductivity depending on the polarization field. In the ionosphere Hall current leads to the polarization which easily leaks away along the lines of force of the geomagnetic field except at the dip equator where the field is entirely horizontal.

The effective specific conductivity to be used in dynamo theory is therefore σ_3. The conductivities can be written in term of the magnetic field B using the equation relating it to the gyro frequency. The total conductivity can be obtained by integrating over the different species such as electrons and ions. One gets then

$$\sigma_0 = \frac{1}{B} \sum_r \frac{n_r \omega_r}{\nu_r} e_r$$

$$\sigma_1 = \frac{1}{B} \sum_r \frac{n_r \omega_r \nu_r}{(\nu_r^2 + \omega_r^2)} e_r$$

$$\sigma_2 = -\frac{1}{B} \sum_r \frac{n_r \omega_r^2}{(\nu_r^2 + \omega_r^2)} e_r$$

and $\sigma_3 = \sigma_1 + \sigma_2^2 / \sigma_1$

Height distribution of σ_0, σ_1, and σ_2 show that σ_1 and σ_2 are smaller than σ_0 and reach maximum at 110 to 140 km. Since $\sigma_2 > \sigma_1$ in the altitude region of interest

Cowling conductivity represents enhancement over the Pederson conductivity. As the ratio σ_2/σ_1 is considerable at height around 100 km, σ_3 shows maximum here.

From the known electric conductivity and assumed wind systems, electric current systems have been computed by Matsushita (1953) and Maeda and Matsumoto (1962). The current system obtained is similar to that estimated from the geomagnetic data.

In a similar way horizontal wind systems in the dynamo region can be deduced from known electric conductivities and the current system from the geomagnetic data (H. Maeda 1955b, 1957, S. Kato 1956, 1957).

I.1.4. Electromagnetic drift

Electromagnetic drifts of ionisation were suggested by Martyn (1947, 1948) to explain the tidal oscillations and the non-Champan layer behaviour of the F-regions of the ionosphere. He suggested that these drifts are due to the electro-dynamic forces associated with the magnetic variations. These drifts have both vertical and horizontal components.

In presence of electric fields and the earth's main magnetic field, the drift velocity of a changed particle with respect to neutrals is shown by the equation

obtained by Martyn (1953) and Kato (1959):

$$\vec{U} = \frac{\vec{J} \times \vec{B}}{\sum_n \eta_n m_n \nu_n}$$

where $\vec{J}$ is the electric current density, $\vec{B}$ is earth's main magnetic field. For simplicity, the axis of earth's rotation is assumed to coincide with that of earth's dipole magnet. In the F- region collision frequency is much smaller than the gryo frequency and assuming that vertical current component vanishes, one obtains:

$$Ux = -(Ey/B) \text{ Sin } I$$

$$Uy = \frac{Ex}{B} \text{ cosec } I$$

$$Uz = \frac{Ey}{B} \text{ cos } I$$

The electric field in the F-region seems to be derived mainly from that in the E-region (electro-static field of the E-region arising due to polarization is transferred to F-region via the highly conducting lines of force) and is given by the relation

$$Ez = - Ex \text{ cot } I$$

The East-West drift in the F-region can be shown to be

$$Uy = (Ex \text{ Sin } I - E_2 \text{ cos } I) /B.$$

Thus near equator

$$Uy \simeq -Ez/Bx.$$

Martyn (1953) studied drift of ionization under the influences of an electric field and atmospheric wind. He derived relations for the horizontal and vertical drift of ionization at all latitudes in a thin ionosphere in which vertical electric currents are prohibited, and concluded that

(1) in the lower E-region and below, the ionization will move horizontally with substantial local wind velocity

(2) In the upper E-region, the horizontal motion of ionization may differ substantially in magnitude and direction from that of local wind

(3) in the F-region ionization cannot be moved by winds transverse to the earth's magnetic field. A local N-S wind causes the F-region ionization to move along the direction of the earth's field. High East-West drift can be produced in F-region by N-S applied electric fields (except at equator where vertical fields transferred from dynamo region produce high drifts).

(4) Vertical drift velocities due to either winds or fields are small below 100 km except in the immediate vicinity of magnetic equator where E-W fields can produce large vertical drifts at heights of 90 km and upwards

(5) in the F-region notable vertical drift is produced by E-W fields or by local N-S winds (blowing of ionization along the field lines).

According to Baker and Martyn (1953) polarization field at any region is given by

$$S = 1.7 \times 10^4 \quad \sin^2 \theta \quad \cos \theta' \quad \cos \phi \quad \text{volts}$$

where θ is the colatitude of a point in any region of the ionosphere, θ' is the colatitude of that point in the dynamo region which is linked to the former point by a field line and ϕ is the longitude measured positively eastward from the midnight meridian. At moderate or high latitudes $\theta \simeq \theta'$ but near the equator $\cos \theta'$ may differ appreciably from $\cos \theta$. The vertical field E_z at the equator was given to be $E_z = 1330 (\sec \theta' - 3 \cos \theta')$ which will give rise to horizontal drift of ionization directed westward by day, and eastward by night with maximum velocity.

$$U = 4300 (\sec \theta' - 3 \cos \theta') \text{ m/sec.}$$

Since θ' is of the order of 9°, U approaches 2×10^4 m/sec or 200 m/sec in the middle of day.

Thus regarding the horizontal drifts in the F-region, the E-W component will be towards West during day and towards East during nighttime at low latitudes, reverse

at high latitudes with change over occurring around 35° lat. At the equator, F-region horizontal drift is entirely E-W while N-S drift is maximum at poles and absent at equator.

I.1.5. Electric fields and drifts from dynamo theory

From the current intensities and the conductivities, the total electric fields can be computed. Maeda (1955a) obtained the field distribution for the second polar year S_q data. The electrostatic field can be obtained as the difference between the total field and the dynamo field. Winds can be calculated from the conductivities and the current systems obtained from the geomagnetic data and substituted to give dynamo fields. Same electrostatic fields can be considered in the F-region and electro-magnetic drifts can be calculated. Maeda (1963) obtained solar daily variations of the three components of the drift speed and a world-wide distribution of the horizontal drift. The N-S component is absent at equator and increases towards poles reaching a maximum of about 50 m/sec. At low latitudes N-S component is towards North during daytime and towards South during night while at high latitudes it is Northward before-noon and Southward afternoon time. E-W component is towards West during day and towards East during night at low latitudes and reverse is the case at high latitudes with change

over occurring in between 40-50^{o} lat. The E-W component is maximum near equator and decreases smoothly becoming practically absent at the point of reversal and again increasing at high latitudes.

The vertical drift is highest at equator and decreases slowly towards poles. All the three components of drift in F-region show mainly diurnal variations.

The horizontal drift distribution show rotation of drift vector at high and middle latitude while there is a sudden reversal without any rotation at equator.

I.1.6. Equatorial zone

Equatorial zone is unique in geomagnetic studies. The earth's magnetic lines of force are nearly horizontal here. As the geographic equator, geomagnetic equator and magnetic (dip) equator are not identical the geomagnetic phenomena will depend on these three equators. Because the solar radiation and air motions are controlled by the geographic equator, conductivity mainly by dip equator.

Equatorial region was defined as the zone lying between 20^{o}S and 20^{o}N of dipole equator for IGY listing (Nicolet 1957). However, Onwumechilli (1964b) has shown that dipole equator has no significant influence on the daily range of H and that away from electrojet region the influence of geographic and dip equators were equal. He

suggested that it is better to define the equatorial region in terms of $20^{o}S$ and $20^{o}N$ geographic or dip latitude which gives widest zone.

I.1.7. Equatorial electrojet

The cause of the equatorial electrojet lies in a special equatorial feature of the electric conductivity of the upper atmosphere. The geomagnetic field being entirely horizontal at the equator, polarization charges cannot leak here and this results in the increased effective conductivity at the equator. Baker and Martyn (1953) estimated the half width of this strip as 3^{o} lat. The current in this strip is west to east for most of the day.

Studying the enhancement of the daily range of H over the magnetic equator in different longitudes Rastogi (1962, 1963) suggested that the electrojet is most intense at Peru and weakest around the Indian zone. Recent rocket measurements have shown the peak current density over dip equator, approximately $0.7 \times 10^{5} Amp/m^{2}$ off the coast of Peru (Maynard 1967, Davils et al 1967) and approximately $4 \times 10^{-6} Amp/m^{2}$ over Thumba, India (Sastry 1968).

The range of H under the electrojet is greater during increased solar activity (Rao et al 1965). Further it is shown that range of H close to electrojet is greater

at the equinoxes than at the solstices (Chapman and Raja Rao 1965).

VHF radar observations at Jicamarca have indicated the presence of currents over the magnetic equator even in the nighttime, the direction being Westward (Balsley 1966). The nighttime currents are small in magnitude due to decreased conductivity during those periods and so are not easily detected on normal magnetograms. However Rastogi et al (1966a, b) have shown that the amplitude of SSC in H or the fluctuations in H during the nighttime are significantly enhanced over the magnetic equator in the American zone and attributed this to the remnant equatorial current system flowing during the nighttime hours. No such enhancement was observed for the Indian zone.

I.1.8. Equatorial E_s.

In addition to the regular E, or F-region traces certain scatter echo configurations are noted on conventional ionograms. Such ionogram configurations at E-region height are known as 'sporadic E' or E_s and such configurations identified on equatorial ionograms as 'equatorial sporadic E' or E_s-q the critical frequency of such echoes often exceeding 10 mc/s.

According to the temporal variation of the occurrence of sporadic E, there are three major zones. The auroral zone in which E_s is predominantly a nighttime phe-

nomenon with little seasonal variation. A middle latitude zone in which E_s is predominantly a summer time phenomenon occurring both by day and night but more intensely by day. An equatorial zone in which E_s is a daytime phenomenon with little seasonal variation. In the middle latitudes, it has been observed that more occurrence of E_s is present nearer the equator.

Matsushita (1951) showed the close relation between the equatorial sporadic E and equatorial electrojet. Plots of f_oE_s and the daily amplitude of the horizontal field variation with magnetic dip showed enhancement in the same zone for both the para_meters.

A further evidence of the correlation between the two was obtained from lunar effects in the E_s-q. The eastward lunar equatorial electrojet reinforces the E_s-q, but the westward lunar electrojet tends to cause a disappearances of E_s-q (Matsushita 1957a, Knecht 1959, Egan 1960). This lunar effect indicates that solar equatorial electrojet, which is an eastward current is much larger than the eastward lunar electrojet and is a major cause of the E_s-q.

Cohen et al (1962) studied the scattering of VHF rader echoes and found that the irregularities that produce the sporadic E configurations are embedded in the equatorial electrojet. The strength of the radar echoes is seen to rise markedly in a discontinuous fashion as the electro-

jet current builds up. From the current threshold Farley (1963) led the idea that the irregularities are as a result of two stream plasma instability in the electrojet.

I.1.9. Equatorial F-region

While the E- and the lower F-region are found to obey the simple Chapman theory to some extent the F_2 region ionization is found to differ in many aspects. The critical frequencies of E and F layers at any place were found to obey approximately the Chapman's law $f_c \propto \cos^n \chi$ i.e. the foE or foF_1 is maximum at noon. The f_oF_2 at Huancayo (dip 0^o) was found to have minimum around noon with two maxima at around 09 and 16 hrs; while f_oF_2 at other latitudes reached a maximum value few hours after the midday.

The establishment of large number of ionospheric stations during the World War II had indicated a geomagnetic control on the F_2 layer i.e. f_oF_2 values were similar at stations having same geomagnetic and not the same geographic latitude (Ranzi 1939, Maeda et al 1942). Appleton (1946) pointed out that a plot of noon f_oF_2 against magnetic dip showed a minimum over the equator with two maxima on either side at 28^o dip. Thus a belt of low values of f_oF_2 centred on magnetic equator was discovered, and is referred to as Appleton anomaly or the equatorial anomaly of the F_2 layer.

Appleton (1954) showed that the anomaly present at noon tends to disappear during the afternoon and by evening is replaced by a crest of abnormally high values at equator.

Rastogi (1959) studied the diurnal development of anomaly during the low sunspot year 1953 and 1954 and showed that before sunrise there is a strong maximum at the equator. At later hour, the maximum flattens and is followed by a week maximum at low latitudes. As the time of day progresses, the peak becomes more pronounced and simultaneously shifts to higher latitudes till about 14 hr., when the anomaly is most pronounced, after which the process reverses and at 20 or 21 hours the anomaly disappears with maximum at equator agqin.

The development of equatorial anomaly is clearly seen by studying the diurnal variation of f_oF_2 at different latitudes. It is well-known that the low latitude stations show two peaks one in the morning and one in the evening (Maeda 1955), whereas at middle latitude stations the f_oF_2 shows a single maximum in the afternoon. Rastogi (1959) studied the diurnal variation at few stations near the equator and showed that from double peak behaviour at equator (Kodaikanal) one gets a single maximum around dip 25^o (Bombay). The morning peak which occurs earliest at

Kodaikanal shifts later similarly the evening peak which occurs latest at Kodaikanal shifts earlier; finally these two peaks come closer and merge to a single peak for Bombay. Thus the anomaly obtained by Appleton is as a consequence of the typical low in noon of the f_oF_2 at equatorial stations which is known as the forenoon bite-out.

Lyon (1963) studied the anomaly for the IGY period on quiet days and showed that the variation of noon f_oF_2 with magnetic dip was symmetrical about magnetic equator but in solstices marked asymmetry is found with f_oF_2 higher in the winter hemisphere.

The diurnal development of the anomaly at two equinox periods of 1958, for selected quiet days, was studied by Lyon and Thomas (1963) for the American, African and East Asian sectors. The anomaly was found to persist at least until 02 hr. and sometimes until sunrise. Further, it was found to persist longer in the African and East Asian zones.

The first explanation of the equatorial anomaly was given by Mitra (1946) suggesting that the electrons formed high above the magnetic equator move along the field lines and would appear over mid-latitudes giving extra ionization. Martyn (1947a, b) proposed the role of electromagnetic drift in the anomaly. He considered the vertical drift due to horizontal air currents in a simple

dynamo theory model of Schuster. Later with the modified dynamo theory Martyn (1955) explained the equatorial bite-out in forms of vertical divergence of drift. The polarization fields from the dynamo region are transferred to F_2 region via the highly conductivity lines of force and they cause drifts of ionization. Later he showed that the horizontal drifts are of importance near the equator. Martyn (1959) stated that horizontal diffusion is important near magnetic equator and the two peaks on either side of the equator are due to the horizontal divergence from the equator. Rastogi (1959) showed that the separation of double maxima at equator is reduced at increasing latitudes before merging to a single maximum, suggesting electro-magnetic lift of ionization at the equator followed by diffusion under gravity along the geomagnetic lines of force. Similar suggestion was given by Duncan (1960).

Lyon and Thomas (1963) reported evening enhancement of the anomaly after 18 hr. as shown earlier on the side of the magnetic equator near to the geographic equator and the layer height was also found to be higher on this side. Earlier Appleton (1960) has shown that h_mF_2 begins to rise rapidly at about 18 hr. in a rather narrow belt centred on magnetic equator. Thus, this enhancement of the anomaly in the evening hours (18 hr.) associated with

the sudden height rise supports the diffusion mechanism.

Hanson and Moffett (1966) and Brameley and Peart (1965) have independently reached comparable solutions by involving vertical electrodynamic drifts. Both papers demonstrate that the main observed features of the daytime equatorial F-region can be produced by drifts of 5 to 20 m/sec. in conjunction with photo-ionization, diffusion and a linear loss process.

I.1.10. Equatorial Spread-F

Like the irregularities in the electrojet, there are intense irregularities in the equatorial F-region. These irregularities are found to be highly field aligned.

The scattering from these irregularities gives rise to what is known as spread-F. Spread-F in the equatorial region was first reported for Huancayo by Booker and Wells (1938) and later for Singapore (Osborne 1951), Ibaden (Wright et al 1956) and at Kodaikanal (Bhargawa 1958). The existence of an equatorial belt of about $\pm 20^{\circ}$ geomagnetic (or magnetic) latitude of high occurrence of spread-F was shown by Singleton (1960) and by Lyon et al (1960).

Equatorial spread-F is mainly a nighttime phenomenon and is closely related to the post sunset height rise preceding the occurrence of spread-F. There is a marked effect (inhibition) of the magnetic activity on equatorial

spread-F. While Martyn's theory (1959) of the amplification of irregularities due to vertical drift of layer explains the association of the peak of the spread-F and the height rise, his theory does not present an adequate source of the electrostatic field to cause the required lifting of the layer. Calvert (1962, 1963) suggested an alternative that the cooling of the neutral atmosphere which gives rise to an electric field. This field causes differential drift velocity between the ionosphere and its irregularities like Martyn's field. Thus the consequent increase in layer height amplifies the irregularities.

The basic cause of the production of the irregularities for spread-F echoes has not been dealt by Martyn or Calvert. Daag (1957) put forward the idea of electrostatic coupling to E-region as the basic cause of irregularities. However, Cohen and Bowles (1961) found the irregularities creating equatorial spread-F too small to be accounted according to this theory.

Singleton (1962) combined the ideas of Dessler (1958) and Martyn (1959) to explain the spread-F at all latitudes. According to this theory, the irregularities in the F-region are created by the hydromagnetic waves and are amplified as suggested by Martyn. So far this theory seems to be most adequate in explaining the equatorial spread-F.

I.1.11. Conclusion

Thus one finds that the equatorial zone is an anomalous zone as regards geomagnetism and ionosphere. The horizontal field at the equator results in enhanced conductivity in the dynamo region, consequently a large current flows in a narrow zone franking the dip equator known as equatorial electrojet. This large current flow gives rise to large range in the diurnal variation of field at equatorial stations. Associated with this large current are intense irregularities which are formed in the electrojet and give strong scatter reflections known as equatorial E_s reflections. The equatorial zone has the property of large vertical drifts in the F-region caused by the E-W electric field and N-S magnetic field which results in the vertical lift of the ionization which moves over to the nearer latitudes by the process of diffusion along field lines giving a noon bite-out phenomenon in the equatorial F_2 layer ionization. In addition, there are large horizontal drifts in the E-W direction caused by the vertical electric fields in conjunction with the N-S magnetic field. Further the equatorial region has the property of large height rise of the F-layer after sunset causing intense spread-F echoes. Most of these phenomena are primarily due to the intense conductivity or electrojet which

arises because of the unique feature of the main magnetic field at equator.

REFERENCES

Appleton E.V. and Barnett M.A.F.	1925	Nature, London, 115,333.
Appleton E.V.	1946	Nature, London, 157, 691.
Appleton E.V.	1954	J. Atmosph. Terres. Phys., 5, 348.
Appleton E.V.	1960	Some ionospheric results obtained during the IGY (ed. by W.J.G. Beynon), page 3, Elsevier, Amsterdam.
Baker W.G. and Martyn D.F.	1953	Phil. Trans. Roy. Soc., London, A246, 281.
Balsley B.B.	1966	Annales Geophys., 22, 2445.
Balsley B.B.	1969	J.Atmosph.Terr. Phys., 31, 475.
Bartels J.	1936	Terr. Mag. Atmosph. Elect., 41, 225.
Bhargawa B.N.	1958	Ind. J. Meteor. Geophys., 9, 35.
Booker H.G. and Wells H.W.	1938	Terr. Mag. Atmosph. Elect., 43, 249.
Bramley E.N. and Peart M.	1965	J. Atmosph. Terres. Phys., 27, 1201.
Breit G. and Tuve M.M.	1925	Nature, London, 116, 357.
Cain J.C., Daniels W.E. and Hendricks J.S.	1965	J. Geophys. Res., 70, 3647.
Calvert W.	1962	N.B.S. Technical Note, 145.
Calvert W.	1963	J. Geophys. Res., 68, 2591.
Chapman S.	1913	Phil. Trans. Roy, Soc., London, A213, 279.
Chapman S.	1919	Phil. Trans. Roy. Soc., London, A218, 1.
Chapman S.	1951	Proc. Phys. Soc., London, B64, 833.

Chapman S. and Raja Rao K.S.	1965	J. Atmosph. Terres. Phys., 27, 559.
Cohen R. and Bowles K.L.	1961	J. Geophys. Res., 66, 1081.
Cohen R., Bowles K.L., and Calvert W.	1962	J. Geophys. Res., 67, 965.
Cowling T.G.	1933	Monthly Notices Roy. Astron. Soc., 93, 90.
Cowling T.G. and Borger R.	1948	Nature, London, 162, 142.
Daag M.	1957a	J. Atmosph. Terres. Phy., 11, 133.
Daag M.	1957b	J. Atmosph. Terres. Phys., 11, 139.
Davis T.N., Burrows K. and Stolanth J.D.	1967	J. Geophys. Res., 72, 1845.
Dessler A.J.	1958	J. Geophys. Res., 63, 507.
Duncan R.A.	1960	J. Atmosph. Terres. Phys., 18, 89.
Egan R.P.	1960	J. Geophys. Res., 65, 2343.
Egedal J.	1947	Terr. Mag. Atmosph. Elect., 52, 449.
Farley D.T.	1963	J. Geophys. Res., 68, 6083.
Hanson W.B. and Moffett R.J.	1966	J. Geophys. Res., 71, 5559.
Hirono M.	1950	J. Geomagn. Geoelec., 2, 1.
Hirono M.	1952	J. Geomagn. Geoelec., 4, 7.
Hirono M.	1953	J. Geomagn. Geoelec., 5, 22.
Kato S.	1956	J. Geomagn. Geoelec., _, 24.
Kato S.	1957	J. Geomagn. Geoelec., 9, 107.

Kato S.	1959	Rept. Ionosph. Space Res., 13, 62.
Knetcht R.W.	1959	J. Atmosph. Terres. Phys., 14, 348.
Lyon A.J.	1963	The Ionosphere, p. 88, Inst. Phys. & PHYS. Soc., London.
Lyon A.J., Skinner N.J. and Wright R.W.H.	1960	J. Atmosph. Terres. Phys., 19, 145.
Lyon A.J. and Thomas L.	1963	J. Atmosph. Terres. Phys., 25, 373.
Maeda K., Uyeda H. and Shinkawa H.	1942	Rept. Phys. Inst. Rad. Waves, No. 2.
Maeda H.	1955	Rept. Ionosphere Research, Japan., 9, 60.
Maeda H.	1955b	J. Geomagn. Geoelec., 7, 121.
Maeda H.	1957	J. Geomagn. Geoelec., 9, 86.
Maeda H.	1963	Proc. Intern. Conf. Ionosphere, 1962, Inst. Phys. and Phys. Soc., London, 187.
Maeda K. and Matsumoto H.	1962	Rept. Ionosph. Space Res., Japan, 16, 1.
Martyn D.F.	1947a	Proc. Roy. Soc., A189, 241.
Martyn D.F.	1947b	Proc. Roy. Soc., A190, 273.
Martyn D.F.	1948	Nature, London, 162, 142.
Martyn D.F.	1949	Nature, London, 163, 685.
Martyn D.F.	1955	Proc. Intern. Conf. Ionosphere, and Phy. Soc., London, p.254.
Martyn D.F.	1959	Proc. I.R.E., 47A, 147.
Martyn D.F.	1959	J. Geophys. Res., 64, 2178.
Martyn D.F.	1953	Phil. Trans. Roy. Soc., London, A246, 306.

Matsushita S.	1951	J. Geomagn. Geoelec., 3, 44.
Matsushita S.	1953	J. Geomagn. Geoelec., 5, 109.
Matsushita S.	1957	J. Atmosph. Terres. Phys., 10, 163.
Maynard M.C.	1967	J. Geophys. Res., 72, 1863.
Mitra S.K.	1946	Nature, London, 158, 668.
Nicolet M.	1957	Annales IGY, VIII, Pergamon Press.
Onwumechilli A.	1964b	J. Geophys. Res., 69, 5063.
Osborne B.W.	1951	J. Atmosph. Terres. Phys., 2, 66.
Parkinson W.D. and Cleary J.	1958	Geophys. J. Roy. Astron. Soc., 1,
Pederson P.O.	1927	Danmarks Nature Samfund, A15, 244.
Pekris C.L.	1937	Proc. Roy. Soc., London, A158, 650.
Ranzi I.	1939	Ricerca Sci., 10, 926.
Rao K.N., Rao D.R.K. and Raja Rao K.S.	1967	Tellus, XIX, 337.
-Rastogi R.G.	1959	J. Geophys. Res., 64, 727.
Rastogi R.G.	1962	J. Atmosph. Terres. Phys., 24, 1031.
Rastogi R.G.	1963	J. Geophys. Res., 62, 2445.
Sastry T.S.G.	1968	J. Geophys. Res., 73, 1789.
Schuster A.	1889	Phil. Trans. Roy. Soc., 180, 467.
Schuster A.	1908	Phil. Trans. Roy. Soc., London, A208, 163.
Singleton D.G.	1960	J. Geophys. Res., 65, 3615.

Singleton D.G.	1962	J. Atmosph. Terres. Phys., 24, 909.
Stewart B.	1882	Encyclopedia Britanica, 16, 159.
Taylor G.I.	1936	Proc. Roy. Soc., London, A156, 318.
Wielkes M.V.	1949	Oscillations of the Earth's Atmosphere, Cambridge University Press, London and New York.
Wright J.W.	1960	J. Geophys. Res., 65, 185.
Wright R.W.H., Koster J.R. and Skinner N.J.	1956	J. Atmosph. Terres. Phys., 8, 55.

******

SECTION - II - IONOSPHERIC DRIFT MEASUREMENTS AT THUMBA

Chapter - II.0 - Introduction and brief survey of methods for wind and drift measurements.

Chapter II.0

II.0.1 Introduction

II.0.2 Methods for wind and drift measurements.

CHAPTER II.0 Introduction and brief survey of methods for wind and drift measurements.

II.0.1. Introduction

Winds in upper atmosphere are known for a long time. Visual observation of noctiluscent clouds provides direct evidence of the existence of winds in upper atmosphere. As early as in the end of the nineteenth century, scientists reported the observations regarding movements of such clouds in the height range upto 90 km. Stormer (1932, 1933 and 1935) studied horizontal drifts of such clouds and found average order of speed between 30 to 80 m/sec.

Noctiluscent clouds are considered to be assemblies of small dust and ice particles and are observed around 80 km. in high latitudes. Movement of these clouds is naturally the neutral wind velocity at these heights. Photographing these clouds from widely spaced cameras, one can determine the height as well as the drift velocity of the clouds. The occurrence of such clouds is very rare and restricted to high latitudes only.

Another evidence of winds in the heights around 100 km. was given by the drift of visible meteor trails. Meteors entering the earth's atmosphere with very high velocity collide with neutral particles and get heated up resulting in its vapourization and thermal ionization of the medium. The hot meteoric particles therefore produce

trail in the atmosphere which is sometimes even visible and is able to reflect radio waves incident to it. Both photographic and radio methods have been used to study the trails. In the photographic method, the changes with time of the visible trail are recorded from different points on ground separated by few km. and winds can be computed (Liller and Whipple, 1953). In the radio method, the ionized trails left behind are tracked by radar technique (Hey, 1947). Assuming that the trail is subject to a uniform wind the speed of the drift of the trail can be determined by using Doppler Technique (Manning et al 1950).

The meteor trail method has the advantage that winds can be measured at definite heights and thus height gradients of the wind can be studied. However, this method is limited to heights from 80 to 110 km. and further the occurrence of meteors is not uniform diurnally and seasonally.

Both the noctiluscent cloud and meteor trail method relate to the neutral winds in the upper atmosphere. The electron drift in the ionosphere was first noticed indirectly by Ratcliffe and Pawsey (1933) and Pawsey (1935) while studying the amplitude fluctuations (fading) of a radio wave reflected from ionosphere. By studying such fading records at two receivers spaced at various distances on the ground, they concluded that the cause of fading

was due to interference of radio-waves reflected from scattering centres in the ionosphere. Pawsey (1935) was also first to notice a consistent time lag of the order of a second between fading records at two receivers. He attributed this to horizontal movement in the ionosphere.

Mitra (1949) developed a method to determine such motions in the ionosphere based on the original ideas of Ratcliffe and Pawsey (1933, 1935). A pulse transmitter was used in his experiment and the amplitude of the reflected signal was recorded simultaneously at three spaced points situated at the vertices of a right angled triangle of sides 100 meters each. The time delays between maxima of similar fades from two pairs of records were measured and the drift speed of electron was calculated. In this technique, one observes the movement of the diffraction pattern over ground formed due to irregularities of ionization in the ionosphere which scatter the radio-waves. Subsequently experiments have been done by various workers all over the world using Mitra's technique. As a source of radio signal ground based transmitters as well as outside source such as radio waves emitted by stars have been employed. The latter is known as radio star method and measures the average drift of the whole of the ionosphere while the former indicates the drift at the level of reflection of the radio waves.

Measurements of neutral winds and drifts in the upper atmosphere gained considerable importance following the development of the dynamo theory which was derived to explain the geomagnetic field variations observed at ground. According to this theory, the air movement across the magnetic field lines, which carries ionization also, generates dynamo field which drives the current system causing the geomagnetic field variations at ground. The concept of electrostatic fields being transferred to F-region heights and causing electro-magnetic drifts was put forward by Martyn (1953). Many of the ionospheric phenomena are explained on the drifts theory. To test the validity of this theory, experiments were performed all over the world to check whether drifts or winds observed do compare to what is estimated on the basis of the dynamo theory.

II.0.2. Methods for winds and drift measurements

With the advent of Rockets and Satellites, many new methods of measuring winds and drifts in ionosphere have come into picture. Kent and Wright (1968) have given an extensive review of all the methods available for measuring the neutral gas motion, bulk plasma motion and the motion of irregularities in the ionized plasma. A brief description of some of the methods which are in prominent use at present are given here.

a) Neutral gas motion

1. Meteor trail method using radio detection:

The ionized trails left behind the meteors move with the neutral wind hence radio tracking of the trails will be indicative of winds at that level. Pulse as well as continuous wave techniques have been developed for the measurements of height and velocity of meteor trails. Manning, Villard and Peterson (1950) in USA have used continuous wave doppler method together with special direction finder. Greenhow (1952) at Jodrell Bank used a coherent pulse doppler technique while Robertson, Liddy and Elford (1953) in Australia used a combination of pulse and continuous wave methods. Extensive work has been done at Jodrell Bank and Adelaide. Diurnal, seasonal variations of winds as well as height gradients have been studied. The method however is limited to certain height ranges at certain latitudes only.

2. Chemical trail method

A method which has come to limelight recently is the release of photo or chemi-luminiscent chemicals in the upper atmosphere. Rocket as well as gunlaunched projectiles have been used for the purpose. In the early stages, alkali metals were used either at sunrise or at sunset

so that the resonant scattering of sunlight made the trail visible from the ground against a darksky. Recently trimethyle aluminium is being used which enables the trail visible at any time of night. The diffusion of the trail and subsequent distortion due to the local wind system is photographed every few seconds from widely spaced cameras at the ground. In this manner the trail is followed and hence winds can be measured.

b) Bulk motion of plasma

1. Rocket ignition of plasma

Artificially created plasma in the atmosphere can be kept in track and its motion can be computed. In case of barium release, both the neutral cloud as well as the ion clouds are formed, both photo luminiscent. The neutral cloud being in the green while the ion cloud in the blue region of the spectrum. With the help of filters both clouds can be photographed and separate motions of the neutral as well as plasma motion can be followed.

c) Motion of irregularities

1. Closely spaced receiver method

One of the most widely used method to measure the drifts of the small scale irregularities of electron density consists in recording the amplitude variations of a radio wave simultaneously at three closely spaced

points on the ground (Mitra 1949). The radio waves traversing through these irregularities get phase variations introduced, which cause a diffraction pattern formed on the ground. Movement of these irregularities results in the movement of the diffraction pattern on the ground giving rise to the amplitude variations observed at a point with respect to time.

Apart from the method described by Mitra which used a pulse transmitter, methods have been devised receiving radio signals of an artificial satellite or radio signals emitted by stars. In the reflection method the motion of irregularities is half the motion of diffraction pattern on ground, it is same as the movement of diffraction pattern on ground in case of radio star signals while it is related to the motion of satellite as well as the heights of satellite and the irregularities when one observes fading of a satellite signal.

Drift measurements of the irregularities in the E- and F-regions employing Mitra's technique were attempted at a large number of high latitude stations after 1949 and a review of all these results is given by Briggs and Spencer (1954). Method of analysis of the fading records was further developed by Briggs et al (1950), Phillips and Spencer (1955) and Fooks (1965) which enables to find the

size and shape of the diffraction patterns as well as the steady and random components of the drift.

Radio star scintillations have been employed by Spencer (1955) and Little et al (1962) at high latitudes and by Koster (1963) at equator to study drift and size of irregularities in the F_2 region. Scintillations of satellite signal was first observed by Slee (1958). Munro (1963) and Kent and Koster (1966) have further described the work on satellite signals.

2. Widely spaced receiver method

Large scale irregularities can be studied by the method of widely distributed receivers with a transmitter or widely distributed transmitters with a receiver; the separation on the ground of the order of several tens to hundreds of km. The waves recorded thus travel in different paths. The reflected signals show sometime similar abnormalities on different records with some time delays. These abnormalities arise due to the passage of large scale irregularities across these paths through the reflection points. In practical observations, these large scale irregularities are generally restricted to F-region, except E_s clouds of high ionized density.

Munro (1948, 1950 and 1953) studied P'f traces at fixed frequency and found abnormalities appearing as

peaks or dips of virtual height, crossing of O and x components or some other abnormality. From the time delays between such abnormalities on different records, one can find the drift of large scale irregularities.

3. Doppler shift method

Motions of relatively intense irregularities have been detected by observing the doppler shifts in radio echoes using VHF. Sporadic E irregularities in the equatorial and auroral regions have been detected by this method (Cohen and Bowles 1963, Cole 1963). Irregularities in the F-region causing spread-F have been studied at equator by Calvert and Cohen (1961) and by Clemsha (1964). Calvert and Cohen have reported East-West extent of these irregularities usually of the order of 150-300 km and moving Eastward most of the nights in the speed range 100-200 m/sec. Clemsha (1964) in Africa reported E-W extent of these irregularities upto 400 km and mean rate of drift about 100 m/sec. The order of the drifts of these patches of irregularities is same as that of small scale irregularities which are of the order of about 100 meters.

CHAPTER - II.1. EXPERIMENTAL SET UP AT THUMBA FOR MEASURING IONOSPHERIC DRIFTS

Chapter-II.1.

II.1.1. Transmitter unit

II.1.2. Receiving set up

II.1.3. Antenna system.

CHAPTER II.1 Experimental set up at Thumba for measuring ionospheric drifts

Horizontal drift measurements of the irregularities of ionosphere over Thumba have been made since January 1964 using closely spaced receiver technique developed by Mitra (1949). The method consists of transmitting radio waves to ionosphere and recording simultaneously the received signal at three spaced sites situated at suitable distances apart. The advantages of this particular method lie in the fact that there exist irregularities in the ionosphre always hence routine observations through-out the day can be carried out. Further, the movements of irregularities can be measured in both E- and F-regions separately by using suitable frequencies.

II.1. Experimental set up at Thumba

The experimental set up at Thumba consists mainly of the following units:

II.1.1. Transmitter

II.1.2. Receiver

II.1.3. Antenna system.

II.1.1. Transmitter unit

The transmitter used at Thumba is a pulsed type. Main characteristics of the transmitter are following:

Peak power	1.5 kw
Pulse repetition frequency	50 c/s
Pulse width	50-300 μsec., variable in five steps
Operational frequencies.	2.2 mc/s and 4.7 mc/s.

Fig. II.1.1. shows the schematic block diagram of the transmitter. The transmitter consists of the following sections:

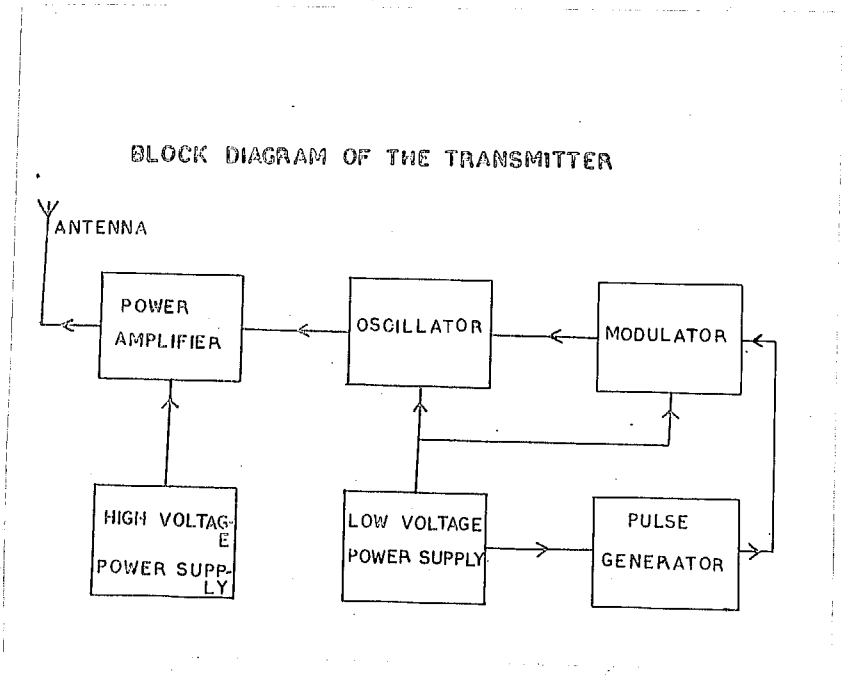

Fig. II.1.1.

a - Mains triggered pulse generator

b - Modulator

c - Master oscillator

d - Power amplifier with tuning unit

e - Power supplies.

a) Mains triggered pulse generator

The circuit diagram of this unit is shown in Fig. II.1.2. A sine wave output of about 20 volts r.m.s.

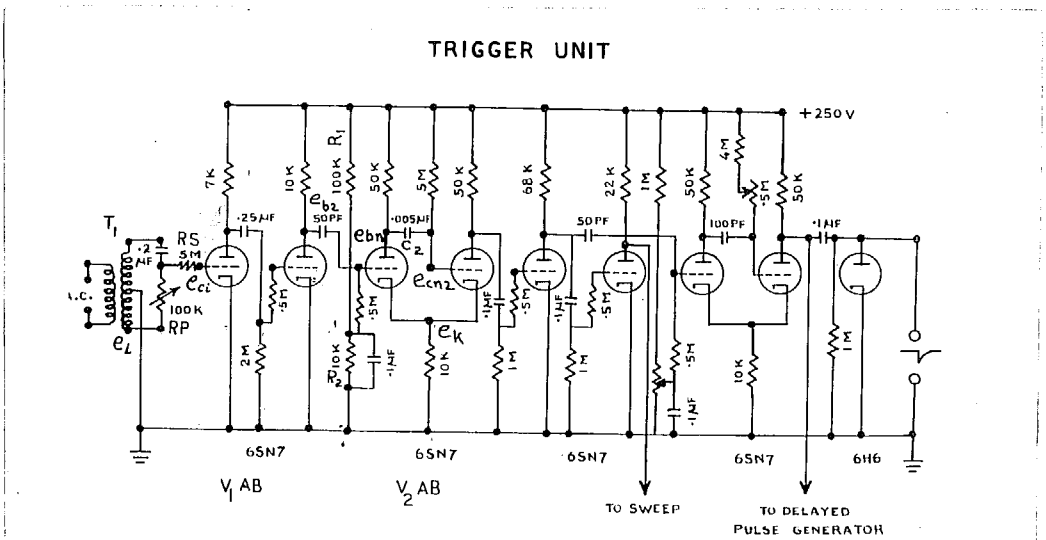

Fig. II.1.2.

is derived from a step down transformer T_1, the phase of which can be varied with a potentiometer RP. Valve V_1 is a double triode 6SN7. The first section functions as an over-driven amplifier. The sine waves are applied to the grid through a high resistor R_s. The grid cathode path

alongwith this resistor R_s act as a diode clipper and the positive peaks of the sine waves are clipped in the process. The second section of the tube converts the sinusoidal input into a nearly square wave. This square wave is differentiated which triggers a one-shot cathode coupled multi-vibrator V_2 A/B. Negative and positive pulse outputs are obtained at the plates of V_2A and V_2 B respectively, the negative pulse output from V_2 A is used to trigger the transmitter.

b) Modulator

The circuit diagram of the remaining sections of the transmitter are shown in Fig. II.1.3. The output of

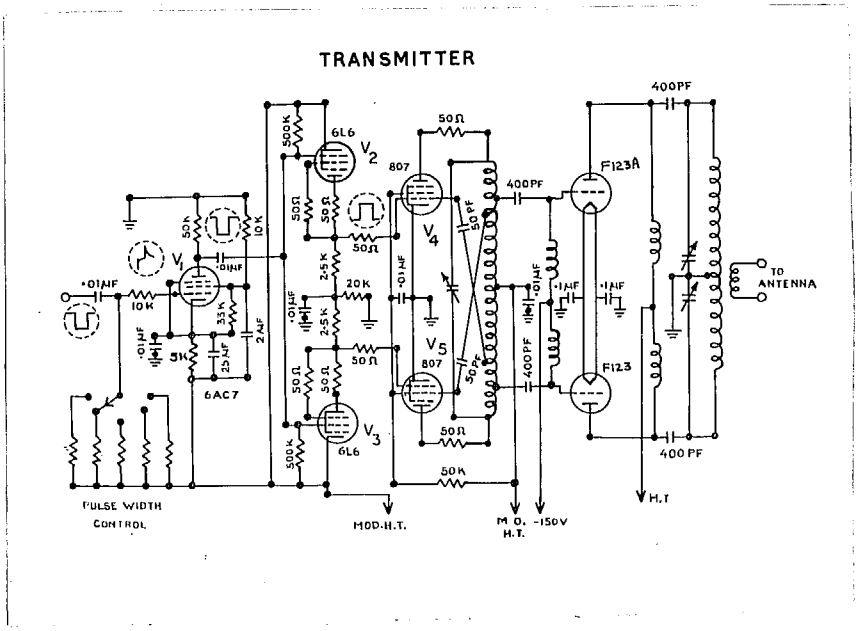

Fig. II.1.3.

the mains triggered pulse generator is fed to the modulator unit. The pulse is first differentiated by a condenser and resistence combination. Five different resistors are provided to select the desired width of the pulse. The negative pulse output of V_1 (6AC7) is applied to the grids of the modulator tubes V_2 and V_3. The plate loads of these tubes are the grid leaks of the two oscillator tubes V_4 and V_5 which are normally biased beyond cut-off. The negative pulses from V_1 momentarily cut-off the tubes V_2 and V_3, the bias is removed from the oscillator which is thus allowed to oscillate for the duration of modulator pulse.

c) Oscillator

A conventional Hartley circuit using two 807 tubes in push-pull is used for the oscillator. Since the oscillator is pulsed with a low duty cycle, the tubes are operated with a plate supply of 750 volts. The oscillator is grid modulated and oscillates only during the duration of pulse.

d) Power amplifier

The power amplifier is a push-pull type using two F123 tubes which are operated with a plate supply of 2.5 kv. To get sufficient power, tuned circuits are used.

The operational frequencies are 2.2 Mc/s and 4.7 Mc/s; the change over is accomplished with the help of additionally fixed condenser which is brought in parallel with the main tuning condenser in the oscillator as well as in the power amplifier stage. The output of the amplifier is coupled to the transmitting antenna through a 75 Ω R.F. cable.

II.1.2. Receiving set up

Block diagram of the receiving and recording set up is shown in Fig. II.1.4. The complete assembly consists of:

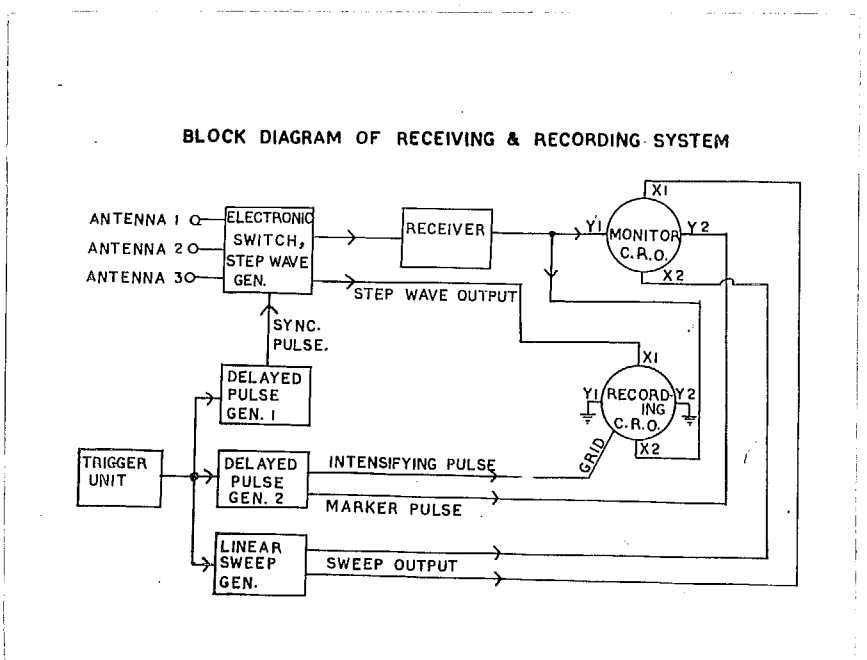

Fig. II.1.4.

a) Trigger unit

b) Delayed pulse generators

c) Electronic switch and step wave generator

d) Linear sweep generator

e) Monitor and recording oscilloscopes

f) Receiver

g) Camera set up for recording the signal variations.

a) Trigger unit

The pulse generator to trigger the various circuits like electronic switch, sweepcircuit etc. is similar to that described in the transmitter section. Two pulses are taken, one positive pulse which is fed to the delayed pulse generators and another a negative pulse which is fed to the sweep circuit.

b) Delayed pulse generator

To select the desired echo to be recorded, a gating circuit is used which gives a pulse whose phase can be varied with respect to the ground pulse. Two pulse delay circuits are used, one for synchronising the electronic switch and another generating two pulses, a 150 v pulse to intensity modulate the recording oscilloscope and another 15 v pulse which appears as a marker pulse on monitor oscilloscope.

The circuit of the pulse delayed generator is shown in Fig. II.1.5. Positive pulse obtained from the

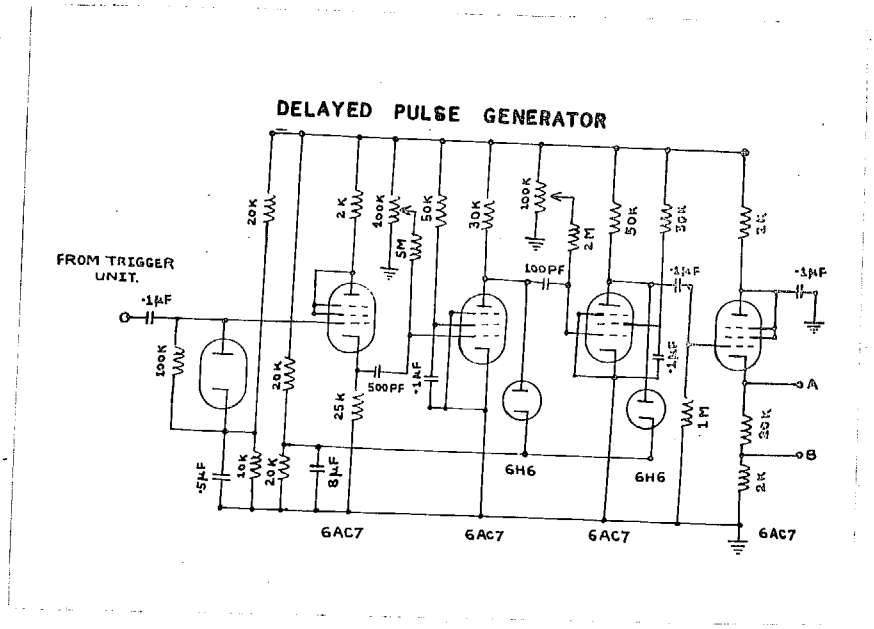

Fig. II.1.5.

trigger unit is applied to the grid of the tube V_1. Potentiometer P_1 controls the phase variation of the outgoing pulse. Similarly P_2 controls the width of the pulse output from value V_2. Final pulse output is taken through a cathode follower stage V_4.

c) Electronic switch and step wave generator

This unit gives the proper switching sequence of the three antenna in succession to the receiver. It also

provides a step wave output with which the signals of three antennas can be recorded separately on a recording oscilloscope. Circuit diagram of this unit is shown in Fig. II.1.6. Screen grids of V_1, V_2 and V_3 are used to produce the multi-vibrator action, but the output is taken from the plates. The wave-forms at A. B. C. switch the grounded grid high frequency amplifier tubes V_4, V_5 and V_6. These wave forms are applied to cathodes

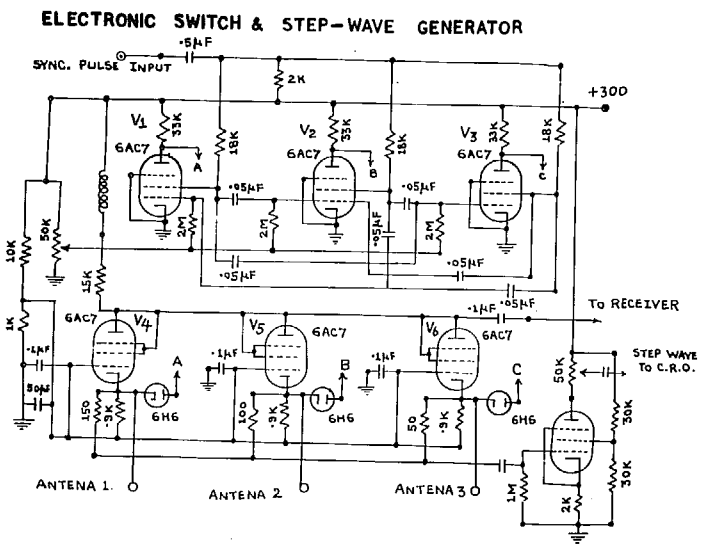

Fig. II.1.6.

through the diodes V_7, V_8 and V_9. During the lower voltage level of the wave forms at A, B, C, the tubes V_4, V_5 and V_6 conduct, thus connecting the antennae to the receiver in equal sequential order. The wave forms at the cathodes of valves V_4,V_5 and V_6 are similar to that at A, B, C. By combining these wave forms with the loads of the ratios 3:2:1 a step wave is obtained and it is amplified in the amplifier V_{10}. This sort of wave gives three spots on the recording scope. Thus the output from different antennae are recorded in a single oscilloscope.

d) Sweep circuit

This circuit uses a sanatron circuit which generates a single stroke linear sweep. The circuit also provides a rectangular pulse, having precisely the same duration as sweep, which is used to brilliance the monitor-oscilloscope. The senatron consists of the Miller integrating circuit of V_4 linked with V_2 to form one semistable stage. The coupling of a similar tube V_5 with V_4 enables to get the push-pull output of the sweep wave form. The output is D.C. coupled to the X plates of the monitor scope.

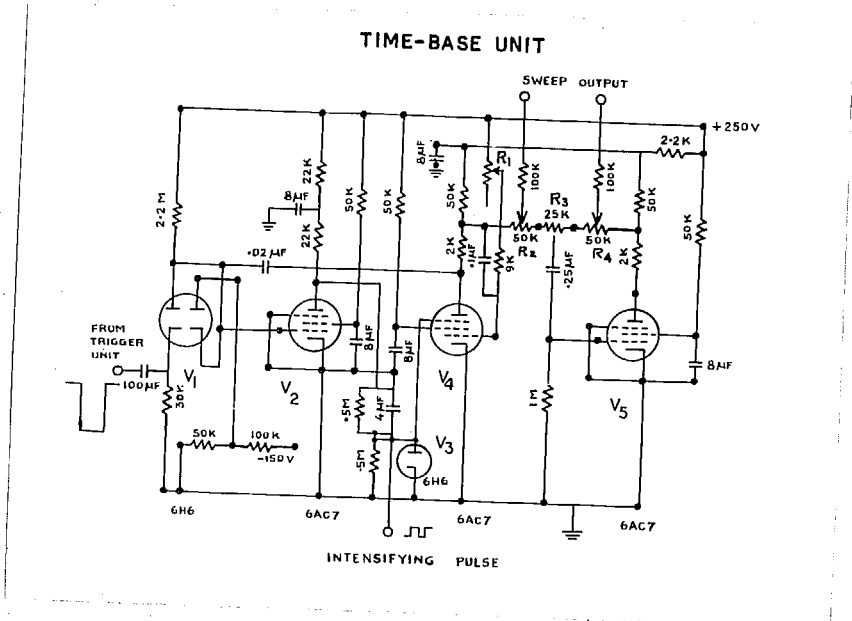

Fig. II.1.7.

e) Monitor and recording oscilloscopes

The circuit diagrams for both the monitor and recording oscilloscopes are of similar type. Oscilloscope tube 5BP1 is used in both the circuits. X and Y shifts are obtained with the help of ganged potentiometers.

In case of monitor oscilloscope the sweep output

is fed to the X plates. Receiver output is fed to one of the Y plates and the gating pulse is fed to other Y plate. To intensify the trace on the monitor scope an intensifying pulse from sweep unit is applied to the grid of the oscilloscope.

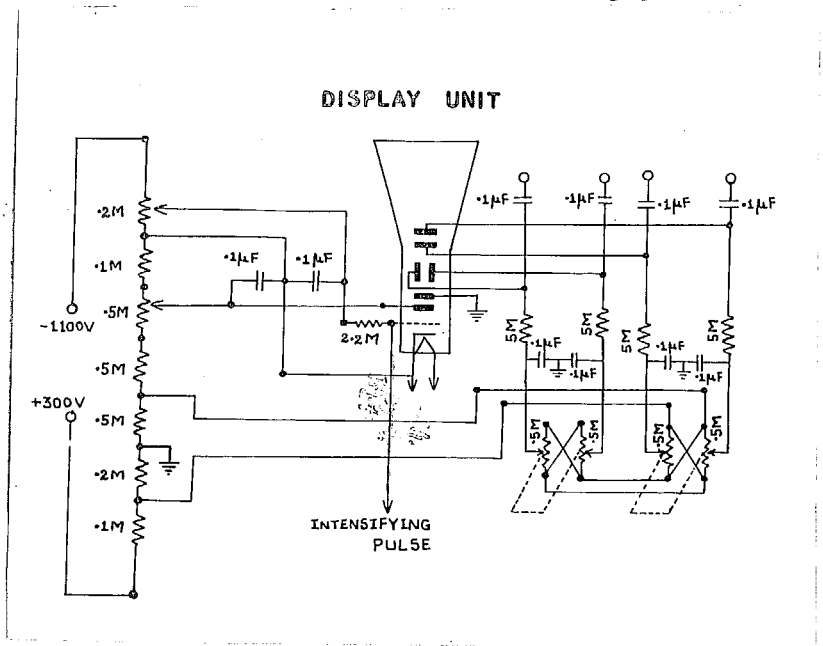

Fig. II.1.8.

In the recording oscilloscope, three spots are obtained one for each antenna, by applying the step wave to one of the X plates. The receiver output is applied to another X plate. The recording scope is made to operate during the time duration of the gate pulse by applying a 150V pulse in synchronous with the gate applied to the grid of the monitor oscilloscope.

f) Receiver

The receiver used for the experiment is a modified receiver of army disposals. The changes which are

made to make it suitable for pulse operation are following:

1) In order to achieve high gain, 6AC7 tubes are used in R.F. stages. AVC control is removed as our interest is in the fading.

2) Band width was increased by suitable damping in the primary and secondary coils of the I.F. transformers.

3) The detector was operated in the linear portion of the characteristic.

4) The detected output is further amplified in a video amplifier stage.

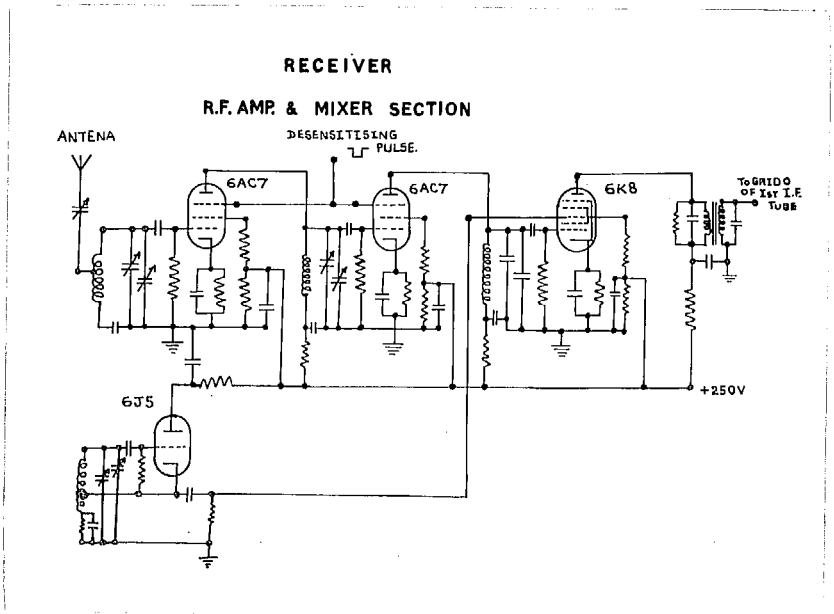

Fig. II.1.9.

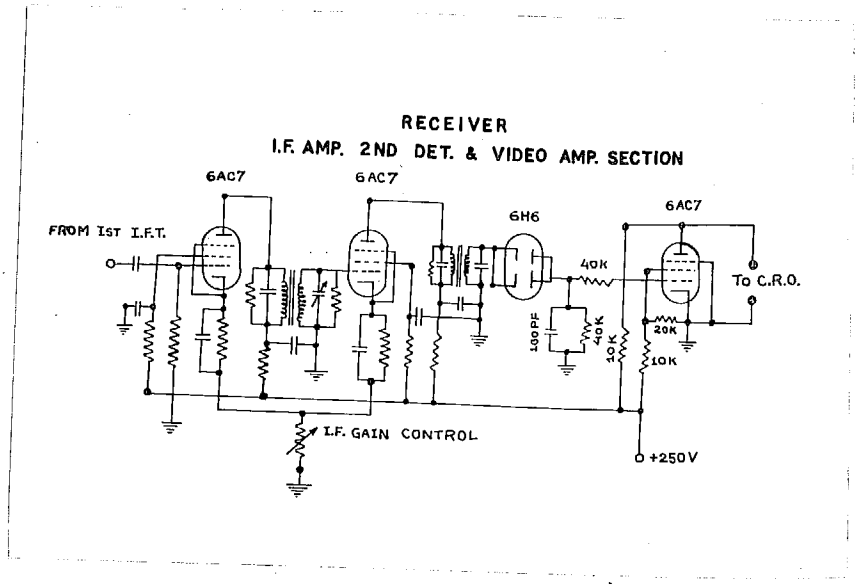

Fig. II1.10

g) Camera unit

Recording was done on a moving 35 mm film. A movie Camera with a motor system was used. The original motor speed was very high for the purpose, hence it was geared down considerably to get a film speed of 28 cm/min.

II.1.3. Antenna system

Half wave centrefed dipoles orientated N-S are used for the transmitting antenna. Two different dipoles are used, one corresponding to the frequency of 2.2 Mc/s and another corresponding to a frequency of 4.7 Mc/s.

75 Ω cables are used to feed power from transmitter final stage to the transmitting aerial.

For receiving purpose, similar half wave dipoles corresponding to a frequency of 2.2 Mc/s are used. To start with three receiving dipoles situated at the vertices of an isoceles right angled triangle were employed with a side of 120 m. One additional antenna was put in 1966 in the N-S line. Further modification of the antenna system was done in the middle of the year 1967. In all, ten aerials were available covering distances upto 480 meters along both E-W and N-S directions, to test the extreme elongation of the ground diffraction patterns obtained at Thumba.

Chapter II.2.

CHAPTER II.2 Fading characteristics observed at Thumba

II.2.1. Fading of radio waves reflected from ionosphere

A radio wave reflected from the ionosphere is observed to have variations in its signal strength at ground, a phenomenon called fading of the radio waves. This fading may be caused by the interference effects between waves which have travelled by different paths such as ground wave, singly or multiply reflected ionospheric waves, waves reflected from different ionospheric regions or the two magneto ionic componenets. It has been possible to isolate a single down coming wave by means of a pulse sender and a gated receiver and or by special aerials and still fading was observed.

The experiments on fading conducted by Appleton and Ratcliffe (1927) and Ratcliffe and Pawsey (1933) showed fading speed roughly proportional to the wave frequency, presence of laterally deviated rays and fadings to be uncorrelated at a separation of about one wavelength which led to believe a diffractive mechanism as the cause of fading. From the measurements of the angle of deviations of the waves, Ratcliffe and Pawsey concluded fading due to interference at the ground of waves scattered from a series of diffracting centres disturbed over an area of radios atleast 20 km. in radias in their experiment.

Based on above experimental findings, Ratcliffe

(1948) gave a theory of the fading of the radio waves considering the ionosphere as a diffractive screen. It is assumed that there exist several scattering centres distributed approximately in a horizontal plane and that each scatters the same power from the incident wave. No attempt was made to define scattering centre exactly. Such 'centres' make up the irregularities which form roughness in the ionosphere. The scattering centres are further assumed in continual random motion in such a way that the velocities in the line of sight are distributed according to Gaussian law, so that the number of scattering centres $P(v)\,dv$ with velocities v and $v+dv$ is given by

$$P(v)\,dv = Ae^{\frac{-v^2}{2v_0^2}}\,dv \qquad \ldots(1)$$

where v_0 is the r.m.s. velocity of a scattering centre. If fo is the transmitted frequency at vertical incidence the radio wave suffers a doppler shift of frequency after scattering from such centres, so that the frequency on returning to the ground is given by

$$f = f_0\left(1 + \frac{2v}{c}\right) \qquad \ldots(2)$$

As the centres are randomly distributed, the phases of the various scattered waves may be assumed to be

randomly distributed. The resultant signal strength at ground will therefore consists of components of different frequencies and the power $W(f)\,df$ in each frequency range can be obtained by combining equations (1) and (2)

$$W(f)\,df = B\,\exp.\left[\frac{-c^2(f^2-f_0^2)}{8f_0^2 v_0^2}\right] df \qquad \ldots(3)$$

The relation can be written in the form

$$W(f)\,df = \frac{\Psi}{\sigma\sqrt{2\pi}}\,\exp.\left[-\frac{(f^2-f_0^2)}{2\sigma^2}\right] \qquad \ldots(4)$$

where $\sigma = \frac{2f_0 v_0}{c} = \frac{2v_0}{\lambda}$ λ being the wave length

and $\Psi = \int_0^\infty W(f)\,df$ = total power in the wave.

The fading of the wave is now seen to result from the beating between the component waves of different frequencies. Furth and Mcdonald (1947) have shown that in a power pass character like equation (3), the amplitude R of the output signal is distributed according to Rayleigh law, so that the probability P(R) of finding an amplitude between R and R + dR is given by

$$P(R) = \frac{R}{\Psi}\,e^{\frac{-R^2}{2\Psi}} . \qquad \ldots(5)$$

In such a case, mean amplitude $\bar{R} = \sqrt{\frac{\pi\Psi}{2}}$

$$\overline{R^2} = \int_0^\infty P(R)\,R^2\,dR = 2\Psi$$

and most probable value $R_m = \sqrt{\Psi}$

The situation is different if in addition to the random components there is a steady component Rice (1945) has given the probability distribution under such circumstances. If B is the amplitude of the steady signal, then the resultant amplitude Q of the envelope is given by the probability distribution

$$P(Q) = \frac{Q}{\Psi} \exp^{-\left(\frac{Q^2+B^2}{2\Psi}\right)} I_o \frac{QB}{\Psi} \qquad \ldots(6)$$

where I_o is the Bessel function of zero order and imaginary argument. In general $\overline{Q^2} = B^2 + 2\Psi$

$$= B^2 + R^2.$$

That is the mean square value of the resultant is the sum of the mean square values of the components. If we define a parameter $b = B/\sqrt{\Psi}$ that is the ratio of the amplitude of steady signal to the most probable value of the random signal. The distribution in case $b < 1$ can be written as

$$P(Q) \simeq \frac{Q}{\Psi} e^{\frac{-Q^2}{2\Psi}} \qquad \ldots(7)$$

which is a Rayleigh distribution. In case $b >> 1$ it approximates to

$$P(Q) \simeq \frac{1}{2\pi\Psi}\left(\frac{Q}{B}\right)^{1/2} \exp\left[-\frac{Q^2-B^2}{2\Psi}\right] \qquad \ldots(8)$$

which is a normal or Gaussian distribution. McNicol (1949)

has shown that above can be put into the form

$$P(Q) = \frac{1}{\sqrt{2\pi\psi}} \exp\left[-\frac{(Q-Q_m)^2}{2\psi}\right] \qquad \ldots(9)$$

where $Q_m = \left[\psi(b^2+1)\right]^{1/2}$

and give the most probable value distribution.

Rice has given theoretical curves of probability distribution for various values of b which are shown in Figure II.2.1. The probability distribution is Rayleigh type when b = 0 and it deviates from it as the value of b increases. For sufficiently high values of b ($>$ 4) the distribution tends to normal type. Thus from the probability distribution curves one can estimate the ratio of steady to random signals.

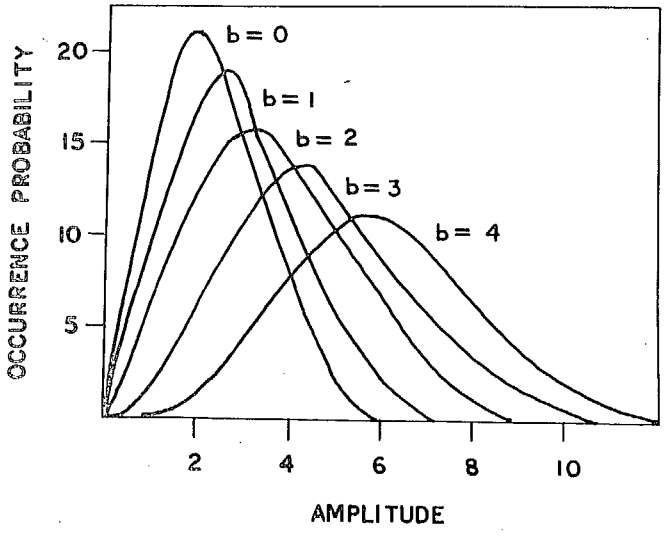

Fig. II.2.1.

Another way of defining this ratio has been shown by Alpert (1960). He has shown that the ratio of the average square of the amplitudes and square of average amplitude

is given by

$$\frac{\overline{R^2}}{\overline{R}^2} = \frac{4(1+b)^2 e^{b^2}}{\pi\left[(1+b^2) I_0\left(\frac{b^2}{2}\right) + b^2 I_1\left(\frac{b^2}{2}\right)\right]^2}$$

where I_0 and I_i are the Bessel functions with imaginary arguments. The limiting values of this ratio are

$$\frac{\overline{R^2}}{\overline{R}^2} \simeq \frac{4}{\pi} = 1.27 \quad \text{for } b^2 \longrightarrow 0$$

$$= 1.0 \quad \text{for } b^2 \longrightarrow \infty$$

Hence, theoritically this ratio must range between 1.0 and 1.27. That is from a Rayleigh distribution when this ratio is 1.27, it decreases with increase of b and tends to unity for normal distributions.

II.2.2. Characteristics of fading records at Thumba

The fading characteristics of the daytime E and F region reflections have been studied by Deshpande (1966). The fading records obtained at Thumba are of impulsive nature with short bursts of signal intensity occurring in the back-ground of practically zero intensity. The rate of fading was found to be much higher than that at non-equatorial station, Ahmedabad. Fadings were found to be as high as 90 per minute for the F-region at 4.7 Mc/s and 60 fades per minute for the E-region reflections at 2.2 Mc/s. The study of amplitude distributions for the daytime records showed that they are neigher Rayleigh nor Gaussian type. Both for the slow fadings (20 to 25 fades per minute) and

fast fadings (about 60-70 fades/min.) the portion of the curve for amplitudes greater than most probable one falls more rapidly than expected from the theoretical Rayleigh curve. About 20 records out of 800 showed M type distribution occurring during very slow fadings. The ratio was higher than theoretical limit $\frac{4}{\pi}$ on about 90% of the occasions with individual values as large as 2.6.

Counting of the fades has been done for each individual record in the period 1964-67 and its variation with solar time of the day, seasonal effects and year-to-year changes in this period have been studied. In addition, some of the features of the fading characteristics of the records in the year 1967, particularly F-region daytime and nighttime records have been studied and are described here.

The daily variations of the fading rate in the entire period 1964-67 are shown in Figs. II.2.2. and II.2.3. Fig. II.2.2 shows the daily variations of the fading rate for E- and F-region reflections in the daytime hours (07 to 18 hr.) during each season of the period 1964, 1965-66 and 1967.

Referring to the E-region fading rates, no marked difference is noticed in the winter season from one year to another year, however in the seasons, equi-

noxes and summer fading rates have decreased from 1964 to 1967. The range of variations as well as the fading rates are smaller during summer in any of the year. A distinct change observed in the year 1967 is marked rise of fading in the late evening hours of the winter and equinoxes seasons. The fading rates are lowest at about 14-15 hrs. during each season. The morning maxima is observed at about 08-09 hr.

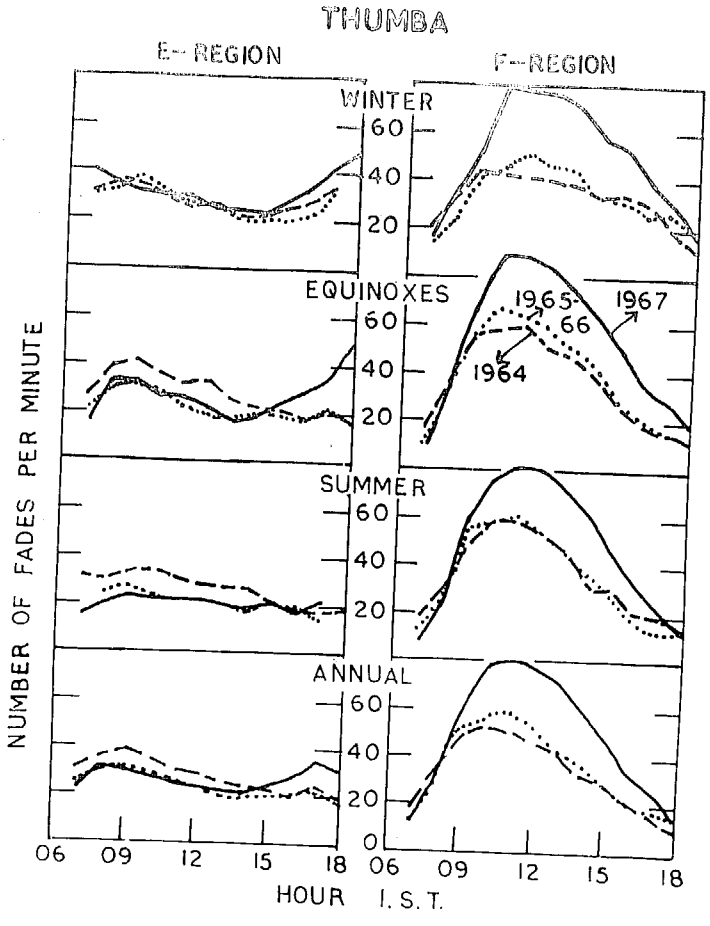

Fig. II.2.2.

The F-region fading rates have increased considerably from the year 1964 to 1967. The nature of the variation is same in each season of the different years with

maxima occurring at about 11 hr. when mean fading rates as high as 80 fades per minute are observed in the year 1967.

The 24 hour variations of the F-region fading rates are shown in Fig. II.2.3. Very low fading rates of the order of 10 fades per minute are observed in the morning (7 hr.) and evening (19 hr.). Apart from the main peak just before noon, a minor peak is observed at about 21-22 hr. Further the peak occurs slightly later during summer season.

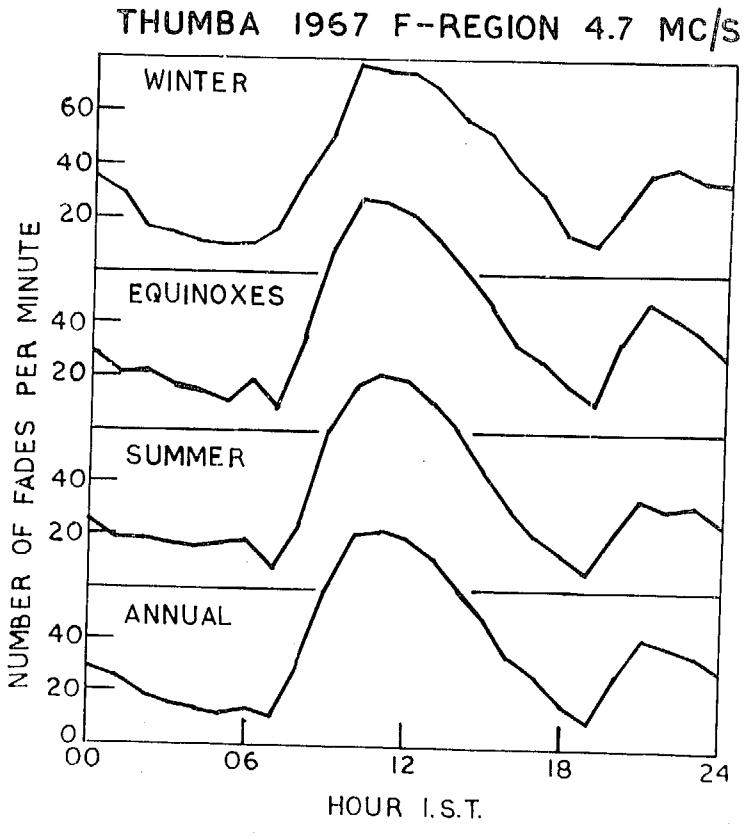

Fig. II.2.3.

Typical examples of the F-region fading records are shown in Figures II.2.4, II.2.5 and II.2.6. Fig. II.2.4 shows some examples of very slow fading rates. Such records

are found to occur everyday at sunrise and just after sunset.

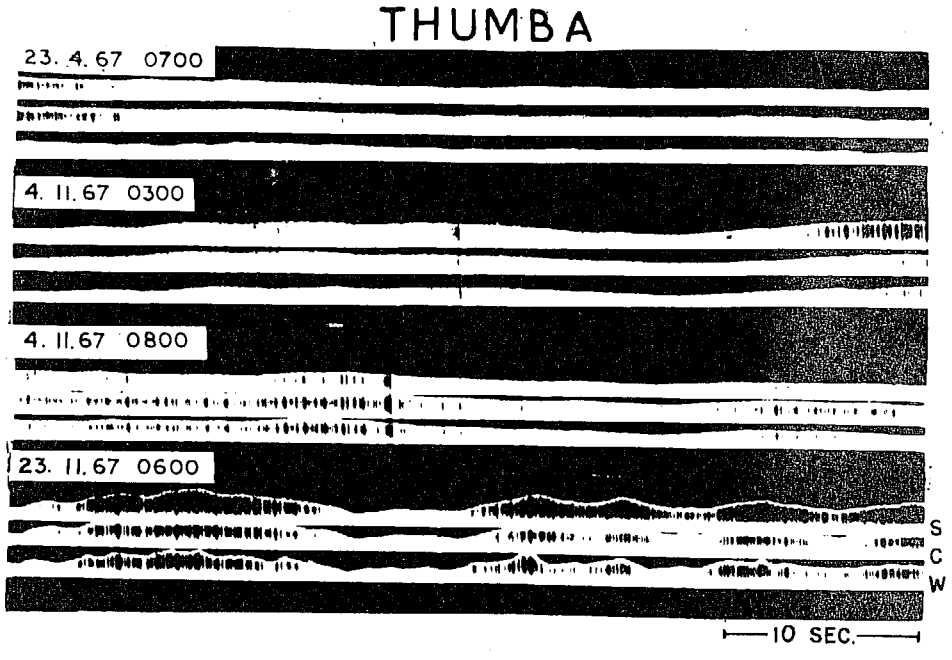

Fig. II·2.4

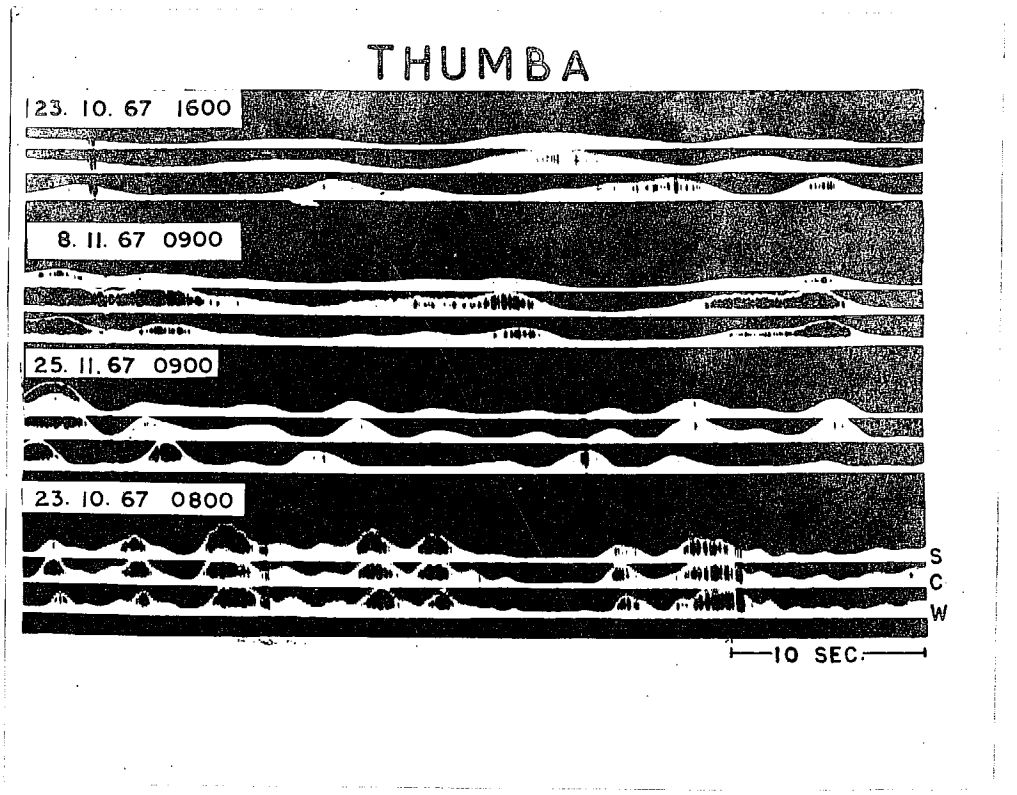

Fig II.2.5

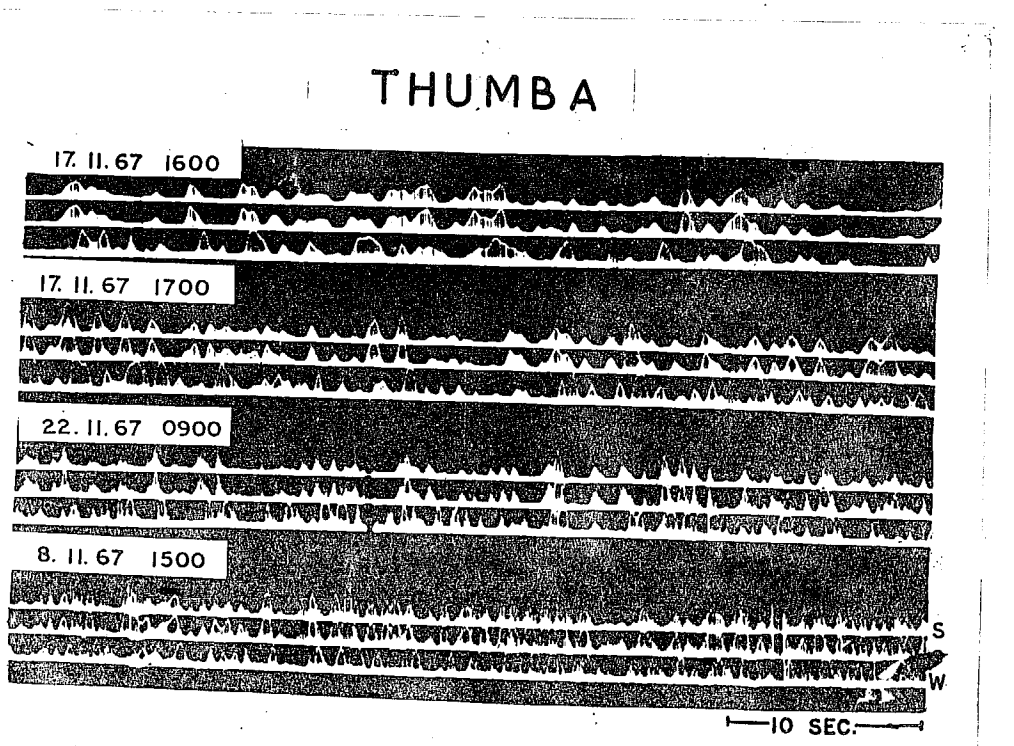

Fig II.2.6

Occasionally they are obtained during night hours also. Such records are seen to have very small amplitude fluctuations with extreme cases when practically steady signal level is recorded. Even in the cases when fades are clear, the signal strength never comes to zero level. On few occasions, a fairly rapid fading superimposed on some steady level have also been obtained.

Fig. II.2.5 shows some of the moderate fading rates obtained at Thumba. Records of this type show smooth fading with clear minima occurring at zero level of the signal strength. This type of records are usually obtained just before and just after the times when the very slow fadings occur.

The fast fading records at Thumba are shown in Fig. II.2.6. These are the typical fading records at Thumba which occur most of the daytime and few hours around midnight. Large and rapid amplitude fluctuations on zero intensity back ground level are the characteristics of such fading records.

The typical F-region fading records at mid-noon, mid-night, morning and evening hours are shown in Figs. II.2.7 and II.2.8. The mid-noon fading rates are very high and look like short bursts of amplitudes arriving at background zero level. The mid-night fading records have same nature as of the fading records at mid-noon but with fading

rates considerably reduced. The fading records obtained

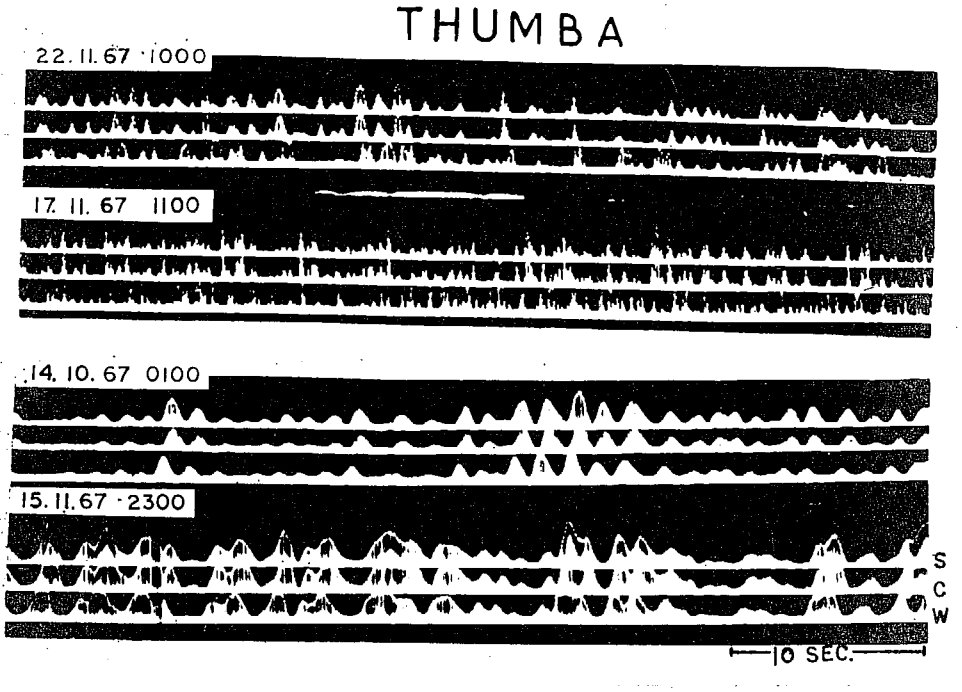

Fig II.2.7

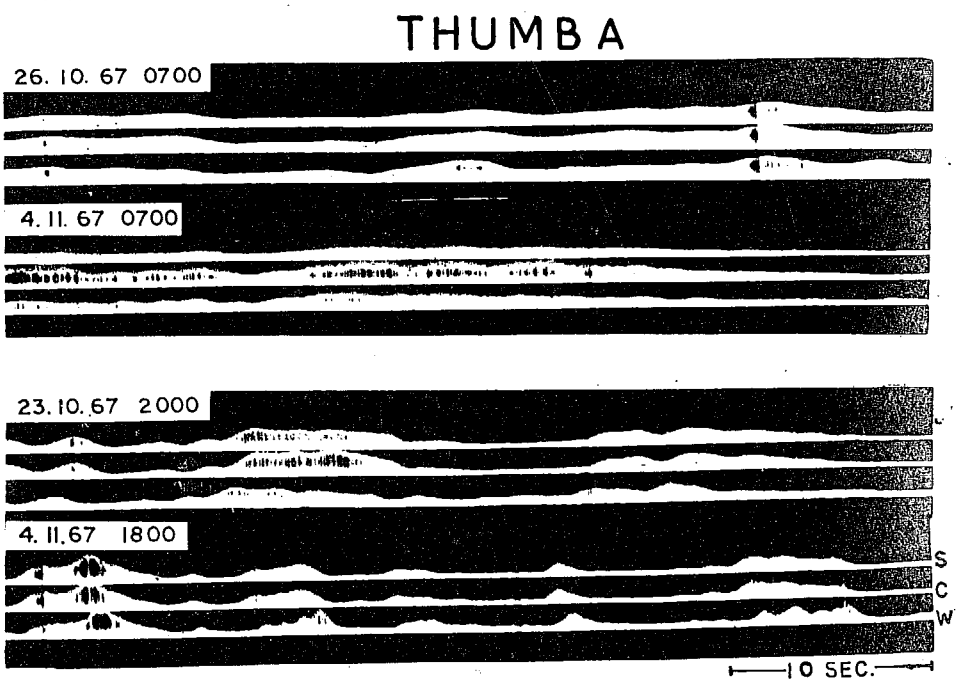
THUMBA
26. 10. 67 0700
4. 11. 67 0700
23. 10. 67 2000
4. 11. 67 1800
S
C
W
10 SEC.

Fig. II-2-8

at morning and evening hours are of very slow or moderate fading rates type, as described earlier.

The amplitude distributions obtained for the fading records at Thumba are of three types, which are shown in Fig. II.2.9.

(1) Typical distribution at Thumba

As described earlier by Deshpande for the daytime records in the year 1964, most of the daytime records show this typical distribution which is neither Rayleigh nor normal distribution. The distribution looks more or less exponential type.

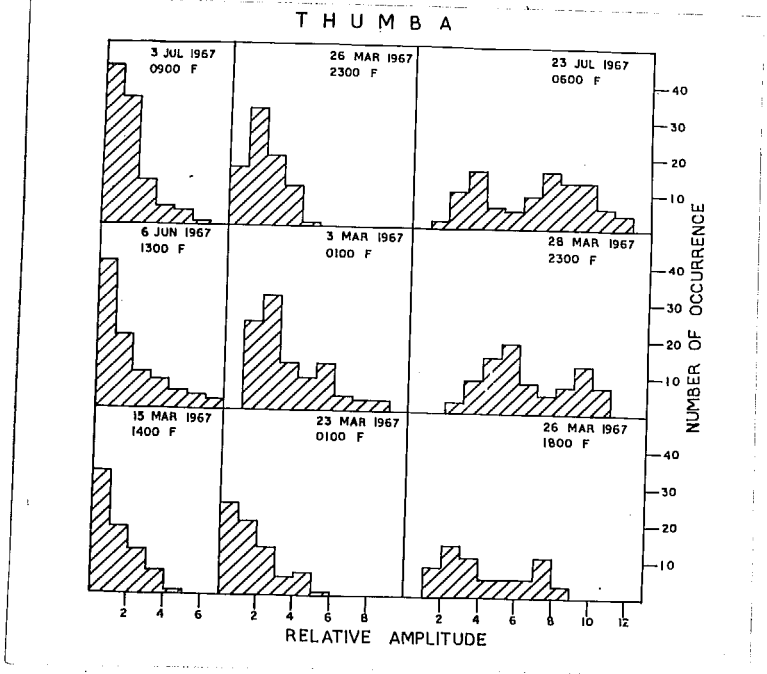

Fig. II.2.9.

(2) Normal or Rayleigh distribution

Distribution of these types as expected from the theory are observed quite rarely at Thumba. Mostly very slow fading records of the morning and evening or

nighttime give this type of distribution.

(3) Double distribution

On few occasions, mostly very slow fading records, have shown this type of distribution which is also known as $\Gamma\gamma$ type distribution. This type of distribution is considered to arise due to addition of two different distributions centred at different amplitude levels, and are restricted to morning, evening or nighttime when very slow fadings are observed.

A study of the ratio $\overline{R^2} / \overline{R}^2$ was made for about 850 E- and F-region records of the year 1967. Fig. II.2.10 shows histograms of percentage occurrence of the ratio $\overline{R^2} / (\overline{R})^2$ in each season. On most of the occasions

this ratio exceeds the theoretical limit of $4/\pi$. Mean values of 1.96 for the daytime E-region records and 1.92 for the F-region records (day and nighttime) are obtained.

This abnormally high values of the ratio $\overline{R^2}/(\overline{R})^2$ seems to be associated with the very high values of fading rates at Thumba which are observed as sharp bursts of intensity on zero ·ach ground intensity. A plot of the ratio $\overline{R^2}/(\overline{R})^2$ versus the fading rate was therefore attempted. Fig. II.2.11 shows the variations of this ratio with the fading rate for both E- and F-regions. A linear increase of this ratio with the fading rate is observed for both the E- and F-region records. Similar study of the probability distribution of the amplitude fluctuations at

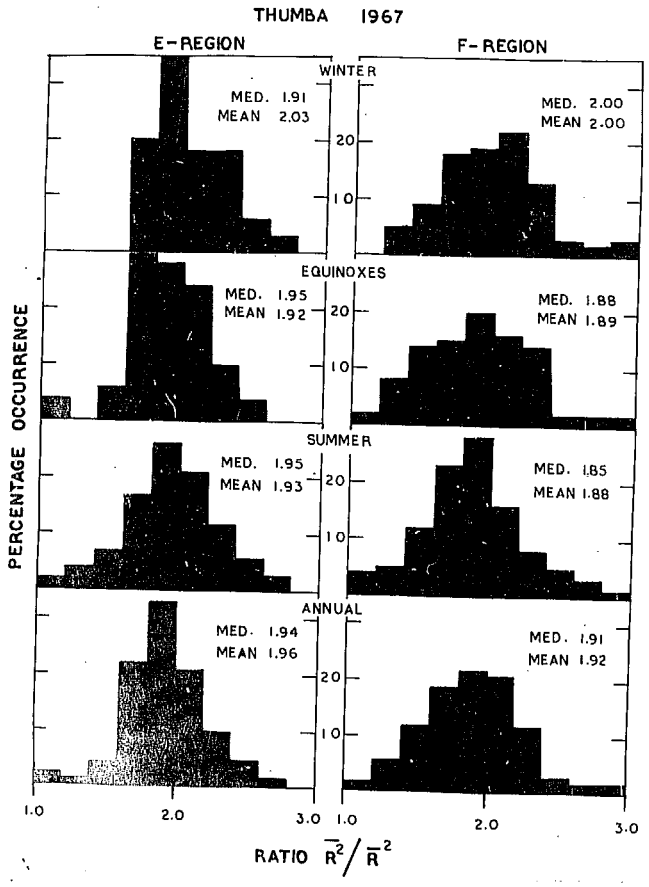

Fig. II.2.10.

Russian stations during IGY programme has shown that the experimental and theoretical amplitude distribution curves agree in most of the cases but the ratio $\overline{R^2} / (\overline{R})^2$ exceeds the theoretical limit on about 20% occasions.

These discrepencies between the theoretical and experimental results indicate limitations of the theory of Ratcliffe and others in the over-simplification of the problem. A rigorous mathematical approach to the fading mechanism involving the particular case at equator is necessary to explain this abnormal behaviour which is found for the fading records at Thumba.

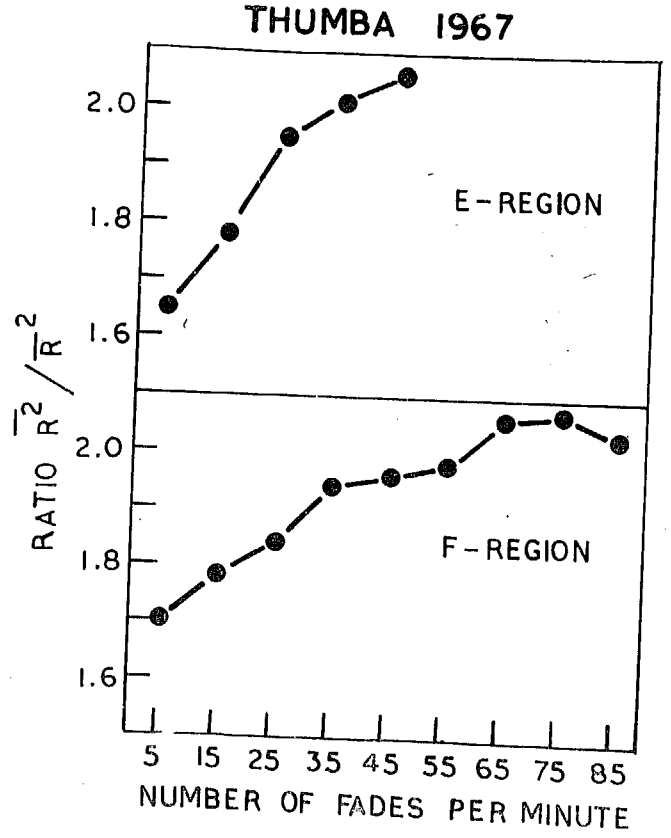

Fig. II·2·11

CHAPTER II.3. RESULTS OF THE DRIFT MEASUREMENTS AT THUMBA IN THE PERIOD 1964-67 USING SIMPLE TIME DELAY METHOD

Chapter II.3.

CHAPTER II.3. Results of the drift measurements at Thumba in the period 1964-67 using simple time delay method

II.3.1. Method of time delay

One of the simplest methods to determine the drifts from fading records obtained at spaced points on the ground is known as 'similar fade method' or 'time delay method'. Considering inhomogeneities in the ionosphere to be fixed in space one would obtain a spatial distribution of amplitude of the echo on the ground not varying with time at any point. But if the inhomogeneities do not change themselves and move uniformly with velocity V then the diffraction pattern on the ground will move with the velocity $2V$ in the same direction as the motion of irregularities, and will give rise to temporal variation of amplitude at a point. Fading could also be produced by an irregularity which changes its from but does not move. Mitra (1949) developed a method for the determination of the horizontal drifts in the ionosphere by comparing the fading records at different sites over the ground assuming

(1) the ground diffraction pattern is moving with a uniform velocity,

(2) the diffraction pattern does not change as it moves, and

(3) the diffraction pattern is isometric i.e. its average characteristics remain same in different directions.

In the similar fade method, time delays are measured between the maxima or minima of similar fades at different spaced points from which one can calculate the the speed as well as direction of the moving ground diffraction pattern.

Let us represent the diffraction pattern by contours of constant amplitude R_1, R_2, R_3 (Fig. II.3.1a) moving with a uniform speed V in a direction which makes an angle θ with respect to reference axis (X axis). If O, A, B are the receiving sites, then as different contours pass over these sites signal strength at these aerials change with time. A maximum of signal strength will be recorded when the contour passes over the receiver tangentially. The locus of the tangential points along the direction of drift is called the line of maximum amplitude and is shown in Fig. II.3.1(b). Under the assumptions

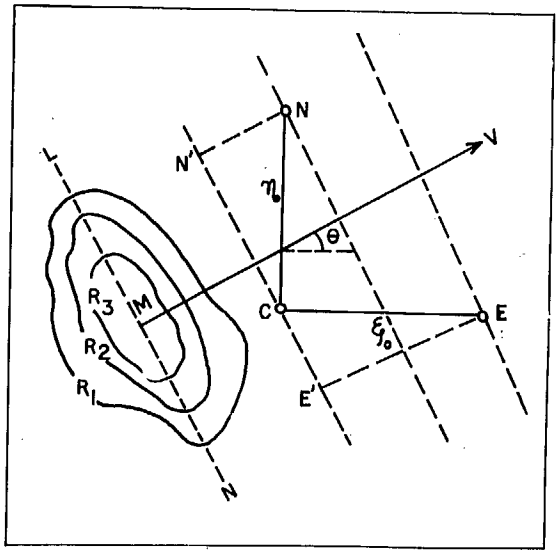

Fig. II.3.1.(a)

made earlier that is when the diffraction pattern is isometric and fairly large as compared to the location sites of the receivers, the line of maxima will be a straight line perpendicular to the direction of motion. When considering the maxima of the fading pattern, one can replace the contours of constant amplitudes by the line of maxima and one immediately finds the relation for V, Θ in terms of distances between receivers and the time lags between the arrival of maxima at different receivers.

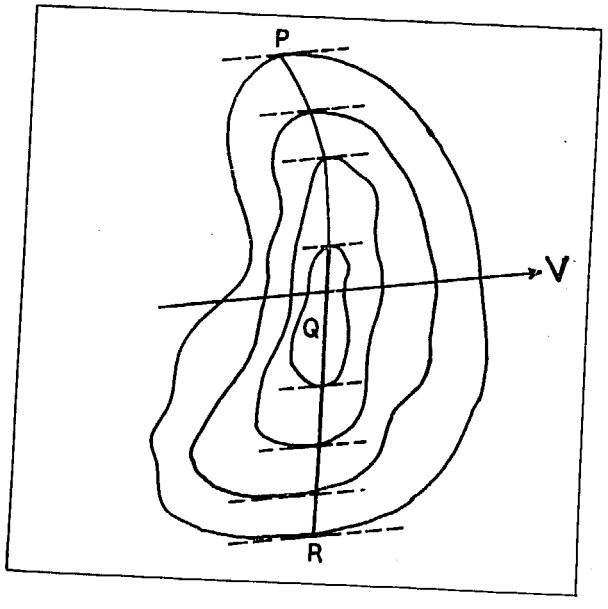

Fig. II.3.1(b)

If one obtains a time lag T_x between the receivers O and A and T_y between O and B, then by simple geometry

$$T_x = \frac{\xi_0 \cos\Theta}{V}$$

$$T_y = \frac{\eta_0 \sin\Theta}{V} \qquad \ldots(1)$$

Let us define $\frac{\xi_0}{T_x} = V_x'$

$$\frac{\eta_0}{T_y} = V_y' \qquad \ldots(2)$$

then from equations (1) and (2)

$$\frac{\cos\theta}{V} = \frac{1}{V_x'}$$

$$\frac{\sin\theta}{V} = \frac{1}{V_y'} \qquad \ldots(3)$$

hence $\frac{1}{V^2} = \frac{1}{(V_x')^2} + \frac{1}{(V_y')^2}$ $\ldots(4)$

and $\tan\theta = V_x' / V_y'$ $\ldots(5)$

In case $\xi_0 = \eta_0 = d$ equation (1) gives

$$V = \frac{d}{\sqrt{T_x^2 + T_y^2}}$$

$$\theta = \tan^{-1} T_y / T_x \qquad \ldots(6)$$

Here V_x', V_y' are two fictitious velocities which do not have any physical significance. They are related to the velocity V by the relations

$$V_x' = V / \cos\theta$$

$$V_y' = V / \sin\theta$$

while actual drift components V_x, V_y are given by

$$V_x = V \cos\theta$$

$$V_y = V \sin\theta$$

The drift speed V thus obtained gives the speed with which the diffraction pattern is moving on the ground. This is divided by 2 to give the movement of irregularities in the Ionosphere. The values of drift speed and direction thus obtained do not contain corrections due to the changes in the irregularities itself and are therefore described as apparent values and are denoted by V' and θ' in the following description.

II.3.2. Drift observations at Thumba

Ionospheric E-region drift measurements have been made at Thumba regularly since January 1964 on 2.2 Mc/s. For F-region drift measurements, another frequency of 4.7 Mc/s was added in February 1964. Observations were taken once each hour for both the E and F-regions between 07 and 18 hrs. I.S.T. In the later part of the year 1964, observations were taken at 4.7 Mc/s during nighttime on few days when echoes were received on 4.7 Mc/s. Attempts to record nighttime E_s reflections failed, as Thumba is situated near the magnetic equator where occurrence of nighttime is quite rare. From January 1967, regular F-region observations during the nighttime were started. Every alternate days full 24 hr. observations were taken and were subjected to routine analysis by measuring the time delays between pairs of aerials along N-S and E-W direction.

Atleast ten time delays were read and calculations were made from the mean time delays. Fading records after a magnification of 8 were read on a centimeter graph paper. The scaling accuracy is kept at 1 mm which corresponds to the accuracy of about .03 sec. in reading the time delay.

II.3.3. Previous results at Thumba

Preliminary results of the daytime drifts in the E-region of ionosphere over Thumba during the period January-February 1964 (Rastogi et al 1966) showed apparent drift velocities higher than reported for any other station and the direction was consistently towards West. The fading records at the N-S pair of antennas showed almost no time lag between them suggesting near absence of the N-S component in the drift velocity. A study of the diurnal and seasonal variations of drifts in the E- and F-regions for the complete year 1964 was made by Deshpande in his Ph.D. Thesis (1966). The important results of this study are described by Deshpande and Rastogi (1966a). The average drift speed in this period was found to be 132 m/sec for the E-region and 161 m/sec for the F-region. The direction was within 270 ± 15^{o} on about 65% of the occasions. Seasonal study showed that tendency for Westward drift was maximum during equinoxes and minimum during summer, departure from Westward drift being less for the F-region. Mean drift speed was

highest during equinoxes and lowest during summer for E-region. In case of F-region, mean drift speed was highest during the equinoxes while no difference could be observed between summer and winter seasons.

II.3.4. Results of present study

Daytime drift results for the entire period 1964-1967 are presented here. The drift direction at Thumba is reversed between the day and night (Deshpande and Rastogi 1968), so to avoid the transition conditions only observations between 08 to 16 hr. are used in the present analysis.

The average picture of the daytime drift is shown in Fig. II.3.2 which has been estimated from more than 2500

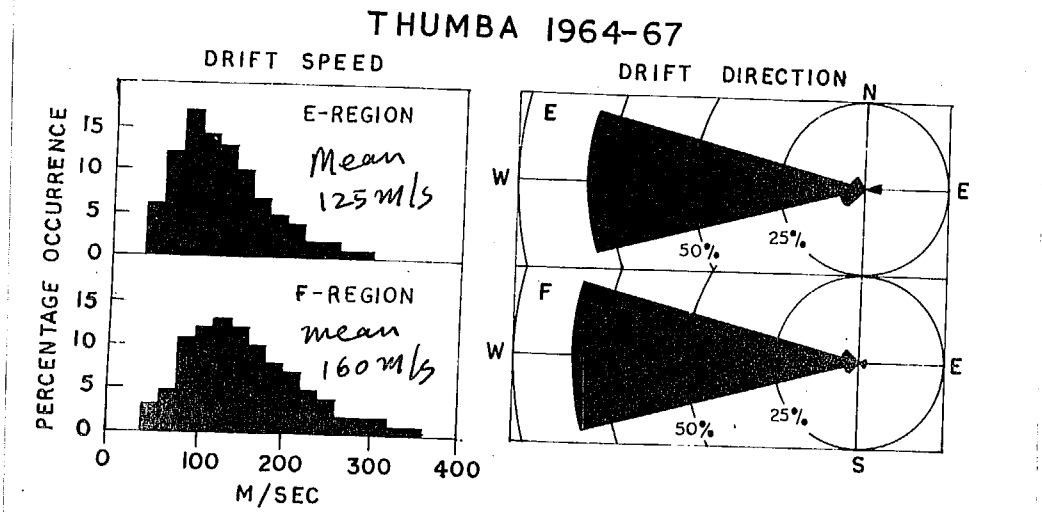

Fig. II.3.2.

records from E-region and more than 3000 records from F-region covering the entire period 1964-67. It is easily seen that drift direction is predominantly towards West; on more than 80% occasions it lies in the range 270 $\pm$ 15° (East of North). The histograms for the drift speed in the E-region range from 40 m/sec to 300 m/sec with a mean speed of 125 m/sec and median value of 111 m/sec. In the F-region speeds range from 40 m/sec to 360 m/sec with a mean speed of 160 m/sec and median value 150 m/sec.

II.3.4(a). Seasonal effect in drift speed

To study the seasonal behaviour, the whole data is divided into the following seasonal groupings:

(1) Winter; consisting of November, December of one year with January, February of succeeding year.

(2) Equinoxes; consisting of March, April, September and October of the same year, and

(3) Summer consisting of May, June, July and August of the same year.

Histograms of percentage occurrences are computed for the speed and direction of drift for each of the seasons in the period, January 1964 to January 1968. Fig.

II.3.3 shows the histograms of drift speed in each season

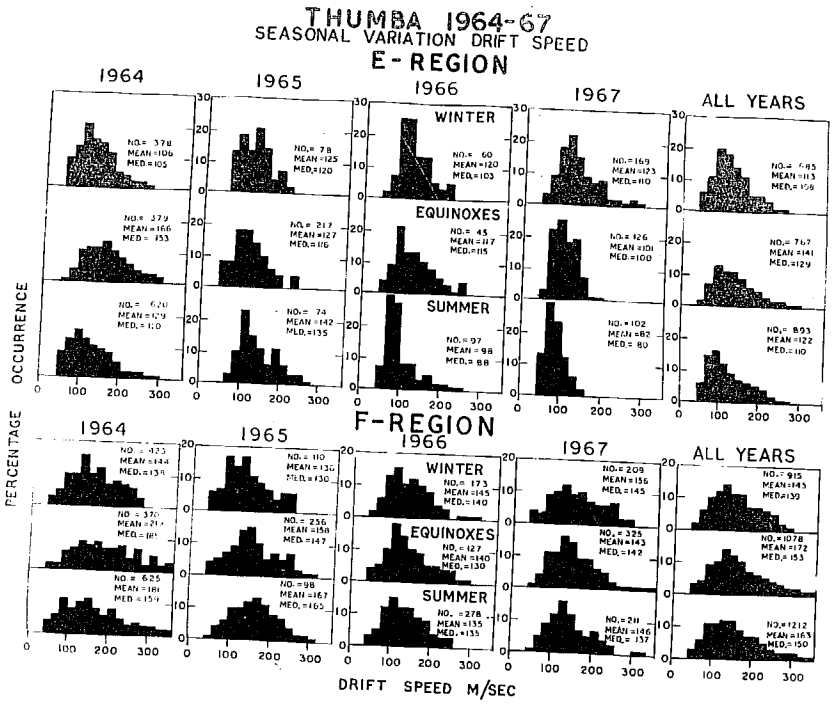

Fig. II.3.3.

for both E- and F-regions. Number of observations, mean value and the median value are given in each histogram and are collected in Table II.3.1 also.

Drift speeds in the E-region for the year 1964 are distinctly higher during equinoxes. Mean drift speeds for the seasons winter, equinoxes and summer are 106, 166 and 129 m/sec. respectively while median values are 105, 153 and

TABLE-II.3.1

Mean and median values of E- and F-region apparent drift speed (m/sec) at Thumba during each of the seasons of 1964 to 1967.

E - REGION

		1964	1965	1966	1967	All years
Winter	Count	378	78	60	169	685
	Mean	106	125	120	123	113
	Median	105	120	103	110	108
Equinoxes	Count	379	217	45	126	767
	Mean	166	127	117	101	141
	Median	153	116	115	100	129
Summer	Count	620	74	97	102	893
	Mean	129	142	98	82	122
	Median	120	135	88	80	110

F- REGION

Winter	Count	423	110	173	209	915
	Mean	144	136	145	156	145
	Median	138	130	140	145	139
Equinoxes	Count	370	256	127	325	1078
	Mean	219	158	140	143	172
	Median	185	147	130	142	153
Summer	Count	625	98	278	211	1212
	Mean	181	167	135	146	162
	Median	159	165	135	137	150

and 120 m/sec respectively. In the year 1965 no difference is noticed between winter and equinoxes, drift speeds are highest during summer. It should be noted that summer 1965 consists of data during the month of August only which makes the values higher than what would be expected from complete season. Mean values in different seasons are 125, 127 and and 142 m/sec respectively while median values are 120, 116 and 135 m/sec respectively. In the year 1966 drift speeds during winter and equinoxes again seem to be equal while lowest speeds are observed during summer. The mean and median values in different seasons winter, equinoxes and summer are 120,117, 98 m/sec and 103, 115 and 88 m/sec respectively. The seasonal changes are well marked in the year 1967. Drift speeds are highest for the winter season and lowest for the summer season. Mean values being 123, 101 and 82 m/sec respectively and median values 110, 100 and 80 m/sec respectively. When the data for all years are combined, the highest drift speeds are found during equinoxes and lowest during winter. In the individual years drift speed is lowest during summer for 1966 and 1967 while for the years 1964 and 1965 lowest drift speeds are during winter. It should be marked that most of the observations during summer season are in the year 1964, hence similar behaviour is found in the combined data also.

In the F-region also highest drift speeds are ob-

served for winter season. In the years 1964 and 1965, drift speeds are lowest during winter while for the years 1966 and 1967 lowest drift speeds are observed during summer. Mean drift speeds for the year 1964 are 144, 219 and 181 m/sec respectively for the winter, equinoxes and summer seasons. The median values are 138, 185 and 159 m/sec respectively. In the year 1965 the mean and median values for different seasons are 136, 158, 167 m/sec and 130, 147, 165 m/sec respectively. Summer 1965 contains observations during the month of August only, hence drift speed are higher than expected during the complete season. Mean and median drift speeds in the year 1966 are 145, 140, 135 m/sec and 140, 130 and 135 m/sec respectively while for 1967 they are 156, 143, 146 m/sec and 145, 142, 137 m/sec respectively. Thus during the years 1966 and 1967 there is not much difference in the median values of different seasons.

No systematic difference in the seasonal behaviour can be judged from the histograms shown in Fig. II.3.4. However, it is certain that the speeds are in general higher during equinoxes. Data for the years 1964 and 1965 show a tendency of highest speeds during equinoxes and lowest during winter, whereas for the years 1966 and 1967 it shows a tendency of highest speeds during winter and lowest during summer.

II.3.4(b). Seasonal effect in the drift direction

A comparison of apparent drift direction (θ') in different seasons of each year is made and is shown in Fig. II.3.4. Results are put as histograms of percentage occurrences plotted in a log linear scale to show the minor groups of directions occurring. In general the directions are mainly towards West.

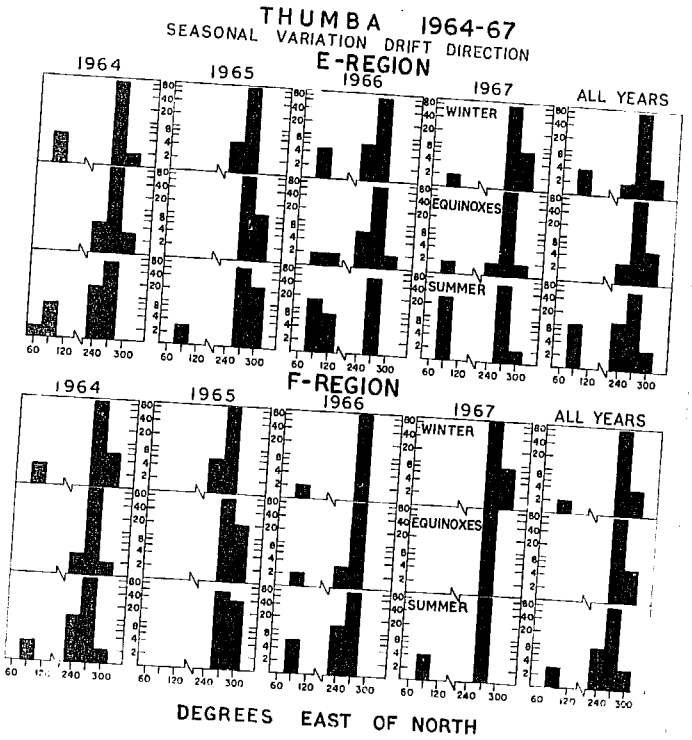

Fig. II.3.4.

In the E-region the percentage occurrences in the range 270 ± 15^{o} are about 90% during winter and equinoxes

of different years and about 65% in the summer season of different years. Another important feature is presence of Eastward drift directions which are quite significant during summer. About 10% occurrence is observed towards East. However, in the year 1965, data is available only for the month August which may not truly represent the summer season. In the year 1966 and 1967 about 25% and 30% of observations during summer indicate Eastward drift. Such daytime Eastward drifts are not observed during equinoxes of the years 1964 and 1965. A small percentage is observed for 1966 and 1967. During winter season, percentage of Eastward drift is slightly more than what is observed during equinoxes.

Referring to F-region histograms, the percentage occurrences in the range 270 ± 15^{o} are more than corresponding E-region percentages. Again there is a tendency during summer for scatter from this range, while on about 90% occasions drift direction is in the range 270 ± 15^{o} during winter and equinoxes it drops down to 80% during summer. The Eastward drift directions are absent during equinoxes. During summer, there are instances of Eastward drift but less than what is observed for E-region. On a few occasions, Eastward drift is observed during winter also.

II.3.4(c). Daily variation of drift speed

Daily variations of drift speed for each season of different years are shown in Fig. II.3.5. As there were no nighttime data except for the year 1967, only daytime values are plotted for each year. Looking at the annual curves for each year the diurnal variations of E- and F-regions are different. In the case of E-region, drift speed increases with the rising of Sun, reaching a maximum around 08-09 hrs, and a slow decrease follows reaching minima at about 13-14 hrs. An increase is observed again in the evening hours. Daily variation curves are of simi-

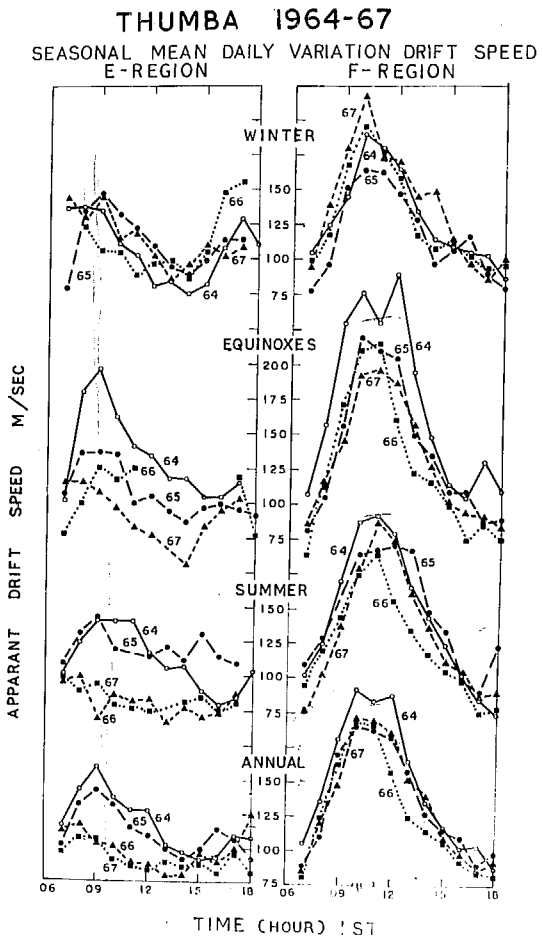

Fig. II.3.5.

lar nature in different years for the winter season. Evening increase is a prominent feature of winter months. There is not much difference in the magnitude of drift speeds for different years in winter. Slight differences are observed in the nature of daily variation curves during equinoxes and summer. The drift speeds are highest for the years 1964 and there is consistent decrease upto 1967. The increase in evening hours which is not observed in the years 1964 and 1965, is present in the year 1967. The range of the variation is much reduced for the summer months. The magnitude of speeds are higher in the years 1964 and 1965 as compared to 1966 and 1967.

Drift speeds for the F-region show a rapid increase after sunrise reaching a maximum around 11 hrs. and a slow decrease afterwards till evening. Referring to different seasons, the nature of the variation remains the same for any season of the different years. During the winter season drift speeds are higher in the years 1966, 1967 as compared to speeds in the year 1964, 1965 while the reverse is the case during equinoxes. During summer the speeds are comparable in 1964 and 1967 while for 1965, 1966 they are

The minima in the morning and evening are of the same order for any season but the range of variation is highest during equinoxes.

The seasonal effect on the peak drift speed is shown in Fig. II.3.6. After combing the data of all the years, maximum speed V_{max} and its time of occurrence is obtained for each month. For both E- and F-regions, maximum drift speed is obtained in the equinoxes; while for F-region, speeds are comparable during solstices, they are minimum during June Solstice months for E-region. F-region drift speeds are always larger than the corresponding E-region drift speeds by about 30-60 m/sec. The time of maximum speed occurs earliest during winter months and latest during

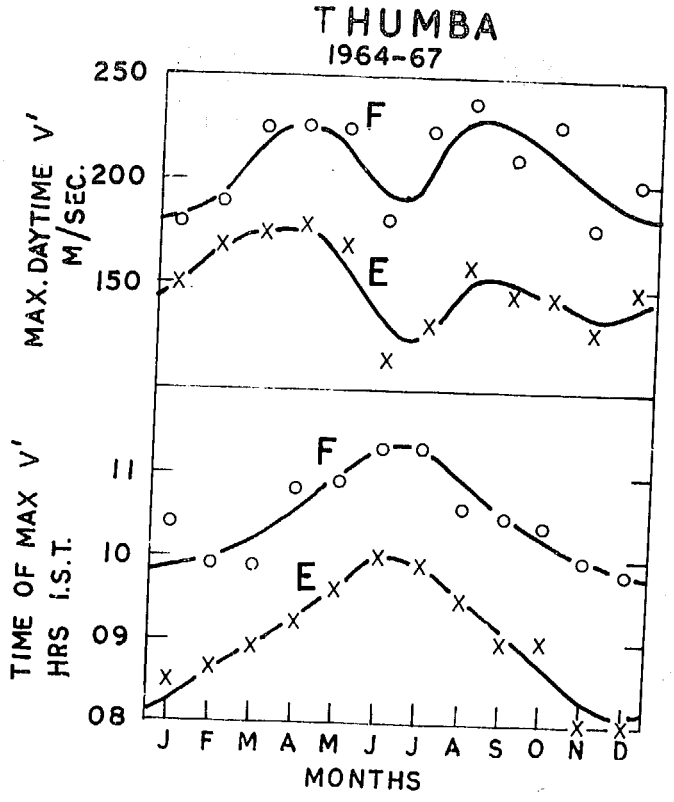

Fig. II.3.6.

summer months. The maximum drift speed in the E-region occurs at about 08 hr. during winter, about 09 hr. during equinoxes and about 10 hr. during summer. The F-region maximum drift speeds occur about one and half hour later than the corresponding times of maxima for the E-region.

II.3.4(d). Solar cycle effect on drift speed and direction at Thumba

To study the solar cycle variation of apparent drift speed and direction, histograms have been computed for the individual years of January 1964 to December 1967 and are presented in the Fig.II.3.7. The apparent drift

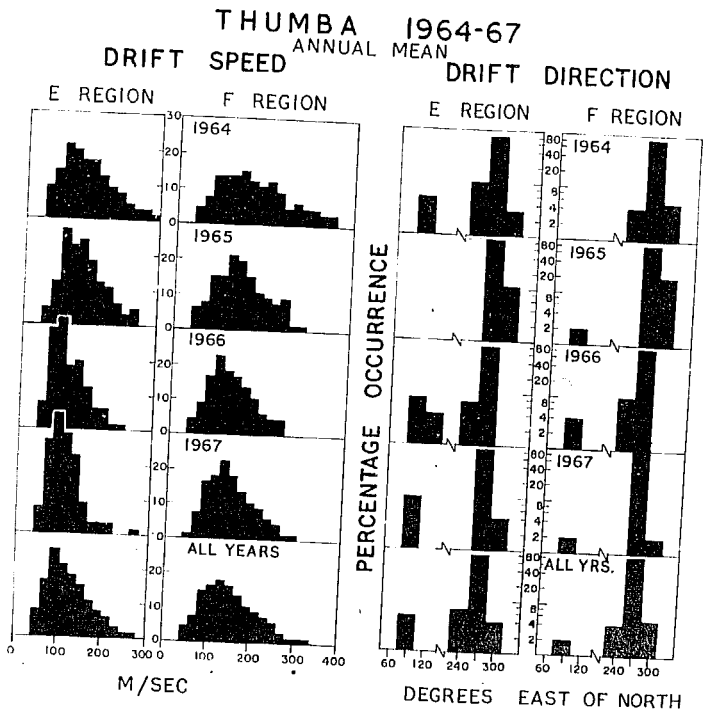

Fig. II.3.7.

speeds (median values) for the years 1964, 1965, 1966 and 1967 are 123, 120, 98 and 99 m/sec respectively for the E-region. Corresponding values for the F-region are 162, 140, 135 and 141 m/sec respectively. Thus with the increase of solar activity, the apparent drift speed decreases for the E-region. While F-region speed is more or less constant. No significant change could be observed in the histograms of drift direction with solar activity.

II.3.4(e). Nighttime F-region drifts at Thumba in the year 1967

From a limited number of nighttime F-region drift observations at Thumba taken during the period, November - December 1964, it was shown that the drift direction is opposite to that found for the daytime i.e. Eastward (Deshpande and Rastogi 1968). Regular nighttime measurements of drifts at Thumba were started from January 1967. Results of the F-region drifts over all hours during the year 1967 are presented here.

A picture of the F-region drifts showing change over from Westward drift to Eastward drift in the post sunset period and change over from Eastward drift to Westward drift in the morning is shown in Fig. II.3.8. It consists of polar diagrams showing apparent drift speed and

direction at few selected hours. Starting from the left

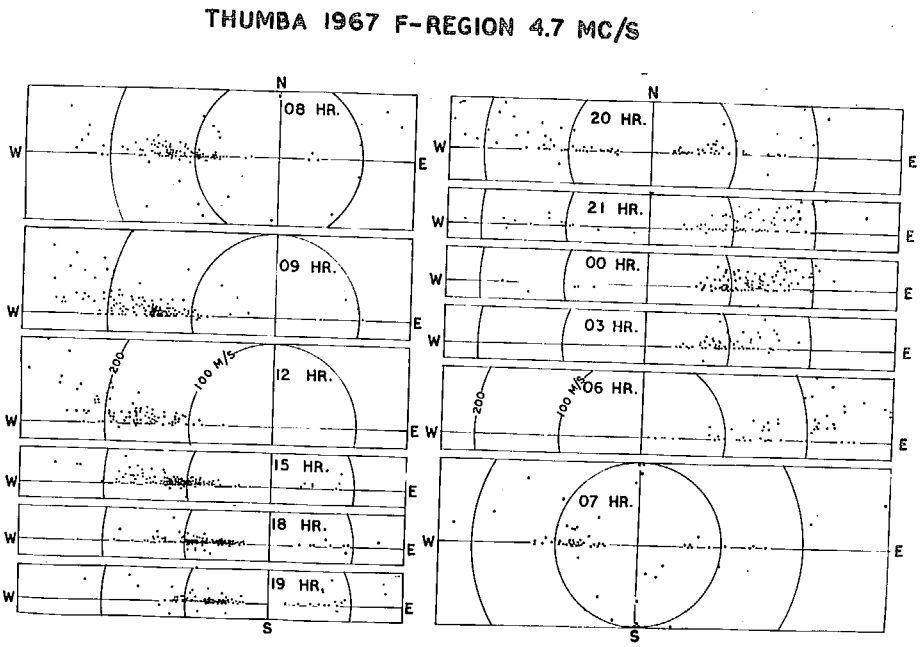

Fig. II.3.8.

hand side of the Fig. II.3.8, one finds a Westward drift at 08 hr. Few points are along the Eastward direction also which show few individual days where change over has not taken place even at 08 hr. The picture at 09 hr. and 12 hr. is of a completely Westward drift. The magnitude of drift is higher than what was observed at 08 hr. The

polar plots at 15 hr., 18 hr. and 19 hr. show consistent decrease in the magnitude of the drift vectors and occurrence of few Eastward drift instances which are on the increase. At 20 hr. the occurrences of Westward drifts are equal to those towards East and magnitude is higher than at 19 hr. 21 hr. shows a chiefly Eastward drift with few points on the West direction indicating days when change over has not taken place even at 21 hr. Drifts at midnight are towards East with 4 or 5 points towards West which were observed sometimes as a second reversal for a short duration. The speed vectors are the same at 21 hr. At 03 hr. there is not a single point in the West direction, the magnitude of drift is reduced. The drift speed again increases at 06 hr. being Eastward. At 07 hr. again, there is scatter. Mostly points are towards West but quite a few are Eastward also. Another feature at 07 hr. is that a few points show N-S drift direction.

Thus one finds reversal of drift at about 07 hr. and 20 hr. An increase in drift speed is observed before reversal both in the morning and in the evening.

A comparison of the apparent drift speeds in the daytime and in nighttime is done for different seasons:

The seasons chosen are:

1) Winter - January, February, November and December.

2) Equinoxes - March, April, September and October.

3) Summer - May, June, July and August.

Fig. II.3.9 shows histograms of the apparent drift speeds in each season as well as the annual picture. Daytime hours are chosen from 08 to 16 and nighttime hours from 20 to 04 to avoid the transition period. The median values for the daytime period are 143, 143 and 138 m/sec respectively for winter, equinoxes and summer. Co-

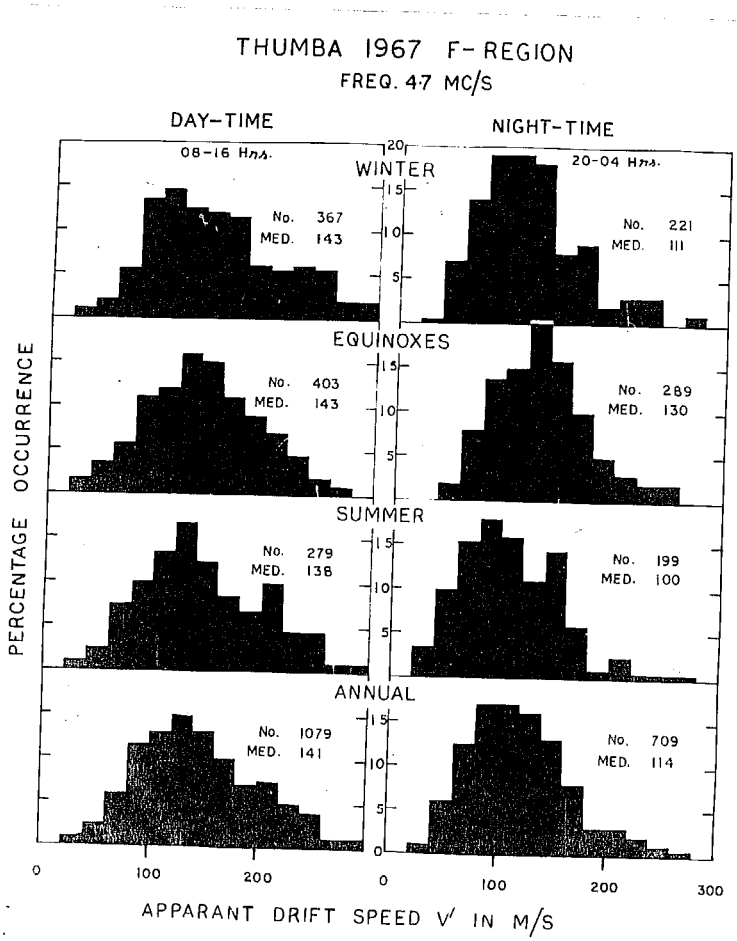

Fig. II.3.9.

rresponding nighttime values are 111, 130 and 100 m/sec respectively. Thus both for the daytime as well as nighttime the speeds are lowest during summer months. Nighttime values are highest during equinoxes while daytime values are comparable during winter and equinoxes.

The apparent drift directions for the above periods are shown in the Fig. II.3.10. During daytime

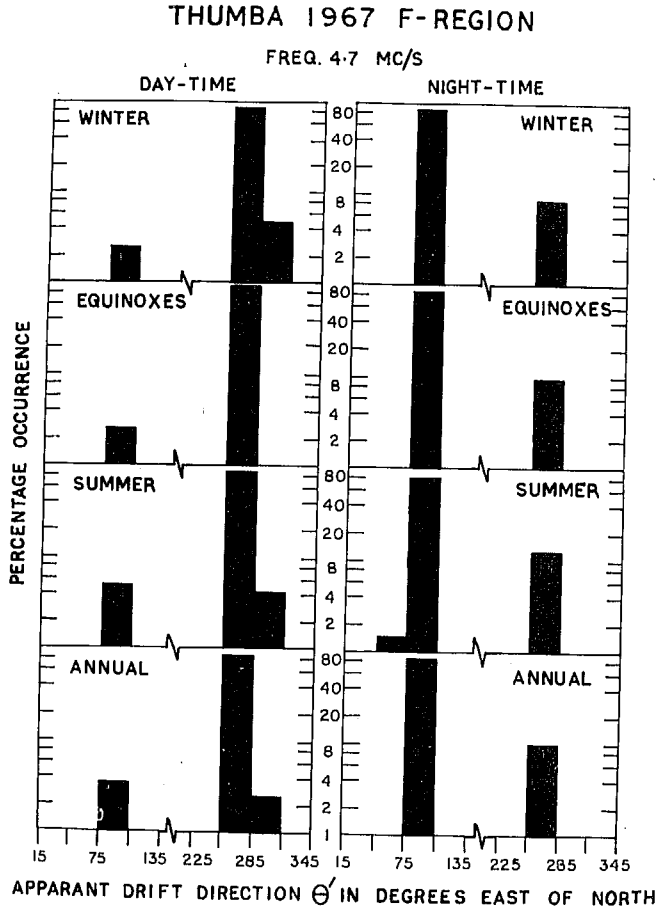

Fig. II.3.10.

drift direction is mainly in the range 270 $\pm$ 15° (more than 90% of occasions) while during nighttime it is mostly in the range 90 $\pm$ 15° (more than 85% of occasions). Drift directions are either around 270° or around 90° at any time.

Seasonal variation of the nighttime drift speed is shown in Fig. II.3.11. Midnight value which is average of 23-00-01 hrs. and maximum nighttime value in the period 20-04 hr. have been plotted against months. Both the curves show maxima during equinoxes and a minima during June. Similar variation has been reported at Ibadan during IQSY (Morriss 1967).

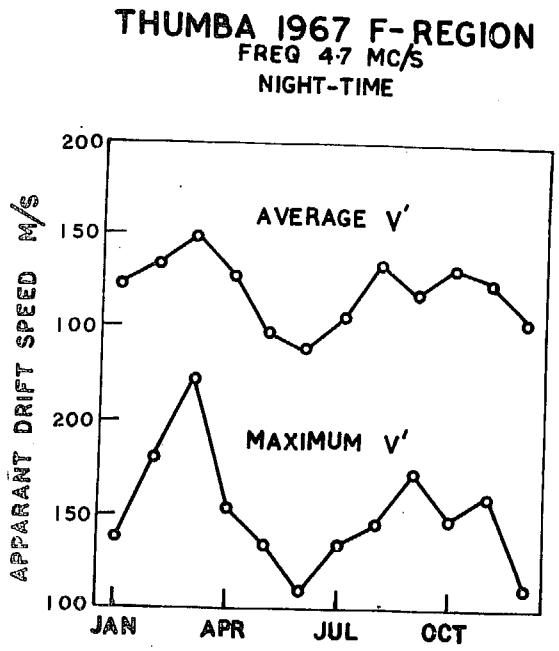

Fig. II.3.11.

As the drifts at Thumba are mainly in a narrow angle band towards East-West direction, only E-W component of drift has been studied. Fig. II.3.12 shows mass plot of the E-W component at each hour of different periods.

To avoid the mixing of points data have been divided into

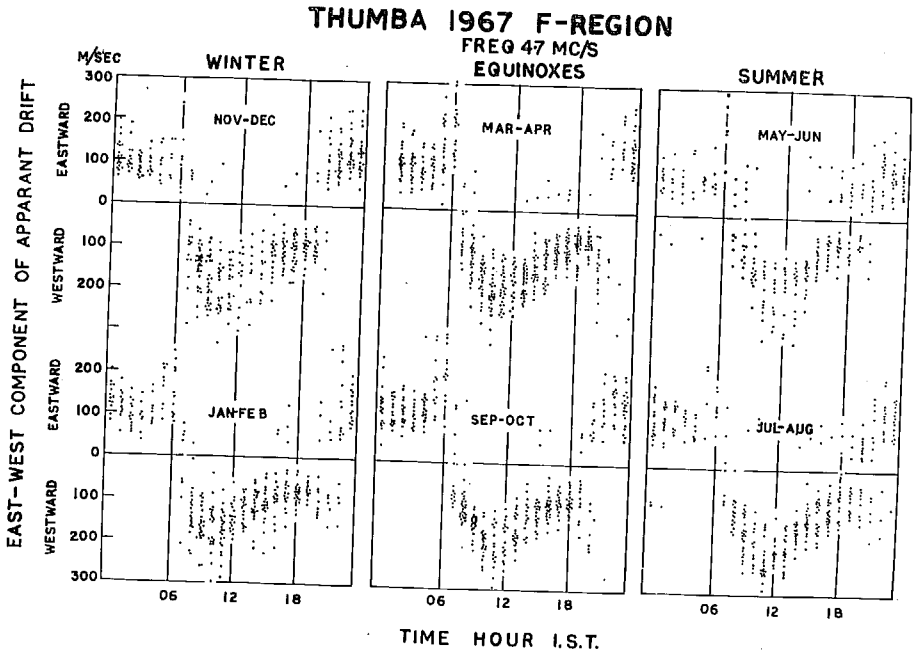

Fig. II.3.12.

6 periods of 2 months each. From the mass plots, one can easily notice the reversals occurring around 07 and 20 hrs. Whereas the morning reversal is quite regular

occurring around 07 hr. during any period, evening reversal is quite variable as seen from the mass plots, the points being distributed on both sides in the period 20 hr. to 22 hr. The mean daily curves of the drift speed for each seasons are shown in Figs. II.3.13 and II.3.14.

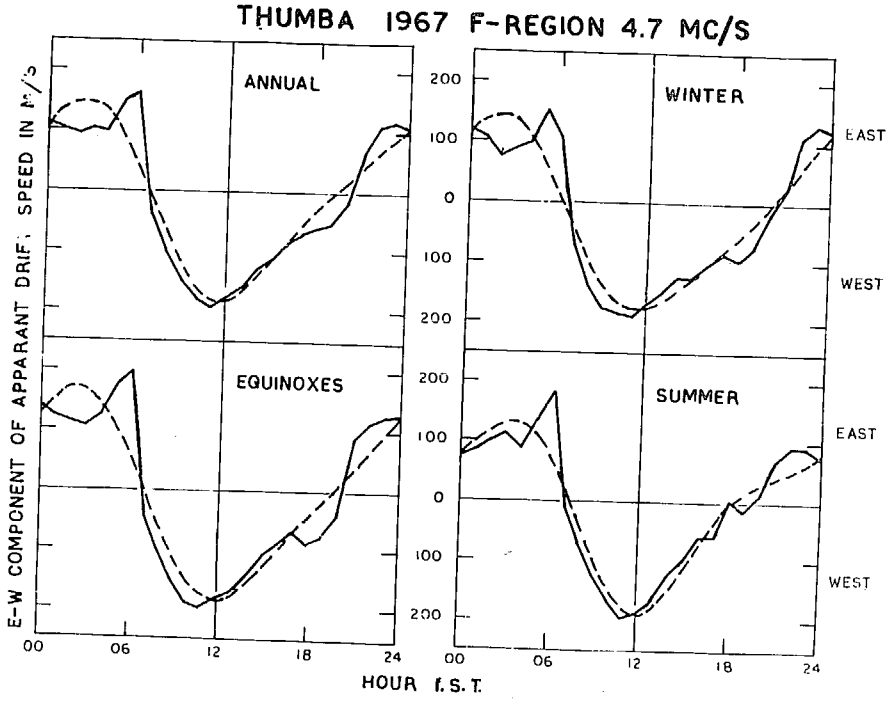

Fig. II.3.13

Fig. II.3.13 shows the observed mean values at each hour (full line) while the built-up curve from two harmonics

is shown with dashed curve. There are significant departures between the two curves especially at the morning and evening time when reversal takes place. To take into account these discrepencies, harmonic analysis was done upto 4 harmonics. In Fig. II.3.14 observed mean values

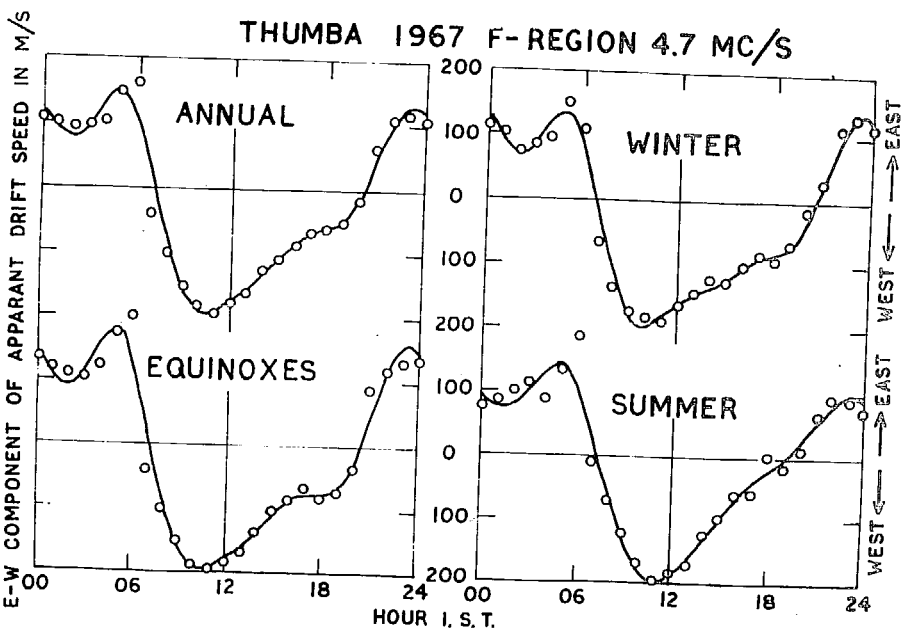

Fig II.3.14.

are shown as open circles while the full line is built-up curve from 4 harmonics. During any season, the variation of drift speed is predominantly diurnal in character. Westward drift during the daytime is strongest at about 09-45 hr. during winter, at about 10.30 hr. during equinoxes and at about 11.00 during summer. Change-over of drift direction takes place at about 7 hr. in the morning during each season while evening reversal takes place at about 19 hr. during summer and at about 20 hr. during equinoxes and winter.

Table II.3.2 gives the coefficients of the first hour harmonics during different seasons. Amplitudes are in m/sec and time of maximum is in hour local time. Predominant harmonic is the diurnal one with amplitudes 153, 165 and 142 m/sec during winter, equinoxes and summer respectively, with maxima at about 01 hr. during each season. The 12 hourly component has amplitudes of about 40 m/sec with maxima occurring at about 04 hr. and 16 hr. The third and fourth harmonics are comparable to the second harmonic and their first maxima also occur at one hour before sunrise.

(Table II.3.2 is given in the next page)

TABLE II.3.2.

Harmonic coefficients of the daily variation of the E-W component of apparent drift speed in F-region at Thumba.

Period	Amplitude A_0 m/sec	A_1 m/sec	A_2 m/sec	A_3 m/sec	A_4 m/sec	Time of maxima in hour (local time) ϕ_1 hour	ϕ_2 hour	ϕ_3 hour	ϕ_4 hour	Morning reversal hour	Evening reversal hour
Winter 1967	-26	152	32	43	22	0.9	3.3	5.8	5.1	6.8	20.4
Equinoxes 1967	-12	165	36	49	38	1.1	4.1	6.0	5.0	7.1	20.4
Summer 1967	- 9	142	50	31	12	0.9	5.1	6.0	5.3	7.3	19.2
Annual 1967	-16	153	36	41	22	1.0	4.3	5.9	5.1	7.1	20.2

II.3.5. Comparison of Thumba results with other equatorial stations

The apparent drift results obtained at Thumba are in close agreement with those obtained at Ibadan and at Tamale. The drift being Westward during daytime and Eastward during nighttime. The drift speeds obtained at Thumba are of-course higher than that observed at Ibadan or Tamale. This can be understood as Thumba is nearest to the magnetic equator amongst the three.

Skinner et al (1958) have shown that at Ibadan there is practically no time shift between the N-S pair of aerials. Westward daytime and Eastward nighttime drift were observed for both E- and F-regions. The variation was a mainly diurnal one with amplitude of about 110 m/sec (F-region).

Rao and Rao (1961) showed daytime average drift speed minimum in summer and maximum in autumn seasons in each year of the period June 1957 to May 1959; while Rao and Rao (1964) reported drift speeds in the E-region for the period May 1960 to April 1962 to be higher in winter than in summer. Thus the seasonal variation of drift study at Waltair shows most probable drift speed value to be higher in winter than in summer. The diurnal variation was shown to have clear presence of semi-diurnal component by Rao and

Rao (1964) with daytime maxima occurring at 11 hr. and 17 hr. The main character of the daily variation being diurnal one. They further reported that at Waltair drift speed increases from the year 1954 reaching a maximum during the sunspot maximum period 1957-59 and then decreasing towards the minimum sunspot period.

F-region study at Waltair by Rao and Rao (1959) showed most probable value of 95 m/sec of the drift speed in the period 1956-58. Further the most probable value was found to be higher in winter than in summer. Rao and Rao (1964b) obtained a most probable drift speed of 100 m/sec in the period 1958-59 while Rao and Rao (1963a) obtained most probable value of 85 m/sec in the period 1960-62 indicating increase of drift speed with solar activity.

II.3.6. Latitudinal variation of the apparent drift speed

Drift measurements at a large number of stations at high latitudes were made in the early fifties. The results were summarised by Briggs and Spencer (1954) in a review paper. Horizontal drift speeds of the order of 80 m/sec were observed. There was a tendency of the F-region drift speeds to be higher than the E-region drift speeds. The E-W component of the drift speed was found to be Eastward during daytime and Westward during the nighttime.

Later measurements at low latitude stations Singapore and Waltair showed an opposite trend, the E-W component of drift being towards West during day and towards East during night (Purslow, 1958 - Rao and Rao 1958). Drift measurements at the mid-latitude station Puerto Rico during the daytime hours showed marked seasonal variation with drift direction predominantly Eastward in summer and predominantly Westward in winter (Keneshea et al, 1965). Such behaviour of the F-region drifts had been predicted by Martyn (1955). According to him a phase reversal of the East-West components should occur at latitudes 35^{o}N and 35^{o}S. Martyn's theory further predicts that at the magnetic equator the Westward drift in the F-layer during the daytime should be the order of 200 m/sec. The measurements at Singapore and Waltair fall short than expected according to Martyn's theory. The drift observations at a station within the equatorial electrojet first obtained at Ibadan showed drift entirely towards West during the daytime and towards East during nighttime with change-over occurring around 07 hr. and 20 hr. The N-S component was either negligible or unmeasurable due to extreme elongation of the irregularities. The drift speed at Ibadan was found to be higher than that at Singapore and Waltair. Observations from Tamale, a still closer station to equator, showed

slightly higher speed. The drifts obtained at Thumba which is almost at the centre of electrojet showed much higher speeds. A comparison of all available data of the apparent drift speed was made to study any latitudinal behaviour. Only daytime speeds have been compared. For the stations, Ibadan, Puerto Rico and Tamale, only the true drift (V) and the ratio of random to true drift components (V_c/V) were availble and the apparent drift (V') was calculated using the relation

$$V' = V(1 + (V_c/V)^2).$$

Some of the stations did not indicate the period of day when the observations were taken and are included in the comparison. Table II.3.3 contains the names of stations compared, magnetic latitudes of the stations and the average daytime speeds. Observations at different stations are at different periods of solar activity and for different duration of the observation period. A plot of the drift speed in the E- and F-regions is shown with the magnetic latitude. From Table II.3.3 and the Fig. II.3.15, it is observed that at most of the stations speed is higher for the F-region than for the E-region. For both the regions the drift speed shows a sharp maximum at the

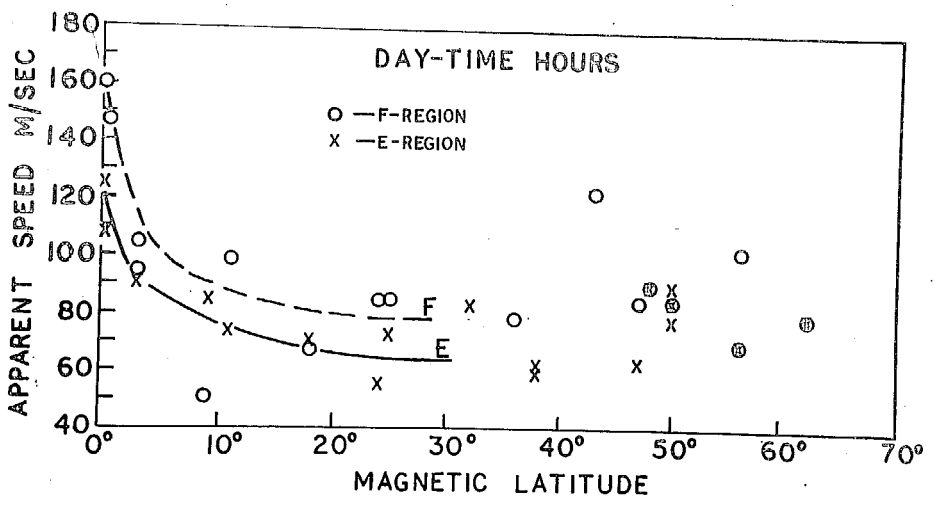

Fig. II.3.15.

magnetic equator.

The sharp maximum of the drift speed over the magnetic equator and consistent Westward drift suggests that there may be close inter-relations between the equatorial ionospheric drifts and the equatorial electrojet.

(Table II.3.3 is given
in the next page)

TABLE-II.3.3

The mean apparent drift speed in the E- and F-regions of the ionosphere during the daytime hours at different stations in the world.

Station	Mag. Lat.	Layer	Year	Time	Speed	Reference
1	2	3	4	5	6	7
Thumba	0.3°S	E	1964-67	day	125	Author
		F	1964-67	day	1[illegible]	
Tamale	0.6°S	E	1962 Feb. Mar.	day	1[illegible]	
		F	1962 Feb. Mar.	day	1[illegible]	Koster (1966)
Ibadan	3°S	E	1957 Aug. Sep.	day	147	
		F	IGY	day	105	Skinner et al (1958)
Bangui	9°S	E	IGY	day	90	Skinner et al (1963)
			1958	day	95	Skinner et al (1963)
Singapore	9°S			day	85	Annals IGY, Vol. 33, 1965.
Waltair	11°N	F	1953-54	day	50	Osborne (1965)
		E	1954-55	day	65	Rao et al (1956)
			1957-59	day	81	Rao and Rao (1961)
			1960-62	all hrs.	75	Rao and Rao (1964)
			Mean		74	
Ahmedabad	18°N	F	1958		99	
		E	1956-66	day	70	Rao and Rao (1964a)
Delhi	24°N	F	1956-62	day	68	Unpublished
		E	1958-59	all hrs.	55	
Yamagawa	25°N	F	1958-59		85	Mitra et al (1960)
		E	1958	day	73	
Puerto Rico	32°N	F	1958	day	85	Rao and Rao (1965)
		E	1958 Mar.- Feb. 1959	day	83	Rao and Rao (1964a)
Ashkabad	36°N	F	1958	day	79	Keneshea et al (1965)
						Rao and Rao (1964a)

....2

1	2	3	4	5	6	7
Brisbane	38°S	E	1952-53	day	78	Burke and Jenkinson(1957)
		E	1953-54	day	57	
			1958	day	51	
Seimiz	43°N	F	Mean		62	Rao and Rao (1965)
Halley Bay	47°S	E	1958	day	123	Rao and Rao (1964a)
			1958	all hrs.	63	Piggott and Barclay (1963)
		F	1957-58	all hrs.	85	Bellchambers and Piggott (1965)
Cologne	43°N	E	Winter (1941-42)	all hrs.	90	Krauthkramer (1950)
Wellington	50°S	E	1958	day	78	Rao and Rao (1964)
De Bilt	50°N	E	1958	day	90	Rao and Rao (1965)
Cambridge	50°N	E & F	1952	all hrs.	85	Phillips (1952)
Washington	56°N	E & F	1950 Mar.Dec.	day	70	Salzberg and Greenstone (1951)
Gorky	56°N	F	1958	day	103	Rao and Rao (1964a)
Ottawa	62°N	E & F	1950 Jun.Oct.	all hrs.	80	Chapman (1953).

Journal of Atmospheric and Terrestrial Physics, 1969, Vol. 31, pp. 1205 to 1215. Pergamon Press. Printed in Northern Ireland

Horizontal drifts in the *E*- and *F*-regions over Thumba, during day-time

HARISH CHANDRA and R. G. RASTOGI
Physical Research Laboratory, Ahmedabad-9, India

(Received in revised form 20 March 1969)

Journal of Atmospheric and Terrestrial Physics, 1969, Vol. 31, pp. 1205 to 1215. Pergamon Press. Printed in Northern Ireland

Horizontal drifts in the *E*- and *F*-regions over Thumba, during day-time

HARISH CHANDRA and R. G. RASTOGI
Physical Research Laboratory, Ahmedabad-9, India

(*Received* 7 *February* 1969; *in revised form* 20 *March* 1969)

Abstract—The paper describes the apparent horizontal drifts in the *E*- and *F*-regions of the ionosphere over Thumba, India (dip. 0·6°S) during the day-time hours of the years 1964–67. The direction of drift is predominantly towards west (about 80 per cent of occasions during any of the seasons of the year). The speed of drift is found to be larger than at any other equatorial stations for which the data are available. The diurnal variation of drift speed in *E*- or *F*-regions shows a forenoon maximum which occurs later during June–July, than during other months. There is no distinct change in the drift speed or direction between the years 1964–67. A comparison of drift speed at other stations shows minimum at mid-latitudes and a sharp maximum over the magnetic equator. Drift observations at other low latitude stations are recommended for a detailed study of the abnormal zone near the magnetic equator.

INTRODUCTION

ONE OF the most widely used methods for determining the horizontal drifts in the ionospheric regions consists of recording the fading of ionospheric echoes at three spaced receivers (MITRA, 1949; KRAUTKRAMER, 1950). A number of stations were started during IGY/IGC but the data for regions close to the magnetic equator are still very few. Ionospheric drift measurements were started at Thumba (Geog. lat. 8°33′N, Geog. long. 76°52′E, Magn. lat. 0.3°S) in January 1964. Preliminary results of the day-time *E*-region drifts during January–February 1964 showed that the apparent velocities were abnormally greater than at any other stations and the direction was remarkably towards West (RASTOGI *et al.*, 1966). The seasonal and diurnal variations of *E*- and *F*-region drifts for the period January–December 1964 have been described by DESHPANDE and RASTOGI (1966*a*). The average drift speed was found to be 132 m/sec for *E* and 161 m/sec for the *F*-region. The direction was within 270° ± 15° for about 65 per cent of occasions. DESHPANDE and RASTOGI (1966b) have shown that the ratio of random to the true drift velocity determined according to the method described by BRIGGS *et al.* (1950) has been about 0·91 for *E* and 0·81 for the *F*-region. Thus the true velocity would be about half of the apparent velocity. The apparent drift speed or direction determined by the time shifts for the maximum cross-correlation were found to be almost the same as those determined by simple time shifts of similar fades (DESHPANDE and RASTOGI, 1967). Therefore, for general analyses of the drift records at Thumba, the similar fade method was utilised. The present paper describes the results of the observations taken during the period January 1964–December 1967.

A pulse transmitter of peak power 1·5 kW and pulse width 100–200 μ/sec was operated at 2·2 MHz for *E*-region and at 4·7 MHz for *F*-region. The receiving aerials are half wave dipoles oriented along N–S direction and situated at the

corners of an isosceles right angled triangle with the two sides along East–West and North–South directions and of length 120 m. The aerials are connected with a single receiver through a three-step-electronic switch and the records are obtained on 35 mm photographic film. The observations were generally taken from 6 to 18 hr on both the frequencies. As reported earlier by DESHPANDE and RASTOGI (1968) the direction of drift at Thumba is reversed between the day and night. To avoid the transition conditions only the observations between 08.00 to 16.00 hr are used in the present analyses.

RESULTS AT THUMBA

Throughout the paper the speed and direction refer to the apparent values derived from the mean time shifts between E–W and N–S pairs of aerials. These values may be affected by the random motions within the ionospheric irregularities themselves. The histograms of the percentage occurrence of drift speed and of the direction for E as well as F-region averaged over the entire period of observations are shown in Fig. 1. It is clearly seen that the direction is predominantly towards West; about 80 per cent of occasions the direction was within 270 $\pm$ 15° East of the North. The side lobes in any other directions are insignificantly small. The histograms of drift speed show a rather sharp rise and slower fall, the values ranging between 40–350 m/sec. The mean value of speed is 125 m/sec. for the E and 160 m/sec. for the F-region which are not significantly different from the values obtained during January–December 1964. The median values of the drift speed for 1964–1967 are 111 m/sec for E and 150 m/sec for the F-region.

The whole data is divided into the following seasonal groups:

(1) Winter—consisting of November, December of one year with January–February of the succeeding year.

(2) Equinoxes—consisting of March, April, September and October of the same year.

(3) Summer—consisting of May, June, July and August of the same year.

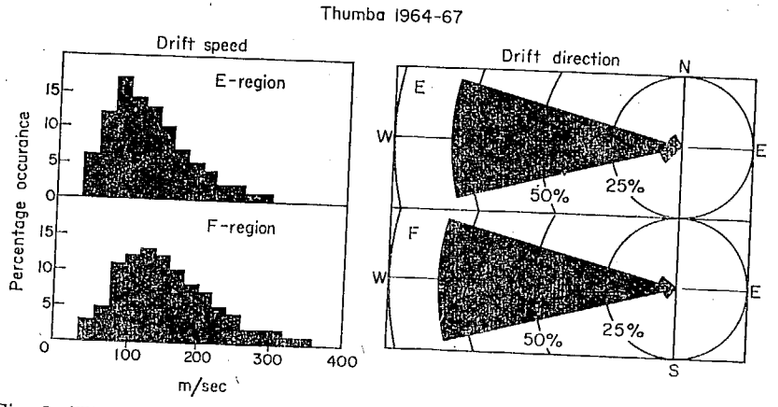

Fig. 1. Histograms of percentage occurrence of speed and direction of drifts in E- and F-regions over Thumba for 08.00–16.00 hr averaged over the entire period January 1964–December 1967.

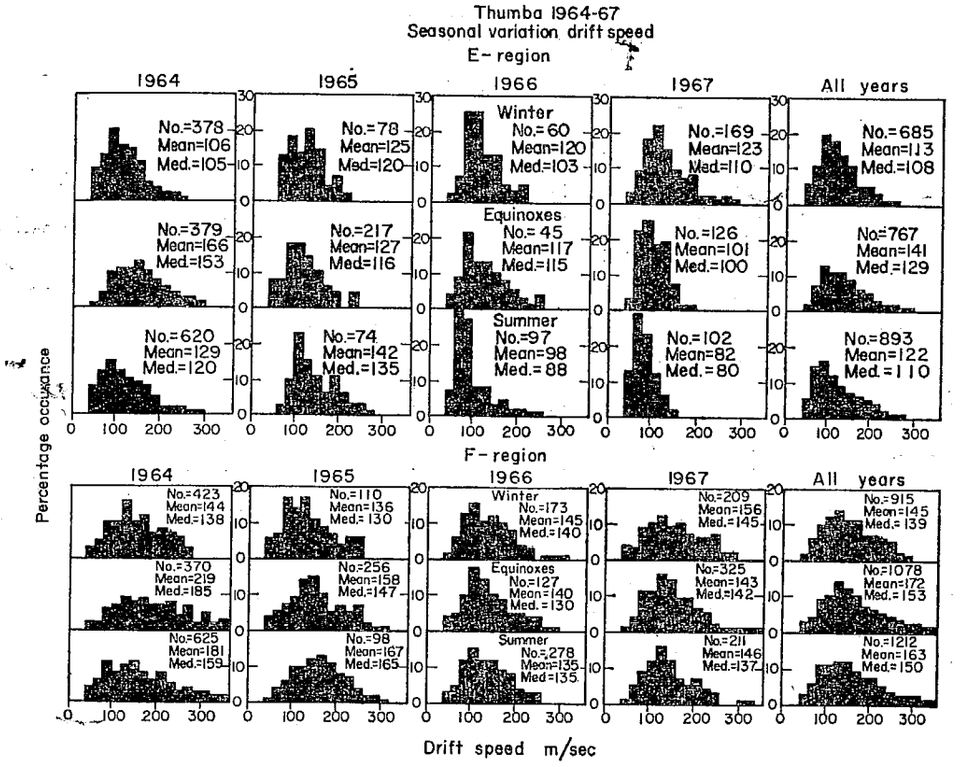

Fig. 2. Histograms of percentage occurrence of speed of the drift in E- and F-regions over Thumba for each of the seasons 1964–1967.

Average histograms are computed for the speed and direction for each of the seasons and for each of the years 1964–67.

The linear histograms of the percentage occurrence of drift speed for each season of the years 1964–67 for both E- and F-regions are shown in Fig. 2. The number of observations, the mean and the median values of drift speed for each season are given in the diagram.

A general glance shows that the histograms are slightly skewed giving the mean value about 10 m/sec larger than the corresponding median value. Further, histograms for F-region are comparatively more spread than those for E-region.

Referring to the E-region histograms and taking all the years together the median drift speeds for Winter, Equinoxes and Summer are 108, 129, 110 m/sec respectively. Similarly for the F-region, the median drift speed averaged over all years is 139 during Winter, 153 during Equinoxes and 150 during Summer. Considering the years separately there is no significant difference in the seasonal mean drift speeds which could be attributed when the scatter of individual observations is taken into account.

The histograms of the percentage occurrence of drift direction for each season of the years 1964–67 for both E- and F-regions are shown in Fig. 3. It is to be

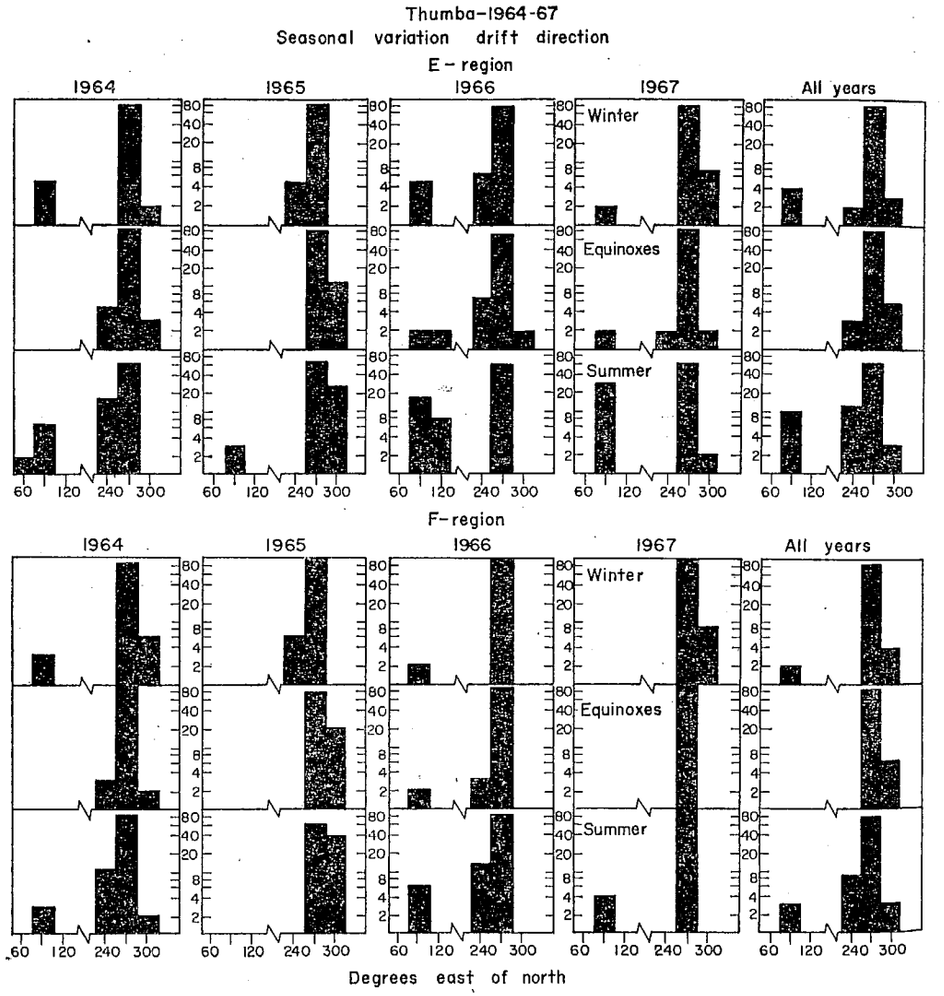

Fig. 3. Histograms of percentage occurrence (in logarithmic scale) of the direction of the drift in the E- and F-regions over Thumba for each of the seasons 1964–1967.

noted that the ordinates giving the percentage occurrences are drawn on a logarithmic scale to show more clearly the smaller values. For either of the E- or the F-region the drift direction is very predominantly towards West (270°). There are some small lobes centering on neighbouring values 240 and 300°. There are absolutely no other directions possible except the East (90°) where one gets about 10 per cent of occurrences during Summer, about 5 per cent occurrences during Winter and absolutely no occurrence during Equinoxes for the E-region. The occurrences of eastward drift in the F-region are still smaller than those in the E-region.

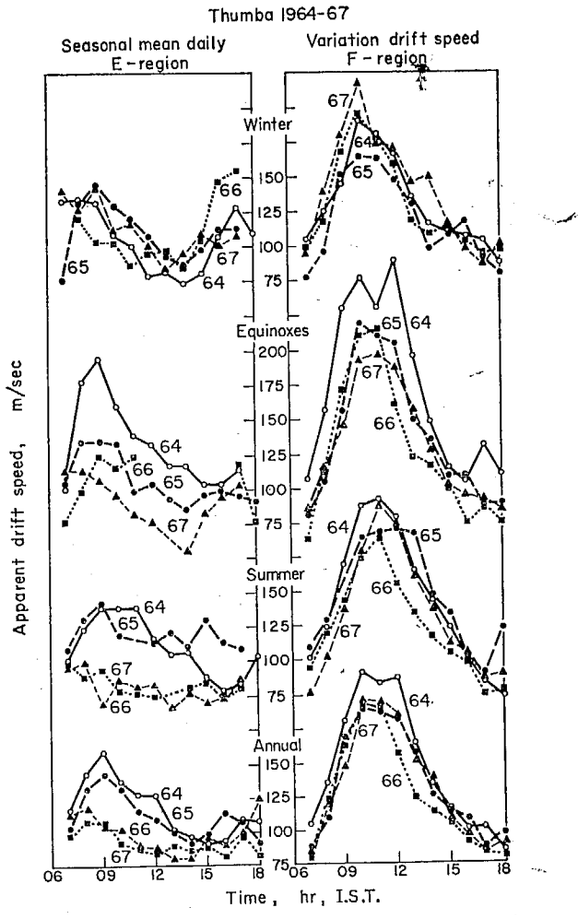

Fig. 4. Solar daily variations of the drift speed for E and F-regions over Thumba for each of the seasons of 1964–67.

The daily variation of the drift speed during each of the seasons of the years 1964–67 are shown in Fig. 4. Referring to the F-region the daily variations are very similar during the individual years, except the values seem to be higher during 1964. The drift speed increases with sunrise, reaches a maximum value at about 10–11 hr, and slowly decreases with the solar time. The daily variation curve is definitely unsymmetrical about noon. The range of drift speed is almost the same during different seasons.

Referring to the E-region curves there seems to be an increase at sunrise, reaching a maximum value at about 8–9 hr, and there is a minimum in the afternoon at about 14–15 hr. The curves for different years are very similar for Winter months, but there are slight differences during Equinoxes and especially during the Summer months. The range of speed during the day is much smaller during Summer than during Winter or Equinoxes.

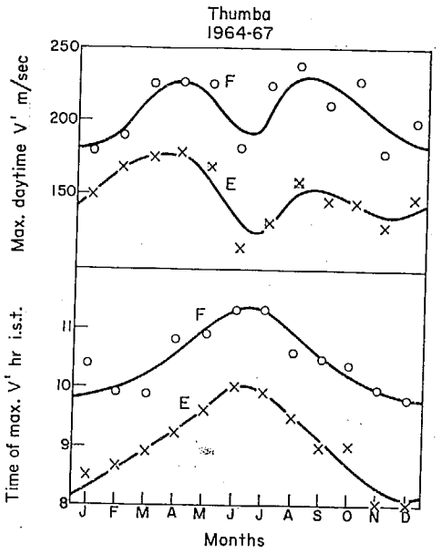

Fig. 5. The value of maximum daytime E- and F-region drift speeds and the time of its occurrence during each of the month averaged over 1964–67.

Figure 5 shows the seasonal variation of the maximum value of speed (V') during the day-time as well as its time of occurrence for both the E- and the F-regions. The maximum for E-region occurs at 08.00 hr during Winter, about 09.00 hr during Equinoxes and about 10.00 hr during Summer. The F-region maximum during different months seems to occur about 1½ hr later than the time of corresponding E-region maximum. The maximum daytime values seem to be largest during the Equinoxes and the values during Winter and Summer are almost equal. The F-region drifts are always larger than the corresponding E-region drift values by about 30–60 m/sec.

The maximum day-time drift speed at Ibadan shows a minimum in May and maximum in January, for either of the E- or F-region (MORRIS, 1967). The time when the velocity is maximum was earliest near the equinoxes and latest in June–July. Thus the results at Thumba are similar to those at Ibadan for the June–July months but there are slight differences during equinoxes.

To study the solar cycle variation in the drift speed and the direction, the average histograms are prepared for each of the year separately, and are shown in Fig. 6.

The histograms for the E- or the F-region show progressively less amount of spread with increasing solar activity from 1964 to 1967. The median drift speed for the E-region is 123, 120, 98, 99 m/sec for the years 1964 to 1967 respectively. Similarly the yearly median F-region drift speed is 162, 140, 135 and 141 m/sec respectively for the years 1964–1967. It may be suggested that the yearly averaged E-region drift speed decreases with the increase of solar activity while the F-region drift speed remains constant. The histograms for the drift direction show the

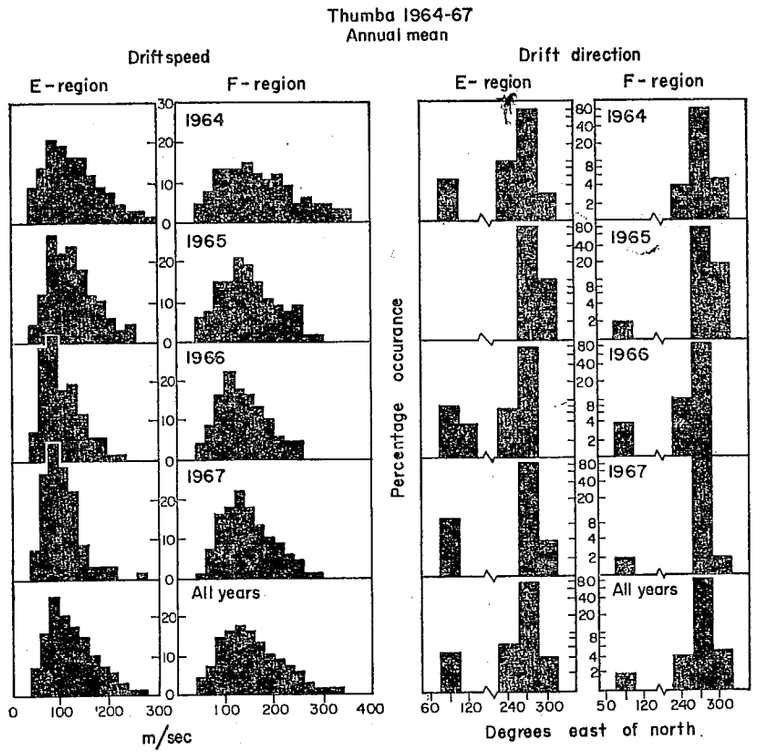

Fig. 6. Histograms of drift speed and direction of E- and F-region drifts averaged over all the months of each of the years 1964–1967.

normal results described earlier, there being the major peak at 270° and a secondary one at 90°. There is no systematic and significant change in the drift direction between 1964 and 1967.

RAO and RAO (1964a) have indicated that the E-region drift speed at Waltair increases with solar activity, the mean value being 83 m/sec during 1957–59 and 75 m/sec during 1960–62. MORRIS and LYON (1966) have found that the velocity of ionospheric drift at Ibadan during equinoxes in the IQSY was reduced by a factor of 1·8 to that during IGY. The data at Thumba so far do not indicate any definite variation of drift speed with solar activity.

COMPARISON WITH THE RESULTS AT OTHER STATIONS

The earliest measurements were made at high latitude and it was observed that the East–West component of the drift was towards east during the day-time and towards West during the night-time (BRIGGS and SPENCER, 1954). Later measurements at the low latitude stations, namely Singapore, and Waltair, showed an opposite trend, the drift being towards West during day and towards East during night (PURSLOW, 1958; RAO and RAO, 1958). Drift measurements at a mid-latitude station, Puerto Rico, during the day-time hours showed marked

Table 1. The mean apparent drift speed in E- and F-regions of the ionosphere during the day-time hours at different stations in the world

Station	Magnetic latitude	Layer	Year	Time	Speed	Reference
Thumba	0·3°S	E	1964–67	day	125	Present article
		F	1964–67	day	160	
Tamale	0·6°S	E	1962—Feb.–Mar.	day	107	KOSTER (1966)
			1962—Feb.–Mar.	day	147	
Ibadan	3°S	F	1957—Aug.–Sep.	day	105	SKINNER *et al.* (1958)
		E	IGY	day	90	SKINNER *et al.* (1963)
		F	IGY	day	95	
Bangui	9°S	E	1958	day	85	*Ann. IGY* **33**, 1965.
Singapore	9°S	F	1953–54	day	50	OSBORNE (1955)
Waltair	11°N	E	1954–55	day	65	RAO *et al.* (1956)
		E	1957–59	day	81	RAO and RAO (1961)
		E	1960–62	—all hours—	75	RAO and RAO (1964a)
		F	Mean	day	99	RAO and RAO (1964a).
Ahmedabad	18°N	E	1956–66	day	70	Unpublished.
		F	1956–62	day	68	
Delhi	24°N	E	1958–59	—all hours—	55	MITRA *et al.* (1960).
		F	1958–59		85	
Yamagawa	25°N	E	1958	day	73	RAO and RAO (1965).
		F	1958	day	85	RAO and RAO (1964a).
Puerto Rico	32°N	E	Mar. 1958—Feb. 1959.	day	83	KENESHEA *et al.* (1965).
Ashkabad	36°N	F	1958	day	79	RAO and RAO (1964a).
Brisbane	38°S	E	1952–53	day	78	BURKE and JENKINSON (1957).
		E	1953–54	day	57	
		E	1958	day	51	RAO and RAO (1965).
			Mean		62	
Seimiz	43°N	F	1958	day	123	RAO and RAO (1964a).
Halley Bay	47°S	E	1958	—all hours—	63	PIGGOTT and BARCLAY (1963).
		F	1957–58	—all hours—	85	BELLCHAMBERS and PIGGOTT (1965).
Cologne	43°N	E	Winter	—all hours—	90	KRAUTKRAMER (1950).
		F	1941–42		90	
Wellington	50°S	E	1958	day	78	RAO and RAO (1965).
De Bilt	50°N	E	1958	day	90	RAO and RAO (1965).
Cambridge	50°N	$(E–F)$	1952	—all hours—	85	PHILLIPS (1952).
Washington	56°N	$(E–F)$	1950 Mar.–Dec.	—all hours—	70	SALZBERG and GREENSTONE (1951).
Gorky	56°N	F	1958	day	103	RAO and RAO (1964a).
Ottawa	62°N	$(E–F)$	1950 Jun.–Oct.	—all hours—	80	CHAPMAN (1953).

seasonal variation in direction being predominantly to the East in Summer and to the West in Winter (KENESHEA *et al.*, 1965). The drift observations at a station within the equatorial electrojet region, first obtained at Ibadan revealed that the drift was entirely towards west during the day-time and towards East during the night-time with a change over happening around 07.00 hr and 20.00 hr. The N–S component was either negligible or unmeasurable due to extreme elongation of irregularities. The drift speed at Ibadan was found to be higher than that at Singapore and Waltair. The results derived from comparatively fewer observations at Tamale, which is still closer to the equator than Ibadan, revealed slightly higher speed being Westward during day. The measurements of drift at Thumba which is almost at the center of the equatorial electrojet showed the values of the drift speed higher than at Ibadan or Tamale. A comparison of drift speed at different stations was therefore attempted.

The values of the drift speed in E- and F-regions only during the day-time hours are calculated. For Ibadan, Puerto Rico and Tamale, only the true drift (V) and the ratio of random to true drift components (V_c/V) were available and so the apparent drift (V') was calculated using the formula $V' = V\{1 + (V_c/V^2)\}$. Some stations did not indicate the period of the day when the observations were taken and these are also included in the present comparison. In Table 1 are given the values of apparent drift speed in the E- and F-regions from the available published literature. It is to be noted that the observations refer to different periods of solar activity and to different length of observation period. Figure 7 shows the mass plot of speed vs. magnetic latitude of the station. It is seen from the Table 1 and Fig. 7 that generally at most of the stations the speed is higher for the F-region than for the E-region. For either of the regions the drift speed shows a very sharp maximum at the magnetic equator. It may be taken into consideration that these are apparent drifts which could be modified when corrections are made for the random motion within the irregularities causing them. SKINNER *et al.* (1958) have shown that the irregularities at Ibadan are elongated along N–S direction, the mean axial ratio of the characteristic ellipse being 5 for the E- and 11 for the F-region. Similar elongations of the order of 6:1 between N–S and E–W

Fig. 7. Variation of the day-time average drift speed with magnetic latitude.

directions are reported for Tamale (KOSTER and KATSRIKU, 1966). RASTOGI *et al.* (1968) have shown that the cross correlation between an E–W pair of aerials falls fairly rapidly with increasing distance between them, being about 0·7 for a separation of about two wavelengths. In the N–S direction the cross correlation between two aerials decreases very slowly with increasing distance such that even at a separation of 8 wavelengths the correlation exceeds 0·8. This clearly indicates that the ionospheric irregularities over Thumba are highly elongated along the magnetic lines of force.

The sharp maximum of the drift speed over the magnetic equator and consistently westward direction of the drift at the magnetic equator as well as the extreme elongation of the irregularities undoubtedly suggests that these drifts are characteristics of the magnetic equatorial zone.

It is recommended that further observation at few more low latitude stations should be undertaken to study the inter-relations between the equatorial ionospheric drifts and the equatorial electrojet. This would define the range of latitude within which such consistent westward drift and the extreme elongation of the irregularities occur.

Acknowledgements—Sincere thanks are due to Professor V. A. SARABHAI, Chairman, Indian National Committee for Space Research, for the encouragement and the facilities provided at Thumba Equatorial Rocket Launching Station and to Professor K. R. RAMANATHAN for his interest and valuable suggestions during the course of study.

REFERENCES

BELLCHAMBERS W. H. and PIGGOTT W. R.	1965	*Ann. IGY* **33,** 278.
BRIGGS B. H., PHILLIPS G. J. and SHINN D. H.	1950	*Proc. phys. Soc.* **B63,** 106.
BRIGGS B. H. and SPENCER M.	1954	*Rep. Prog. Phys.* **17,** 245.
BURKE M. J. and JENKINSON I. S.	1957	*Aust. J. Phys.* **10,** 378.
DESHPANDE M. R. and RASTOGI R. G.	1966a	*Annls Géophys.* **23,** 418.
DESHPANDE M. R. and RASTOGI R. G.	1966b	*Proc. IQSY Symp. New Delhi.*
DESHPANDE M. R. and RASTOGI R. G.	1967	*Proc. Ind. Acad. Sci.* **66,** 272.
DESHPANDE M. R. and RASTOGI R. G.	1968	*J. Atmosph. Terr. Phys.* **30,** 293.
KENESHEA T. J., GARDNER M. E. and PFISTER W.	1965	*J. Atmosph. Terr. Phys.* **27,** 7.
KOSTER J. R. and KATSRIKU I. K.	1966	*Annls Géophys.* **22,** 440.
MITRA S. N.	1949	*Proc. IEE,* **96,** Part III, 441.
MITRA S. N., VIG K. K. and DASGUPTA P.	1960	*J. Atmosph. Terr. Phys.* **19,** 172.
MORRIS R. W. and LYON A. J.	1966	*Nature, Lond.* **310,** 617.
MORRIS R. W.	1967	*J. Atmosph. Terr. Phys.* **29,** 651.
OSBORNE B. W.	1955	*J. Atmosph. Terr. Phys.* **6,** 117.
PIGGOTT W. R. and BARCLAY L. W.	1963	*Proc. Int. Conf. Ionosphere,* p. 323. The Physical Society, London (1962).
PURSLOW B. W.	1958	*Nature, Lond.* **181,** 35.
RAO B. R., RAO M. S. MURTHY D. S. N.	1956	*J. scient. ind. Res.* **A15,** 75.
RAO B. R. and RAO E. B.	1958	*Nature, Lond.* **181,** 1612.
RAO B. R. and RAO B. R.	1961	*J. Atmosph. Terr. Phys.* **22,** 81.
RAO A. S. and RAO B. R.	1964a	*J. Atmosph. Terr. Phys.* **26,** 399.
RAO G. L. N. and RAO B. R.	1964b	*J. Atmosph. Terr. Phys.* **26,** 399.
RAO G. L. N. and RAO B. R.	1965	*J. Geophys. Res.* **70,** 667.
RASTOGI R. G., DESHPANDE M. R. and KAUSHIKA N. D.	1966	*J. Atmosph. Terr. Phys.* **28,** 137.
RASTOGI R. G., DESHPANDE M. R. and HARISH CHANDRA	1968	*J. Atmosph. Terr. Phys.* **30,** 1597.
RAWER K.	1965	*Ann. IGY* **33,** 9 Compiled by RAWER K.
SKINNER N. J., LYON A. J. and WRIGHT R. W.	1958	*Nature, Lond.* **102,** 1363.
SKINNER N. J., LYON A. J. and WRIGHT R. W.	1963	*Proc. Int. Conf. on the Ionosphere.* (Edited by STICKLAND A. C.), p. 301. Physical Society London.

(Accepted for publication as 'Short Paper' in JATP)

DAILY VARIATION OF F-REGION DRIFTS AT THUMBA

by

H. CHANDRA & R.G. RASTOGI

Physical Research Laboratory
Ahmedabad-9, INDIA.

ABSTRACT:- The measurements of F-region electron drifts at Thumba during the year 1967 indicate the direction to be Westward during the daytime and Eastward during nighttime, the reversals occurring between 06-07 hr. and 19-20 hr. A significant increase of drift speed occurs about an hour before the morning as well as the evening reversal. The results are in excellant agreement with the electron drifts measured by Doppler shift of V.H.F. scatter echoes at Jicamarca.

The present article describes the results of round the clock measurement of F-region drift at Thumba (Magnetic latitude 0.3°S) for the year 1967. In Fig. 1 are shown the mass plots of apparent drift speed and direction at a few selected hours. F-region drifts at

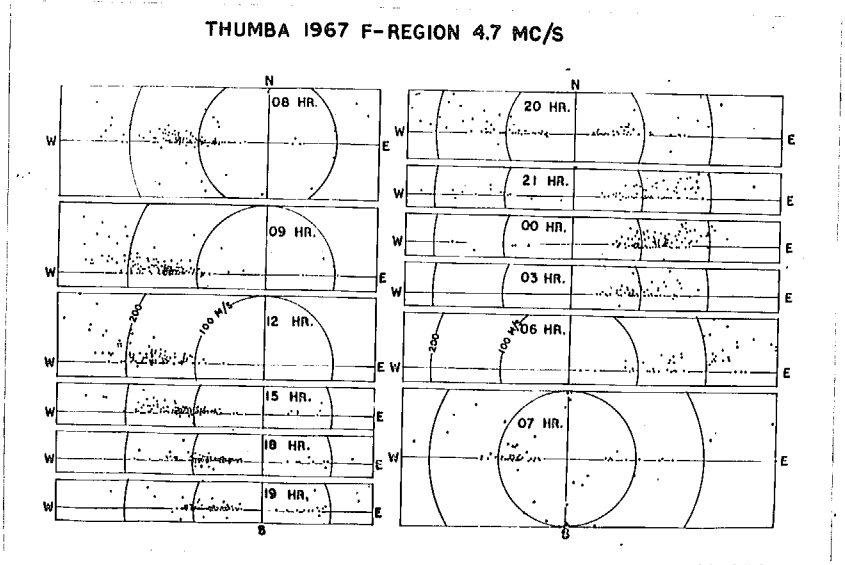

Fig. 1 - Mass polar plots of the apparent drift velocities at few selected hours.

Thumba are seen to be predominantly towards West between 07 and 19 hours and predominantly towards East between 21 and 06 hours. The time of evening reversal is found to have appreciable day-to-day variability as evident from the scatter of points at 20 and 21 hrs. The N-S drift directions seem to be negligible even during the periods of reversal.

The mean daily variations of E-W component of drift speed for each season are shown in Fig. 2; the smooth line drawn through

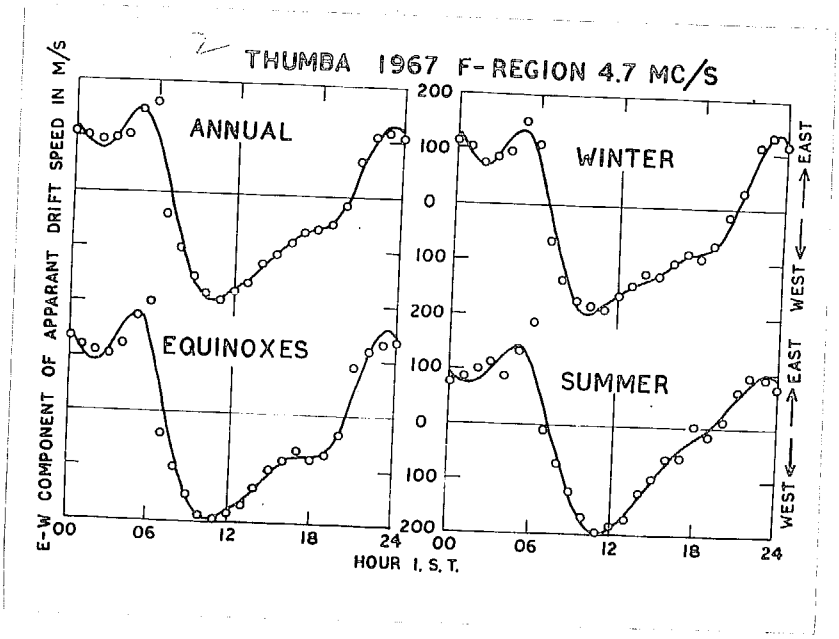

Fig. 2 - Mean daily variation curve of E-W component of apparent drift speed.

the experimental points is built up of the first four harmonics of the daily variation. The different harmonic coefficients for Thumba are given in Table 1, together with similar coefficients for other equatorial stations. A significant increase of the drift speed is seen before the morning reversal during each of the seasons. Similar increase of speed is suggested shortly before the evening reversal,

TABLE-1

Harmonic coefficients of the daily variation of the E-W component of apparent drift speed in F-region at equatorial stations.

Place	Magnetic latitude	Period	Amplitude in m/sec.					Time of maxima in hour local time				Reference
			a_o	r_1	r_2	r_3	r_4	ϕ_1	ϕ_2	ϕ_3	ϕ_4	
Thumba	0.3°S	Winter 1967	-26	152	32	43	28	0.9	3.3	5.8	5.1	
		Equinoxes 1967	-12	165	36	49	38	1.1	4.1	6.0	5.0	
		Summer 1967	-9	142	50	31	12	0.9	5.1	6.0	5.3	Present article
		Annual	-16	153	36	41	22	1.0	4.3	5.9	5.1	
Ibadan	3°S	Aug.-Sep. 1957	-10	111	26			1.5	1.2			Skinner et al. 1958..
Waltair	11°N	1957	8	89	6			1.8	7.6			Rao and Rao 1958.
Singapore	9°S	Sep.'53-Aug.'56.	18	45	22	10		0.4	0.5	5.9		Rurslow 1958.

specially during the equinoxes.

The measurements of true electron drifts from the Doppler shifts in V.H.F. scatter echoes at Jicamarca (Magnetic Latitude 1°N), indicate that the echoing centres in the electrojet move Eastward during the night and Westward during the day. The reversal times are centred about 06.30 hr. and 20.30 hr. with a marked increase in the drift velocity about an hour before both the morning and evening reversals (Balsley 1966, 1969). Balsley and Woodman (1969) have shown an intimate relation between horizontal drifts in the E-region and vertical drifts in the F-region. These results which indicate true electron motion are in remarkable agreement with the results obtained at Thumba.

It is concluded that the ionospheric drift measurements near the magnetic equator do indicate the true motions of electrons and these motions are intimately associated with the equatorial electrojet.

REFERENCES

Balsley B.B.	1966	Ann. Geophys., 22, 460.
Balsley B.B.	1969	J. Atmosph. Terr. Phys., 31, 475.
Balsley B.B. and Woodman R.F.	1969	J. Atmosph. Terr. Phys., 31, 565.
Purslow B.W.	1958	Nature, London, 181, 35.
Rao B.R. and Rao E.B.	1958	Nature, London, 181, 1612.
Skinner N.J., Hope J. and Wright R.W.	1958	Nature, London, 182, 1363.

******

CHAPTER - II.4 CORRELATION METHODS FOR THE COMPUTATION OF DRIFTS AND ANISOTROPY PARAMETERS AND THE RESULTS OBTAINED AT THUMBA EMPLOYING CORRELATION TECHNIQUE

CHAPTER - II.4(a) Correlation methods for computing drift and anisotropy parameters of the irregularities

II.4a.1 Correlation methods to determine uniform drift motion

II.4a.2 Extension of the method to anisotropic case

II.4a.3 Calculation of correlation coefficients, optimisation of sampling interval and length of the records

II.4a.4 Comparison of the different methods.

CHAPTER - II.4(b) Steady and random drift components at Thumba

II.4b.1 True drift parameters in the year 1964

II.4b.2 Daily variations of true drift parameters during 1964

II.4b.3 True drift parameters during the year 1967

II.4b.4 Daily variation of true drift parameters during 1967

II.4b.5 Comparison of the true drift parameters in the years 1964 and 1967

II.4b.6 Comparison with the results obtained at other equatorial stations.

CHAPTER - II.4(c) Size and shape of the ionospheric irregularities at Thumba

II.4c.1 Anisotropy parameters during 1964

...

CHAPTER II.4 contd..

Chapter II.4(c)

CHAPTER - II.4(a) CORRELATION METHODS TO DETERMINE DRIFT PARAMETERS

INTRODUCTION

Time delay method assumes that the fading produced is entirely due to the steady drift of the diffraction pattern on the ground and that contours of constant amplitude have circular symmetry. In practical cases, the diffraction pattern itself undergoes random changes in it as it moves. Consequently, the fading observed at ground is produced by the steady drift as well as due to changes in the diffraction pattern.

II.4a.1(a) Correlation method to determine uniform drift motion

A method to deduce the uniform steady motion of the diffraction pattern was originated by Briggs, Phillip and Shinn (1950) taking into account the random changes in its shape as it moves. The principle of this method is to consider the general similarity of the fading records and then to compare it with the case when it is moving with a uniform speed. The difference gives a measure of the random changes. Thus the steady motion of the pattern and the rate at which the pattern alters as it moves can be obtained. The method is based on the calculations of auto and cross correlations between fading records at different aerials.

II.4a.1(b) Auto and cross correlation functions

A variation of the amplitude R against time can be represented by an auto correlation function $\rho(t)$ defined as

$$\rho(t) = \frac{\{R(t) - \bar{R}\}\{R(t+\tau) - \bar{R}\}}{\{R(t) - \bar{R}\}^2} \qquad \ldots(1)$$

where $\bar{R}$ = mean amplitude of the record

τ = a small time interval over which amplitudes are studied

which gives the measure of average correlation between the values of R separated by time interval τ. It has value unity for t = 0 and decreases smoothly as τ increases. A typical auto correlation curve is shown in Fig. II.4.1.

In practical case amplitude R is a function of space coordinates x, y and a time coordinate t. For simplification let us treat a one dimensional ground. In such case correlation coefficient can be defined as

$$\rho(\xi, t) = \frac{\{R(x,t) - \bar{R}\}\{R(x+\xi, t+\tau) - \bar{R}\}}{\{R(x,t) - \bar{R}\}^2} \qquad \ldots(2)$$

From a one dimensional ground we can know an auto-correlation function $\rho(0, t)$ from either of the record obtained at x = 0 or at $x = \xi_0$, where ξ_0 is the receiver separation and a function $\rho(\xi_0, t)$ which is the cross correlation

between the two fading records. Fig. II.4.1 shows the auto and cross correlation functions from such set of fading records. Cross correlation function is maximum at some definite time interval as the two fading records are slightly shifted from each other. Further its maximum value may not be unity as the two fading records may not be exactly similar.

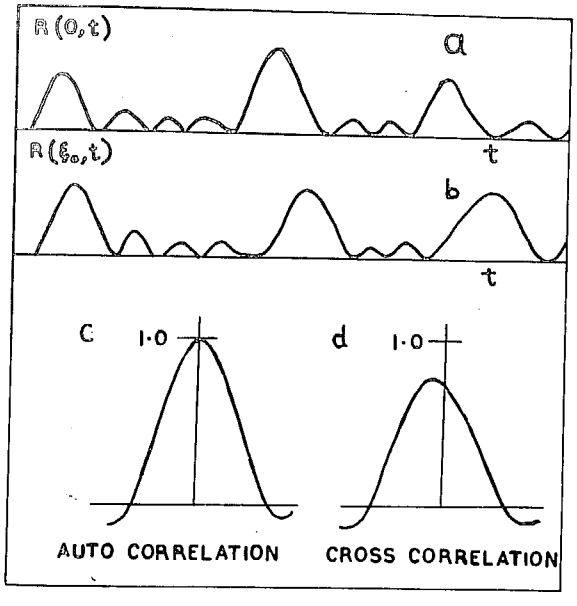

Fig. II.4.1.

In a smilar way, one can write correlation coefficients in terms of two space coordinates x, y and one time coordinate t.

$$\rho(x,y,t) = \frac{\{R(x,y,t)-\bar{R}\}\{R(x+\xi,y+\eta,t+\tau)-\bar{R}\}}{\{R(x,y,t)-\bar{R}\}^2}$$

where ξ_0, η_0 are receiver separations. Thus one can find from

three fading records obtained by spaced receiver method, three cross correlation curves, one each for the different pairs of fading records.

II.4a.1(c). Definitions

Briggs et al defined four velocities to describe the movement of the diffraction pattern. They are described here in terms of correlation function for a one dimensional ground.

(1) Fading velocity Vc'

This is defined as a ratio of space shift to time shift needed to produce on the average same change in the value of R.

Mathematically $Vc' = \frac{xo}{to}$

where $\rho(x_o, o) = \rho(o, t_o)$ . ...(4)

Physically fading velocity Vc' is the velocity of drift that would be needed to explain the fading entirely in terms of a drifting pattern with no random changes. On the assumptions mentioned earlier (isotropic ground pattern) this quantity is independent of the direction.

(2) Drift velocity V

This is the velocity of the moving observer with which he finds the slowest speed of fading. Thus if a dis-

placement ξ_1 in time τ_1 is required to experience slowest fading then

$$V = \frac{\xi_1}{\tau_1} \qquad \ldots(5)$$

For a two dimensional ground V has direction and can be represented by components $V_x = V \cos\phi$, $V_y = V \sin\phi$ where ϕ is the direction of the V.

(3) Characteristic velocity Vc

This is the fading velocity observed by an observer moving with a uniform drift V. To this observer, the ratio of space shift to time shift needed to produce a similar change in R is

$$Vc = \frac{x_0}{\tau_1} \qquad \ldots(6)$$

where $\rho(x_0, o) = \rho(\xi_1, \tau_1)$

(4) Apparent drift velocity V'

If a receiver situated at $x = \xi_0$ is examined with another at $x = 0$ and maximum correlation is obtained at time interval τ_0 then this velocity is defined by

$$V' = \frac{\xi_0}{\tau_0} \qquad \ldots(7)$$

For a two dimensional ground, supposing receivers spaced ξ_0 along OX and spaced η_0 along oy have best correla-

tions at time lags τ_{ox}, τ_{oy} then

$$V_x' = f_o / \tau_{ox}$$

$$V_y' = f_o / \tau_{oy}$$

These two components are related by the equation

$$\frac{1}{(V')^2} = \frac{1}{(V_x')^2} + \frac{1}{(V_y')^2} \qquad \ldots(8)$$

and are the same qualities as described in the time delay method.

II.4a.1(d). Relation between different velocities and their determination

For isotropic diffraction patterns Briggs et al found the relations between different velocities by the following equations:

$$(V_c')^2 = V_c^2 + V^2 \qquad \ldots(9)$$

and $$(V_c')^2 = V'V \qquad \ldots(10)$$

Determination of Vc'

If one compares the cross-correlation value at t = 0 to same value of auto-correlation at time τ_s then from above definitions

$$V_c' = f_o / \tau_s \qquad \ldots(11)$$

Determination of V'

V' can be determined by knowing the time lag for maximum cross correlation value. If t_o is the lag for best correlation between fading records at two points spaced ξ_o from each other, then

$$V' = \xi_o / t_o \qquad \ldots(12)$$

Substituting the values of Vc' and V' in equation (10), one can solve for the value of V.

II.4a.1(e). Other methods to find drift velocities

Another way to find the drift velocity V is from time $\tau = \tau_e$ when auto and cross correlations are equal. V can be found using the relation

$$V = \xi_o / 2\tau_e \qquad \ldots(13)$$

The best way described by Briggs et al was to plot complete auto and cross correlation values and then to find time τ and τ' for equal correlation values in the cross and auto correlation curves. A plot of $\tau'^2 - \tau^2$ against different time interval value τ is a straight line,

$$\tau'^2 - \tau^2 = (\xi_o^2 - 2V\xi_o\tau) / V_c'^2$$

The intercepts of which are τ_e and τ_ξ^2. From these inter-

prets, one can find V and V' using the relations

$$\xi_{o}/2V = \tau_{e}$$
$$\xi_{o}^{2}/V_{c}'^{2} = \tau_{s}^{2} \qquad \ldots(15)$$

Above equations can be generalized to the case of a two dimensional ground. If ϕ is the angle between the drift direction of the pattern and x axis then

$$V_{x} V_{x}' = V_{c}'^{2}$$
$$V_{x} = V\cos\phi = \xi_{o}/2\tau_{ex}$$
$$V_{x}' = V'/\cos\phi = \xi_{o}/\tau_{ox}$$

and
$$\tau'^{2} - \tau^{2} = (\xi_{o}^{2} - 2V_{x}\xi_{o}\tau)/V_{c}'^{2} \qquad \ldots(16)$$

Similar set of equations can be written for the y axis representing another pair of fading records. These equations are derived on the basis that variations of R are equal on the average for equal displacements in any direction. That is the correlation surfaces in the plane show circular symmetry or contours of constant correlation are circular.

Another important relation obtained by Briggs et al is
$$\tau_{s}^{2} = t_{o}^{2} + \tau_{o}^{2} \qquad \ldots(17)$$

where to is the time lag required to give an auto-corre-

lation value equal to the maximum cross correlation value. The advantage of this equation lies in the fact that Vc' can be calculated from top portion of the correlation curve which is less liable to error. This relation will be further discussed later.

II.4a.2. Extension of the method to anisotropic case

The main drawback of the method as described by Briggs et al lies in the fact that it can be applied to isotropic cases only. That is if Vc' values along three different directions calculated by the three pairs of records come out to be same then only we can apply this method. Since the presence of magnetic field creates anisotropy in the free electron motion, irregularities are field aligned in general and the diffraction pattern on the ground are elongated along the magnetic lines of force. Particularly at the magnetic equator, the diffraction patterns are highly elongated in N-S direction.

Phillips and Spencer (1955) extended the analysis of Briggs et al to anisotropic diffraction patterns. As an extreme case, consider a pattern in which the amplitude contours are so elongated that they appear as a set of parallel lines. In such a case, any motion parallel to the lines can never be detected. When the pattern is

finite in structure, there will be errors depending on the degree of elongation.

An anisotropic diffraction pattern can be described by contours of constant correlation which will be similar concentric eclipses. A pattern of this type could be produced if a statistically isometric pattern is stretched in one direction. Distortion of this type may be represented by a characteristic ellipse similar to contours of constant correlation and may be said to represent an average shape of the contours of constant amplitude of the diffra-

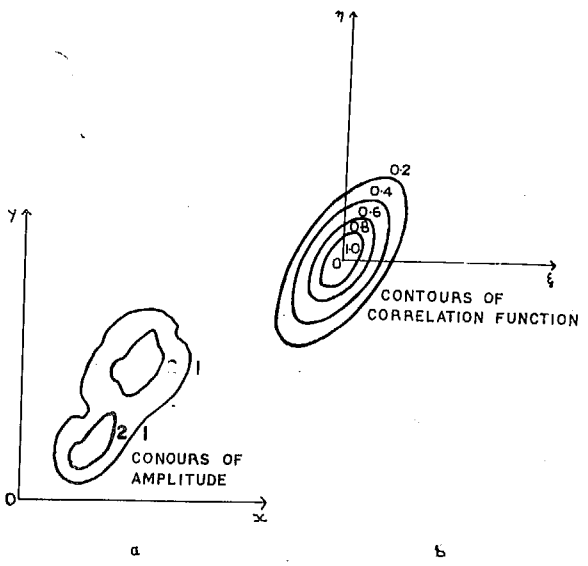

Fig. II.4.2.

pattern. Complete curves of constant correlation can be deduced if one knows the axial ratio, orientation of ellipse and auto-correlation function along one direction. For the knowledge of the shape of the contours only axial ratio and orientation of ellipse are sufficient.

II.4a.2(b). Determination of the characteristic ellipse

From the fading records at three points situated at the corners of an isoceles right angled triangle of side a, one can obtain auto-correlation function $\rho(o,o,\tau)$ at a number of values of τ. A plot of this function against τ will give the time correlogram. Cross correlations $\rho(a,o,o)$, $\rho(o,a,o)$ and $\rho(a,-a,o)$ can be determined at $\tau = 0$ between three pairs of the fading records. If τ_1, τ_2 and τ_3 are the time values on the time correlogram which give same ρ values as at $\tau = 0$ on cross correlograms, then from the definition of Briggs et al

$$(V_c')_1 = a/\tau_1$$

$$(V_c')_2 = a/\tau_2$$

and $$(V_c')_3 = \sqrt{2}\, a/\tau_3 \qquad \ldots(18)$$

which are the fading velocities in the three directions defined by the spaced points where fadings are observed. The simplest example of spacings in these direction which have a fixed correlation is given by putting $\tau = 1$ which gives correlation $\rho(0,0,1)$, the spacings are then equal to Vc'. As any constant correlation surface is an ellipse, Vc' when plotted on a polar plot, must be one of the ellipses of constant correlation. The known values

of Vc' give the length of the semi-diameter of the ellipse for the three directions. This is sufficient to determine the axial ratio ρ and orientation ψ of minor or major axis.

If one considers the equation of an ellipse with its axes rotated clockwise by an angle ψ from the coordinate axes and substitutes the values of fading velocities as intercepts of this ellipse on the three lines joining the three pairs of spaced points at which fading records are observed, one gets three equations which can be solved to give axial ratio ρ ($\rho > 1$) and ψ. One gets then

$$\rho^2 = \frac{R + (P^2 + Q^2)^{1/2}}{R - (P^2 + Q^2)^{1/2}} \qquad \ldots(19)$$

and $$\tan 2\psi = P/Q \qquad \ldots(20)$$

where $P = \tau_1^2 + \tau_2^2 - \tau_3^2$

$Q = \tau_1^2 - \tau_2^2$

$R = \tau_1^2 + \tau_2^2$

and ψ is the orientation of minor axis from x axes measured in the clockwise sense.

II.4a.2(c). Determination of drift parameters of an anisotropic pattern

An anisometric pattern can be considered as a result of streching of an isometric pattern in one direction

by an amount μ . Phillips and Spencer applied the results of Briggs et al to an equivalent isometric pattern and then corrected to take into account the anisotropy. They showed that when an anisometric pattern is wrongly assumed to be isometric the drift direction as well as apparent drift speed are affected; apparent speeds are lowered depending on the value of μ and the angle between the drift direction and the minor axis of the ellipse.

Consider an anisometric pattern as shown in Fig. II.4.3(a) where O, A, B are the points forming a right angled triangle where fadings are observed. Its velocity diagram is shown in Fig. II.4.3(b), where V_1', V_2' are apparent drift components along OA, OB and Vc' ellipse is shown with its minor axis at an angle ψ from the V_1' direction.

Its equivalent isometric pattern and velocity diagram are shown in Fig. II.4.3(a) and II.4.3(b). In this diagram Vc' ellipse changes to a form of a circle. The triangle OAB is no longer a right angle in this case as the lines along V_1', V_2' have a slope reduced by a factor of μ in the diagram. As the fadings observed hence time shifts are identical in two diagrams, ratio of the velocities V_1', V_2' is similar to that of base line OA, OB in two diagrams. Only difference being that velocity diagram of II.4.3(d) will give rise to velocity diagram of II.4.3(b)

with a vertical expansion by a factor μ_2 .

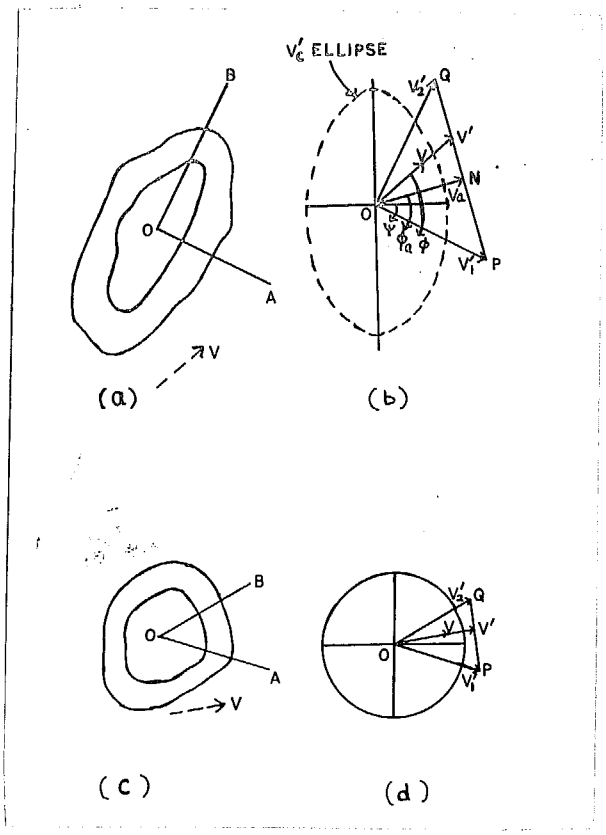

Fig. II.4.3
(a, b, c and d)

The results of Briggs et al were derived for a right angled system. They can be generalized to the case when axes are not at right angles. Thus we can write

$$V_n = V \cos \phi_n \qquad (21)$$

$$V' = V_n' \cos \phi_n \qquad (22)$$

$$V'V = (V_c')^2 \qquad (23)$$

The vector V' in Fig. II.4.3(d) is obtained by drawing a perpendicular from O to the line PQ joining the end points of the vectors V_1', V_2'. Similarly V' can be obtained in Fig. II.4.3(b), but as the lines representing V_1', V_2' in Fig. II.4.3(b) are having slopes μ_2 times to that in Fig. II.4.3(d). Consequently vector V' has a slope μ_2^2 times to that of the perpendicular on to line PQ. Thus without anisotropic correction, the vector ON will give the apparent drift. Let us represent

it by V_a and its direction measured from the V_1' direction as ϕ_a . The correction has to be applied to get true vector V', since it has a slope μ^2 times the slope of line ON. If we represent corrected drift V' having an angle ϕ from V_1' direction

$$\tan(\phi - \psi) = \mu^2 \tan(\phi_a - \psi) \qquad \ldots(24)$$

which can be written in another form as

$$\tan(\phi - \phi_a) = \frac{(\mu^2 - 1)\tan(\phi_a - \psi)}{1 + \mu^2 \tan^2(\phi_a - \psi)} \qquad \ldots(25)$$

The relation between the vector V' and V_a is given by

$$V_a = V' \cos(\phi - \phi_a) \qquad \ldots(26)$$

where $\frac{1}{V_a^2} = \frac{1}{V_1'^2} + \frac{1}{V_2'^2}$

These equations show that the corrections depend on the value of axial ratio μ and the angle $\phi_a - \psi$, that is between the apparent drift direction and the minor axis of the ellipse. When this direction is along the minor or major axis there is no correction for the direction hence for the drift speed.

True drift speed can be computed from the equations derived by Briggs et al. $(V_c)'$ along the direction of drift can be calculated by the equation:

$$(V_c')_V = \frac{1 + (\mu^2 - 1)\cos^2\psi\,(V_c')_1^2}{1 + (\mu^2 - 1)\cos^2(\phi - \psi)} \qquad \ldots(27)$$

where $(V_c')_l$ is the fading velocity along the vector V_l'. True drift will be therefore given by

$$V = (V_c')^2_V \; / V' \qquad \ldots(28)$$

In short the method of Phillips and Spencer consists in finding the fading velocity in three directions. An ellipse is drawn through these points and parameters λ_2 and ψ are calculated. Uncorrected drift speed V_a and direction ϕ_a are found applying ordinary Briggs et al method. They are corrected from the known value of λ_2 and ψ. Fading velocity $(V_c')_V$ is calculated along the corrected drift direction. From corrected apparent drift V' and this fading velocity $(V_c')_V$, true drift speed V is calculated using equation (28).

II.4a.2(d). <u>Further modification of the correlation method as applied to anisometric patterns</u>

Fooks (1965) has suggested two modifications to use the correlation method of an analysis.

(a) Mean auto correlation function from the three fading records should be used to reduce statistical deviations.

(b) The time values τ'_{12} etc. can be derived from equation (17) given by Briggs et al which in the notation of Fooks is

$$\tau^2_{12} = (\tau')^2_{12} + (\tau_m)^2_{12} \qquad \ldots(29)$$

where $(\tau')_{12}$ is the time displacement giving maximum cross correlation between the fading records 1 and 2, and $(\tau_m)_{12}$ is the time displacement on the mean auto-correlation function giving auto correlation value equal to maximum value of cross correlation between the fading records 1 and 2. In a similar manner, τ_{13} and τ_{23} can be calculated. This equation was derived by Briggs et al (1950) for isometric patterns. Kelleher (1965) has shown that this relation is valid for anisometric patterns also. The advantages of this modification are:

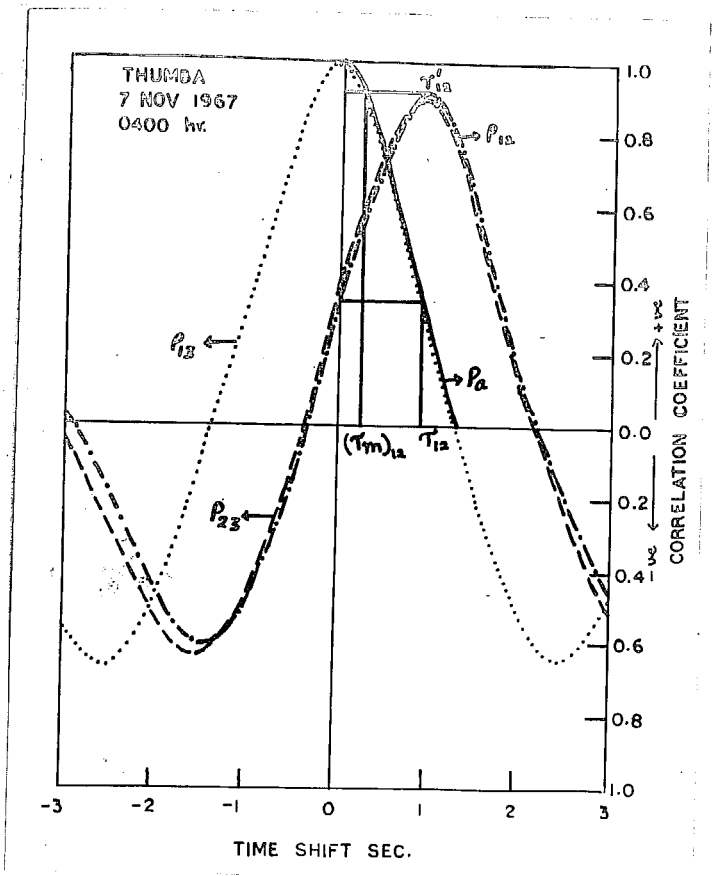

Fig. II.4.4.

(1) It uses the points at a higher level on the correlation functions and hence results are less affected by statistical variation.

(2) Using this equation V' always comes higher than V

and thus removes the occurrences of negative V_θ^2 values which some authors have reported.

II.4a.2(e). Average size of irregularities in the pattern

Phillips and Spencer derived the axial ratio ρ and orientation ψ of the characteristic ellipse, however, the size of this ellipse was not mentioned by them.

From the V_c' values, one can find the major axis a and the minor axis b. This ellipse has dimensions of velocity and can be converted to distances to give average size and shape of the irregularities in the pattern. Generally they are multiplied by $\tau_{0.5}$, the value of time displacement required to give $\rho = 0.5$ on the mean autocorrelation curve, and gives the separation to give a correlation 0.5 between the fadings as measured at different points on the ground.

To determine the average size, shape and tilt of ellipse, we give here treatment according to Fook's (1965).

An ellipse with its centre at the origin is represented by the equation in polar coordinates

$$\frac{\cos^2\theta}{a^2} + \frac{\sin^2\theta}{b^2} = \frac{1}{r^2} \qquad \ldots(30)$$

If the ellipse is rotated through an angle θ_0 we get the

equation

$$\frac{\cos^2(\theta-\theta_0)}{a^2}+\frac{\sin^2(\theta-\theta_0)}{b^2}=\frac{1}{r^2} \qquad \ldots(31)$$

Let (r_1,θ_1), (r_2,θ_2) and (r_3,θ_3) be three points along the three directions θ_1, θ_2, θ_3 where correlation falls to 0.5 at separations r_1, r_2, r_3. Substituting these values in equation (31), one can solve for θ_0 which is given by the expression

$$\tan 2\theta_0=\left[\frac{D_{12}(\cos 2\theta_1-\cos 2\theta_3)-D_{13}(\cos 2\theta_1-\cos 2\theta_2)}{D_{12}(\sin 2\theta_1-\sin 2\theta_3)-D_{13}(\sin 2\theta_1-\sin 2\theta_2)}\right]$$

where $D_{12}=\frac{1}{r_1^2}-\frac{1}{r_2^2}$ etc. $\qquad \ldots(32)$

$2\theta_0$ will lie between $+\pi/2$ to $-\pi/2$ and is tilt of either the major or the minor axis. Using the value of obtained from equation (32), one can solve two equations of the form (31) for a and b. In case $b>a$, the value of θ_0 must be altered by $\pi/2$ and values of a and b must be interchanged. θ_0 can be altered by π if necessary to keep it in the range 0 to π.

The results of analysis are generally quoted with angles measured from North in the clockwise sense.

II.4a.2(f). Definition of Vc for anisometric patterns

Briggs et al defined Vc as the value of Vc' found

by an observer moving with velocity V. For such an observer, entire fading will be due to random changes in the pattern. Vc' is defined as the ratio of shift in space to the shift in time needed to produce on the average same change in the value of correlation. For a stationary pattern, the time shift needed to reduce the correlation to 0.5 can be defined as the mean life time of the pattern. Therefore

$$Vc = \frac{\text{Pattern size}}{\text{mean life time}} \qquad \ldots(33)$$

For an isometric pattern there is no need to identify Vc with any specific velocity component in the pattern. The anisometric patterns were dealt by Phillips and Spencer, however, Vc was not defined by them for such patterns. In such cases Vc will be a function of direction. As mean life time will be independent of direction, so Vc for any direction will be porportional to the corresponding radias of the characteristic ellipse. As pattern size and mean life time are not affected by V definition for Vc will be same for a moving pattern.

Fooks and Jones (1961) gave the value of $(V_c)_V/V$ where $(Vc)v$ is the value of V_c corresponding to the direction of V to indicate the effect of random changes.

II.4a.3 CALCULATION OF CORRELATION COEFFICIENTS - OPTIMISATION OF SAMPLING INTERVAL AND LENGTH OF RECORD

II.4a.3(a) - Sampling theory

In the theories concerned so far involving the correlation coefficients, it is assumed that each record is a sample taken from an infinitely long record with auto-correlation coefficient. Due to finite length of the record, errors will arise in the calculation of correlation coefficients represented by r .

Soper (1915) has derived the distribution of sample correlation coefficients given by

$$\bar{r} = \rho\left[1 - \frac{1-\rho^2}{2N}\right] \qquad \ldots(34)$$

and

$$\sigma(\rho) = \frac{1-\rho^2}{\sqrt{N-1}}\left[1 + \frac{1+\rho^2}{4N}\right] \qquad \ldots(35)$$

where $\bar{r}$ = mean value of the correlation coefficients

$\sigma(\rho)$ = standard deviation in the calculated correlation coefficients.

N = number of sampling points used in compiling the correlation coefficients.

For large value of N

$$\bar{r} = \rho \qquad \ldots(36)$$

and $\sigma(\rho) = \frac{1-\rho^2}{\sqrt{N-1}}$ ...(37)

In case of a finite length of the record a good estimate of variance is

$$\sigma(A) = \frac{1-A^2}{\sqrt{N-1}} \qquad \ldots(38)$$

From this expression, it is evident that to increase the variance, number of scaled points on the amplitude record should be increased. However, there must exist a number N such that scaling at more than N points does not decrease the variance. This N is called the number of independent points.

Bartlett (1956) has shown that the variance of a computed correlation coefficient from a time series is related to the complete auto-correlation function by

$$Var[A(T)] \approx \frac{1}{T}\int_{-\infty}^{\infty} \rho^2(v)\, dv \qquad \ldots(39)$$

where T is the length of the sample. Hence, if amplitudes are scaled at intervals smaller than T/N, these amplitudes are not independent of each other. Substituting the value of variance by squaring $\sigma(A)$ in equation (38)

$$\frac{(1-\rho^2)^2}{N-1} = \frac{1}{T}\int_{-\infty}^{\infty} \rho^2(v)\, dv \qquad \ldots(40)$$

which gives $$N = \frac{T}{\int_{-\infty}^{\infty} \rho^2(v)\, dv}(1-\rho^2)^2 + 1 \qquad \ldots(41)$$

Maximum value of N occurs at $\tau = 0$ where $\rho = 1$, hence

$$N = \frac{T}{\int_{-\infty}^{\infty} \rho^2(v)\,dv} + 1 \qquad \ldots(42)$$

For a Gaussian form of correlation function $\rho(v) = \exp(-v^2/2b^2)$ where b is defined by $\rho(b) = 0.61$.

Hence $N = T/\sqrt{\pi}\, b$. $\qquad \ldots(43)$

This gives the maximum number of points for independent amplitude measurements. Bowhill (1956) has shown that average fading period for a Gaussian autocorrelatogram is given by

$$T_2 = \frac{T}{\text{no. of maxima of the amplitude in time T.}}$$

$$= 3.63\ b. \qquad \ldots(44)$$

Substituting this value in equation (43)

$$N = 2 \text{ (no. of maxima in time T).} \qquad \ldots(45)$$

which shows that a record should be scaled at a number of ordinates atleast twice the number of maxima occurring on the record. Scaling at closer intervals gives no increase in the accuracy of the estimate of the correlation coefficient while scaling at wider intervals increases the variance of the distribution.

II.4a.3(b). Optimisation of sampling interval and length of the record

The effect of varying the sampling interval for a given sample record on the calculations of correlation coefficients has been studied for about 15 cases to optimise the sampling interval suitable for the general correlation analysis of the fading records at Thumba. As the fading rates at Thumba show very large variations with fading rates as high as 100 fades per minute, and as low as practically zero, records of different fading rates were selected for this analysis. In a similar fashion sample record was read with the smallest sampling interval (0.1 sec. in the present analysis) and correlation coefficients were calculated by taking different lengths of the sample record to find a suitable length of the record which would give reasonable reliability in calculations of the correlation coefficients. Examples of the correlation coefficients calculated from a fixed length of the record with different sampling intervals are shown in Fig. II.4.5 as auto-correlation curves. Similarly Fig. II.4.6 shows auto-correlation curves of sample records with a sampling interval constant but different lengths.

In Fig. II.4.5 are shown auto-correlation curves of sample records of length about 48 sec each. Amplitude

readings of the entire length was done at intervals 0.1 sec., 0.2 sec., 0.3 sec., 0.4 sec., 0.6 sec. and 1 sec. The fading rates of the records chosen vary from 12 fades per minute to 60 fades per minute. Small deviations in the auto-correlation curves are noticed at sampling interval 1.0 sec. for records with fading rates of about 40 fades per minute and at sampling interval 0.6 sec. for records with fading rates of about 50 fades per minute and more.

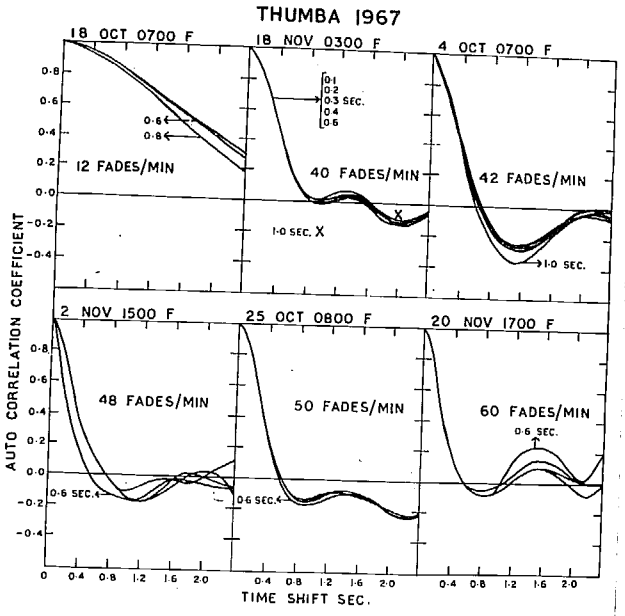

Fig. II.4.5.

Converting in terms of samplings per fade, deviations in the auto-correlation coefficients occur at sampling rates of 2 samples per fade or less while for sampling rates of 3 samples per fade or more there is no difference in the auto-correlation coefficients except at the very large time shifts. As these portions are in the 2nd peak of the auto-correlation curves and are not needed in the analysis

of drift parameters one can safely take 3 samples per fade in the routine amplitude readings. As a safety measure, samplings at least 4-5 per fade has been used as the criteria for the analysis of the fading records at Thumba.

The auto-correlation curves from different sample lengths are shown in Fig. II.4.6. Appreciable difference is noticed if very small length of the record is taken but as the length is increased the curves come out to be more and more similar. For a moderate fading rate (25-40) or fast fading (> 40 fades per min.) a record of 20 sec. length is enough to get reliable correlation coefficients.

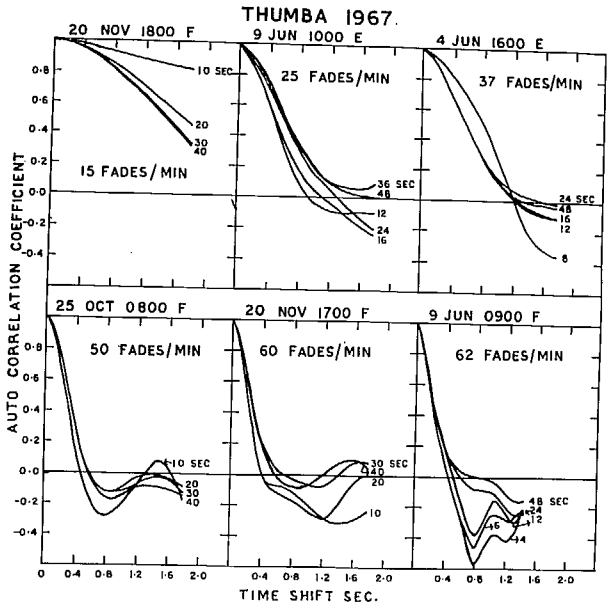

Fig. II.4.6.

But for slow fading, it may not be as much reliable. In terms of fadings, one can say that at least 12-15 fades are necessary to get sufficient reliability.

Keeping in mind the above consideration, the amplitude readings for the fading records at Thumba has been divided into the following categories namely:

(1) Very fast fadings (60 fades per minute)

The records with fading rates 60 have been traced for a length of 20 sec. and amplitude readings are done at each 0.1 sec.

(2) Moderate fadings (30-60 fades per minute)

The records with fading rates 30-60 are traced for a length of 20 sec. and amplitudes are read at each 0.2 sec. interval.

(3) Slow fadings (15-30 fades per minute)

The fading records in this range have been traced for a length of 40 sec. and amplitudes are sampled at each 0.2 sec. interval.

(4) Very slow fadings (less than 15 fades per minute)

Records of this range have been traced for a length of 80 sec. and amplitude readings are done at each 0.4 sec. interval.

II.4a.4. Comparison of different methods

II.4a.4(a). As the correlation method of drift analysis is a laborious one it is not possible to use it on a routine

basis. However, it is desirable to know the relation between the actual steady drift of the diffraction pattern on ground and the results calculated by the routine method. Deshpande and Rastogi (1967) have shown that apparent drift speed and direction determined from mean time shifts between similar fades of the fading records are almost same as those obtained using time lags for the maximum cross correlation between the pairs of fading records. Similar analysis has been done for the data for 1967. Fig. II.4.7

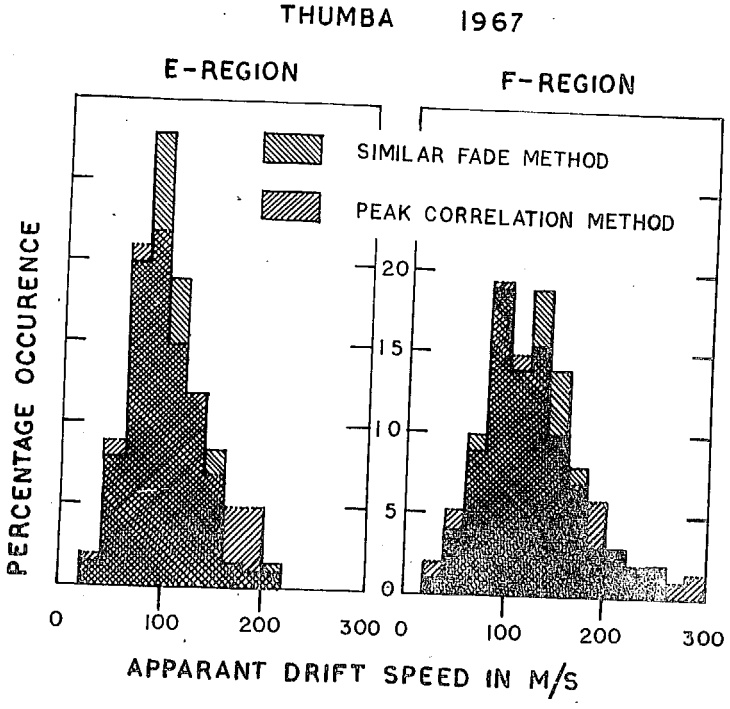

Fig. II.4.7.

shows the histograms of percentage occurrences for the apparent drift speeds calculated by two methods. Histograms for E-region and F-region have been computed separately. The area with crossed lines shows common results while the area with single lines shows deviations from the common percentage. There does not appear much difference in the results of the two methods. The nature of histograms remains same for the two methods. Similar histograms for the apparent drift directions are shown in Fig. II.4.8

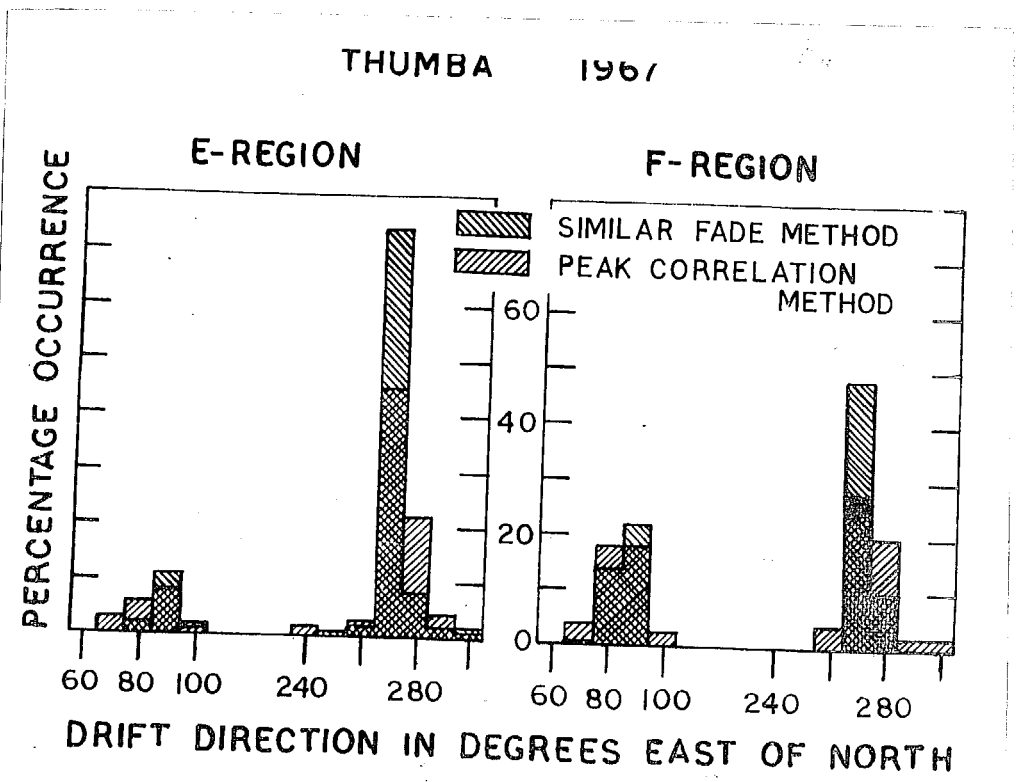

Fig. II.4.8.

The basic drift directions are same, that is a group of directions centred around 270^{o} and another centred at 90^{o}, but there is a tendency of the percentage occurrence of the direction in the range 270 ± 5^{o} being more by the time delay method.

II.4a.4(b). Apparent drift and anisotropic corrections at Thumba

Phillips and Spencer (1955) have shown that serious errors may arise when patterns are wrongly assumed to be isometric. From an analysis of 15 records, they showed that average errors in the direction was 15^{o} while greatest error was 53^{o}. The ratio V_a / V' had a mean value 0.9 and smallest value 0.60 showing that while on the average errors are not serious, individual error could be considerably large. They further showed that the apparent direction ϕ_a tends to lie in the direction of minor axes as expected on theoretical grounds.

An estimate of the anisotropic corrections has been made for the diffraction patterns at Thumba in the year 1964. Over 600 records were analysed using the method of Phillips and Spencer. As the diffraction patterns at Thumba are highly elongated along N-S (the axial ratios for the diffraction patterns at Thumba for the period

January - December 1964 range from 1 to 10 with mean value of 3) correction in the direction ($\phi - \phi_a$), ratio V_a/V' and the quantity ($\phi_a - \Psi$) were computed for eachpattern and grouped in three ranges of axial ratios:

(1) $2 \leq r \geq 1$

(2) $3 \leq r \geq 2$

and (3) $r > 3$

For a particular group of axial ratios, correction factors $\phi - \phi_a$ and V_a/V' were calculated in different ranges of the parameter ($\phi_a - \Psi$). Figure II.4.9 shows the effect of r and the factor ($\phi_a - \Psi$) on the correction of direction. The points plotted show the corrections as observed while curves represent the theoretical estimates of

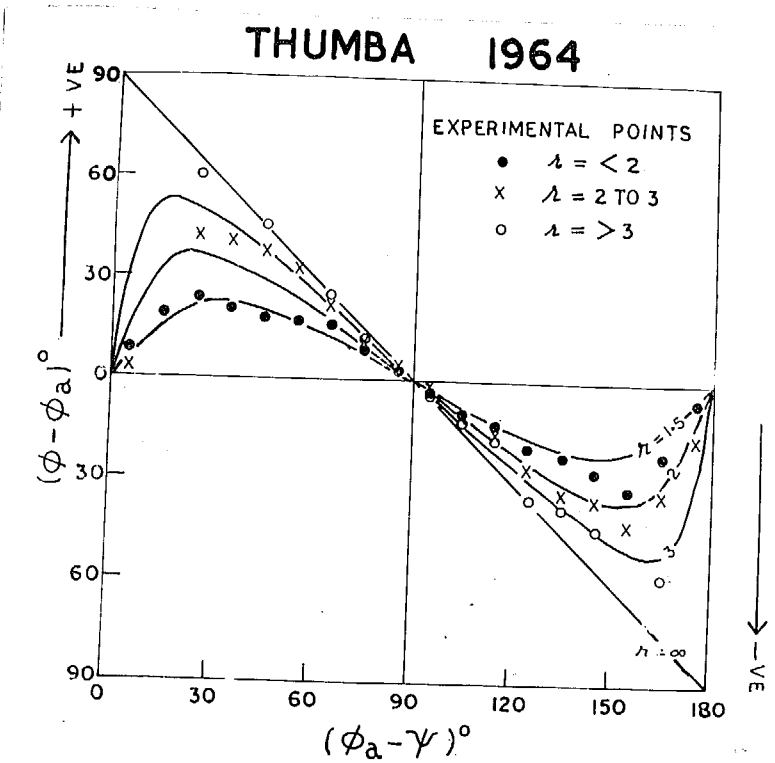

Fig. II.4.9

the correction as a function of axial ratio r and $(\phi_a - \psi)$. Thus for a particular value of $(\phi_a - \psi)$ correction increases with the value of r. Corrections as high as 60° have been observed. Highest correction theoretically possible is 90° for $r = \infty$, and $\phi_a - \psi = 0$ or π that is when motion is along the elongation and is unable to be detected. There is no correction for $\phi_a - \psi = 90°$. For any particular value of r the maximum correction occurs at a certain value of $\phi_a - \psi$, let us call it θ; the maxima occur at θ and $\pi - \theta$, with the increase of r, θ decreases approaching 0 at $r = \infty$.

The factor V_a / V' as a function of r and $(\phi_a - \psi)$ is shown in Fig. II.4.10. There is no correction at $(\phi_a - \psi) = \pi/2$. Theoretical curves show maximum correction at $\phi_a - \psi = 0$ or 180° for $r = \infty$ when motion is along the elongation. From experimental values correction factor as low as 0.50 has been observed.

It should be remarked that corrections of this order are very rare statistically. Most of the points lie around $\phi_a - \psi = 90°$ where correction is very low. Histograms have been computed for $\phi_a - \psi$, $\phi - \phi_a$ and V_a / V' and are shown in Fig. II.4.11 as percentage occurrences. $\phi_a - \psi$ generally ranges from 20° to 160° with median value 95°.

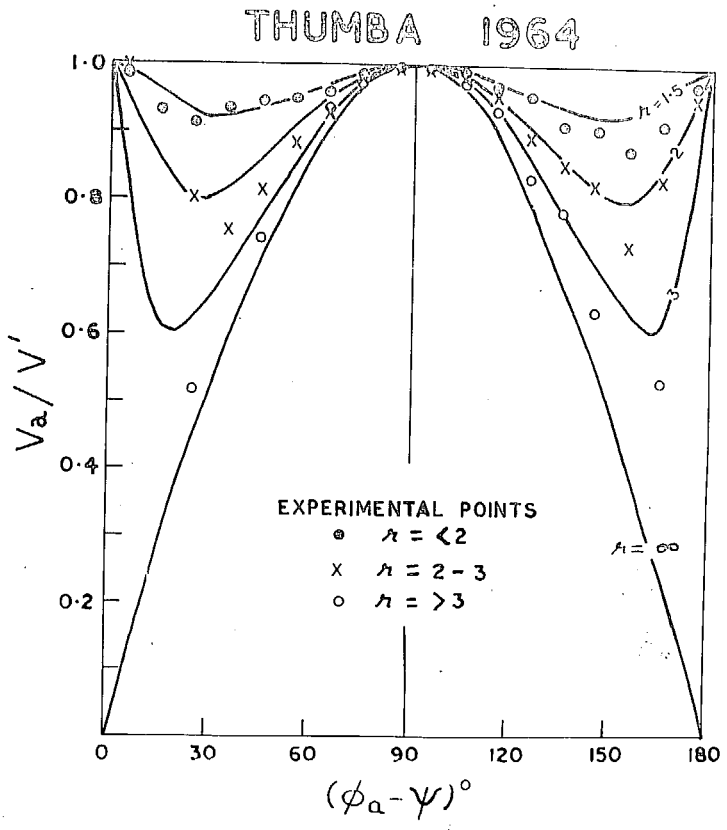

Fig. II.4.10.

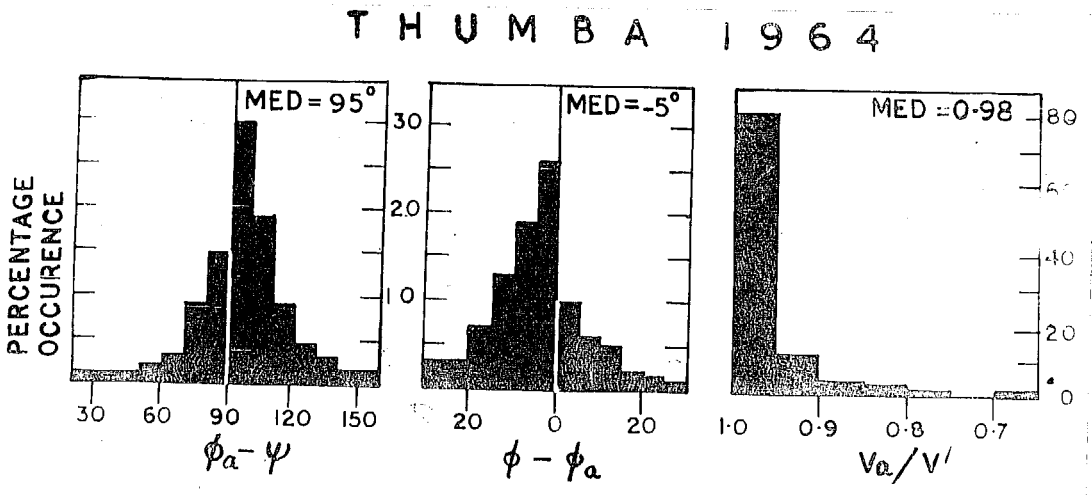

Fig. II.4.11.

On 80% of the occasions, it lies between 70° and 110°.

The correction in direction ranges from -30° to 30° with median value -5°. The correction is within $\pm 10^{\circ}$ on more than 50% occasions.

The correction factor V_a/V' ranges from 1.0 to 0.6 with a median value of 0.98, on 80% occurrences it is within the limits .95 to 1.0.

Thus even for the highly elongated diffraction patterns obtained at Thumba, there is no siginificant error introduced in the determination of apparent drifts, because of the tendency of the drift along the minor axis of the pattern.

Further as already shown the apparent drifts calculated by mean time delays are not significantly different from those calculated by correlation peaks, the routine analysis from mean time delays is justified. Only other parameter that remains to be evaluated is V_c/V to find the relation between steady drift of the pattern and apparent drift. Next sub-chapter describes the correlation analysis done at Thumba to study the relation between true drift speed and the apparent drift speed.

CHAPTER - II.4(b) - STEADY AND RANDOM DRIFT COMPONENTS AT THUMBA

INTRODUCTION

As described in the previous section, the drifts calculated by mean time delays or by peak cross correlation lags are in general higher than the steady drifts of the pattern. The differences arising due to the contributions in fading of the changes in the ground diffraction pattern as it moves past the observing points. The relationship between the apparent drift and the steady drift is given by the equations

$$V_c'^2 = V_c^2 + V^2 \qquad \ldots(1)$$

$$V_c'^2 = V' V \qquad \ldots(2)$$

where V_c' is the fading velocity as defined earlier and V_c the random component of the drift. The ratio V_c/V has been interpreted as the factor showing the relative stability of the diffraction pattern as it moves. For a pattern moving uniformly without any changes in it, (V_c/V) is zero and for such a case $V' = V$.

In general the quantities V' and V are related by the relationship

$$V' = V\left[1 + \left(\frac{V_c}{V}\right)^2\right] \qquad \ldots(3)$$

which shows that V' is in general greater than V depending on the ratio V_c/V. As it is not possible to determine all drift parameters on a routine basis, time delay method has been employed on day-to-day basis. However, it is essential to know parameter V_c/V and its variation with solar time, so that apparent drifts can be connected to actual drifts.

A study of the steady (V) and random (V_c) components of drifts was done for the Thumba data in the year 1964 and results are described by Deshpande and Rastogi (1966). The method of Briggs et al was applied to about 800 records. An average value 0.91 of the ratio V_c/V was obtained for E-region and 0.81 for F-region records. Daily variation of V_c and V was of same nature during each season.

The ground diffraction patterns were found to be elongated along N-S direction with mean axial ratio (r) of the order of 3 for both E- and F-regions, when size and shape of the patterns were calculated using the method described by Fooks (1965). Owing to the high elongation of the patterns obtained at Thumba, the analysis of records is redone using Phillips and Spencer method which takes into account the anisotropy of the pattern. The method consists of evaluating the characteristic ellipse parameters and

then various velocities can be calculated as described in the last section. (value of V_c/V has been given for the direction of drift following Fooks and Jones, 1961).

II.4b.1. True drift parameters in the year 1964

Figure II.4.12 shows the histograms of the percentage occurrence of the ratio V_c/V along the direction of drift for each season. This ratio shows the relative importance of the random changes of the pattern to the steady drift. Individual values range from nearly zero to more than 3.0. The median values of this ratio are 0.95 for the E-region and 0.70 for the F-region. Thus the apparent drift speeds for the E-region are 1.9 times the true drift speed while for the

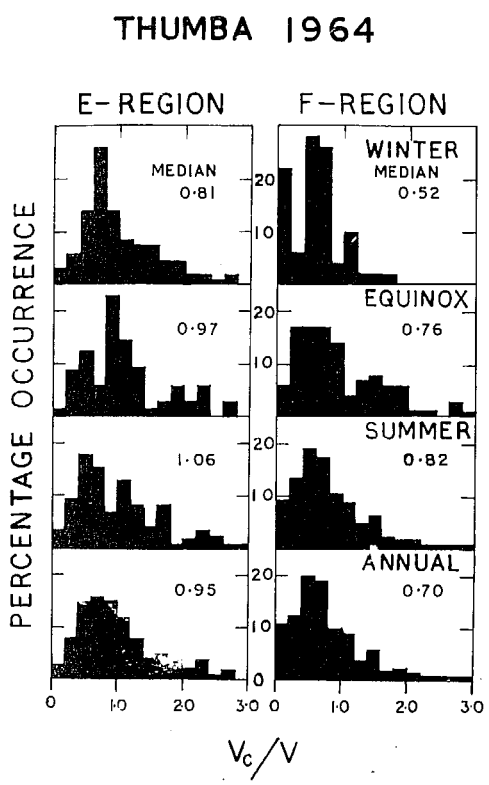

Fig. II.4.12

F-region they are 1.5 times the true drift speed. This means that the random changes in the diffraction pattern are more in case of E-region reflections, or the irregularities are less stable in the E-region. Seasonally the median values of V_a/V for E-region are 0.81, 0.97 and 1.06 for winter, equinoxes and summer respectively. For F-region, the values are 0.52, 0.76 and 0.82 respectively in different seasons. Thus the ratio V_a/V is minimum during winter season and maximum during the summer season.

The apparent drift speed without anisotropic correction V_a as calculated from the correlation peaks which is more or less the same as that calculated from mean time delays, the true drift speed V and the true drift direction ϕ in each season are shown in Fig. II.4.13.

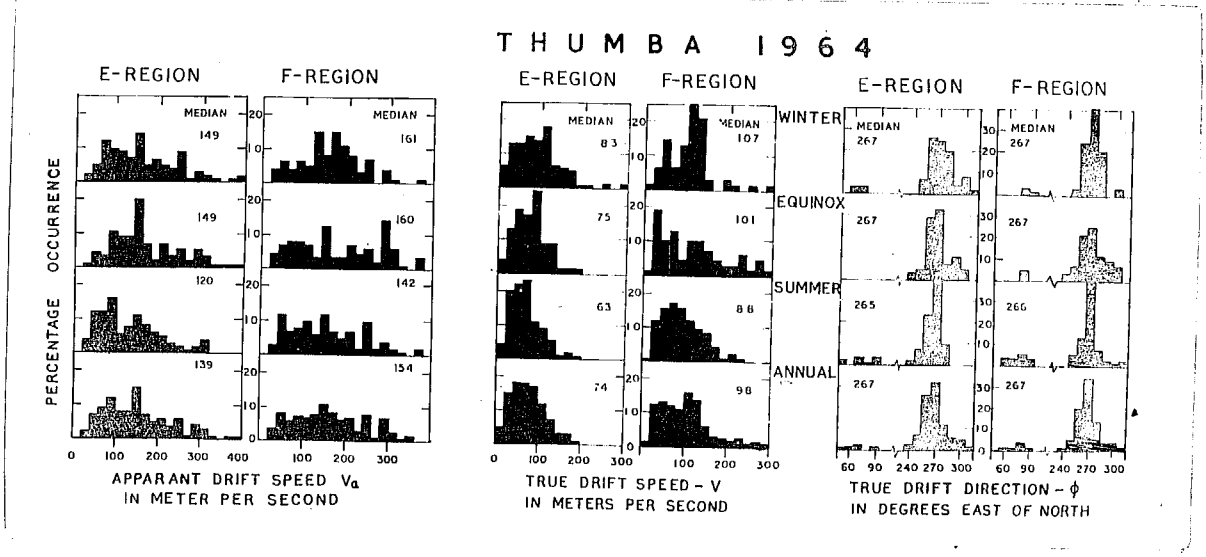

Fig. II.4.13

as histograms of percentage occurrences. Histograms for V_a and V have been computed in the speed steps of 20 m/sec each. V_a ranges from 20 m/sec to 400 m/sec while values of V range from less than 20 m/sec to 300 m/sec. The histograms for V_a show scatter in the high speed ranges which are removed in the histograms for V. The median values of V_a are 139 m/sec for the E-region and 154 m/sec for the F-region. Corresponding values of true drifts V are 74 m/sec for the E-region and 98 m/sec for F-region, which give the ratio V_a/V as 1.9 for the E-region and 1.6 for the F-region. The median values of for different seasons, winter, equinoxes and summer are 149, 149 and 120 m/sec for E-region and 161, 160 and 142 m/sec for F-region respectively. Thus for both E- and F-regions apparent drifts are lowest during summer and equal during winter and equinoxes. Referring to the median values of V, they are 83, 75 and 63 m/sec for the E-region and 107, 101 and 88 m/sec for F-region during individual seasons. Thus the true drifts are also lowest during the summer season. However, true drifts are highest during winter in contrast to equal values of apparent drifts during winter and equinoxes. This being because of the fact that the ratio V_a/V is lowest during the winter season.

True drift direction ϕ is mostly towards West.

TABLE-II.4.1

Daytime drift parameters during 1964

Period	Counts	Apparent drift speed V_a (in m/sec) Mean	Med.	True drift speed V (in m/sec) Mean	Med.	Ratio random to steady drift V_c/V Mean	Med.
			E-REGION - 2.2 Mc/s				
Winter	144	163 ± 8	149	92 ± 5	83	1.04 ± .04	.81
Equinoxes	86	177 ± 10	149	78 ± 5	75	1.17 ± .07	.97
Summer	120	166 ± 5	120	71 ± 4	63	1.33 ± .09	1.06
Annual	350	169 ± 8	139	80 ± 5	74	1.18 ± .07	.95
			F-REGION - 4.7 Mc/s				
Winter	70	165 ± 8	161	110 ± 5	107	0.59 ± .05	.52
Equinoxes	91	188 ± 11	160	115 ± 9	101	1.08 ± .13	.76
Summer	105	177 ± 10	142	96 ± 6	88	1.10 ± .09	.82
Annual	266	177 ± 10	154	107 ± 7	99	0.92 ± .10	.70

Histograms for ϕ have been divided in small steps of 10^{o} each. Over 90% of occasions, direction lies in the range 235^{o} to 315^{o} measured East of North while over 65% occasions it lies in the range 270 ± 15^{o}. There is no seasonal effect which could be observed.

II.4b.2. Daily variations of drift parameters during 1964

Daily variations of the ratio V_c/V and V during daytime hours (07-18) are shown in Fig. II.4.14. There is

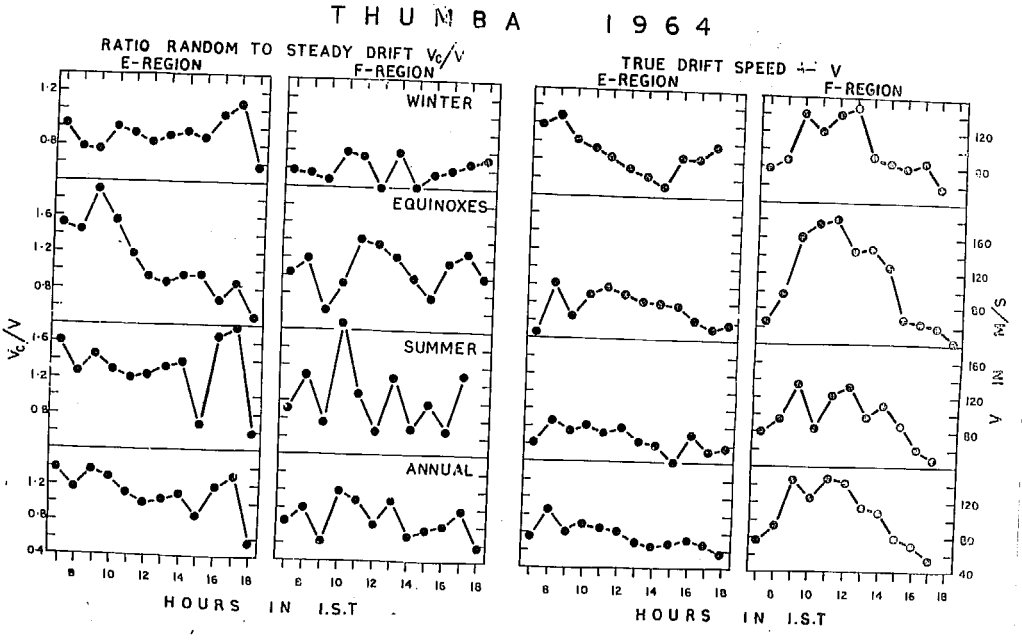

Fig. II.4.14

no significant systematic variation in the mean values of V_e/V which could be observed for either of the regions. Daily variation of true drift speed V is practically of same nature as of the apparent drifts obtained at Thumba. For the E-region, the nature of the variation is different during the winter season. There is maximum at 08 hrs. followed by decrease till 14 hrs. and then again an increase in the evening hours. During equinoxes and summer there is a maximum at 08 hrs. followed by slow decrease till evening. The range of variation is least during summer for any of the regions. Peak value of mean drift speed obtained in the E-region is about 125 m/sec during the winter, about 100 m/sec during the equinoxes and about 85 m/sec during summer. Corresponding values for F-region are about 140 m/sec during winter, about 180 m/sec during the equinoxes and about 130 m/sec during the summer season.

Daily variation of the mean drift direction is shown in Fig. II.4.15. The drift direction is Westward throughout the daytime hours (07 to 18) for both the E- and F- regions. Annual picture shows drift direction for both the regions centred about 270° North of East with departures upto $\pm 10^{\circ}$ at individual hours. Drift direction lies North of West before noon while it is South of West in the afternoon. Seasonally in the E-region, there is a tendency of drift

direction to lie North of West during winter, along true West during equinoxes and South of West during summer. In the F-region, there is no such seasonal differences. However, Southward component is observed in the evening hours during any of the seasons.

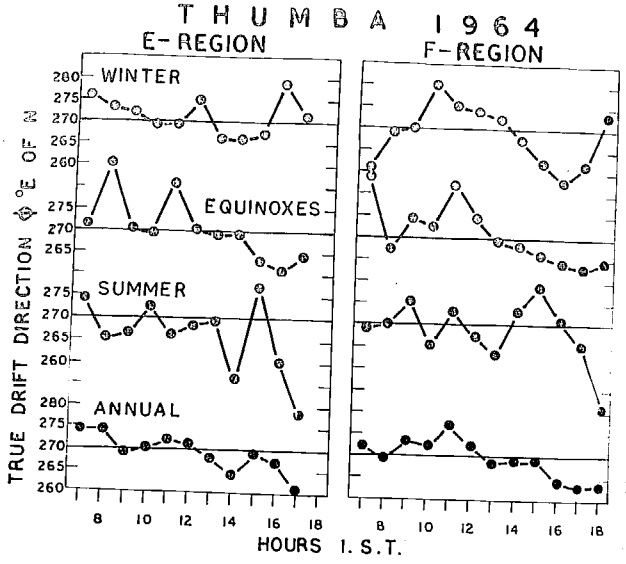

Fig.II.4.15.

II.4b.3. True drift parameters during the year 1967

The correlation analysis was applied to more than 800 fading records taken during the year 1967, out of these a large number of records were taken for the F-region to study the complete daily variation in the F-region drifts.

True drift parameters for the E-region are shown in Fig. II.4.16. Referring to the parameter V_d its median values are 100 m/sec during winter, 115 m/sec during equinoxes and 83 m/sec during the summer. True drift speed (V) for the corresponding seasons are 78, 75 and 65 m/sec. respectively (median values). Thus again one finds the lowest drift speeds to occur during summer. The values of

the ratio V_a/V are 0.56 during winter, 0.70 during the

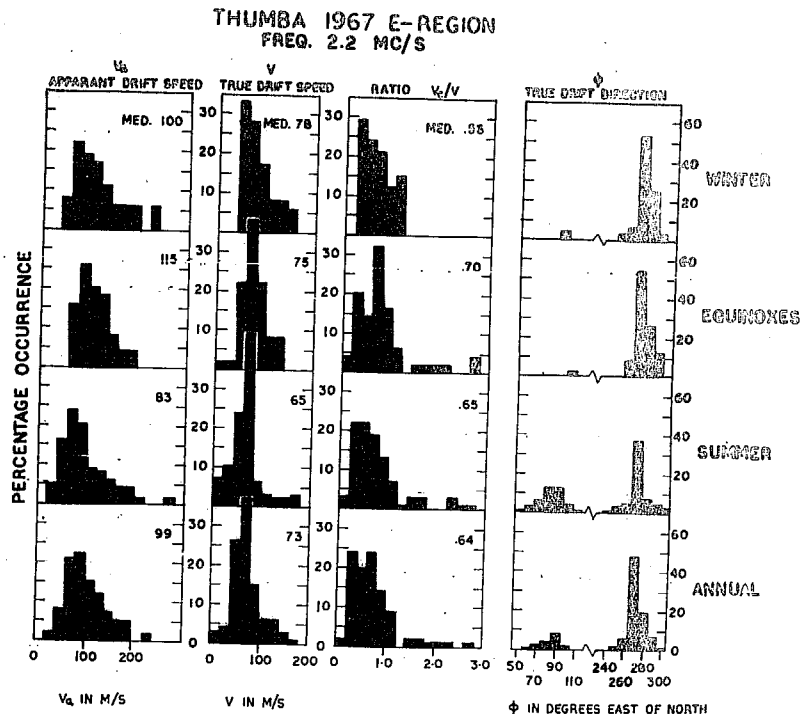

Fig. II.4.16.

equinoxes and 0.65 during summer. It should be noted that the ratio V_a/V was lowest during winter in the year 1964 also. The direction of the true drift is mainly Westward lying in the range of 235° to 305° measured from North in the clockwise sense. During the seasons winter and equinoxes, more than 50% of occasions, the drift direction lies

TABLE-II.4.2

Daytime drift parameters at Thumba during 1967 -

E - REGION 2.2 Mc/s

Period	Counts	Apparent drift speed V_a (in m/sec)		True drift speed V (in m/sec)		Ratio random to steady drift V_c/V	
		Mean	Med	Mean	Med	Mean	Med
Winter	36	112 ± 8	100	80 ± 5	78	.58 ± .05	.56
Equinoxes	51	125 ± 10	115	77 ± 5	75	.78 ± .08	.70
Summer	67	93 ± 6	83	65 ± 4	65	.76 ± .08	.65
Annual	154	105 ± 8	93	74 ± 5	73	.69 ± .07	.63

in the range 270 ± 5° and is in the range 265° to 285° on about 80% occasions. During the summer, the percentage of occasions in the range 270 ± 5° is less than 40% and in the range 265° to 285° less than 50%. A marked difference during summer season is Eastward drift on about 35% of occasions. Most of such Eastward drift directions are observed either in the morning hours or in the evening hours.

Similar histograms for the parameters of true drift in the F-region are shown in Figs. II.4.17, II.4.18 and II.4.19. The F-region histograms have been computed separately for daytime (07 to 18 hrs.) and nighttime (19-06 hrs.). In Fig. II.4.17 are shown the histograms of percentage occurrences of the ratio V_c/V. Histograms have been computed upto a ratio 3.0 but there are only a few values of V_c/V beyond the value 2.0. The median values of this ratio in daytime are 0.56 for winter, 0.46 for equinoxes and 0.59 for the

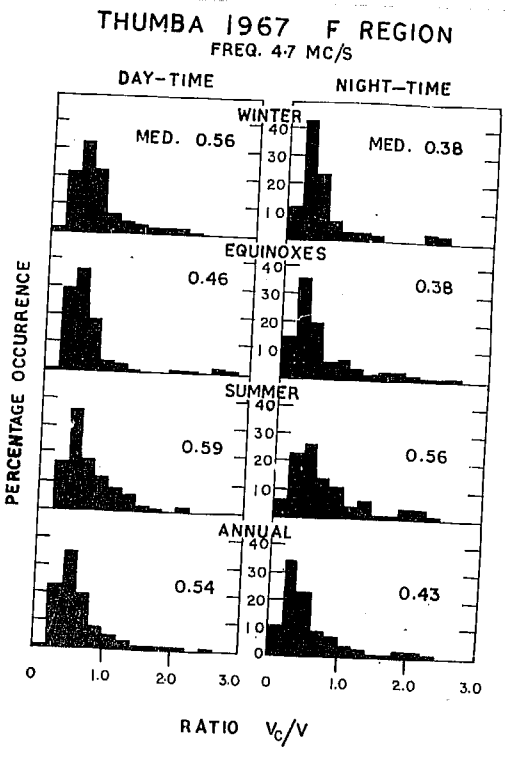

Fig. II.4.17.

summer season. Corresponding values in the nighttime are 0.38 during the winter, 0.38 during the equinoxes and 0.56 during summer seasons. Thus, the daytime values of V_a/V are the higher one than the nighttime values during any of the seasons. Seasonally the values seem to be highest during summer for both daytime as well as nighttime. Histograms for V_a and V are shown in Fig. II.4.18. The histograms for V_a

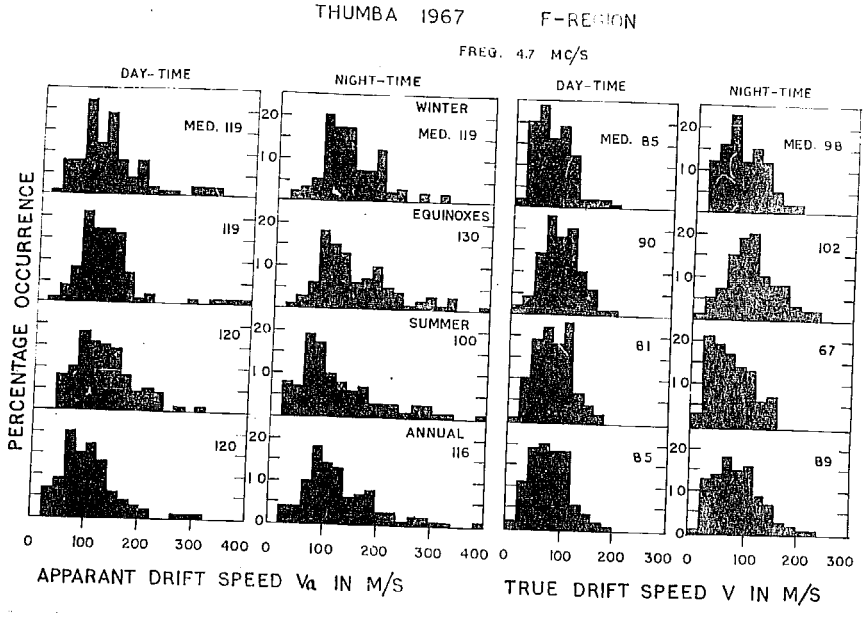

Fig. II.4.18

show scatter in the higher side of the histograms which are smoothed out in the histograms of true drift speed V. This is expected as records with high values of V_a/V give

rise to very high apparent drift speeds. The median values of apparent drift speed V_d in the daytime are 119 m/sec during winter and equinoxes and 120 m/sec during summer while in nighttime it is 119 m/sec during winter, 130 m/sec during equinoxes and 100 m/sec during summer. Thus the apparent drift speeds are equal in the daytime and nighttime during winter. During the equinoxes, nighttime values are higher while during summer daytime values are higher.

True drift speeds after anisotropic correction and separation of random components are reduced by about 25 to 30%. During daytime, the true drift speeds are 85 m/sec during winter, 90 m/sec during equinoxes and 81 m/sec during summer. Corresponding values in the nighttime are 98, 102 and 67 m/sec respectively. Thus drift speeds are highest during equinoxes and lowest during summer for both daytime and nighttime periods. However, the differences are quite less in the daytime.

The histograms for the F-region drift directions are shown in Fig. II.4.19. During daytime, the direction is closely Westward with more than 70% of occasions lying in the range 270 ± 5^{o} during winter, about 60% of occasions during equinoxes and about 50% of occasions during summer. On few occasions, there is Eastward direction for the drift which is maximum during the summer season (about 20%) and least during equinoxes (about 4%). This Eastward drift

during daytime hours which is quite significant during equinoxes (about 4%). This Eastward drift during daytime hours which is quite significant during summer is as a result of late reversal of drift direction in the morning and early reversal in the evening. Nighttime drift direction is again Eastward with 75% of occasions direction lying within the range 270 $\pm$ 15°.

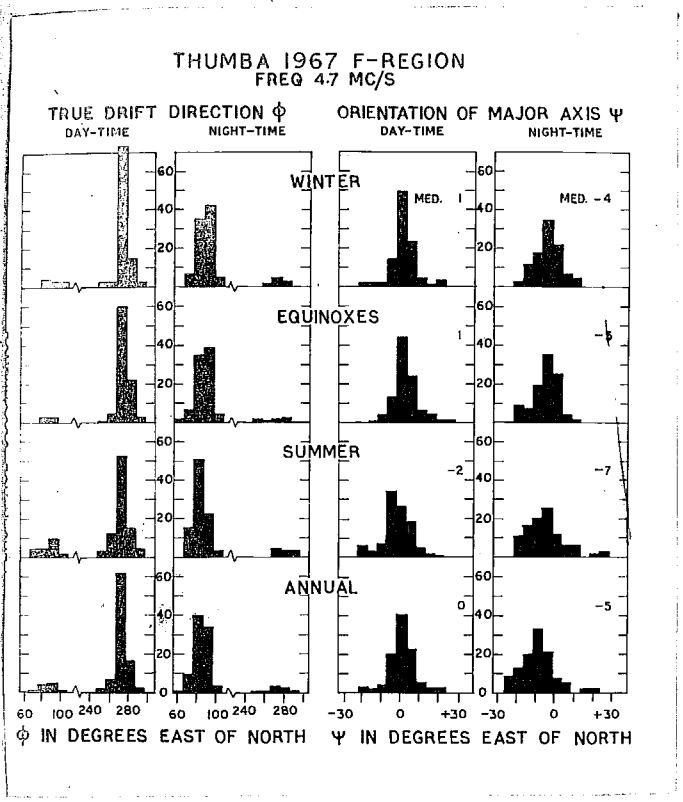

Fig. II.4.19

II.4b.4. Daily variations of true drift parameters during 1967

Daily variations of the true drift speed V and the ratio V_E/V for E-region are shown in Fig. II.4.20. As the records analysed for E-region are only about 150 seasonal study is not done. The daily variation of true drift speed V shows a rise in the morning reaching a maximum at

08 hrs. It is followed by decrease till noon. Another increase is observed in the evening hours. The daily variation of V_c/V does not show any significant change. It remains more or less steady in the range 0.60 to 0.90. The values at 13 hrs. and 14 hrs. seem to be quite low but as the observations around noon time are very few in the E-region due to the insufficient power of the transmitter importance should not be given to these points.

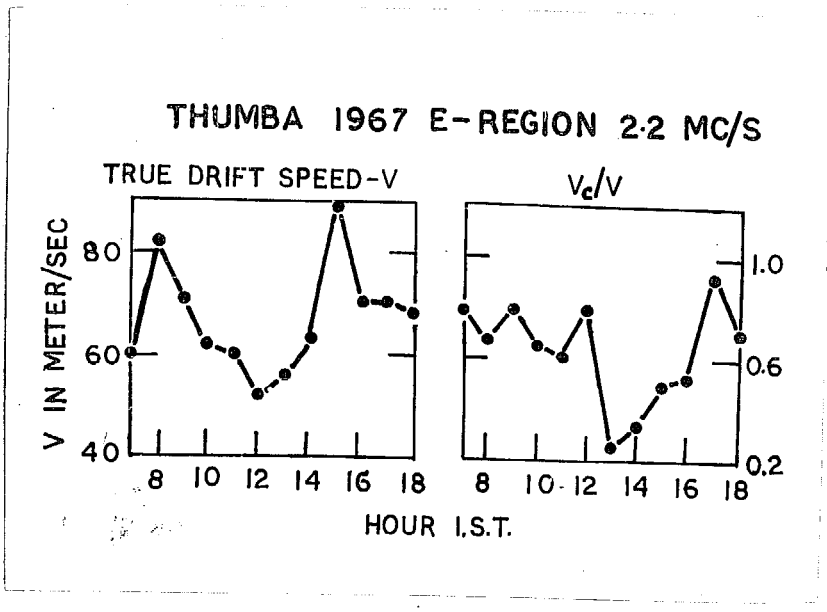

Fig. II.4.20.

The diurnal variation of the true drift speed V and the ratio V_c/V for F-region are shown in Fig. II.4.21. Nature of the variations for both the parameters are same during any of the seasons. Referring to the annual variation for V, its value decreases from midnight upto 04 hrs., there is sudden increase at 05 and at 06 hrs. The value decreases suddenly reaching minimum at 07 hrs. Another maximum is observed about noon. There is again slow decrease till evening

TABLE-II.4.3

Drift parameters at Thumba during 1967

F - REGION - 4.7 Mc/s

Period	Counts	Apparent drift speed V_a (in m/sec)		The drift speed V (in m/sec)		Ratio random to steady drift V_c/V	
		Mean	Med	Mean	Med	Mean	Med
DAYTIME							
Winter	121	130 ± 4	119	89 ± 4	85	.63 ± .03	.56
Equinoxes	159	125 ± 5	119	90 ± 3	90	.58 ± .04	.46
Summer	105	126 ± 5	120	82 ± 3	81	.70 ± .05	.59
Annual	385	127 ± 5	120	87 ± 3	85	.60 ± .04	.52
NIGHTTIME							
Winter	59	130 ± 7	119	103 ± 6	98	.47 ± .05	.38
Equinoxes	119	155 ± 7	130	107 ± 4	102	.55 ± .06	.38
Summer	73	134 ± 9	100	75 ± 5	67	.63 ± .09	.56
Annual	251	140 ± 8	116	95 ± 5	89	.55 ± .07	.44

Once again maxima is observed at about 22 hr. in the night.

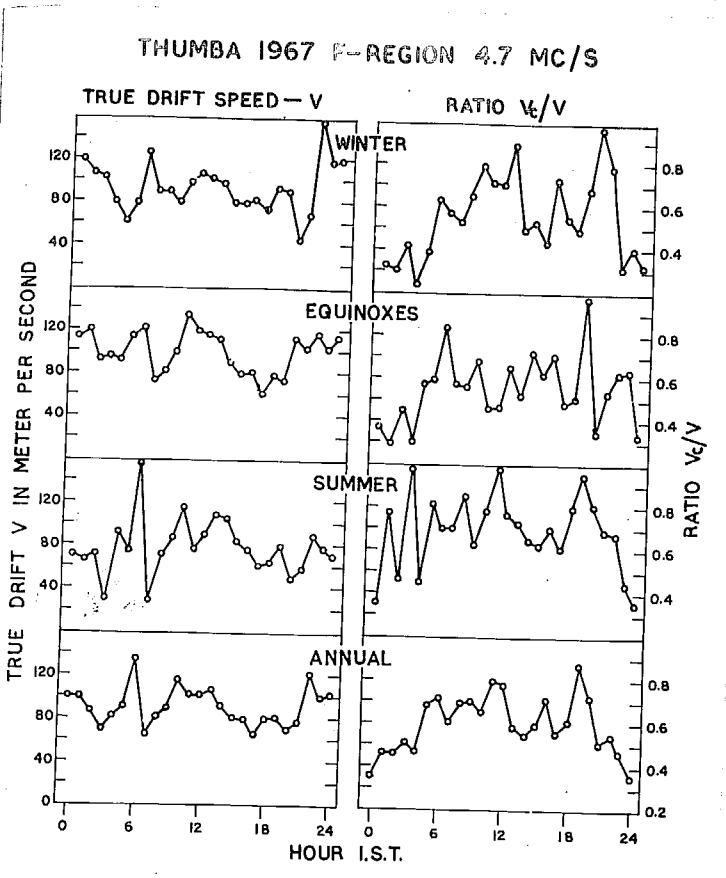

Fig. II.4.21

The values of V are plotted irrespective of the direction to make a comparison with the variation of V_c/V. Diurnal variation of V_c/V shows much smoother variation with maximum value around noon and minimum value during night hours. A sudden increase is observed at 19 hrs. during any of the season. Thus the daytime apparent drifts will be much higher to the true drifts compared to nighttime apparent drifts.

As the true drift direction is always true West or East, harmonic analysis was applied to the E-W component of true drift only. In Fig. II.4.22 are shown the mean diurnal variation of the East-West component of true drift speed. Open circles represent the mean values at different hours and the smooth curve is built up from the first four har-

monics of the Fourier analysis. The coefficients of first four harmonics are given in Table II.4.4. Nature of the curve is mainly diurnal with maximum Eastward drift at 23.00 hr. and maximum Westward drift at 10.00 hr. An important feature of the daily variation curve is a significant increase in the drift speed prior to morning reversal which is observed in each season. Similar increase seems to occur before evening reversal during winter and equinoxes but is not observed in summer season. Morning reversal occurs shortly before 07 hrs. during winter and equinoxes and shortly before 08 hrs. during summer. Evening reversal occurs shortly before 20 hr. during winter, shortly after 20 hr. during equinoxes, and shortly before 19 hr. during the summer. Thus Eastward drifts are observed for longest time during summer while Westward drifts are observed for

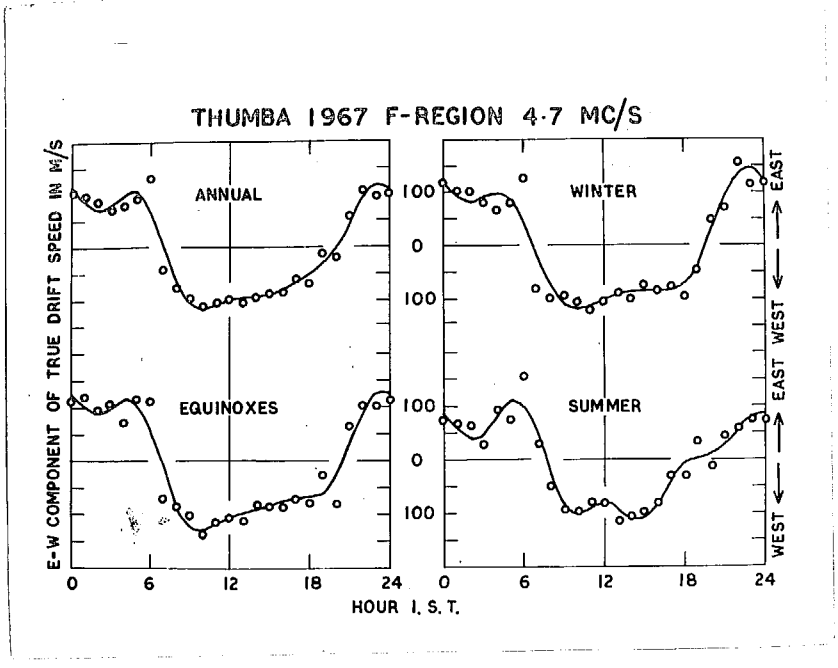

Fig. II.4.22

TABLE-II.4.4

Harmonic coefficients of the daily variation of the E-W component of true drift speed at Thumba.

Period	Amplitude in m/sec					Time of maxima in hour (Local time)				Morning reversal hour	Evening reversal hour
	a_0 m/sec	A_1 m/sec	A_2 m/sec	A_3 m/sec	A_4 m/sec	ϕ_1 hour	ϕ_2 hour	ϕ_3 hour	ϕ_4 hour		
Winter 1967	-3	124	15	36	14	0.7	1.0	5.6	4.6	6.7	19.6
Equinoxes 1967	-9	122	27	28	20	1.2	2.4	5.9	5.1	6.8	20.4
Summer 1967	-3	96	24	21	28	1.4	6.0	5.6	3.6	7.7	18.5
Annual 1967	-5	114	11	28	18	1.1	3.2	5.7	5.3	7.0	20.0

longest time during equinoxes.

The amplitude of the first harmonic is 124 m/sec during Winter, 122 m/sec during equinoxes and 96 m/sec during summer respectively with maxima occurring around 01 hr. in each season. The second, third and fourth harmonics are of comparable order ranging from 15 m/sec to 35 m/sec in different seasons.

II.4b.5. Comparison of true drift parameters in the years 1964 and 1967

A comparison of the true drift speed V and the ratio V_c/V in the years 1964 and 1967 can be made from Tables, II.4.1, II.4.2 and II.4.3. Number of observations, mean values with probable errors and the median values for each season are quoted in the table. Referring to the E-region the annual mean values for the drift speed V are, 80 $\pm$ 5 m/sec. in the year 1964 and 74 $\pm$ 5 m/sec. in the year 1967 while the median values are 74 m/sec and 73 m/sec. respectively. Thus there is no significant difference between the drift values in the years 1964 and 1967. Seasonally one finds a decrease in the drift speed in the year 1967 during winter season while there is no difference during equinoxes and summer. The drift speeds are highest during winter and lowest during summer in both the years.

Annual mean value for V_c/V is 1.18 $\pm$ .07 in the year

1964 and .69 ± .07 in the year 1967; the median values are .95 and .63 respectively. Thus there is appreciable decrease in the ratio V_c/V from 1964 to 1967, which shows that the random changes in the diffraction pattern are less in the year 1967. During any of the season V_c/V has lower values in the year 1967. The values of V_c/V are lowest during winter season in both the years while higher values are observed during summer than during equinoxes in the year 1964 and comparable values are observed in the year 1967.

Referring to F-region, the drift speeds seems to be higher in the year 1964. The annual mean values for the years 1964 and 1967 are 107 ± 7 m/sec and 87 ± 3 m/sec respectively while the median values are 99 m/sec and 85 m/sec respectively. There is decrease in the drift speed in the year 1967 for each season. In the year 1964, highest drift speeds are during equinoxes and lowest during summer, but in the year 1967 drift speeds are equal during winter and equinoxes with lowest speed during summer. The values of V_c/V show a decrease in the year 1967 during any of the seasons. Annual mean values for the year 1964 and 1967 are .92 ± .10 and .60 ± .04 respectively. The median values are .70 and .52 respectively.

It may be concluded that the ratio V_c/V has lower values in the year 1967 for both E- and F-region records. E-region values are higher than the F-region values during

each season of both the years showing that the diffraction patterns are more stable for the F-region reflections. True drift speed in the E-region does not show any significant difference from 1964 to 1967 but a decrease in the true drift in the F-region is observed for the year 1967.

II.4b.6. Comparison with the results obtained at other equatorial stations

True drift parameters have been computed using correlation analysis at the equatorial stations namely Ibadan (Skinner et al, 1963), Tamale (Koster and Katsriku, 1966) and Waltair (Rao and Rao 1963). The results obtained for these stations are quoted in the Table II.4.5. For comparison, the results obtained at high latitude station, Cambridge (Fooks and Jones, 1961), are also quoted. The true drift speed V is found to be higher at stations near the magnetic equator. For the E-region in daytime hours the true drift speed is about 80 m/sec at Thumba, 67 m/sec at Tamale and 55 m/sec at Ibadan showing a gradual decrease in the drift speed away from the equator. The true drift speed obtained at Waltair is about 80 m/sec. However, while at Thumba and Ibadan the values of true drift speeds are much less than the corresponding apparent drift speeds, they are equal at Waltair, even though the ratio V_c/V is quoted to be 0.71. Similarly, the daytime F-region drift

speeds are higher near the magnetic equator except at Waltair where true drift speed is again higher than apparent drift speed. It should be remarked that the true drift quoted for Waltair is higher than the apparent drift and is not understood considering the ratio V_c/V to be 0.67.

The mean ratio V_c/V is found to be 0.9 - 1.2 at Thumba in the year 1964 and 0.6 - 0.7 in the year 1967. For Ibadan and Tamale also, the ratio V_c/V is between 0.6 - 0.8. Thus, in general, the value of V_c/V in the equatorial region is in the range 0.6 - 0.8 which shows that the steady drift has got more contribution in the fading pattern obtained on the ground. At each station, V_c/V is found to be higher for the E-region.

Skinner et al (1958) have studied true drift at Ibadan during IGY period. They obtained drift direction to be Westward during the daytime and Eastward during the nighttime with reversal occurring at about 06 hr. and 19.30 hr. From the harmonic analysis of the true drift speeds in the F-region, they obtained the amplitude of the first harmonic 99 m/sec on quiet days and 68 m/sec on distrubed days. Further the amplitudes of the first harmonic in the seasons winter, equinoxes and summer were 112 m/sec, 97 m/sec and 76 m/sec respectively for quiet days; 85 m/sec, 66 m/sec and 56 m/sec respectively for the disturbed days,

the maxima in each season occurring at about 01 hr. These results are in good agreement with those obtained at Thumba. The maxima occurring at 01 hr. with first harmonic amplitudes of 124 m/sec, 122 m/sec and 96 m/sec respectively in the seasons winter, equinoxes and summer.

Morris (1967) has studied the true drift speeds at Ibadan during IQSY. The nature of variation remained same with change over of direction occurring at about 06 hr. in the morning and at about 20 hr. in the evening. However, the magnitude of drift speed was significantly lower than that obtained by Skinner et al during the IGY period. The diurnal curve shown by them shows similar variation as that at Thumba with increase in the drift speed before reversal in the morning and suggestion of similar increase before the reversal in the evening. Maximum daytime velocities were found to occur in January and minimum in May while maximum nighttime velocities occurred during equinoxes with minimum in June. Time of occurrence of the maximum daytime velocity was found to be earliest during equinoxes and latest during summer.

TABLE - II.4.5

Comparison of the true drift parameters at different stations

Station	Mag.Lat.	Period of study	Region	Counts	V_a	V	V_c/V	Reference
Thumba	0.3°S	1964	E - Day	350	169	80	1.18	
			F - Day	266	177	107	0.92	
		1967	E - Day	154	105	74	0.69	
			F - Day	385	127	87	0.60	
			F - Night	251	140	95	0.55	
Tamale	0.6°S	Feb -Mar. 1962	E - Day	43		67	0.8	Koster and Katsriku (1966)
			F - Day	83		115	0.5	
			F - Night	38		70		
Ibadan	3.0°S	IGY	E - Day	1000		55	0.8	Skinner et al (1963)
			F - Day			70	0.6	
			F - Night					
		IGY	E - Day	24				Skinner et al (1958)
			F	25				
Waltair	11°N	Sum. 60	E	75	80	79	0.71	Rao and Rao (1963)
		Win. 61	F	95	87	93	0.67	
Cambridge	50°N	Mar -Apr. 1955	E - Day	39			0.08	Fooks and Jones (1961)
			F - Day	37			1.2	
		Feb 1958	F - Night	35			0.7	
Ashkhabad	36°N	1960	E_s				0.9	Mirkotan (1962)
Moscow		1959	F_2				1.6	Mirkotan (1962).

CHAPTER II.4c. SIZE AND SHAPE OF THE IONOSPHERIC IRREGULARITIES AT THUMBA

Introduction

A study of the parameters of the characteristic ellipse such as axial ratio r, orientation Ψ and the semi-minor axis b, which represent an average size of the diffraction pattern on ground, was made for the daytime E- and F-region reflections at Thumba in the year 1964. The results obtained from the analysis following Fooks (1965) have been described by Deshpande and Rastogi (1966). The patterns were found to be aligned almost along the magnetic N-S; on about 60% of occasions, the major axis was found to be within 10° from the magnetic N-S for either of the E- or F-regions. The patterns were highly elongated with mean axial ratio of 3.16 and 3.24 for the E- and F-regions respectively. The semi-minor axis b having a mean value of 105 meters for the E-region patterns and 99 meters for the F-region patterns.

Seasonal study of the anisotropy parameters for the daytime E- and F-region reflections in the year 1964 has been described by Deshpande in his Ph.D. thesis. The mean axial ratio was found to be maximum in summer for both E- and F-regions. No significant difference was observed in the mean values of b in different seasons except that the mean

value of b for the F-region records during winter season was smaller than those of other seasons.

II.4c.1. Anisotropy parameters during 1964

The anisotropy parameters of the records analysed earlier were redone when the method of Phillips and Spencer (1955) was applied in the determination of true drift velocities. The only difference in this method and that described by Fooks (1965) lies in the fact that while the first one reads the correlation values at time $t = 0$, later one calculates them from the peak portions of the correlation curves giving statistically better results. The results obtained are described here and compared to those obtained by earlier analysis.

The individual results for the parameter ψ, r and b at different hours are first collected together seasonally for both the E- and F-regions. Histograms of percentage occurrences are computed for each parameter in different seasons and are shown in the Fig. II.4.23. The mean and median values alongwith the number of observations in each season are collected in Table II.4.6.

Referring to the Fig. II.4.23, there are no seasonal differences in the histograms for the orientation ψ, its values ranging from 30° West of geographic North to 30° East of the geographic North. The annual median values

being 6^{o} West of North in case of E-region and 4^{o} West of North in case of F-region. Taking into consideration that the declination at Thumba is -3^{o} (West of geog. North) it can be concluded that the diffraction patterns obtained at Thumba are almost magnetic field aligned. The annual mean

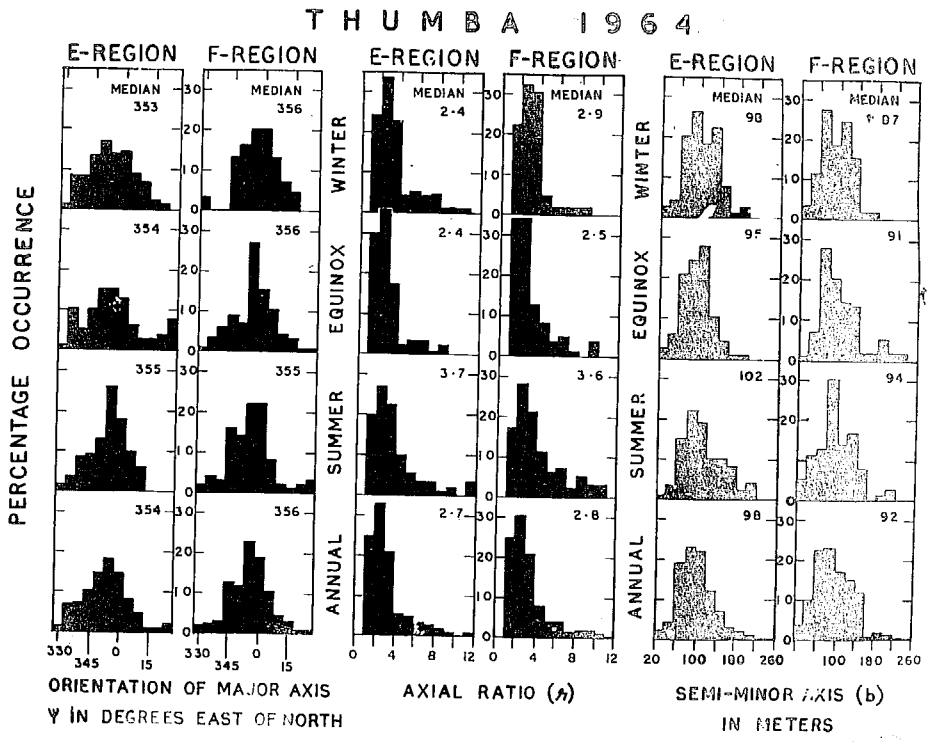

Fig. II.4.23

values of ψ are -4.0 ± 1.5^{o} for the E-region and -3 ± 1.0^{o} for the F-region measured from the geographic North.

TABLE-II.4.6.

Daytime anisotropic parameters at Thumba during 1964.

Period	Counts	Semi-minor axis b (in meter)		Axial Ratio r		Orientation of characteristic ellipse in degrees each of North ψ	
		Mean	Med	Mean	Med	Mean	Med
		E - REGION - 2.2 Mc/s					
Winter	144	99 ± 2	98	3.2 ± .2	2.4	356 ± 2	353
Equinoxes	86	102 ± 5	95	2.9 ± .2	2.4	356 ± 2	354
Summer	120	115 ± 5	102	4.0 ± .1	3.7	355 ± .5	355
Annual	350	105 ± 4	98	3.4 ± .2	2.7	356 ± 1.5	354
		F- REGION - 4.7 Mc/s					
Winter	70	90 ± 3	87	3.0 ± .3	2.9	357 ± 1	356
Equinoxes	91	105 ± 6	91	2.8 ± .2	2.5	358 ± 1	356
Summer	105	105 ± 7	94	3.9 ± .2	3.6	355 ± 1	355
Annual	266	100 ± 5	91	3.2 ± .2	2.8	357 ± 1	356

The axial ratio 'r' at Thumba is found to vary in the range 1 - 12, most of the values lie in the range 1-4. The scatter in the higher axial ratio side of histograms is rare except in summer when significant percentage lies in the higher axial ratio groups. The median values of the axial ratios for the E- and F-regions for the whole year are 2.7 and 2.8 respectively. Thus the axial ratio of the patterns formed due to the reflections from the E- or F-regions are nearly same. The median values in the individual seasons are 2.4, 2.4 and 3.7 for the E-region and 2.9, 2.5 and 3.6 for the F-region during winter, equinoxes and summer seasons respectively. Thus for both the E- and F-regions, the axial ratio is largest during summer. The annual mean values 3.4 ± 0.2 for the E-region and 3.2 ± 0.2 for the F-region are not much different from those obtained earlier by Deshpande (1966). Even individually the axial ratios come out to be practically same as obtained earlier.

The semi-minor axis (b) obtained lie in the range 20-240 meters while most of the values lie in the range 60-140 meters. The annual median values are 98 meters for the E-region and 92 meters for the F-region. Seasonally the values are found to be slightly higher in summer than winter for both the regions. The median values being 98, 95 and 102 meters for the E-region and 87, 91 and 94 meters

for the F-region in the seasons winter, equinoxes and summer in that order. The annual mean values of 105 meter for the E-region and 100 meters for the F-region are same as obtained earlier by Deshpande (1966). Even seasonal mean values are practically identical. Thus the anisotropy parameters calculated according to Phillips and Spencer (1955) and Fooks (1965) using different portions of the correlation curves give practically same results as seen from the analysis of the data for the year 1964.

II.4c.2. Daily variations of anisotropy parameters in the year 1964

The hourly mean values of the parameters r and b are plotted in Fig. II.4.24. There is no systematic daily

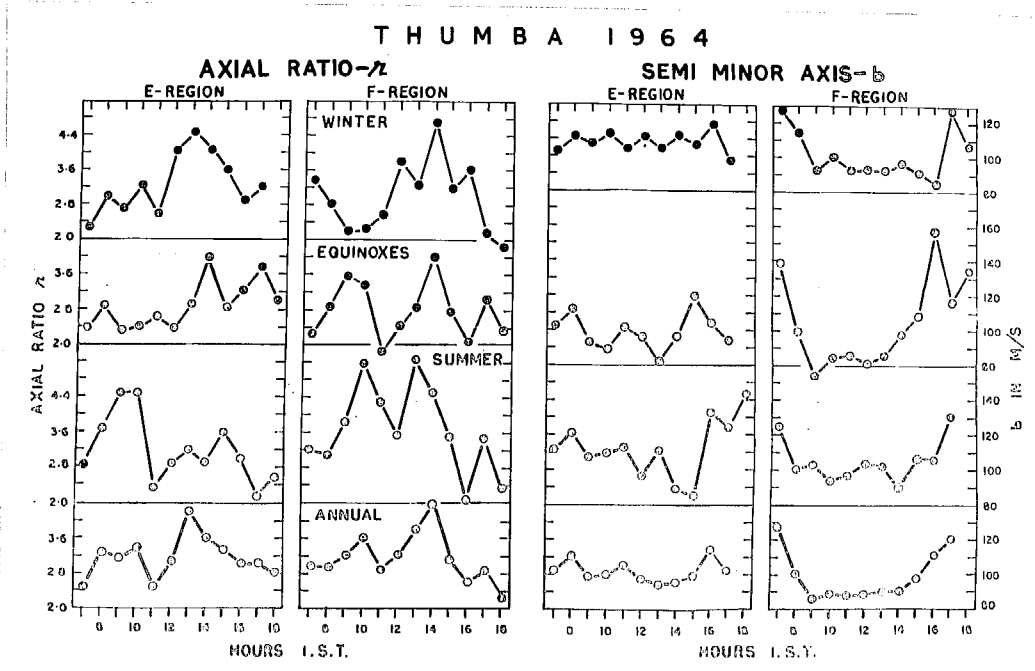

Fig. II.4.24.

variation of the axial ratio r, however the values seem to be lower during early morning and late evening hours, suggesting a maxima during midday hours. The daily variation of the semi-minor axis b is not so clear in the E-region, but a broad minima in the hours 09-14 is found in the F-region. The value of b increases very significantly in the morning and evening hours for the F-region records. In the E-region, the value of b is practically constant with time during winter, but decrease in the midday is clear during equinoxes and summer. For the F-region, the behaviour is similar during each season. The value of b decreases rapidly after sunrise, reaching minima around 09 hrs. and remaining more or less constant upto 14 hr. and again increases in the evening hours.

Daily variation of the orientation ψ is shown in Fig. II.4.25. For the E-region, there is not much variation in the orientation from hour to hour, the orientation being centred at about 5° West of geographic North at all hours. However, F-region records show definite

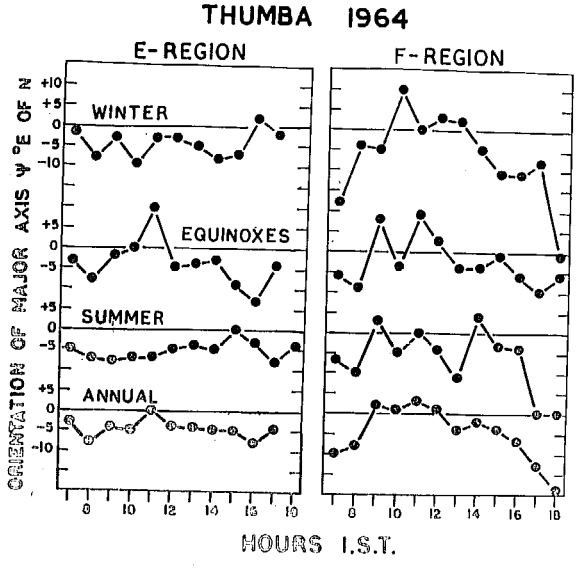

Fig. II.4.25.

daily variation, orientation being more Westward of the geographic North in the morning and evening hours and nearer to the north in midday hours. There is no seasonal difference in the daily variation of orientation.

II.4c.3. Anisotropy parameters in the year 1967

The anisotropy parameters for the daytime E-region reflections and 24 hour F-region reflections have been calculated using the method described by Phillips and Spencer (1955) and Fooks (1965). Seasonal results have been grouped together and histograms have been computed for the E-region daytime, F-region daytime and F-region nighttime records. Figs. II.4.26, II.4.27 and II.4.28 show histograms of the parameters b, r and ψ in each season of the E- and F-region records. The number of records analysed in each season with mean and median values are given in Tables II.4.7 and II.4.8.

Fig. II.4.26 shows the parameters b, r and ψ for the E-region records in each season of the year 1967. Most of the values of b lie in the range 40-140 meters, annual median value being 70 meters which is considerably smaller than the value 98 meters obtained for the year 1964. The seasonal median values are 66, 69 and 74 meters/sec. respectively for winter, equinoxes and summer. Thus the

TABLE-II.4.7.

Daytime anisotropic parameters at Thumba - 1967

E-REGION - 2.2 Mc/s

Period	Counts	Semi-minor axis b (in meter)		Axial ratio $\frac{a}{b}$		Orientation of characteristic ellipse in degrees East of North. ψ	
		Mean	Med.	Mean	Med.	Mean	Med.
Winter	36	70 ± 3	66	6.4 ± .5	5.6	0 ± 1.5	359
Equinoxes	51	71 ± 3	69	6.0 ± .5	5.2	5 ± 0.5	362
Summer	67	85 ± 4	74	5.4 ± .4	5.1	357 ± 1.5	358
Annual	154	75 ± 3	70	5.9 ± .5	5.3	1 ± 1.5	360

TABLE-II.4.8

Anisotropic parameters at Thumba during 1967

F - REGION-4.7 Mc/s

Period	Counts	Semi-minor axis b (in meter)		Axial ratio		Orientation of characteristic ellipse in degrees East of North	
		Mean	Med	Mean	Med	Mean	Med
				DAYTIME			
Winter	121	82 ± 4	68	8.7 ± .6	6.5	1 ± 1	1
Equinoxes	159	71 ± 4	64	13.1 ± .8	8.1	2 ± 2	1
Summer	105	80 ± 6	69	7.0 ± .5	5.6	359 ± 1.5	358
Annual	385	78 ± 5	67	9.6 ± .7	6.7	1 ± 1.5	0
				NIGHTTIME			
Winter	59	135 ± 7	84	8.0 ± .7	6.2	355 ± 1	356
Equinoxes	119	140 ± 4	98	8.6 ± .4	5.9	354 ± 1.5	355
Summer	73	116 ± 8	80	7.0 ± .8	4.6	353 ± 3	353
Annual	251	130 ± 7	87	7.9 ± .7	5.6	354 ± 2	355

semi-minor axis of the pattern seems to be greater in

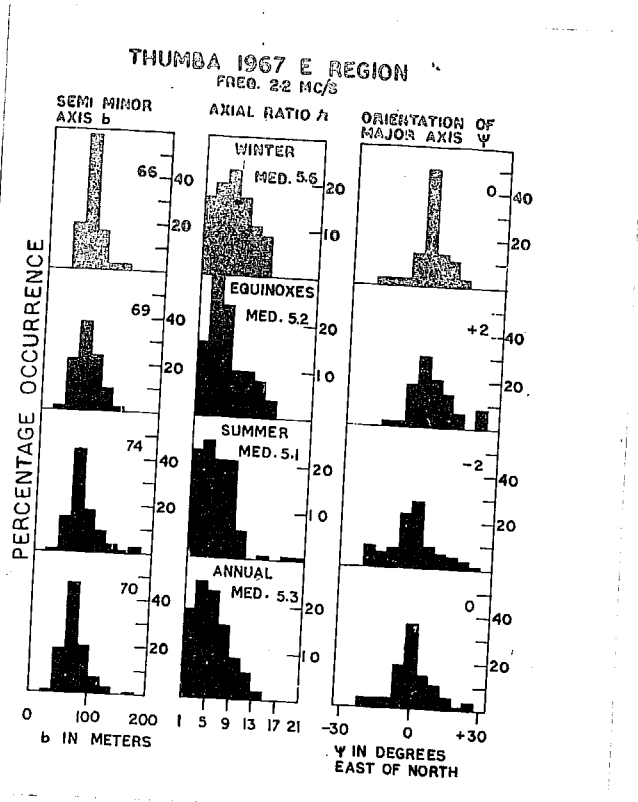

Fig. II.4.26.

summer season than in winter or equinoxes.

The axial ratio r lies mostly in the range 1-14 with annual median value of 5.3. Thus the range as well as the median value of r has increased in the year 1967. The seasonal median values do not indicate any significant difference, being 5.6, 5.2 and 5.1 for the seasons Winter, equinoxes and summer respectively. However, the mean values are 6.4, 6.0 and 5.4 and do show a little decrease

in summer season.

The orientation, measured from the magnetic North, shows the values for ψ lying $\pm 25^{\circ}$ from North with annual median value 0° indicating highly field aligned irregularities in the ionospheric E-region over Thumba. There is no seasonal difference, orientation being mostly along magnetic N-S in each season.

The parameters for the F-region are shown in Figs. II.4.27 and II.4.28. Separate histograms have been computed for the daytime (07-18 hr.) and nighttime (19-06 hr.). The histograms for the semi-minor axis b range upto 300 meters. During daytime, most of the values are within 140 meters but they extend upto 300 meters during nighttime. The annual median values are 67 meters in the daytime hours and 87 meters in the nighttime hours. Thus daytime diffraction patterns are smaller in size. Comparing to daytime 1964 value, there is considerable decrease in the value of b in the year 1967. Seasonally there is no significant difference in the median or mean values for winter and summer, however, values for equinoxes are little smaller. During nighttime, the mean and median values are lowest in summer and highest in equinoxes. But, as the observations in the early morning hours , 04-06 hrs., are least in summer and maximum in equinoxes, nothing significant can be said from the mean or the median values during nighttime.

The axial ratio r obtained at Thumba vary in the range 1-30 with annual median values 6.7 for the daytime and 5.6 for the nighttime. Corresponding mean values are 9.6 for the daytime and 7.9 for the nighttime. Thus the elongation of the ground diffraction patterns have increased considerably from 1964 to 1967. There is definite seasonal variation obtained in the parameter r, for the daytime the mean and median values are highest for the equinoxes and lowest for the summer. During nighttime again axial ratio has lowest values for summer, but the values are of same order for the seasons, winter and equinoxes.

The histograms for the orientation ψ in the daytime and nighttime hours in each season are shown in Fig. II.4.28. In the daytime most of the values lie in the range $\pm 20^{\circ}$ from magnetic North while in the nighttime most of the values lie in the range -25° to $+10^{\circ}$ from magnetic North showing the nighttime values shifted slightly Westward from the North. The annual median values being 0° for daytime and -5° for nighttime. Thus while the pattern are aligned almost along magnetic N-S in the daytime, they are aligned slightly West of the magnetic N-S during nighttime. Seasonally, the values for the summer months seem to be more Westward than the values obtained for Winter and equinoctial months.

(Figure II.4.28 is given in the next page)

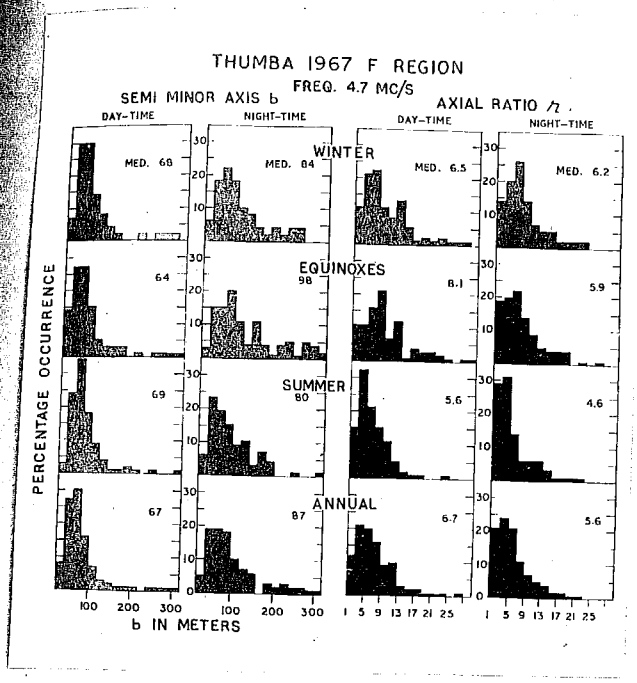

Fig II. 4.27

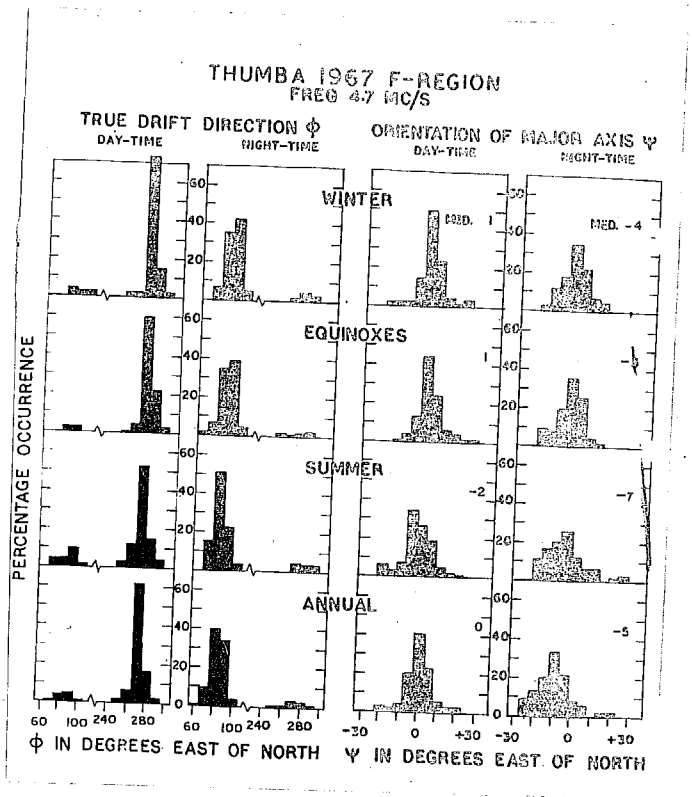

Fig. II.4.28.

II.4c.4. Daily variations of the anisotropy parameters during 1967

Daily variations of the anisotropy parameters b, r and Ψ for the E-region are shown in Fig. II.4.29. As the number of records analysed were not sufficiently large

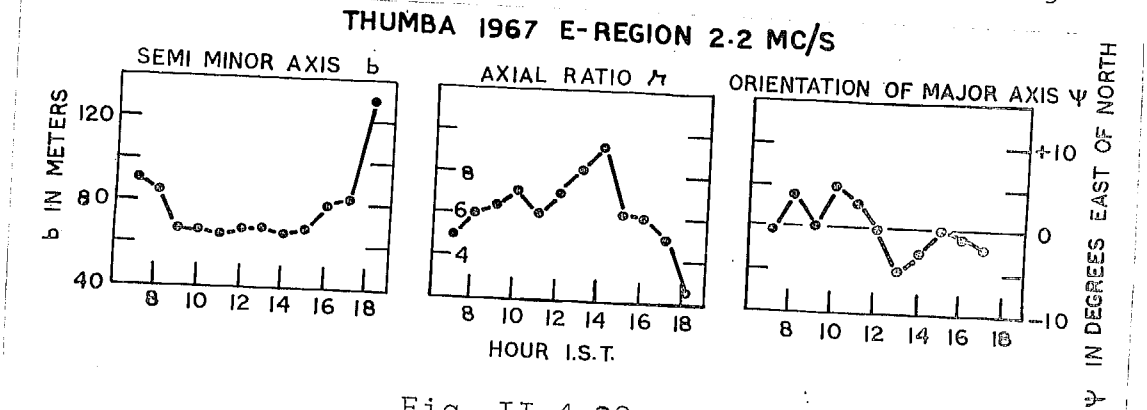

Fig. II.4.29.

for E-region (about 150 records) only annual variations are given.

The variation of b shows a constant from 09 hr. to 15 hr. with a value about 65 meters. An increase in the early morning and late evening hours is seen.

The axial ratio r seems to be lower on the early morning and late evening hours compared to a broad maxima obtained in the midnoon hours.

The orientation ψ does not indicate any systematic variation but it can be observed that orientation is East of the magnetic North in the forenoon period while it is West of the magnetic North in the afternoon period.

The daily variation of the anisotropy parameters for the F-region in each season are shown in Fig. II.4.30.

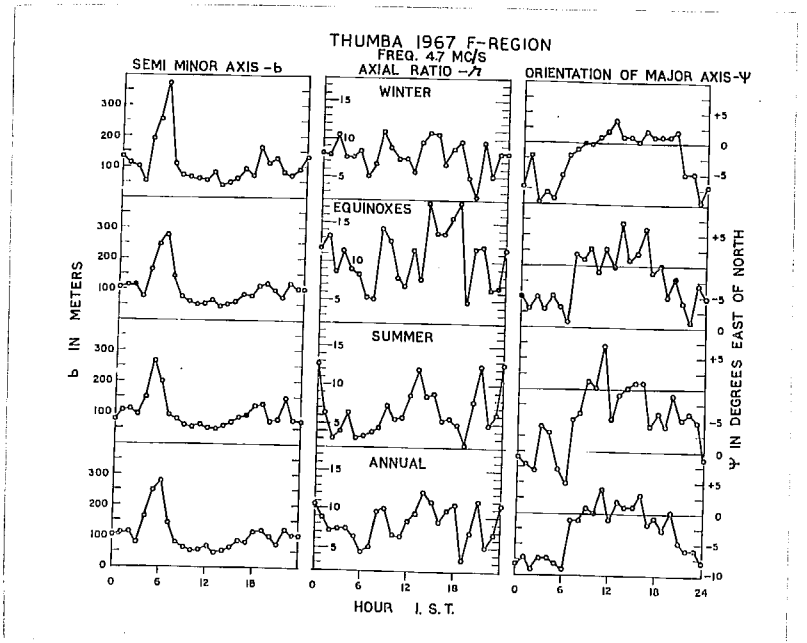

Fig. II.4.30.

Referring to the parameter b it shows a systematic similar variation during each season. The value of b is nearly constant at 100 meters in the period 0-3 hrs., then there is increase upto 06 hr. reaching a value of about 300 meters. Sudden decrease is observed from 06 to 07 hr., followed by slow decrease with minima (about 50 meters) at about noon. Slow increase follows upto 19 hrs. reaching a value more than 100 meters. Another decrease is observed at about 21 hr. with an immediate increase and remaining constant, in the midnight period, at about 100 meters.

The axial ratio r does not show any smooth daily variation, however, it is clear that there are two minima occurring at 06 and 19 hrs. There is an indication of a broad maximum around midday and a steady decrease from midnight to 06 hr. The range of variation is minimum during winter and maximum during equinoxes.

The orientation ψ has a systematic similar diurnal variation during each season. The value of ψ remaining about 7-8 degrees West of magnetic North in the night hours. A sudden change occurs at 07 hr. The value of ψ in daytime hours remaining centred about magnetic N-S.

II.4c.5. Comparison of the results in the year 1964 and 1967

Comparing the results of the daytime (07-18 hrs.)

E- and F-region records of the years 1964 and 1967, one finds a considerable decrease in the semi-minor axis b and a considerable increase in the axial ratio r. The orientation being along the magnetic meridian. The semi-minor axis b has a mean value 105 meters for the E-region records in the year 1964 which is reduced to a value of 75 meters for the records in the year 1967. Thus there is about 30% reduction in the mean value of b from 1964 to 1967. Similarly for the F-region the semi-minor axis b has mean value of 100 meters in the year 1964 and 67 meters in the year 1967, showing a reduction of about 30%. The mean value of the axial ratio for the E-region diffraction patterns is 3.4 in the year 1964 and 5.9 in the year 1967. Thus axial ratio has nearly doubled for the E-region records. For the F-region corresponding values are 3.2 and 9.6. Thus elongation of the F-region irregularities in the year 1967 is three times the elongation in the year 1964.

II.4c.6. Comparison of Thumba results with the result obtained at other equatorial stations

Anisotropy of the irregularities near equator were first studied by Skinner et al (1958). They reported the diffraction patterns obtained from the E- and F-region reflections at Ibadan to be highly elongated and aligned along the magnetic N-S. Axial ratio of 5 was obtained for

the E-region and 11 for the F-region.

Later Skinner et al (1963) studied the transverse size of the diffraction patterns. Average daytime value of about 50 meters was obtained for daytime hours for the F-layer reflections. The daily variation showed a broad minima in the daytime hours while high values were obtained at 06 hr. and 18 hr. The size of the irregularities was found to be nearly same for quiet and disturbed days except in the period 19-24 hrs. when the size was considerably higher for disturbed days. The nautre of the daily variation of the semi-minor axis shown by them is almost similar to that obtained at Thumba. The daytime values of b at Thumba go as low as about 40 meters for the year 1967 and agree remarkably to that obtained at Ibadan during IGY.

At Tamale, Koster and Katsriku (1966) studied the anisotropy for the E- and F-region reflections in the period February - March 1962. Axial ratio of 5.5. for the E-region and 6.6 for the F-region reflections were obtained. Orientation of the diffraction pattern was found to be almost along the magnetic N-S. The size of irregularities was found to lie most probably between 40-60 meters for the E-region and 92 meters for the F-region. The daily variation of the transverse size of the diffraction pattern showed a borad minima around noon. Very high values were observed in the morning at 06 hrs. and near midnight. Nighttime values

were found to be considerably higher than during daytime. However, these results are based on about 100 records analysed for the F-region. Thus the results obtained at Ibadan and Tamale are in close agreement with the results obtained at Thumba.

II.4c.7. Lat. variation of the anisotropy parameters

A comparison of the anisotropy parameters at different latitudes was done by Rao and Rao (1963) for the E-region irregularities. In all, about 100 records were analysed for the stations, Waltair, Yamagawa, Debilt and Halley Bay. The period of study was August - October 1958, for all the four stations. They concluded that i) the axial ratio is found to decrease systematically with increase in latitude except near poles, 2) the orientation of the semi-major axis of the characteristic ellipse is found to rotate systematically from North to West with increase of latitude, 3) the length of the semi-major axis also shows a systematic decrease in the average value with the increase in latitude except near the poles.

Similar study for F-region has been made by Rao (1966) from about 75 records obtained from Waltair, Yamagawa, Debilt and Halley Bay during the period August-October 1958. Conclusions of this study were similar to those reported earlier for the E-region study. However, these studies are

made on the basis of very few records. With the results available for few more stations particularly near the equatorial region comparison of the anisotropy parameters have been made.

The anisotropy parameters for the equatorial stations are given in Table II.4.9. For comparison, few parameters for high latitude stations are also given. The period of study as well as the number of records analysed at each station are also quoted in the Table.

The elongation of the irregularities is considerable for the stations near the equator. At Thumba, the axial ratio is about 3:1 for both the regions in the year 1964. Data for the year 1967 shows axial ratio of the order 6:1 for the E-region, 10 : 1 for the daytime F-region and 8 : 1 for the F-region nighttime records. Thus the diffraction patterns obtained at Thumba are highly elongated indicating highly elongated irregularities in the ionosphere over Thumba. Skinner et al (1958) reported axial ratio 5 and 11 for the E-region records and F-region records respectively, obtained at Ibadan in the year 1958, however their results comprise of only about 25 records for each layer. At Tamale, records analysed for the period February - March 1962 show axial ratio of 5.5 for the E-region daytime and 6.6 for the F-region records (Koster and Katsriku, 1966). All these stations

TABLE-II.4.9

Comparison of the anisotropy parameters at different stations.

Station	Mag.lat.	Period of study	Region	Counts	r	ψ	b	Reference
Thumba	0.3°S	1964	E-day	350	3.4	-4	105	
			F-day	266	3.2	-3	100	
		1967	E-day	154	5.9	1	75	
			F-day	385	9.6	1	67	
			F-Night	251	7.9	-6	130	
Tamale	0.6°S	Feb-Mar. 1962	E-day	43	5.5	-2.4	40-60	Koster and Katsriku (1966)
			F-day	83		-2.7	92	
			F-Night	38				
Ibadan	3.0°S	IGY	E-day F-day F-Night	1000			50	Skinner et al (1963)
		IGY	E-day	24	5	0.0		Skinner et al (1958)
			F-	25	11	0.0		
Waltair	11°N	Sum. '60	E-	75	2.1	-16	135	Rao and Rao (1963)
			F-	95	2.3	-11	147	
Singapore	9°S		F-		1.7			Harriston (1965)
Cambridge	50°N	Mar-Apr. 1955	E-day	39	1.5	N-W	235 Med.	Fooks and Jones (1961)
		Feb.'58.	F-day	37	1.6	N-W	296 val-	
			F-Night	35	1.8	N-W	140 ues	
Ashkhabad	36°N	1960	E_s		2.7	**		Mirkotan (1962)
Moscow		1959	F_2		3.3	50@		Mirkotan

**along the meridian in daytime.
@ large scatter.

are within 3^{o} magnetic latitude. Thus the irregularities near the equator are highly elongated. Rao and Rao (1963) reported the axial ratio 2.1 for the E-region and 2.3 for the F-region at Waltair (11^{o}N mag. lat.), from the records analysed in the period Summer 1960 to Winter 1961-62. Thus there is a sharp change in the elongation of the irregularities within 10^{o} from the equator. Harrison (1965) has reported an axial ratio of 1.7 for the F-region at Singapore (9^{o}S). Thus the elongation at latitudes about 10^{o} from the equator is of the order of 2. At a high latitude station Cambridge, axial ratio is shown to be 1.5 for the daytime E-region and 1.6 for the daytime F-region (Fooks and Jones, 1961). The records analysed by them were mostly in the period March - April 1955 and a few records during February 1958. Mirkotan (1962) has reported an axial ratio of 2.3 for the F_2-region over Moscow based upon 362 records analysed during the year 1959. Thus the axial ratio seems to be of a order of 2 at all latitudes, for which data are available except near equator where it is as high as 10.

Axial ratio of 2.6 has been reported for the E-region at Ahmedabad by Patel (1967) for the data in the period March 1960 - February 1961 and by Kaushika (1968) for the data in the period March 1965 - February 1966. Tsukamato and Ogata (1959) reported axial ratio of 1.6 for

the E-region at Yamagawa for the IGY data. At Puerto Rico axial ratio of about 1.8 has been reported for the E-region data in the period February 1954 and June 1954 and for the F-region data in the period June 1954 and February 1955 (Yerg, 1956).

Thus one finds a high axial ratio very close to the magnetic equator (stations upto 3^{o} mag. lat.). For stations in the latitude region 10^{o} to 50^{o} there is a slow decrease in the axial ratio. For very high latitude stations much data has not been subjected to correlation analysis to give the anisotropy parameters. Hence, there is a need for the measurements near the auroral zone to find the variation from above 50^{o} lat. to the pole region. Similarly there is no station in the range 3^{o} to 10^{o} lat. Hence the sharp change over to equatorial behaviour is to be studied.

The orientation of the characteristic ellipse is along the magnetic meridian at the equatorial stations, Thumba, Tamale and Ibadan; about 10-15^{o} West of North at Waltair, N-W at high latitude station Cambridge and almost perpendicular to N-S at a station like Halley Bay. Thus while at equatorial stations within 3^{o} (mag. lat.) the orientation is along the magnetic meridian it tends to be Westward at higher lat. However, data for the anisotropy parameters at high latitudes is not sufficient to draw any

definite conclusion in that zone.

The semi-minor axis of the characteristic ellipse was found to be about 50 meters for the daytime F-region records at Ibadan during IGY. At Thumba, it is of the order of about 100 meters in the year 1964 and 70 meters in the year 1967. At Tamale, the transverse size of the characteristic ellipse is shown to be in the range 40-60 meters for the E-region and 92 meters for daytime F-region for the year 1962. Thus the average size of the irregularities (semi-minor axis) is definitely lower than 100 meters in the daytime hours. These may be compared with the size of 135 meters and 147 meters for the E- and F-region records at Waltair and 235 meters, 296 meters respectively for the daytime E- and F-region records at Cambridge. Thus the transverse size of the irregularities is considerably reduced near the equator.

CHAPTER - II4d. Multi-antenna fading records at Thumba to study the elongation of diffraction patterns.

Multi-antenna measurements at Thumba

The analysis of the fading records obtained at Thumba showed a complete similarity between the N-S pair of aerials with practically no time shift between them, while the E-W pair of aerials showed appreciable time shift and maintained a reasonable similarity so that analysis either by ordinary time delay method or by correlation technique can be applied.

The correlation analysis of the fading records at Thumba, which were obtained by recording the fadings at three aerials situated at the corner of a right angled triangle with sides 120 m. each, in the year 1964 showed very high correlations (more than 0.9) between the N-S pair of aerials at all hours while the E-W pair showed slight variation with time, being about 0.8 in the morning and evening hours and comparatively low (0.5) during the midday hours.

An additional antenna was put in the N-S line, so that the fading records could be obtained at aerials with a separation of 240 m. in N-S direction. Even at this separation, there was no appreciable time shift seen between the N-S pair. The fading records along the N-S line were found to be exactly similar with no time shift, suggesting high elongation of the irregularities over Thumba.

To study the diffraction patterns at Thumba more precisely additional aerials were set up making it a 10 aerial system; six along E-W direction and 5 along N-S direction. Thus fadings could be recorded at distances upto 480 meters along both E-W or N-S direction. The new antenna system employed for this purpose is shown in Fig. II.4.31. They are described as N_1, N_2 etc. where the

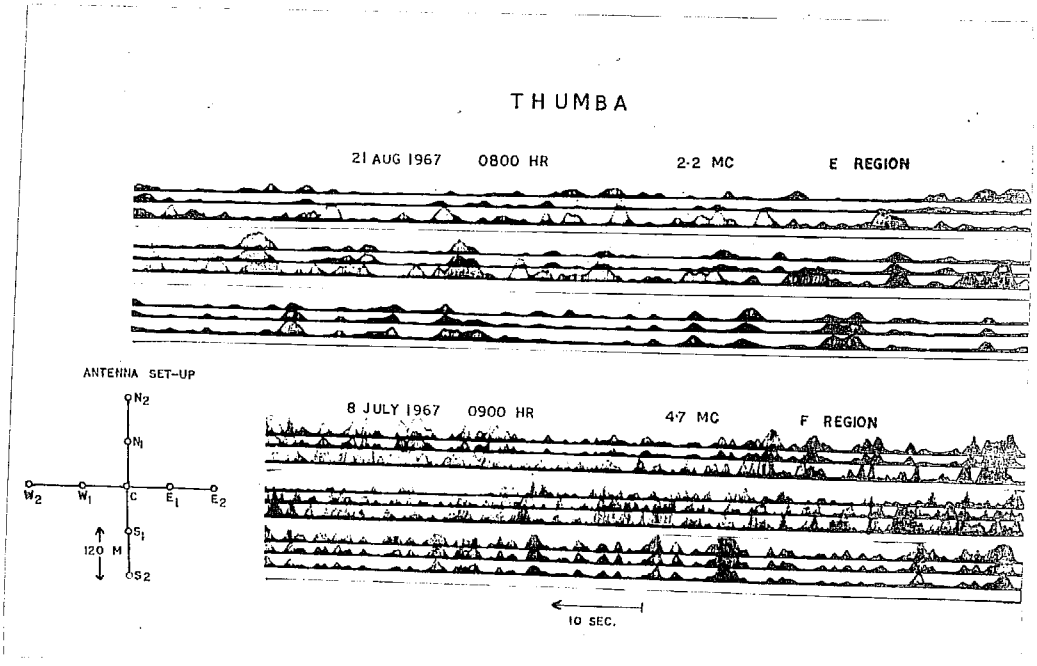

Fig. II.4.31.

alphabets indicate the direction with respect to central antenna (c), and the subscripts indicate the distances in unit of 120 meters from the central antenna. Thus N_3 means aerial situated at a distance of 3 x 120 meters in the direction North of the central antenna. Observations were taken with three antennas at a time and immediately switching over to another three antennas. Most of the observations were taken on three sequence of amplitude recordings, namely:

(1) $N_2\ N_1\ S_2$,

(2) $W_2\ W_1\ E_2$ or $W_1\ C\ E_{\frac{1}{2}}$, and

(3) $W_2\ C\ S_2$.

Recordings were made for 2 min. each for a sequence. About half a minute was taken in the change over of the antenna sequence. Thus a total of about 7 minutes were taken for one complete set of recording. More than 50 sets of such observations have been taken in the year 1967 in the period June to November 1967. It has been tried to cover different hours possible so that diffraction patterns during the course of a day can be studied. Most of the records were taken for the F-region while few E-region records also have been recorded.

A short note (Rastogi et al, 1968) describes the results of two such sets of F-region fadings records. A

detailed study from more of such analysis is presented here.

Figs. II.4.31, II.4.32, II.4.33 and II.4.34 show some example of the multi-antenna fading records. The aerials in the N-S line show very high similarity in the fading records. Time shifts between the N-S pairs of aerials seem to be unappreciable even at a separation of 480 meters. However, some of the records indicate little time shift between the N-S pairs of aerials. Time shifts being proportionate to the distance between the aerials. Similarity between the fading records of E-W sequence is rather poor, particularly during mid-day hours when even at a distance λ correlation is poor. The fadings are completely uncorrelated at a distance 2λ. However, the records of early morning or mid-night hours show better correlation, the time shifts seem to be again proportionate to the

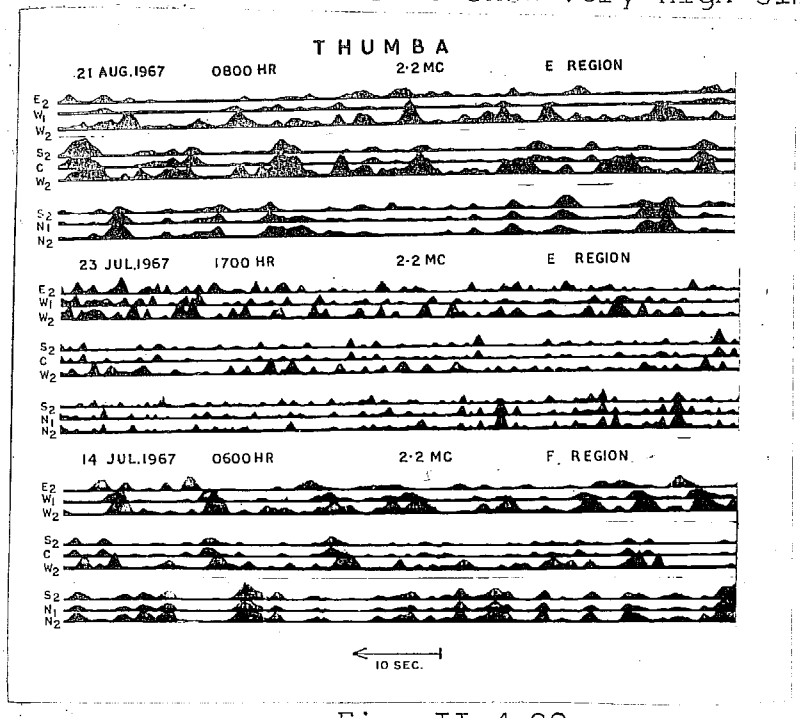

Fig. II.4.32.

distance between the aerials.

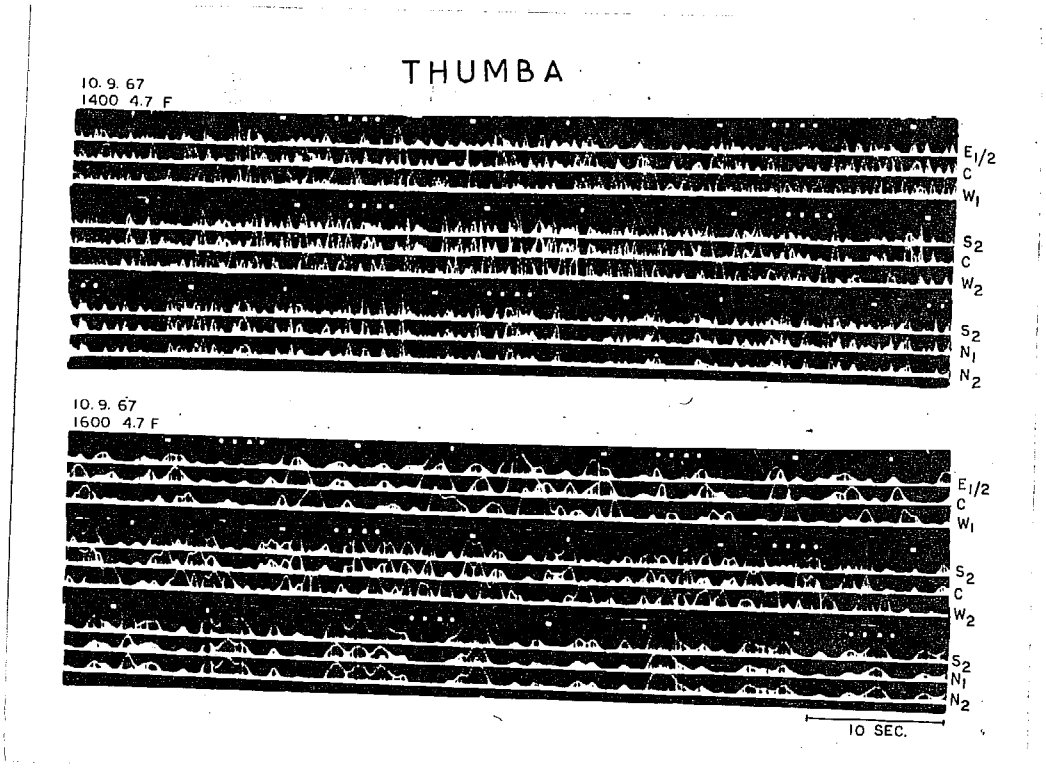

Fig. II.4.33.

The above results are clearly seen in Fig. II.4.35 where correlation curves for different aerial separations are pbtted along both E-W and N-S directions for few cases. Closer the separation, higher is the correlation and smaller the time shifts.

Fig. II.4.36 shows the variations of the correlation with separation along N-S and E-W directions. The

crosses represent the correlation along N-S direction and

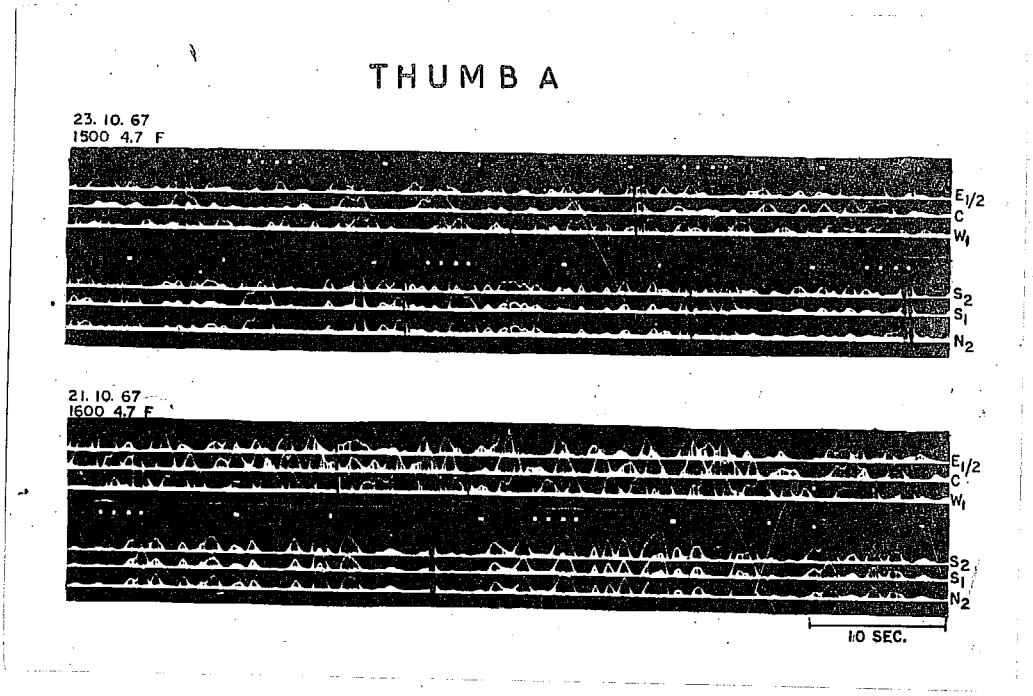

Fig. II.4.34.

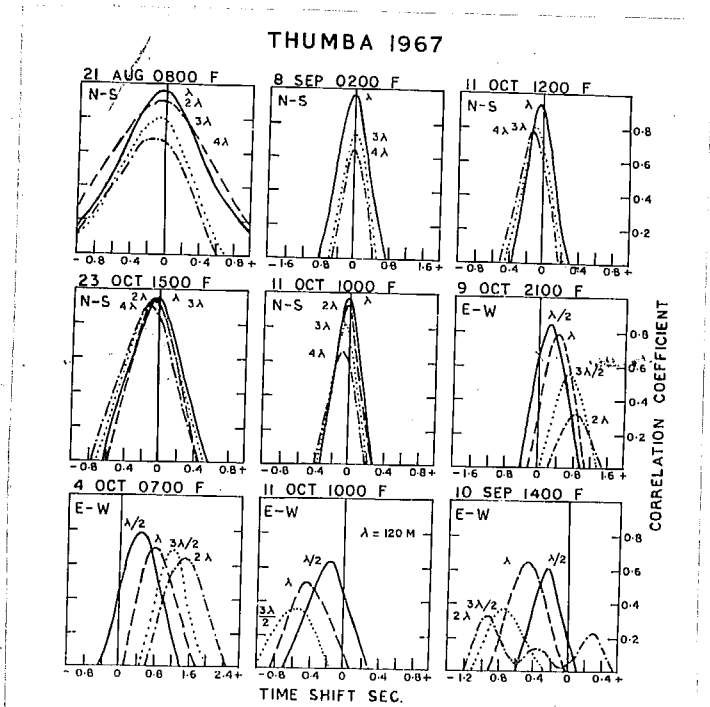

Fig. II.4.35.

the circles represent the correlation along E-W direction. The correlation of the two records, one at 05 hr. and another at 06 hr., are high along both E-W and N-S directions, being about 0.95 at a separation λ and about 0.90 for N-S direction and 0.80 for E-W direction at a separation 4λ, indicating a large size of the ground diffraction pattern along and across the field lines. The high correlation along N-S is seen again for the record at 07 hr. but it drops to 0.60 at separation $3\lambda/2$ for E-W direction. Thus while N-S extent is maintained the E-W extent of the pattern is reduced. The patterns are still thinner for the records one at 09 and another at 10 hr. The correlation

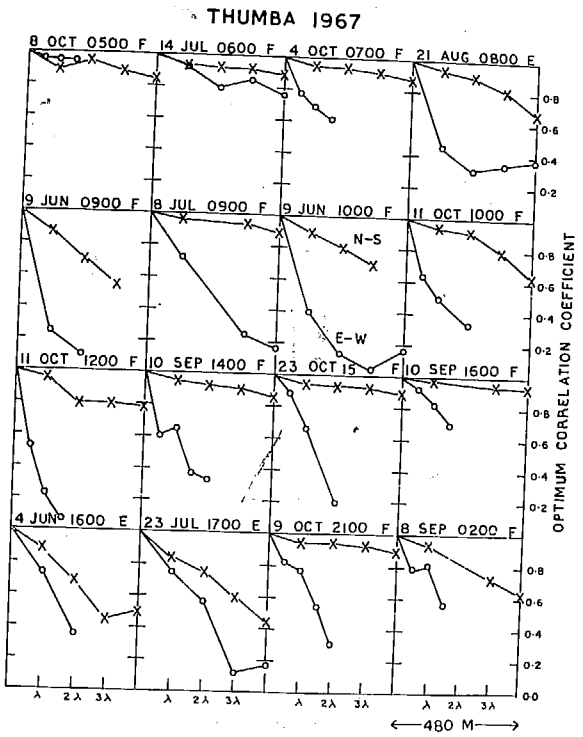

Fig. II.4.36.

drops along N-S as well as E-W direction. Correlation of about 0.5 is obtained at a separation λ along E-W while correlation is more than 0.65 along N-S even at a separation 4λ.

A case of extreme elongation is noticed for the record at 12 hr. with correlation dropping to 0.50 at a separation $\lambda/2$ along E-W and to 0.80 at separation 4λ along N-S.

The next three examples at 14-16 hr. show slightly higher correlation along both the E-W and N-S directions. The two examples of the nighttime fading records, one at 2100 and another at 0200 hours show a correlation of about 0.50 at 2λ separation along E-W. The correlation is much higher along N-S direction being 0.90 and 0.64 respectively at 4λ separation.

Thus from the above examples, one finds that the F-region fading records at Thumba show a very high correlation along N-S direction. On the average correlation between 0.80 - 0.90 is found at 4λ separation in this direction. The correlation along E-W direction changes with the time of day. The variability is quite large with correlation falling to 0.50 even at a distance $\lambda/2$ and remaining as high as 0.80 at 4λ distance. In general, the cases of extreme elongation are observed around midday

when the size of the irregularities is found to be minimum. A fairly large size is observed in the early morning hours when high correlation is maintained along E-W direction also as seen in the exaples of 05 hr. and 06 hr. shown here.

From the few E-region records of morning and evening periods, one finds a fairly good correlation along N-S direction or along E-W direction. Roughly, one obtains a correlation of 0.50 at 4 λ separation along N-S direction and at 3 λ /2 along E-W direction. Thus the size of the E-region diffraction pattern along E-W direction is not much different than the size of the F-region diffraction pattern of the corresponding hour. However, the size along N-S is much less indicating a less degree of the elongation along the magnetic field lines.

The above results are in agreement with the conclusions obtained in the last sub-chapter from a normal antenna sequence. The size of the minor axis of the characteristic ellipse was shown to be minimum around noon; of the order of 50 meters, while very large size of the order of 300 meters was obtained in the early morning hours. The axial ratio was found to be higher around noon compared to early morning and late evening hours. Further the axial ratio was shown to be much higher for the F-region records

than for the E-region records. All these results are reflected in the few examples of multi-antenna records which are shown here.

Reprinted from

Journal of Atmospheric and Terrestrial Physics, 1968, Vol. 30, pp. 1597–1599. Pergamon Press. Printed in Northern Ireland

SHORT PAPER

Elongation of irregularities in ionospheric *F*-region over the magnetic equator in India

PERGAMON PRESS
OXFORD NEW YORK LONDON PARIS

Journal of Atmospheric and Terrestrial Physics, 1968, Vol. 30, pp. 1597–1599. Pergamon Press. Printed in Northern Ireland

SHORT PAPER

Elongation of irregularities in ionospheric *F*-region over the magnetic equator in India

R. G. RASTOGI, M. R. DESHPANDE and HARISHCHANDRA
Physical Research Laboratory, Ahmedabad-9, India

(*Received* 23 *November* 1967; *in revised form* 28 *February* 1968)

Abstract—The diffraction pattern of the field strengths of pulsed radio waves of frequency 4·7 Mc/s reflected from the *F*-region of the ionosphere near the magnetic equator in India are studied with the help of ten receiving aerials, six in the E–W and five in the N–S directions at distances of 60–480 m. The cross-correlation between the signal strengths at paired aerials along the N–S direction decreases very slowly with increasing separation, while along the E–W direction the correlation decreases very rapidly with increasing distance between the aerials. This suggests that the irregularities causing the fading of short radio waves near the magnetic equator are highly elongated along the N–S direction.

MEASUREMENTS of ionospheric drift at Thumba (Geog. lat. 8·5°N, Geog. long. 76·9°E) have been continued since January 1964, using the conventional technique of recording the fadings of ionospheric echoes at three dipoles aligned along N–S direction and situated at the corners of an isosceles right angled triangle with the equal sides of about one wavelength. The amplitude fading records of *E*- or *F*-region reflections received at the E–W pair of aerials have been found to be very similar with significant time shifts between them while at the N–S pair of aerials fadings are almost identical with generally negligible time shifts indicating predominantly westward drifts (RASTOGI *et al.* 1966*a*, *b*). The correlation analyses of the fading records have shown that the maximum cross-correlation between the N–S pair of records is about 0·8 while with the E–W pair it is about 0·6 for a separation of 120 m between the aerials. DESHPANDE and RASTOGI (1967) have shown that the N–S component of the drift, though very small compared to the E–W component, has significant diurnal and seasonal variations. To measure the N–S component more accurately and to study in detail the characteristics of the diffraction pattern on the ground, the number of aerials in the N–S and E–W directions were increased to five and six respectively. With respect to the Central aerial (C), the East, West, North and South aerials are designated as E, W, N and S respectively. The suffixes attached to these letters indicate the distances of the aerials from the Central aerial in units of 120 ms. The antenna set-up is shown in Fig. 1. Two examples of fading records on 4·7 Mc/s at the set of three aerials in the N–S or E–W directions are shown in Fig. 2 and 3. One set of three fading records were taken for 2 min and the aerials were immediately changed to obtain another set of 2-min records. Only small portions of such records are shown in

Figs. 2 and 3. The correlograms calculated from the full length of the records are also shown in the diagrams.

The fadings of radio reflections at Thumba are usually sporadic consisting of short bursts of signal strength over a relatively low average intensity. Individual fadings are almost sinusoidal in shape. The probability distribution of the amplitude of signal strength does not fit the theoretical Rayleigh or Gaussian distributions (RASTOGI *et al.* 1966*c*). To check whether the fadings are due to magneto-ionic interference, another dipole in E–W direction was installed and signals were received separately at two mutually perpendicular aerials. Signals at E–W

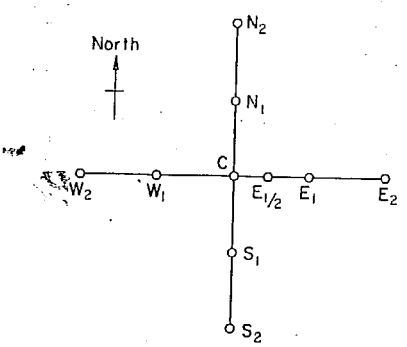

Fig. 1. Antenna set up for ionospheric drift measurement at Thumba.

dipoles were found to be almost negligible as compared to those received at N–S dipoles. The fadings were thus found to be caused by only the ordinary component of the radio waves.

Figure 2 shows an example of slow fadings (30 fades/min). Record (A) incorporates fadings at aerials along the E–W direction with separations of 60, 120 and 180 m. The fadings at all three aerials are very similar but are shifted with respect to one another and the amount of shift is proportional to the separation of the aerials. The time shifts of the maximum correlation coefficients for E–W pairs of aerials indicate a systematic increase with the increasing aerial separation. The value of the maximum correlation coefficient has decreased from a value of 0·93 at 60 m separation to a value of 0·72 at 180 m separation. Record (B) incorporates fadings at aerials along N–S direction with separations of 120, 360 and 480 m. It is seen that every peak is reproduced almost simultaneously at all the three aerials. The correlograms at pairs of N–S aerials do not show any apparent difference for different pairs of aerials selected and the shift of the peak correlation coefficient in different pairs cannot be accurately determined. The maximum correlation factor for any of the pairs of these aerials exceeds 0·9.

Figure 3 shows an example of rapid fadings (80 fades/minute). Here again every peak is recorded almost simultaneously at all the three N–S aerials. The correlograms at N–S aerials are very similar for different pairs, the maximum correlation coefficients and the time shifts are almost similar for different pairs. Regarding the E–W pairs of aerials at short distances viz. W_1W_2 pair, the fadings are seen to be reasonably similar with a distinct time-shift. Fadings at aerials with greater separations i.e. W_1E_2 or W_2E_2 do not show any similarities. No

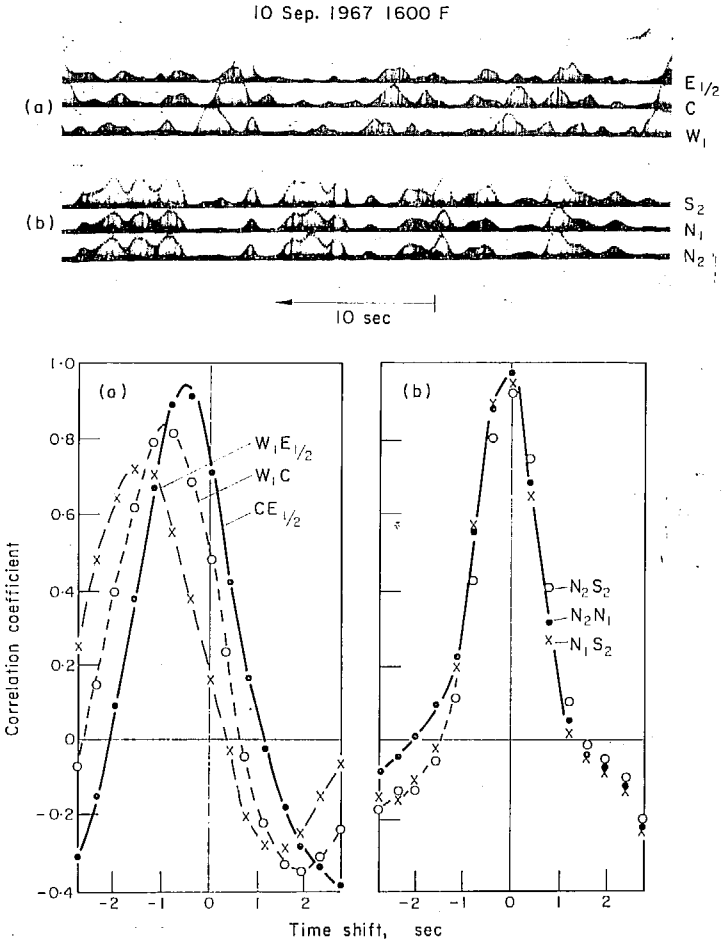

Fig. 2. Fading records of F-region reflections (4·7 Mc/s) at different pairs of aerials in E–W and N–S directions with cross-correlograms on 10 September 1967 at Thumba.

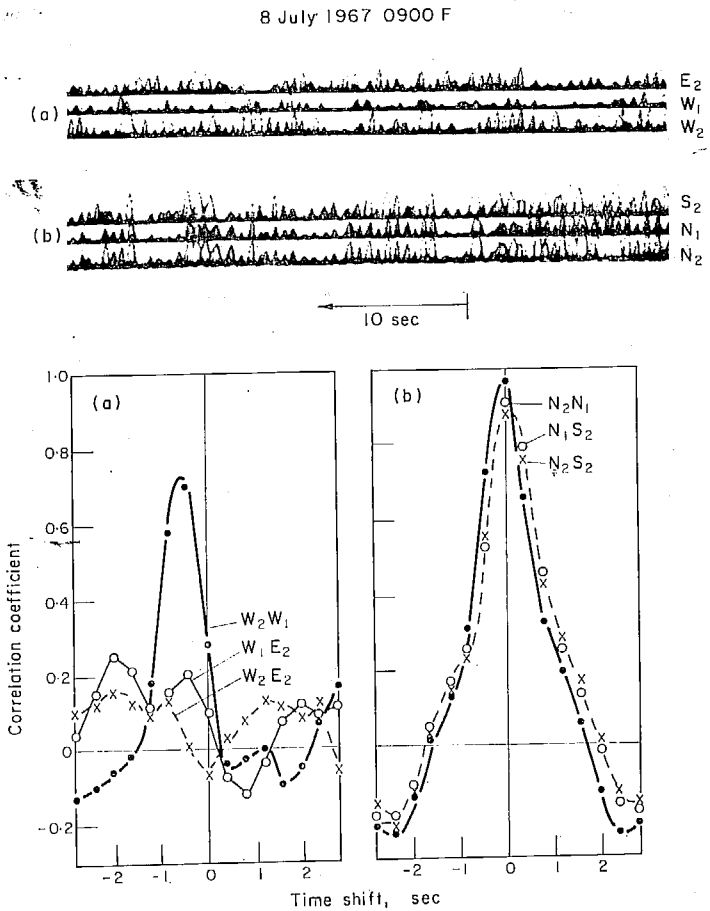

Fig. 3. Fading records of F region reflections (4·7 Mc/s) at different pairs of aerials in E–W and N–S directions with cross-correlograms on 8 July 1967 at Thumba.

significant peak in the correlograms is observed for E–W aerials separated by 360 or 480 m.

The maximum correlation-coefficients of pairs of aerials in the E–W and N–S directions are plotted against the separation between the aerials in Fig. 4. The wavelength scale is also indicated in the diagram. It is seen that for 10 September 1967 the optimum correlation-coefficient at the E–W pairs of aerials drops to about 0·7 when the separation is 180 m, whereas the N–S pairs of aerials the correlation even at 480 m is greater than 0·9. For 8 July 1967 the optimum

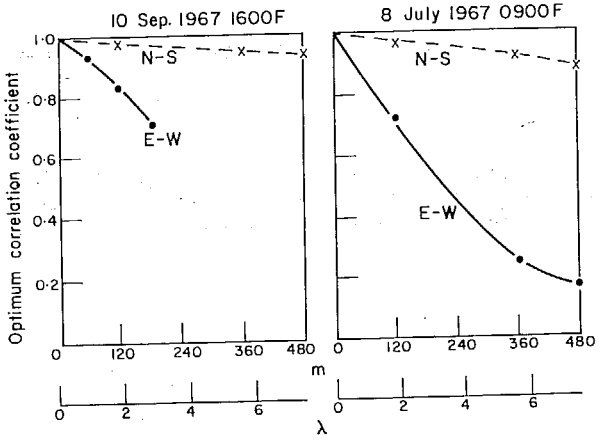

Fig. 4. Variation of the optimum cross-correlation-coefficients with the antenna separation at Thumba on 4·7 Mc/s.

correlation coefficients at the N–S pair of aerials decrease very slowly with increasing distance such that even at 480 m separation, i.e. at 8λ (wavelength) distance it is about 0·9. The optimum correlation-coefficients at E–W pairs of aerials decrease much faster, so much so, that at 8λ it drops to 0·2.

It is concluded that the extent of irregularities at Thumba is greater than 480 m along the N–S direction and only 200 m along E–W direction. For reliable measurements of N–S component of the drift for the computation of the size of irregularities at an equatorial station, the aerials should have much largerse paration along N–S than along E–W direction. Further measurements of drift at Thumba with more separated aerials in N–S direction are being continued.

Acknowledgements—Thanks are due to Prof. K. R. Ramanathan for helpful discussions and Miss Nila. M. Deshpande for the computational assistance. Thanks are also due to Indian National Committee for Space Research for the facilities provided at their Rocket Range in Thumba.

References

Rastogi R. G., Deshpande M. R. and Kaushika N. D.	1966*a*	*J. Atmosph. Terr. Phys.* **28**, 137.
Deshpande M. R. and Rastogi R. G.	1966*b*	*Annls Géophys.* **22**, 418.
Deshpande M. R. and Rastogi R. G.	1968	*J. Atmosph. Terr. Phys.* **30**, 319.
Rastogi R. G., Kaushika N. D. and Deshpande M. R.	1966*c*	*Annls Géophys.* **22**, 380.

(Accepted for publication as 'Short Paper' in JATP)

Drift and anisotropy parameters of the irregularities in the E- and F-regions of ionosphere over Thumba during 1964.

BY

R.G. RASTOGI, H. CHANDRA and M.R. DESHPANDE
Physical Research Laboratory
Ahmedabad-9
INDIA.

ABSTRACT:- Fading records of the E- and F-region reflections at Thumba for the daytime hours in the year 1964 have been analysed by full correlation method applying the anisotropy corrections. The random component of the drift is found to be 0.95 and 0.70 times the steady component in the E- and F-regions respectively thereby reducing the true drift speed to 74 m/sec in the E-region and 98 m/sec in the F-region. The true drift direction is found to be towards magnetic west (267°E of geog. N) for either of the regions. The characteristic ellipse defining the diffraction pattern is elongated along the magnetic N-S, the minor axis being about 100 metres and the axial ratio about 3.

INTRODUCTION

The results of the ionospheric drift measurements at Thumba using Mitra's method (1949) for the period 1964-67 have been described by Chandra and Rastogi (1969). The present article describes the results of analyses according to full correlation method suggested by Briggs, Phillips and Shinn (1950) and modified by Phillips and Spencer (1955). The method has been applied on 350 records for E-region and 266 records for F-region, taken between 07-18 hr. at Thumba in 1964.

Under the assumption that the diffraction pattern is statistically isometric in nature, the true (steady) drift speed (V) and the apparent drift speed (V') obtained from time delays are related by the expression:

$$V' = V\left[1 + \left(\frac{V_c}{V}\right)^2\right] \qquad \ldots\ldots(1)$$

where V_c defines the random component of drift. When $V_c = 0$ that is, when the diffraction pattern moves without any change, $V' = V$. For any definite value of V_c the true drift speed V is always smaller than the apparent speed V'. The average diffraction pattern as seen on the ground can be defined by a characteristic ellipse such that any radial distance gives the seperation required for the correlation to be reduced to half in that particular direction. The orientation of the major axis (Ψ, expressed here in degrees East of North), the axial ratio (r) and the semi-minor axis (b) of the ellipse have been calculated using the method by Phillips and Spencer (1955), and Fooks (1965).

Corrections due to the anisotropy of the diffraction pattern are applied to the apparent drift speed (V_a) and direction (ϕ_a) obtaining corrected apparent speed V' and direction ϕ. Following Fooks and Jones (1961), the characteristic velocity V_c is calculated along the true drift direction.

Results at Thumba

The analyses have been done separately for each season and the results are given in Table - 1. Both the mean and median values of the parameters are given. In Table - 2, the results of Thumba are compared with those available for other equatorial stations. Only the annual average histograms of different parameters are shown in Fig. 1.

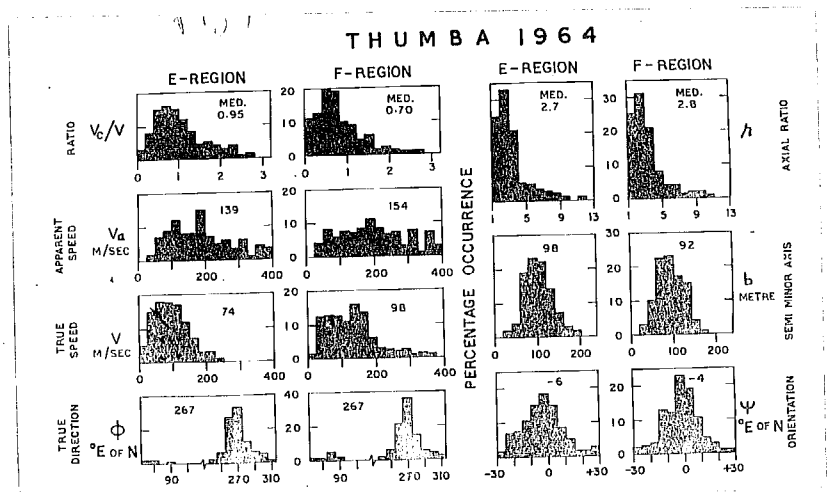

Fig. 1 - Annual average histograms for the true drift and anisotropy parameters V_c/V, V_a, V, ϕ, r, b and Ψ.

The data for the whole period have been grouped again according to the local time and the annual average daily variations of different parameters are shown in Fig. 2. The main features of these parameters are described here.

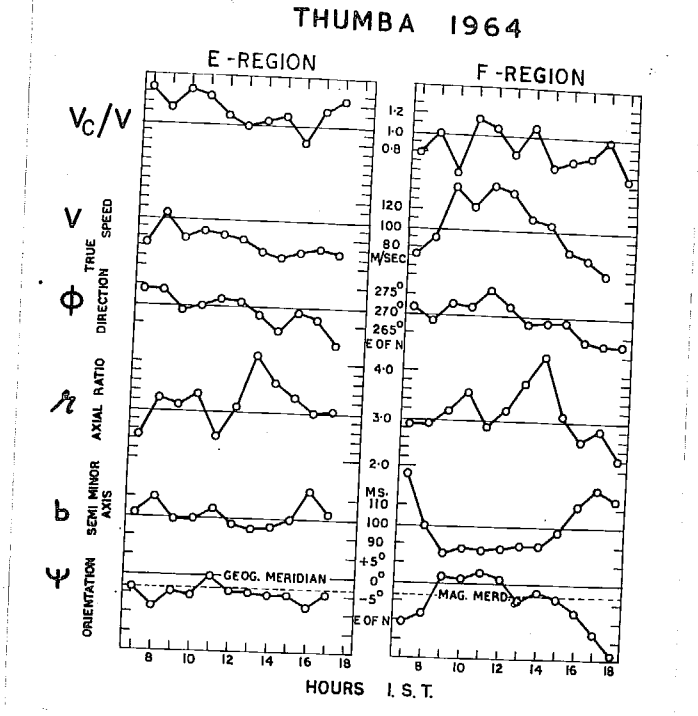

Fig. 2 - Annual average daily variations of the true drift and anisotropy parameters V_c/V, V, r, b and Ψ.

1. Ratio, V_c/V

Individual values of V_c/V range between 0 and 3 with mean value being very close to 1. For any of the seasons the ratio V_c/V is higher for the E-region than for the F-region indicating that the life time of irregularities is larger in the F-region than in the E-region.

Seasonally, for either of the E- or F-regions, the ratio is smallest during winter suggesting that the irregularities are most long lived during winter months. The ratio V_c/V does not show any significant variation with the time of day.

2. True drift speed, V.

The annual average histograms of V are much narrower than those for V_a indicating that the scatter in V_a are mostly due to the fluctuations of V_c than due to V. The annual average ratio V/V_a is .53 for the E- and .62 for the F-region. Thus the apparent drift speed at Thumba are about twice the true drift speeds. The true drift speeds are definitely smaller in summer than in winter months for either of the regions and these results are not similar to those of the apparent drifts due to large seasonal variations of the ratio V_c/V. The F-region drift speed shows a pronounced peak around 10 hr, while no distinct maxima is seen for the E-region although the speeds seem to decrease from 10 hr. onwards.

3. True drift direction, ϕ.

The direction of drift is mainly towards West. There are few observations indicating Eastward drift, but drifts towards North or South are almost inhibited. It is interesting to note that the median direction of drifts is 267° East of geographic North which is true magnetic West, that is the drift of irregularities is exactly at right angles to the magnetic field lines. The daily variation of the angle is small but systematic suggesting the existence of small Northward component in the forenoon and Southward component in the afternoon hours.

4. Axial ratio, r.

The individual values of the axial ratio range between 1 and 10 with the average being 3 for either of the regions. There is

Table-1. - True drift and anisotropy parameters in the E- and F-regions of ionosphere over Thumba in the year 1964.

Period	Counts	Apparent drift speed V_a m/sec.	True drift speed V m/sec.	Ratio random to steady drift V_c/V	Axial ratio r	Orientation E of N (geog.)	Semi-minor axis b in meters
1	2	3	4	5	6	7	8
			E-REGION - 2.2 Mc/s				
Winter	144 Mean	163 ± 8	92 ± 5	1.04 ± 0.04	3.2 ± 0.2	-4.0 ± 2.0	99 ± 2
	Med.	149	83	0.81	2.4	-7.0	98
Equinoxes	86 Mean	177 ±10	78 ± 5	1.17 ± 0.07	2.9 ± 0.2	-4.0 ± 2.0	102 ± 5
	Med.	149	75	0.97	2.4	-6.0	95
Summer	120 Mean	166 ± 5	71 ± 4	1.33 ± 0.09	4.0 ± 0.1	-5.0 ± 0.5	115 ± 5
	Med.	120	63	1.06	3.7	-5.0	102
Annual	Mean	169 ± 8	80 ± 5	1.18 ± 0.07	3.4 ± 0.2	-4.0 ± 1.5	105 ± 4
	Med.	139	74	0.95	2.7	-6.0	98
			F-REGION - 4.7 Mc/s				
Winter	70 Mean	165 ± 8	110 ± 5	0.59 ± 0.05	3.0 ± 0.3	-3.0 ± 1.0	90 ± 3
	Med.	161	107	0.52	2.9	-4.9	87
Equinoxes	91 Mean	188 ±11	115 ± 9	1.08 ± 0.13	2.8 ± 0.2	-1.0 ± 1.0	105 ± 6
	Med.	160	101	0.76	2.5	-4.0	91
Summer	105 Mean	177 ±10	96 ± 6	1.10 ± 0.09	3.9 ± 0.2	-5.0 ± 1.0	105 ± 7
	Med.	142	88	0.82	3.6	-5.0	94
Annual	266 Mean	177 ±10	107 ± 7	0.92 ± 0.10	3.2 ± 0.2	-3.0 ± 1.0	100 ± 5
	Med.	154	98	0.70	2.8	-4.0	91

no significant seasonal or daily variation of the axial ratio.

5. Semi-minor axis, b.

The values of the semi-minor axis of the ellipse are between 20 and 200 meters with mean being about 100 meters. There is no significant seasonal variation of b. Further, b for the E-region seems to be practically constant with the time of day, while b for the F-region seems to have larger values during the morning and evening periods.

6. Orientation, ψ.

The values of ψ are mostly between $\pm$ 30° from geographic North with mean value being 3-4° West of geographic North. It is interesting to note that the magnetic declination at Thumba is 3° West. Thus the orientation of the irregularities seems to be aligned along the magnetic meridian. There is no significant seasonal difference in the value of ψ. Orientation of E-region irregularities has practically no variation with solar time. The F-region irregularities are closely aligned along the magnetic meridian in the midday hours, but, the orientation shifts towards West from North during the morning and evening hours by as much as 20°.

Discussion and comparison with other stations

The ratio V_c/V at other equatorial stations is shown to range between 0.5 to 1.0 and thus the results of Thumba are in fair agreement with those at other equatorial stations.

The comparison of V_a and V values are not available at all the stations. Skinner et al. (1963) have shown that there was larger scatter in apparent drift than in true drift at Ibadan. Further, the true drift speeds were invariably smaller than the corresponding apparent speeds even in individual cases. Rao and Rao (1963) reported

Table-2. True drift and anisotropic parameters at equatorial station

Station	Mag. lat.	Period of study	Region	No. of observations	Apparent drift speed V_a m/sec.	True drift speed V m/sec.	Ratio random to steady drift V_c/V	Axial ratio r	Orientation ψ oE of N.	Semi-minor axis b meters.	Reference
Thumba	0.3°S	Jan-Dec. 1964	E-day	350	169± 8	80±5	1.18±0.07	3.4± 0.2	-4.0±1.5	105±4	Present article
			F-day	266	177±10	107±7	0.92±0.10	3.2± 0.2	-3.0±1.0	100±5	
Tamale	0.6°S	Feb-Mar. 1962	E-day	43		67	0.8	5.5	-2.4±1.5 (mag.)	40-60	Koster and Katsriku (1966).
			F-day	121		115	0.5	6.6	-2.7±1.4 (mag.)	92	
Ibadan	3.0°S	I.G.Y.	E-day	24				5	0.0° (mag.)		Skinner et al. (1958).
			F-day	25				11	0.0° (mag.)		
		I.G.Y.	E-day	1000		55	0.8				Skinner et al. (1963).
			F-day			50	0.6			50	
Waltair	11.0°	Summer 1969	E	75	80	79	0.71	2.1	-16.0	135	Rao and Rao (1963)
		Winter 1971	F	95	87	93	0.67	2.3	-11.0	147	
Singapore	9.0°S		F					1.7	N-S		Harrison (1965).

that the true drifts at Waltair were not significantly different from the corresponding apparent drift speeds. The Table given by them showed that in certain seasons, the true drift was even higher than the apparent drift. This difference between the results at Thumba and Waltair is not understood, especially in view of equation (1).

The E-region drift speeds (V) at Thumba are higher than at any other stations while the F-region drift at Tamale are only slightly greater than corresponding values for Thumba. These results confirm that the ionospheric drifts have a sharp maximum near the magnetic equator.

The values of axial ratio at Thumba are higher than those at Waltair and Singapore but lower than those obtained at Tamale and Ibadan. The preliminary analysis of the records at Thumba have indicated significant increase of the axial ratio with solar activity and mean values of 7 for the year 1967 and about 11 for the year 1968 have been found. This suggests that the higher values of the axial ratio at Ibadan and Tamale than at Thumba are due to the solar cycle effect. Thus the axial ratio is also found to have a maximum close to the magnetic equator.

The orientation of the irregularities at stations, Thumba, Tamale and Ibadan, is within 3° from the geographic North. At Waltair, it is 16° West of North indicating that at stations within the equatorial electrojet, the orientation of the major axis of the irregularities is almost along the magnetic meridian while at higher latitudes the orientation departs significantly towards West of the magnetic meridian.

Conclusion

The above results indicate that the drift measurements near the magnetic equator are closely associated with the equatorial electrojet. A closer study between ionospheric drifts and the magnetic variations are necessary to understand to equatorial ionospheric drifts.

Acknowledgement

Thanks are due to Prof. V.A. Sarabhai, Chairman, Indian National Committee for Space Research, for the facilities provided for the Ionospheric Research Station at Thumba Rocket Range and to Prof. K.R. Ramanathan for his keen interest during the course of work.

REFERENCES

Briggs B.H., Phillips G.J. and Shinn D.H.	1950	Proc. Phys. Soc., B63, 106.
Chandra H. and Rastogi R.G.	1969	J. Atmosph. Terr. Phys., 31, 1205.
Deshpande M.R. and Rastogi R.G.	1966a	Ann. de. Geophys., 23, 418.
Deshpande M.R. and Rastogi R.G.	1966b	Proc. IQSY Symp., New Delhi.
Fooks G.F.	1965	J. Atmosph. Terr. Phys., 27, 979.
Fooks G.F. and Jones I.L.	1961	J. Atmosph. Terr. Phys., 20, 229.
Harrison V.A.W.	1965	Proc. 2nd Int. Symp. on Eq. Aeronomy, edited by F. de. Mendonca, 290.
Koster J.R. and Katsriku I.K.	1966	Ann. de. Geophys., 22, 440.
Mitra S.N.	1949	Proc. I.E.E., 96, Part III, 441.
Phillips G.J. and Spencer M.	1955	Proc. Phys. Soc., B68, 481.
Rao P.B. and Rao B.R.	1963	Proc. Int. Conf. on the Ionosphere (edited by Stickland A.C.) p. 363, Physical Society, London.
Rastogi R.G., Deshpande M.R. and Chandra H.	1968	J. Atmosph. Terr. Phys., 30, 1597.
Rastogi R.G., Chandra H. and Misra R.K.	1969	Proc. 3rd Int. Symp. on Equatorial Aeronomy (in press).

Skinner N.J., Hope J. and Wright R.W. 1958 Nature, 182, 1363.

Skinner N.J., Lyon A.J. and Wright R.W. 1963 Proc. Int. Conf. on the Ionosphere (edited by Stickland A.C.) p. 301, Physical Society, London.

CHAPTER - II.5 EFFECT OF MAGNETIC ACTIVITY ON DRIFT AND SIZE OF THE IRREGULARITIES

Chapter - II.5

Chapter II.5 Effect of magnetic activity on the drift and size of the irregularities

Introduction

According to the dynamo theory, the geomagnetic field variations observed at ground are due to the currents in the dynamo region driven by the electric fields induced due to the air motion across the field lines. Theoretical work on the ionization drift in ionosphere under the influences of electric fields and neutral winds by Martyn (1953) and Kato (1959) has shown that below the E-region, the horizontal movement of the ionization will be substantially same as the local wind velocity. However, the ionization in the F-region cannot be moved across magnetic field lines by neutral winds. The E-W drift in the F-region can be produced only by the applied electric fields which are communicated from the dynamo region. Hence the drifts of ionization in the E-region or in the F-region are dependent on the neutral wind blowing in the dynamo region. Occasionally the geomagnetic field measurements at ground show large perturbations at times of intense solar activity. Fluctuations of the order of few hundred gammas are observed at low latitudes.

The drifts of ionization in the E- or F-region under such magnetic conditions are therefore important to study from the aspect of dynamo theory. Apart from the

measurements at times of severe magnetic activity, a comparison of the drifts at times of normal conditions of the magnetic field variations and at times of such perturbations have been made by many authors.

II.5.1. Magnetic activity - its indices

To depict the character of the magnetic activity throughout the day, a large number of indices have been defined. One of the indices is K-index which was adopted in 1939 by IATME (now IAGA). This is intended to be a measure of solar corpuscular radiation based upon the intensity of geomagnetic activity caused by the electric currents produced by such radiation.

Each observatory assigns an integer from 0 to 9 to each of the 3 h. intervals of the day beginning at 0000, 0300, ...2100 UT. A permanent scale is adopted for each observatory from which K-index can be assigned from the limits of amplitude ranges R in gammas. For each magnetic element, the difference between the highest and lowest deviations from the regular daily variations within the 3 h. interval is defined as the range R. Most disturbed element (excluding Z) has been taken as the basis for K (through 1963).

All observatories could not have the same conversion scale for range R to K index because for the same magnetic storm the range will be many times great at auroral zone stations compared to at equatorial stations.

K-index from 12 observatories between geomagnetic latitudes 47 and 63 degrees are used to derive the planetary index K_p. K-indices are first translated into standardized indices Ks which are freed from local variations. Ks is a continuous variable from 0.0 to 9.0 and is given in thirds of an integer such as 2-, 2_o, 2+ etc. K_p is therefore an index in 28 grades with extreme values 0 (very quiet) to 9 (extremely disturbed).

Based upon the K_p-indices, five magnetically quietest and five magnetically most disturbed days are selected for each month and are known as international quiet and disturbed days. The rankings are based upon the following three criteria with equal weight $\sum K_p$, $\sum K_p^2$ and (Kp) Max.

Drift parameters have been compared with the K-index of nearest observatory by many authors. In the present analysis of the drift results at Thumba, five international quiet and five international disturbed days have been taken as the criterion for studying the effect of magnetic activity on drifts.

II.5.2. Drift and anisotropy parameters during magnetically quiet and disturbed days at Thumba

First, the fading rates and the apparent drift speeds have been studied, because these parameters are tabulated on a routine basis for each record and this gives a good statistics of the comparison. Fig. II.5.1. shows

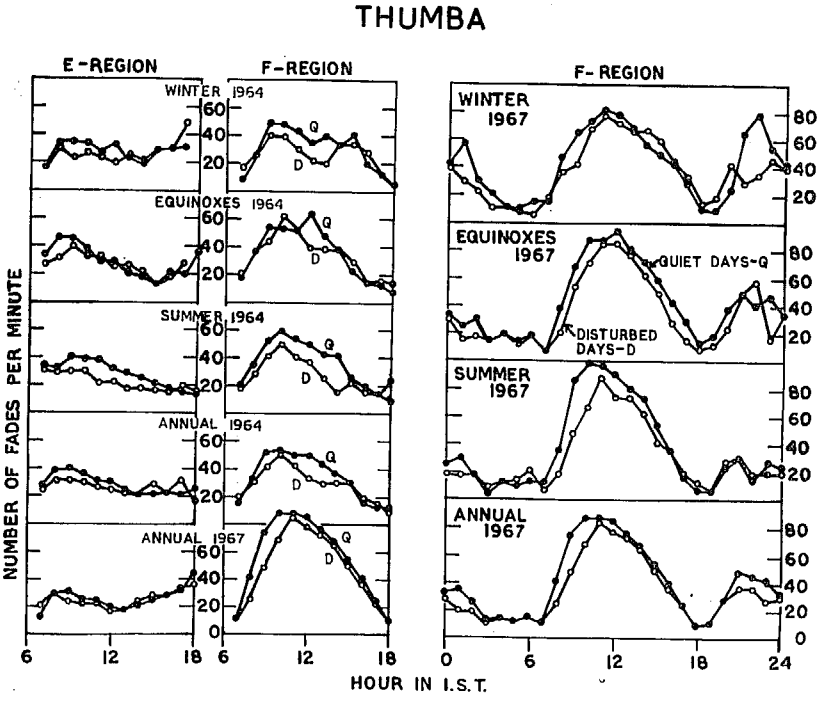

Fig. II.5.1.

the daily variations of the fading rates on quiet and disturbed days during each season in the years 1964 and 1967.

In the year 1967, E-region records were not sufficient and so only annual daily variation is shown. The curve drawn through the full circles represents the daily variation on quiet days while the curve drawn through the open circles represents the daily variation on disturbed days. Referring to the annual daily variation curves fading rates are higher on quiet days than on disturbed days for both E- and F-regions. The difference is most clear in the summer months for both E- and F-regions and least in the equinoxes. In the year 1967 also, the difference is most clear during summer for nighttime hours. Thus it can be noticed that the fading rates are reduced on disturbed days.

The daily variations of the apparent drift speeds on quiet and disturbed days for the daytime hours in each season as well as annual variation in the year 1964 and the annual variation in the year 1967, both for E- and F-regions are shown in Fig. II.5.2, while the daily variations for the F-region during each season in the year 1967 are shown in Figure II.5.3. The E-region drift speed is higher on quiet than on disturbed days in 1964 while in 1967, no significant difference is noticed. In the individual seasons of 1964, the effect is most clear during the solstices (summer and winter). During equinoxes, the speeds are

higher on quiet days in the forenoon period while these are

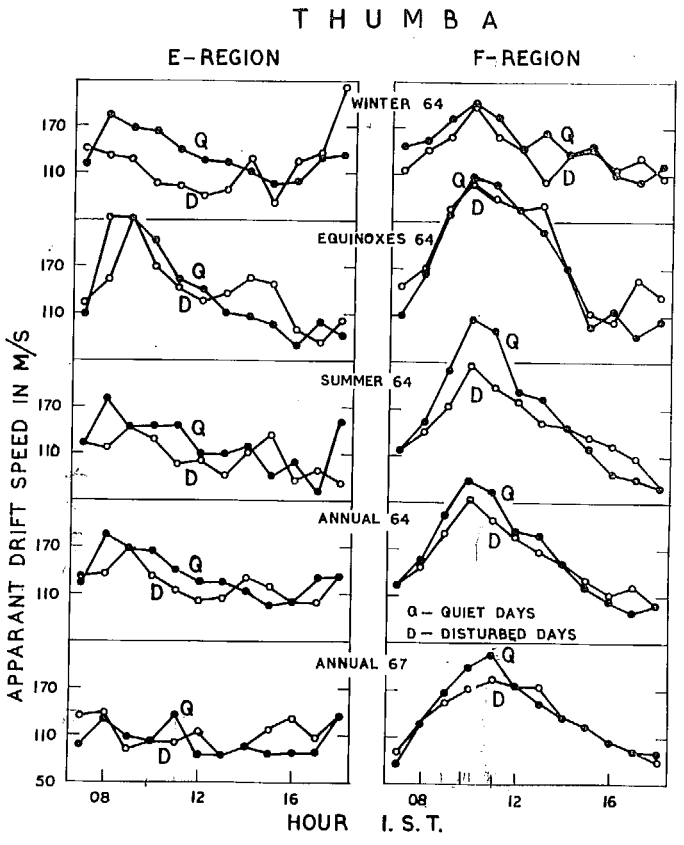

Fig. II.5.2.

higher on disturbed days in the afternoon period.

The F-region results of 1964 and 1967 show an indication of the drift speeds being higher on quiet days than

on disturbed days for both daytime and nighttime. The daytime difference is most clear in summer season, while nighttime difference is most clear in winter season.

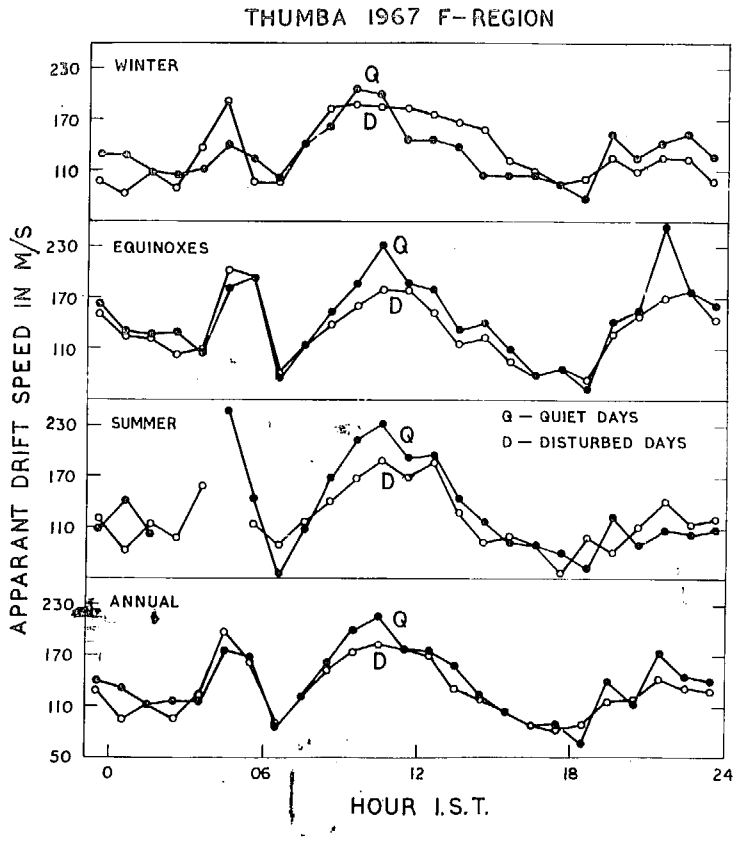

Fig. II.5.3.

Comparison of the true drift and anisotropy parameters on quiet and disturbed days was attempted for the records analysed in the year 1964 and 1967. As the records analysed for the year 1964 were mostly for quiet periods, comparison was undertaken only for the year 1967. In all, 25 quiet period and 31 disturbed period records were available for the E-region while 100 quiet period and 7[illegible] disturbed

period records were available for the F-region. The results are described as histograms of percentage occurrence for each parameter viz. true drift speed V, ratio V_c/V, axial ratio r, orientation and semi-minor axis b and are shown in Figs. II.5.4 to II.5.8. The mean with standared error and median values for each parameter are collected in Table II.5.1.

The histograms of true drift speed on quiet and disturbed days for both E- and F-regions are shown in Fig. II.5.4. The median values for the E-region speeds are

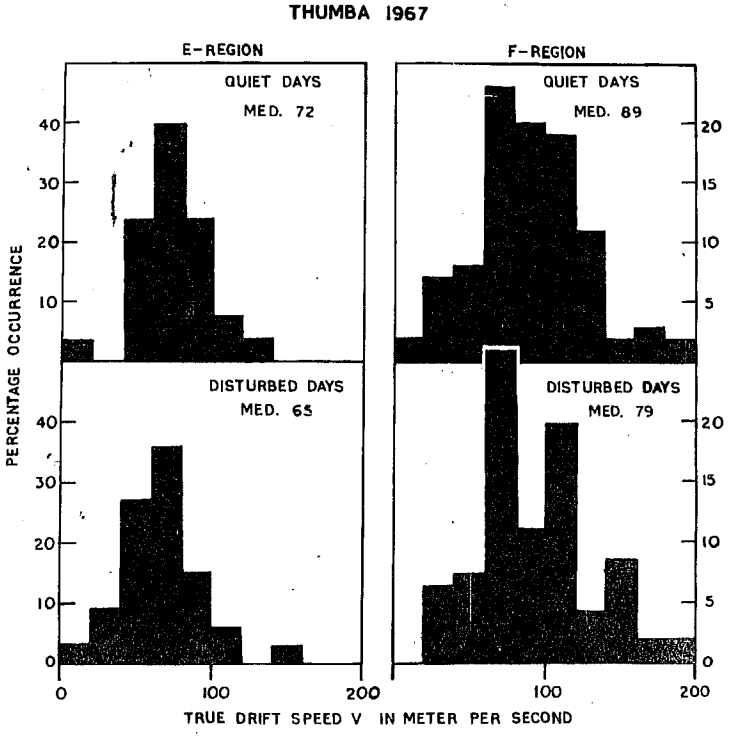

Fig. II.5.4.

89 m/sec. on quiet days and 79 m/sec. on disturbed days indicating decrease in the true drift speed on disturbed days for both E- and F-regions.

The ratio V_c/V on quiet and disturbed days is shown in Fig. II.5.5 as histograms of percentage occurrence.

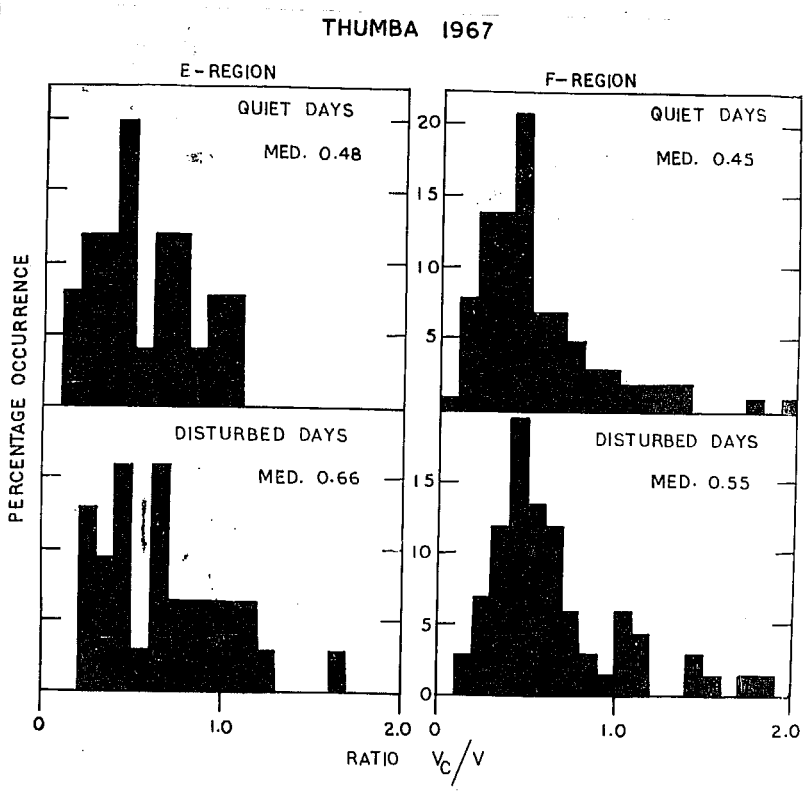

Fig. II.5.5.

The histograms for disturbed days seem to have shifted to higher side. The median values obtained are 0.48 on quiet

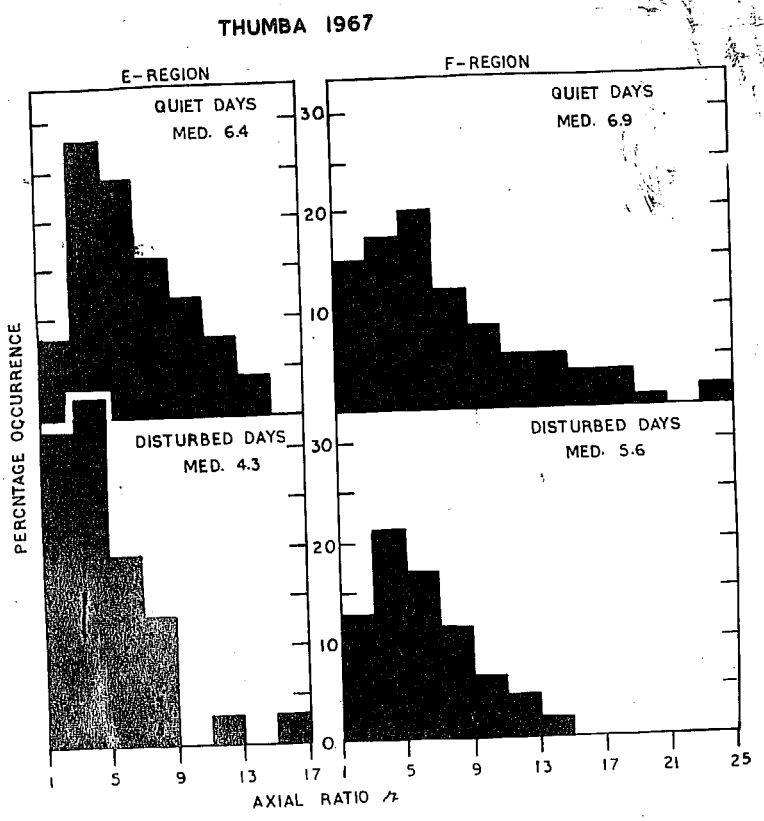
THUMBA 1967
E-REGION
F-REGION
QUIET DAYS
MED. 6.4
QUIET DAYS
MED. 6.9
DISTURBED DAYS
MED. 4.3
DISTURBED DAYS
MED. 5.6
PERCNTAGE OCCURRENCE
30
20
10
30
20
10
0
1
5
9
13
17
1
5
9
13
17
21
25
AXIAL RATIO

Fig II. 5. 6

days and 0.66 on disturbed days for the E-region while for F-region, the median values are 0.45 and 0.55 respectively for quiet days and disturbed days. Thus the ratio V_c/V seems to increase on disturbed days for both E- and F- regions.

The histograms for the axial ratio are shown in Fig. II.5.6. There is a clear indication that while on quiet days individual values of the axial ratio are scattered widely, they are concentrated in the lower value side on disturbed days. The median value of r is 6.4 on quiet days and 4.3 on disturbed days for the E-region while for F-region median value is 6.9 on quiet days and 5.6 on disturbed days. Thus there is clear indication that the elongation of the irregularities is reduced on the disturbed days.

The orientation of the major axis of the ellipse as measured from the magnetic North is shown in Fig. II.5.7. For the E-region, the orientation which is along N-S for most of the occasions on quiet days departs from that on disturbed days, the median values being 2^o East of North on quiet days and 3^o West of North on disturbed days. F-region results show no difference in the nature of histograms or in the median values. Thus there is no marked

effect seen in the orientation ψ , alignment being along

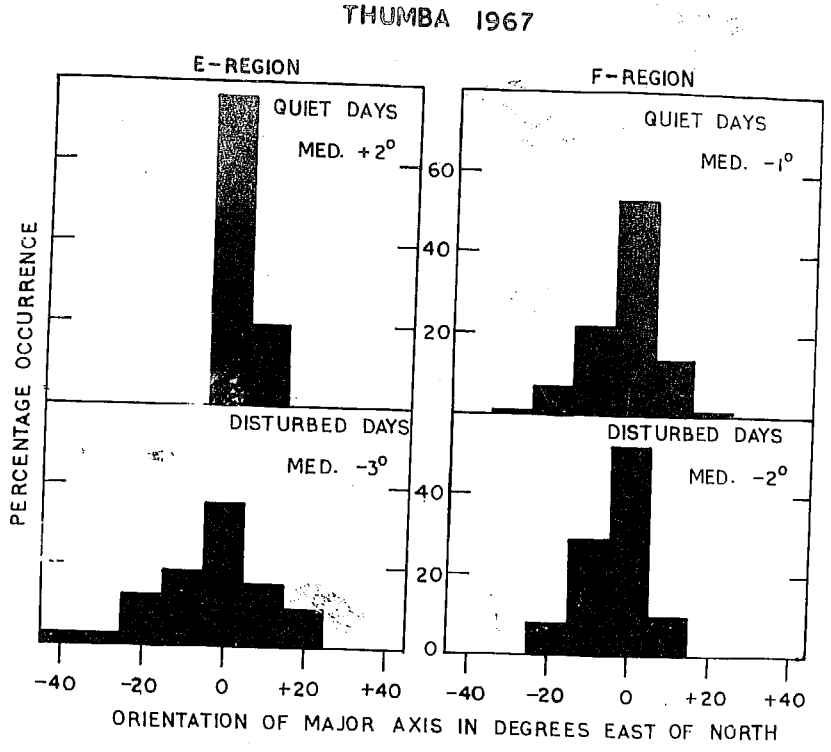

Fig. II.5.7.

magnetic N-S for both quiet and disturbed days.

The size of the irregularities (diffraction pattern at ground) is shown in Fig. II.5.8 which shows the histograms for the length of the semi-minor axis b. From the nature of histograms, it looks that b is larger on disturbed days than on quiet days for E-region while the histograms look alike on quiet and disturbed days for F-region. The median values for the E-region are 70 meters

and 72 meters on quiet and disturbed days respectively which are not different from each other. However, the mean values for the E-region are 72 metres on quiet days and 85 metres on disturbed days. The median value of b for the F-region are 76 metres on quiet days and 80 metres on disturbed days, while the mean value is 95 metres, on both quiet and disturbed days. Thus a little increase of b can be suggested on disturbed days.

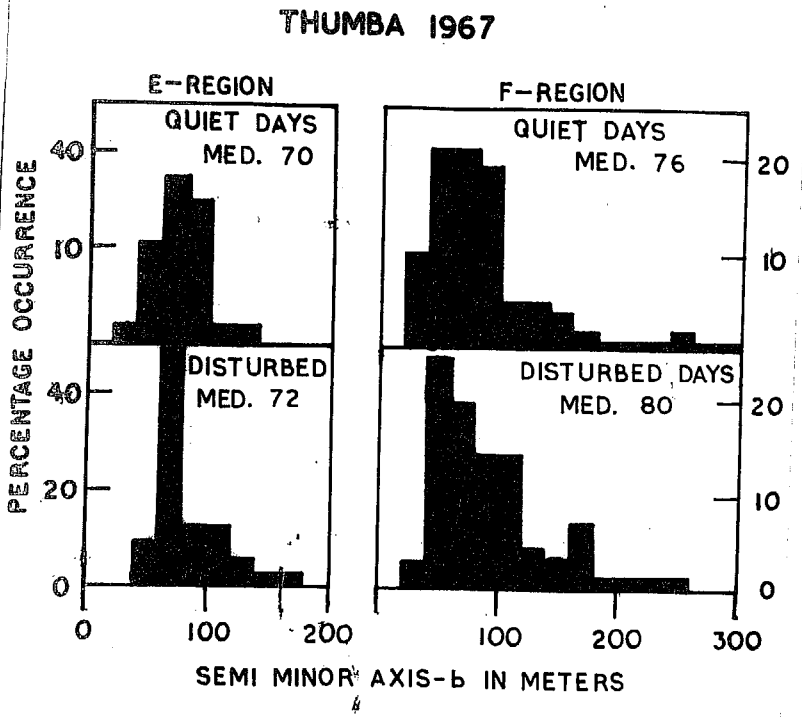

Fig. II.5.8.

(Table II.5.1 is given in the next page)

TABLE-II.5.1.

Drift and anisotropic parameters at Thumba during magnetically quiet and disturbed days in the year 1967.

Parameter	E-region				F-region			
	Quiet days Count = 25		Disturbed days Count = 31		Quiet days Count =100		Disturbed days Count = 74	
	Mean	Med	Mean	Med	Mean	Med	Mean	Med
True drift speed V in m/sec.	74 ± 5	72	66 ± 5	65	93 ± 4	89	87 ± 5	79
Ratio V_c/V	.57 ± .01	.48	.78 ± .06	.66	.59 ± .05	.45	.67 ± .06	.55
Semi-minor axis b in meters.	72 ± 5	70	85 ± 3	72	95 ± 7	76	95 ± 6	80
Axial ratio $\frac{a}{b}$	7.0 ± .7	6.4	4.9 ± .5	4.3	10.0 ± 1.0	6.9	8.4 ± .6	5.6
Orientation of characteristics eclips in degrees East of Mag. North	1 ± 2	2	357 ± 2	357	357 ± 2	359	357 ± 1	358

II.5.3. Results at other stations

Chapman (1953) obtained positive correlation between the apparent drift speed obtained at Ottawa - Montreal and the magnetic K-figure. For the E-region, the drift speed was independent upto K-figure 4, but increased with further increase of the K-figure. F-region drift showed a steady slow increase with K-figure from 0 to 5 and a more rapid increase as the K-figure exceeded 5. Briggs and Spencer (1954) reported drift speeds for the E-region at Cambridge to be independent of K-figure between 1 and 5; however, on one occasion high drift speeds were recorded when there was a severe magnetic storm. For the F-region drift speeds were found to be approximately constant upto K-figure 5, after which E-W component was found to increase steadily.

Rao and Rao (1961) studied E-region drift data at Waltair for the period, June1957 to May 1959, with magnetic activity and found that drift speed increases linearly with magnetic K-figure in the range 0-5. For the same station, Rao et al (1961), obtained drift speed decreasing linearly with the K-figure for the F_2-region. Resolving the drift speed into E-W and N-S components, they found that the N-S component more or less remains constant with the K-figure while a decrease was observed for the E-W component. Thus

while the results for E-region were same as observed at high latitudes the effect f magnetic activity was found to be opposite at low latitude as compared to that found at high latitudes.

A study of the latitudinal variation of the effect of magnetic activity on E-region drifts was undertaken by Rao (1963). I.G.Y. data for the stations, Waltair, Yamagawa, De Bilt, Brisbane and Wellington were compared. K-figure was taken from the magnetic observatories located at the nearest geomagnetic latitudes. For all stations, there was increase in drift speed with the K-figure, the rate of increase being more at high latitudes.

Rao and Rao (1964) studied the effect of magnetic activity on the horizontal drift and anisotropy of the ionospheric irregularities in the E-region at Waltair using full correlation analysis. Both apparent and true drift speeds were found to increase with K-figure. The ratio V_c/V was found to increase on disturbed days, the axial ratio of the characteristic ellipse increased and semi-minor axis decreased. The orientation was found closely aligned along magnetic North in the disturbed days.

Similar study at high latitude station Cambridge by Fooks and Jones (1961) and Fooks (1961) showed that while the axial ratio is nearly same for quiet and disturbed days,

length of the semi-minor axis is reduced considerably and irregularities are aligned closer to magnetic field. Moreover, the ratio V_c/V was quiet low during magnetic storms.

A comparison of the effect of magnetic activity on the true drift and anisotropic parameters of the irregularities in the E-region over Waltair and Yamagawa was made by Rao G. L. N. (1965) for the period October 1958. For both the stations, Waltair and Yamagawa, the drift speed was more on disturbed days, the difference being more for Yamagawa. The axial ratio and the size of the irregularities were found to be more on disturbed days which was more clearer for Yamagawa. The orientation was nearer to the magnetic meridian during disturbed days.

Rao (1966) studied F-region apparent drift speeds with K-figure at Waltair, Yamagawa, Ashkhabad, Simeiz and Gorky. It was found that at low latitude station, Waltair, drift speed decreased with K-figure, at mid-latitude stations, Yamagawa and Ashkhabad, it remained constant and at high latitude stations, Simeiz and Gorky, it increased with the K-figure.

In the equatorial region drift study during quiet and disturbed days was done by Skinner et al (1963) and showed that true drift speed in the F-region on disturbed days is substancially reduced during night, but is hardly

affected by day. Nighttime Eastward drift speed of 90 m/sec was obtained on quiet days and 50 m/sec on disturbed days. The size of irregularities was also found to be more on disturbed nights than on quiet nights while the size was practically same during daytime on quiet and disturbed days.

Osborne and Skinner (1963) correlated the F-region apparent drift speed V' obtained at Tamale (0.6° mag. lat.) with the field H_L at Legon (dip 10°S), i.e. the normal S_q field, and with the jet field at Tamale given by H_T-H_L. About 68 drift measurements during daytime hours were analysed and it was found that V' is more closely related to the jet field H_T-H_L. The apparent drift speed V' was found to increase with the strength of the jet current.

A comparison of the true drift speeds at Ibadan during IGY and IQSY was done by Morris and Lyon (1966) for the equuinoctial months. In the F-region, the drift speed was shown to be reduced by a factor of about 1.8 both near noon and near midnight. In the E-region, there was not much significant difference but a little decrease in the low sunspot years was suggested. They further showed that the daily range of the horizontal component of earth's magnetic field R_H decreased by a factor of about 2 from the solar maximum of IGY to the solar minimum of IQSY indicating close

association of the drift speed with the range of the magnetic field R_H.

II.5.4. Discussion

Results obtained at Thumba show a decrease in the fading rate as well as in the drift speed on magnetically disturbed days for both E- and F-regions. It has been shown that there is a slight decrease in the electrojet strength (difference between the horizontal range at magnetic equator & horizontal range at a station about 6^o away from the magnetic equator gives the jet contribution to the large diurnal variation in the horizontal magnetic component near the magnetic equator and is a measure of the electrojet current strength) on magnetically disturbed days (Osborne, 1963). Hence, it seems that the drift speed of the irregularities in the equatorial ionosphere depends on the electrojet strength.

The axial ratio r significantly decreases on disturbed days for both E- and F-region which shows the elongation of the irregularities is again dependent on the electrojet current strength.

The orientation does not show any significant change but there is indication that on disturbed days it shifts slightly West of magnetic North in the E-region.

No significant change in the semi-minor axis b is observed, but an indication of increase in b is suggested on the disturbed days for E- and F-regions.

Comparing with the results obtained by earlier workers, it is found that on magnetically disturbed days, there is a decrease in the drift speeds at equatorial stations and an increase at high latitude stations. For the E-region, one finds a decrease at Thumba, a small increase at Waltair and a rapid increase at higher latitudes, indicating reversal occurring in between Thumba and Waltair. For the F-region, a decrease is observed at Thumba, Ibadan and Waltair, practically no effect at Yamagawa and Ashkhabad and increase at high latitude stations, Gorky and Simeiz reversal occurring at mid-latitudes. Thus this reversal occurs nearer to equator for E-region than for F-region. Another important difference observed is that for the E-region diffraction patterns at Waltair, the semi-minor axis decreased on disturbed days and orientation became more closely aligned along magnetic North. Similar results were obtained at Cambridge where the semi-minor axis was found to reduce considerably on the distrubed days and orientation being more closely aligned along the magnetic North. The ratio V_c/V was found to be quiet low on disturbed days at Cambridge. The resulsts at Thumba show in-

crease of the ratio V_c/V, suggestion of an increase of the semi-minor axis b both in the E- and F-regions on disturbed days. It seems therefore that that the effect of the magnetic disturbance at equatorial stations is just opposite to that at high latitude stations. However, it is necessary to analyse more data both in the equatorial and high latitude stations to find the exact effect of the magnetic activity on irregularities and their drift.

CHAPTER - II.6. Discussion and comparison of the drift study at Thumba with those at other stations

CHAPTER II.6. Discussion and comparison of the drift study at Thumba with those at other stations

The resulsts of the horizontal drift and anisotropy parameters of the irregularities in the E- and F-regions of ionosphere over Thumba have been compared to those obtained at other stations, particularly at other equatorial stations in the preceeding chapters; namely II.3, II.4 and II.5. The important points are collected here.

For either of the E- or F-regions, there is a sharp increase in the apparent drift speed in a very narrow zone near the magnetic equator which suggests a close association of the drifts in this zone with the electrojet currents. The speeds are lowest near 30^{o}-50^{o} magnitude latitude. A small increase is suggested to occur at high latitude stations.

The direction of drift at Thumba is entirely Westward during daytime and Eastward during nighttime. The N-S drift directions seem to be negligible even during the periods of reversals. Thus the reversals of the drift direction in the morning or evening do not indicate a smooth rotation of the drift vector. Similar E-W drifts have been reported at other stations near magnetic equator, namely at Ibadan and Tamale. The N-S components are significant at stations, Waltair and Singapore, and the drift vectors show smooth rotation with the solar time in accordance with the dynamo theory of S_q variations. The high latitude

drifts have been shown to have daytime East-ward and night-time Westward component with a smooth rotation of drift vector. These observational results agree fairly well with the F-region drift systems as calculated by Maeda (1963) from the dynamo theory.

The reversal times of the drift direction in F-region at Thumba in the morning and evening agree very well with the reversal times of E-region direct electron drifts measured at Jicamarca by Doppler shift technique. The F-region vertical drifts at Jicamarca have been shown to reverse direction exactly when E-W current reversals occur in the E-region. Further, nighttime electron drifts at Jicamarca are shown to have nearly same magnitude as during daytime. These results agree well with the results obtained at Thumba which show that the drift of the irregularities near equator indicate the electron motion itself.

Another interesting result obtained is the late morning reversal and early evening reversal of the drift direction during summer season. The evening reversals are shown to have day-to-day variability.

The true drift speeds calculated at Thumba show drift speed of about 75-80 m/sec in the E-region and about 85-100 m/sec in the F-region. The drift speeds are found to be lowest during summer for either of the region.

The study at other stations also show lowest drift speeds to occur during summer.

The results at Ibadan show maximum drift speed during D-months and lowest during J-months. At Thumba, similar results are obtained for the E-region while for F-region winter and equinoctial values are equal. The time of the daytime maximum is shown to be latest during summer. Similar result has been obtained at Ibadan. Nighttime drift speeds show a clear maxima in the equinoxes and dip during summer at both the stations, Thumba and Ibadan.

E-region drift speeds at Thumba are of same order in the years 1964 and 1967, but there has been a little reduction in the value of drift speed in the F-region. These results are in contrast to the results obtained at Ibadan where there was a considerable decrease of the true drift speed in the F-region and a suggestion of decrease in the E-region from IGY period to IQSY.

The ratio V_c/V at Thumba is of the order of unity in the year 1964 and about 0.6 - 0.7 for the year 1967. The ratios obtained at Ibadan and Waltair also lie in the range 0.6 - 0.8. Thus there is no significant latitude variation in V_c/V. Further, at all low latitude stations, the ratio V_c/V is higher for the E-region than for the F-region. Thus the life-time of the irregularities in the

E-region is comparatively shorther than in the F-region. Again the ratio for the F-region is higher during daytime than during nighttime. These results do indicate a dependence of the life-time of irregularities on the collisions in the region of the irregularities.

The anisotropy of the irregularities is maximum near equator. Axial ratio is found to be 3 for the E- and F-region records at Thumba during the year 1964. However, the value increases to about 6 for the E-region and 10 for the F-region in the year 1967. These values agree fairly well with those obtained at Ibadan for a few records during IGY period. There seems to be a sudden drop in the value of axial ratio at stations away from equator (mag.) as evident from the values obtained at Waltair and Singapore which are of the order of 2. The values are lowest at Cambridge.

The size of the irregularities at ground is lowest at the equator where the transverse size is less than 100 meters. Size as low as 40 meters is obtained during daytime hours of 1967 at Thumba. This value increases towards higher latitudes and at Cambridge sizes exceed 200 meters.

The irregularities are perfectly field aligned at the equatorial stations of Thumba, Tamale and Ibadan, about 10-15^{o}West of North at Waltair and in the N-W qua-

drant at Cambridge.

Thus control of the field lines is maximum near equator where rather thin irregularities are observed. The abnormal behaviour at equator restricted to a very small zone seems to be associated with the presence of large currents flowing in this zone. A marked rise in the axial ratio and marked reduction in the transverse size of the irregularities at Thumba is seen in the year 1967 which is a relatively higher sunspot year than the low sunspot year, 1964. The drift velocities at equatorial stations have been found to be dependent on the jet field.

The fading rate, drift speed and the axial ratio are considerably reduced at equatorial stations on magnetically disturbed days. Further it is well-known that the drift speed increases on magnetically disturbed days, at high latitude stations. The change-over of this phenomenon is seen to occur in the intermediate latitudes which is nearer to the equator for the E-region and slightly away for the F-region.

The diffraction patterns at equatorial stations are more closely field aligned on magnetically quiet days than on disturbed days while reverse is the case at high latitudes. Similarly, the semi-minor axis increases at equatorial stations on magnetically disturbed days and de-

creases at high latitudes.

Thus as far the ionospheric drifts are concerned, one can divide the world-wide pattern into three different zones.

(1) An equatorial zone - where the irregularities and their motion are controlled by electrojet. A true East-West drift is observed which is reduced on magnetically disturbed days. N-S direction are not observed even at the time of reversals. The irregularities are thin, elongated and field aligned. Departure from these properties is observed on magnetically disturbed days.

(2) A high latitude region - where drifts have East-West component which are in reverse direction than those observed at equator. Smooth rotation of the drift vector is observed. Magnetic activity acts opposite to what is observed at equator. Irregularities are here controlled by charged particles precipitation.

(3) An intermediate zone - where the behaviour changes from season to season with drifts like at high latitudes in some season and like at low latitudes in other season. Martyn had predicted a phase reversal of drifts occurring at latitude of about 35^{o}.

Thus the stations in this region have variability because of the positions of the current loops changing from season to season. Magnetic disturbance-wise also, this intermediate zone will have drift speeds independent of the magnetic activity.

However, more study of the drift and anisotropy of irregularities in the E- and F-regions of ionosphere is required particularly at middle latitudes before some conclusion is made on a firm basis.

World-wide drift and the dynamo theory

The external current systems calculated from the observed magnetic field variations show:

(1) In the equatorial zone, there is a daytime East-ward current flow and a weak nighttime West-ward current flow. No N-S currents are observed in this zone.

(2) In the high latitudes, there is daytime West-ward current flow.

(3) Currents are mainly N-S during most of the daytime at intermediate latitudes. An Eastward current around noon is observed at latitude less than that of the current focus and Westward current

at latitudes higher than that of current focus. At a particular latitude, the direction of the current flow changes smoothly with the solar time. The observed world-wide pattern of the drifts therefore agrees fairly well with the expected behaviour according to the dynamo theory.

REFERENCES

Alpert Ya. L.	1960	The Propogation of Radio Waves and the Ionosphere, Moscow, Izd-vo, ANSSSR.
Appleton E.V. & Ratcliffe J.A.	1927	Proc. Roy. Soc., A115, 315.
Balsley B.B.	1966	Ann. de. Geophys., 22, 460.
Balsley B.B.	1969	J. Atmosph. Terr. Phys., 31, 475.
Balsley B.B. & Woodman R.F.	1969	J. Atmosph. Terr. Phys., 31, 865.
Bartels J.	1949a	IATME Bull. No. 12b, p. no. 97-120.
Bartels J.	1949b	J. Geophys. Res., 54, 296.
Bartlett M.S.	1956	Stochastic processes, Cambridge University Press, Cambridge.
Bellchamber W.H. & W.R. Piggott.	1965	Annales of the IGY,, 33, 278.
Bowhill S.A.	1956	J. Atmosph. Terres. Phys., 8, 120.
Briggs B.H., J.S. Phillips & G.J. Shinn	1950	Proc. Phys. Soc., B63, 106.
Briggs B.H. & Spencer M.	1954	Rep. Prog. Phys., 17, 245.
Burke M.J. and I.S. Jenkinson.	1957	Australian Journal of Phys., 10, No. 3, 378.
Calvert W. & Cohen R.	1961	J. Geophys. Res., 66, 3125.
Chapman J.H.	1953	Canad. J. Phys., 31, 120.
Clemsha B.R.	1964	J. Atmosph. Terres. Phys., 26, 91.

Cohen R. & Bowles K.L.	1963	J. Geophys. Res., 68, 2503.
Cole K.D.	1963	Planet. Space Sci., 10, 129.
Deshpande M.R. & R.G. Rastogi	1966a	Ann. 'e. Geophys., 23, 418.
Deshpande M.R. & R.G. Rastogi	1966b	Proc. IQSY Symp., New Delhi, p. 167.
Deshpande M.R. & R.G. Rastogi	1967	Proc. Indian Academy of Sci., 66, 272.
Deshpande M.R. & R.G. Rastogi	1968	J. Atmosph. Terres. Phys., 30, 293.
Fooks G.F.	1965	J. Atmosph. Terres. Phys., 27, 979.
Fooks G.F. & Jones I.J.	1961	J. Atmosph. Terres. Phys., 20, 229.
Furth R. and Medonald D.K.C.	1947	Proc. Phys. Soc., 59, 388.
Greenhow J.S.	1952	J. Atmosph. Terres. Phys., 2, 282.
Harrison V.A.W.	1965	Proc. IInd Int. Symp. on Equatorial Ionosphere, ed. F. de. in endonca, 1290.
Hey J.S.	1947	Nature, 159, 119.
Keneshea T.J., M.E. Gardner & W. Pfister.	1965	J. Atmosph. Terres. Phys., 27, 7.
Kent G.S. & Koster J.R.	1966	Ann. de. Geophys., 22, 405.
Kent G.S. & Wright R.W.H.	1968	J. Atmosph. Terres. Phys., 30, 657.
Koster J.R.	1963	J. Geophys. Res., 68, 2579.
Koster J.R. & Katsriku I.K.	1966	Ann. de. Geophys., 22, 440.
Kelleher R.F.	1965	Proc. IInd Int. Symp. on Equatorial Ionosphere, ed. F. de. Mendonca, p. 272.

Liller W. & Whipple F.L.	1954	Spec. Supple. to J. Atmosph. Terres. Phys., 1, 112.
Little C.B., Reid G.C., Stilther E. & Merritt R.P.	1962	J. Geophys. Res., 67, 1763.
Manning L.A., Villard P.G. & Peterson A.M.	1950	Proc. I.R.E., 38, 877.
McNicol R.W.E.	1949	Proc. Instn. Elect. Engrs., Part III, 96, 517.
Martyn D.F.	1953	Phil. Trans. Roy. Soc., London, A246, 306.
Mitra S.N.	1949	Proc. Inst. Elect. Engrs., 96, 441.
Mitra S.N., K.K. Vig & P. Dasgupta.	1960	J. Atmosph. Terres. Phys., 19, 172.
Mirkotan S.F.	1962	Geomag. and Aeronomy, 2, 578.
Morris R.W. and Lyon A.J.	1966	Nature, 210, 617.
Morris R.W.	1967	J. Atmosph. Terres. Phys., 29, 651.
Munro G.H.	1948	Nature, 162, 386.
Munro G.H.	1950	Proc. Roy. Soc., A202, 208.
Munro G.H.	1953a	Proc. Roy. Soc., A219, 447.
Munro G.H.	1953b	Nature, 171, 693.
Munro G.H.	1963	J. Geophys. Res., 68, 1851.
Osborne B.W.	1955	J. Atmosph. Terres. Phys., 6, 117.
Osborne D.G.	1963	J. Geophys. Res., 68, 2435.
Osborne D.G. & Skinner N.J.	1963	J. Geophys. Res., 68, 2441.

Patel C.M.	1967	J. Inst. Telecom. Engrs., 13, 414.
Pawsey J.L.	1935	Proc. Camb. Phil. Soc., 31, 125.
Phillips G.J. & Spencer M.	1955	Proc. Phys. Soc., 68B, 106.
Piggott W.R. & Barclay L.W.	1963	Proc. Int. Conf. Ionosphere, p. 323, The Physical Society, London, 1962.
Purslow B.W.	1958	Nature, 181, 35.
Rao B.R., M.S. Rao & D.S.N. Murthy.	1956	J. Scientific Industrial Research, A15, 75.
Rao B.R. & E.B. Rao	1958	Nature, 181, 1612.
Rao R.R. & B.R. Rao	1961	J. Atmosph. Terres. Phys., 22, 81.
Rao A.S. & B.R. Rao	1964a	J. Atmosph. Terres. Phys., 26, 399.
Rao G.L.N. & B.R. Rao	1965	J. Geophys. Res., 70, 667.
Rao P.B. & Rao B.R.	1963	Proc. Int. Conf. on the Ionosphere (edited by Stickland A.C.), p. 363, Physical Society, London.
Rao G.L.N. & Rao B.R.	1963	J. Atmosph. Terres. Phys., 25, 553.
Rao P.B. & Rao B.R.	1964	J. Atmosph. Terres. Phys., 26, 445.
Rao G.L.N.	1966	Aeronomy Report No. 9, University of Illinois, Urbana.
Rao G.L.N.	1965	Aeronomy Report No. 6, University of Illinois, Urbana.
Rao B.R., Rao E.B. & Murthy Y.V.R.	1961	Proc. IGY Symp., CSIR, New Delhi, 205-211.

Rao G.L.N. & Rao B.R.	1964	J. Inst. Telecom. Engrs., New Delhi, 10, 537.
Rastogi R.G., M.R. Deshpande and N.D. Kaushika.	1966	J. Atmosph. Terres. Phys., 28, 137.
Rastogi R.G., M.R. Deshpande and Harish Chandra.	1968	J. Atmosph. Terres. Phys., 30, 1597.
Ratcliffe J.A. & Pawsey J.L.	1933	Proc. Camb. Phil. Soc., 29, 301.
Ratcliffe J.A.	1948	Nature (Lond.), 162, 9.
Rawer K.	1965	Annales IGY, 33, Compiled by K. Raswer.
Rice S.O.	1945	Bell System Technical Journal, 23, 282.
Rice S.O.	1949	Bell System Technical Journal, 24, 46.
Robertson D.S., Liddy D.T. and Elford W.G.	1953	J. Atmosph. Terres. Phys., 4, 255.
Skinner N.J., Lyon A.J. & Wright R.W.	1958	Nature, 182, 1363.
Skinner N.J., Lyon A.J. & Wright R.W.	1963	Proc. Int. Conf. on the Ionosphere (edited by Stickland, p. 301, Physical Society, Londoan, AC).
Slee O.B.	1958	Nature, 181, 1610.
Spencer M.	1955	Proc. Phys. Soc., London, 68B, 493.
Soper H.W.	1915	Biometrica, 11, 328.
Stormer C.	1932	Geofys. Pubs. Oslo., 9, 6.
Stormer C.	1933	Vid. Akd. Arch. M.N.M., No. 2.

Stormer C.	1935	Nature, 135, 103.
Tsukamato K. & Ogata Y.	1959	Rep. Ionos. Space Res., Japan, 13, 48.
Yerg D.G.	1959	J. Geophys. Res., 64, 27.

SECTION - III FURTHER STUDIES OF THE IONOSPHERE AT THUMBA AND OTHER EQUATORIAL STATIONS

CHAPTER - III.1 Characteristics of ionosphere over Thumba, Trivandrum and Kodaikanal.

III.1.1 Introduction

III.1.2 Brief description of the ionospheric recorder at Thumba

III.1.3 Characteristics of the ionosphere over Thumba, Trivandrum and Kodaikanal.

CHAPTER - III.1 IONOSPHERE OVER THUMBA, KODAIKANAL AND TRIVANDRUM

III.1.1. Introduction

One of the most common methods of investigating the ionosphere has been the pulse echo technique originated by Breit and Tuve in 1925. The instrument is essentially a type of radar which is capable of obtaining echoes from the ionosphere over a wide range of operating frequencies and is known as ionosonde. Pulses of radio energy are transmitted vertically by special wide band aerial system and received on similar adjacent aerial. The time interval (t) between the transmitted pulse and the reflected pulse is equal to twice the height of the layer divided by the average velocity of the radio-waves. If the velocity of the radio-waves is assumed to be constant and equal to that in vaccum, one obtains only the virtual height of reflection. Since the group velocity of the radio waves is reduced in the ionized media, the virtual height is always greater than the real height of reflection. As the frequency of the transmitted pulse is increased slowly, the radio waves penetrate deeper and deeper in the ionosphere until the radio-waves penetrate through the level of maximum ionization and are not returned back. This limiting frequency is known as the critical

frequency of that particular layer. The ionosonde indicates on the oscilloscope screen the time delay or the virtual height of the reflection of the radio-waves between the various layers and ground. Photographs of these traces are taken on a moving film producing graphs of the virtual height versus the frequency of the radio waves which are called ionograms. A large number of ionosondes were installed for the IGY programme all over the world. The All India Radio (India) installed a manual ionosphere recorder at Trivandrum near magnetic equator in October 1957. With the establishment of the rocket launching station at Thumba which is very close to Trivandrum, an automatic recorder was installed by Physical Research Laboratory, Ahmedabad, and regular sounding started from October 1964.

III.1.2. Brief description of the ionospheric recorder at Thumba

The ionospheric recorder at Thumba has been the model C4 ionosonde designed by National Bureau of Standards (U.S.A.) for IGY programme.

The instrument consists of a single sweep transmitter covering a frequency range from 1 Mc/s to 25 Mc/s accomplished by mixing signals of a variable frequency oscillator (range 31 to 55 Mc/s) with a fixed frequency oscillator

of 30 Mc/s. The receiving system is a double conversion superhetrodyne type. Incoming ionospheric echoes (in the range of 1 to 25 Mc/s) are mixed with the variable frequency oscillator signal (31 to 55 Mc/s) producing a first intermediate frequency of 30 Mc/s. This is again hetrodyned with another fixed frequency oscillator to produce the second intermediate frequency of 1.4 Mc/s. As the variable frequency oscillator is same as used to generate the transmitter pulses, the receiver is always in tune with the incoming signal. The detected pulses are fed to the two oscilloscopes, one for monitoring purposes and the other for recording purposes. Frequency markers are provided at each mega cycle from 1 to 25 Mc/s. Records are obtained on a 35 mm film camera attached with a motor and gear system for obtaining different film speeds.

The equipment can be operated manually or with a programming device controlled by a motor clock. Continuous sweepings can be used for observing rapidly changing phenomena.

The antenna system consists of two separate and identical delta type vertical antennas for the transmitting and the receiving system, both supported by the same central pole. The plane of the two antennas are orientated at right angles to each other to minimise direct coupling between

the transmitter and the receiver. Each antenna is orientated at 45^{o} with respect to the magnetic meridian. In each element of the aerials three wires are used to give a more stable impedence characteristics over the frequency range 1 - 25 Mc/s.

The height of the system is 70' above the ground and the horizontal leg 6' above the ground. The length of the horizontal leg was about 60' in the beginning which was later increased to 100' to give better response in the low frequency range. The antennas are terminated with 600 Ω impedences.

The basic characteristics of the instruments are as follows:

Frequency range	1 to 25 Mc/s logarithmic
Peak power	10 kw
Pulse repetition frequency	10 to 70 variable
Sweep time	15 sec, 30 sec, 120 sec adjustable
Height range	500 km, 1000 km, 4000 km adjustable
Height markers	50 km, 100 km - adjustable
Pulse width	50 - 100μ sec. variable.

III.1.3 Characteristics of the ionosphere over Thumba, Trivandrum and Kodaikanal

Ionospheric soundings at Thumba have been made since October 1964. To start with a sounding was made ach hour which was increased to every half an hour interval from July 1966 and every fifteen minutes from January 1967. The ionosonde at Trivandrum operated till June 1965. As the separation between Thumba and Trivandrum ionosondes was less than 5 Km, a detailed comparison of the ionospheric data from the two instruments was necessary to find any difference, due to different instruments in use at the two stations.

An automatic ionospheric recorder model C2 has been in operation at Kodaikanal since May 1952. The instrument C2 is of similar type as C4, hence differences between the data at two stations Thumba and Kodaikanal may be considered as genuine spatial variations.

A preliminary study of the F-layer characteristics at the three stations was reported earlier by Rastogi and Harish Chandra (1966). Some additional features of this study are described here.

The daily variations of the F-layer parameters over Thumba, namely the critical frequency of F_2-layer (f_oF_2)

the minimum virtual height of F_2-layer ($h'F_2$), the critical frequency of the F_1-layer (f_oF_1) and the minimum virtual height of F_1-layer ($h'F_1$), during each month of the years, 1965 and 1967, are shown in Fig. II.1.1. The full lines show the curves for the year 1967 while dashed lines indicate the same for the year 1965.

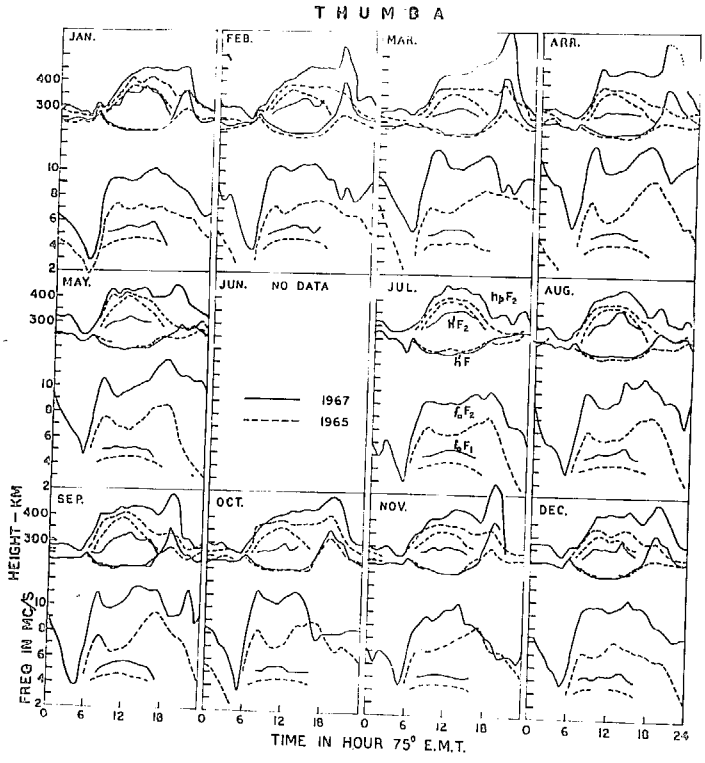

Fig. III.1.1.

The F_2-layer parameters f_oF_2, h'F and h_pF_2 are further grouped season-wise for both the years and their

daily variations are shown in Fig. III.1.2. The contour maps of f_oF_2 and h_pF_2 at Thumba in the entire period, January 1965 to December 1967, are shown in Fig. III.1.3 and Fig. III.1.4.

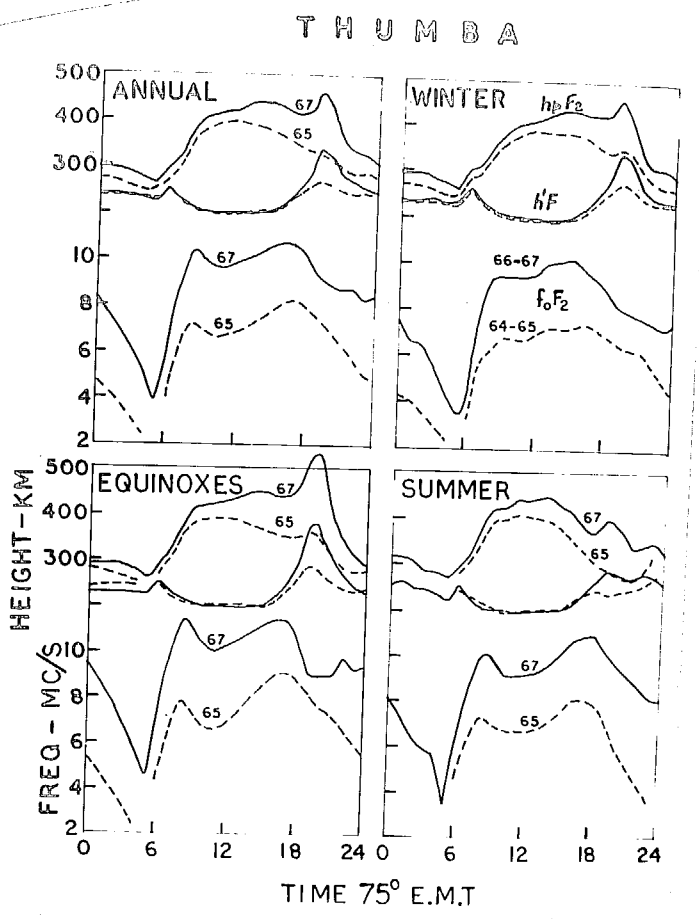

Fig. III.1.2.

(Figs. III.1.3 and III.1.4 are given in the next page).

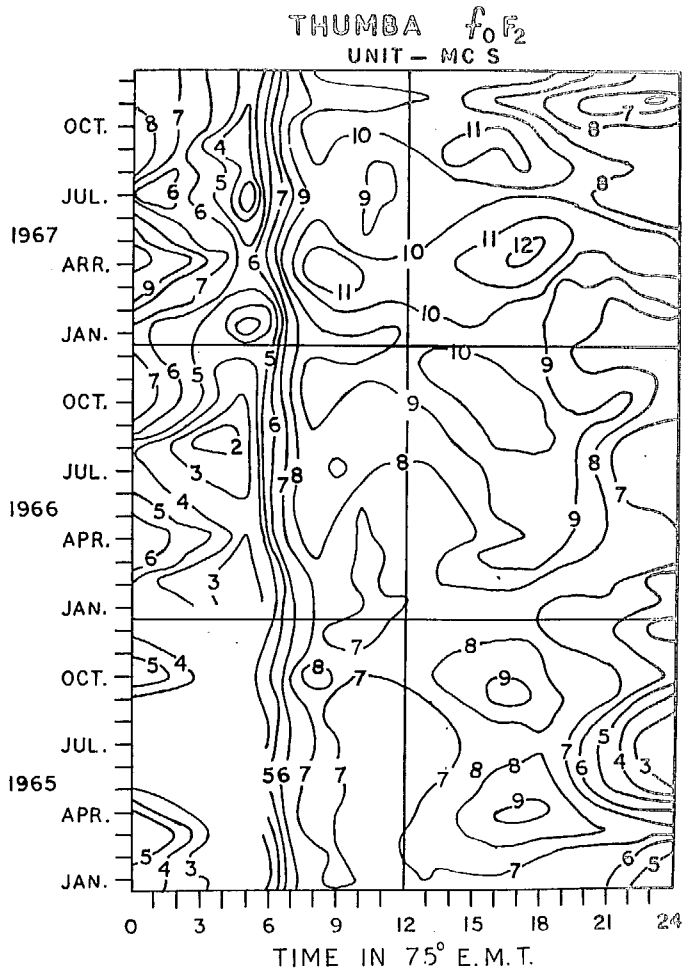
THUMBA f_0F_2
UNIT – MC S
OCT.
JUL.
1967
APR.
JAN.
OCT.
JUL.
1966
APR.
JAN.
OCT.
JUL.
1965
APR.
JAN.
0 3 6 9 12 15 18 21 24
TIME IN 75° E.M.T.

Fig. III.1.3.

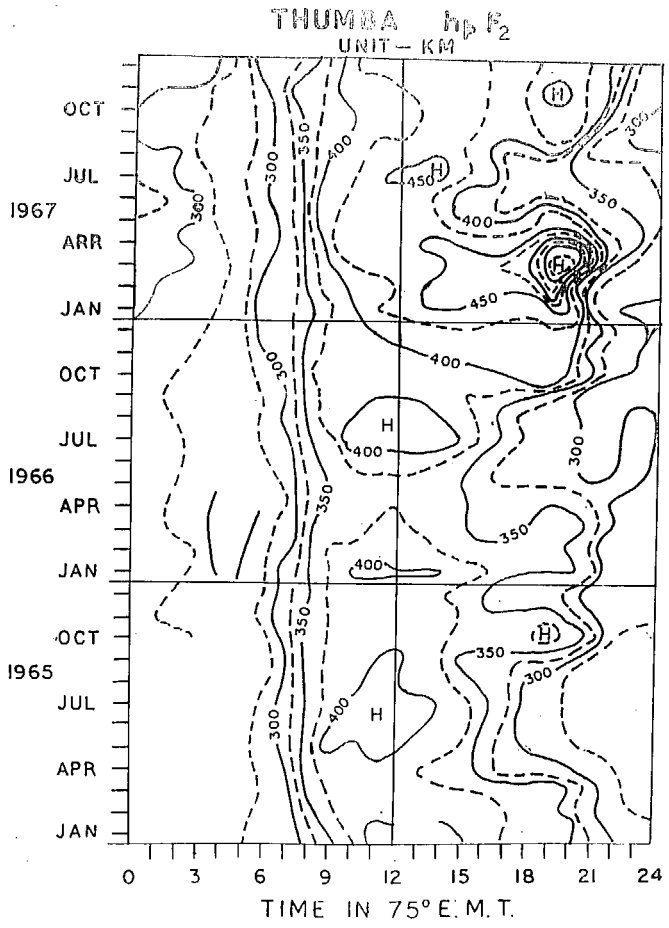
THUMBA $h_p F_2$
UNIT – KM
OCT
JUL
1967
ARR
JAN
OCT
JUL
1966
APR
JAN
OCT
1965
JUL
APR
JAN
0
3
6
9
12
15
18
21
24
TIME IN 75° E.M.T.

Fig. III.1.4.

The important conclusions drawn from the above study are summarized below:

(1) A considerable increase of the critical frequencies f_oF_1 and f_oF_2 is noticed in the year 1967, a year of higher solar activity.

(2) Fore-noon bite-out is observed in the daily variation of f_oF_2 in either of the years with peaks occurring at 08 hr. in the morning and at about 17-18 hr. in the evening. Bite-out is quite pronounced in the equinoxes and summer, but is suppressed in winter months. A prominent evening peak is observed in the year 1965, but the two peaks are of same order in the year 1967.

(3) The h'F values are practically identical for both the year except for a marked post sunset height rise observed for the year 1967. Similarly h_pF_2 values show sudden rise after sunset for the year 1967. In general, h_pF_2 values are higher for the year 1967 than for the year 1965.

(4) h_pF_2 contour map shows maxima around noon in the years 1965 and 1966 during summer months while in the year 1967 very high values of h_pF_2 are observed after sunset particularly during the months, February - April. This height rise after

sunset in the high sunspot year is a typical of equatorial stations.

A comparison of f_oF_2 variations at Thumba and Kodaikanal during each season of the years 1965-67 is shown in Fig. III.1.5. The nature of variations at the two stations is similar. The f_oF_2 values at Kodaikanal are shown to be slightly higher than those at Thumba during winter and equinoxes while they are equal or uncertain during summer season. To check it more precisely, individual day's mid-

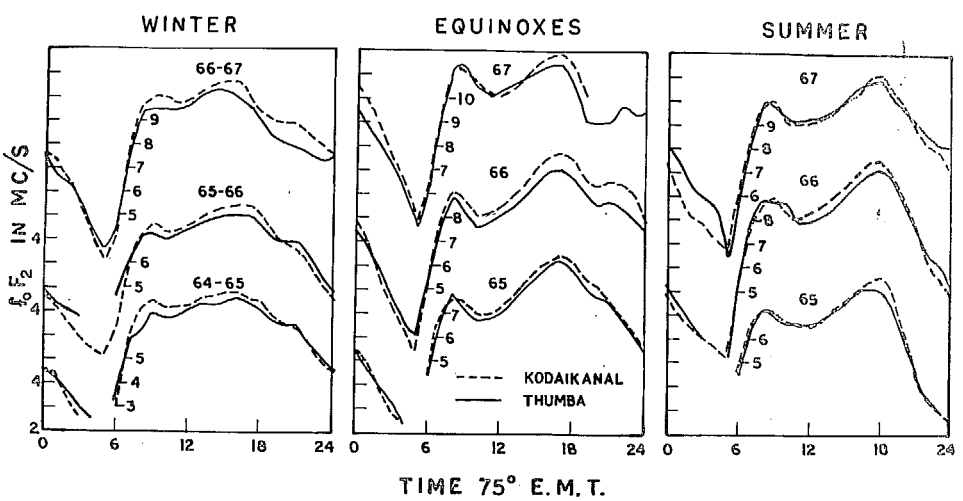

Fig. III.1.5.

day (11-12 hrs.) f_oF_2 values of the two stations were

plotted for the typical winter month (January) and typical summer month (July) and are shown in Fig. III.1.6. It is

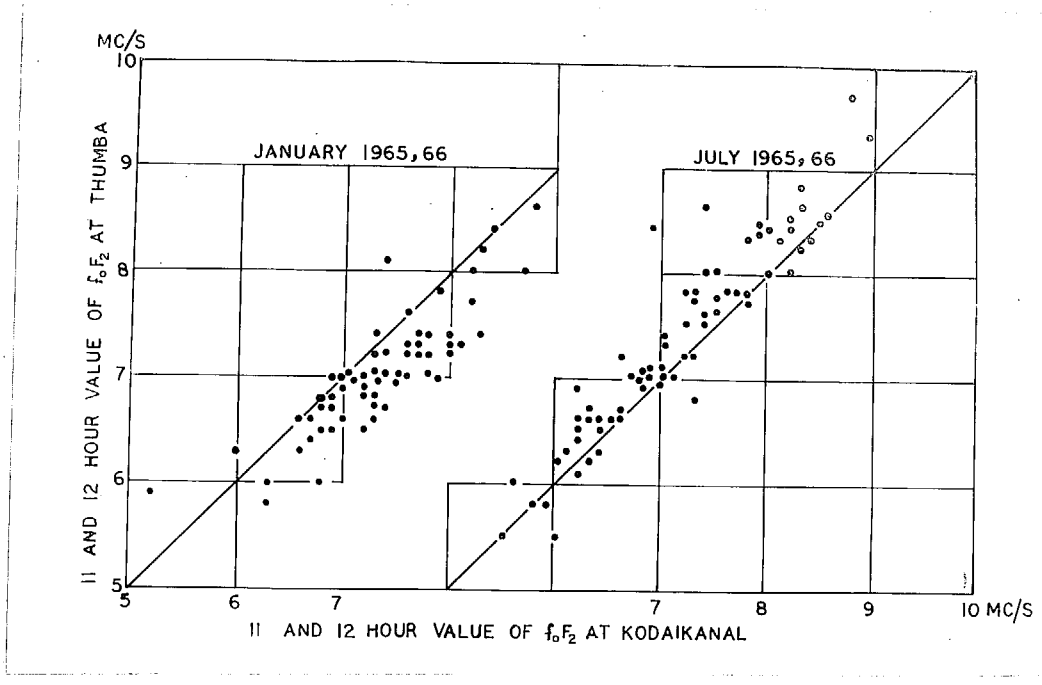

Fig. III.1.6.

clearly noticed that while in the month of January, f_oF_2 values at Kodaikanal are higher than at Thumba, reverse is the case in the month July, suggesting change-over of f_oF_2 equator from one season to another season.

A study of f_oF_2 and hmF_2 variations on magnetically quiet days over a solar cycle at Ibadan in the period

of 1957-64 (Olatunji, 1966) showed well-known systematic decrease of f_oF_2 with solar activity as the sunspot number decreased from 1957 to 1964. The summer and equinoctial months (August-September-October) showed typical midday dip with predominant pre-noon peak of f_oF_2 in the year 1956, predominant evening peak in the year 1964 and nearly equal morning and evening peaks in the year 1961. The predominanat peaks were not observed for the winter solstice months (November-December-January); midday dip was not observed in the year 1957, while a small dip was observed in the year 1961 and 1964. These results indicate that the bite-out phenomenon is reduced during winter months.

Present results at Thumba show predominant evening peak for the seasons summer and equinoxes in 1965 a low sunspot year and nearly equal peaks in the year 1967. The bite-out is least pronounced for the D-months. Earlier, it has been shown by Satyanarayanmurthy (1962) that during the high sunspot years 1957-59, the diurnal variation of f_oF_2 at Trivandrum was a double humped curve with predominant morning peak in all the seasons with marked bite-out during summer and equinoxes and reduced bite-out during winter. Hence, from the study of f_oF_2 variations at Ibadan and Thumba it is clearly evident that (1) marked bite-out is present during summer and equinoxes, but is considerably reduced

during winter, (2) the high sunspot years show a predominant morning peak of ionization while the low sunspot years show predominant evening peak.

h_pF_2 variations

Study of hmF_2 at Ibadan for the months, May, June & July during the years 1957-64 showed post sun-set increase around 19 hr. which is much more pronounced at sunspot maximum. Similar conclusion is obtained from the h_pF_2 variations at Thumba during the years 1965-67.

The F region of the ionosphere over the magnetic equator in India during I. Q. S. Y.

R.G. Rastogi and Harish Chandra

Physical Research Laboratory, Ahmedabad. (India)

ABSTRACT

The article compares the Ionosonde observations at Thumba located near the magnetic equator (dip 0.6°S) with those of the neighbouring stations of Trivendrum (only a couple of Kilometers distance) and Kodaikanal(dip 0.7°N).

To supplement the then existing network of ionospheric stations in India upto the magnetic equator, a manually operated ionospheric recorder was installed in Trivandrum during IGY by All India Radio. With the establishment of Rocket Launching Site near Trivandrum, it was felt necessary to install an automatic ionosonde near the Rocket Range. With the generous loan of a C4 type ionosonde by Wireless Planning and Co-ordination Branch of the Government of India and with the facilities made available at Thumba Rocket Launching Site, a regular vertical ionospheric Sounding Station was established by the Physical Research Laboratory, Ahmedabad. The article describes a comparison of Thumba data with the data simultaneously obtained at Trivandrum and Kodaikanal. The coordinates of Thumba are (Geog. lat. 8°33'N, Geog. long. 76°52'E, Magnetic Dip=0.6°S). Ionospheric soundings at Thumba were started in October 1964 and have been continued since then. The ionosonde at Trivandrum continued operation till June 1965. Thus simultaneous observations are available at Thumba and Trivandrum for about six months. The two stations were only a couple of kilometers apart and one should expect the mean as well as the individual values of the parameters to be identical. In Fig. 1 are shown the daily variations of f_0F_2 and h_pF_2 at the two stations for a winter (Jan.1965) a summer (may 1965) and an equinoxial month (March 1965). It is seen that in general the character of the daily variations are very similar but there are some significant differences, between the two curves. The daytime values of h_pF_2 are slightly lower at Trivandrum than at Thumba. The nighttime values of Trivandrum h_pF_2 are not

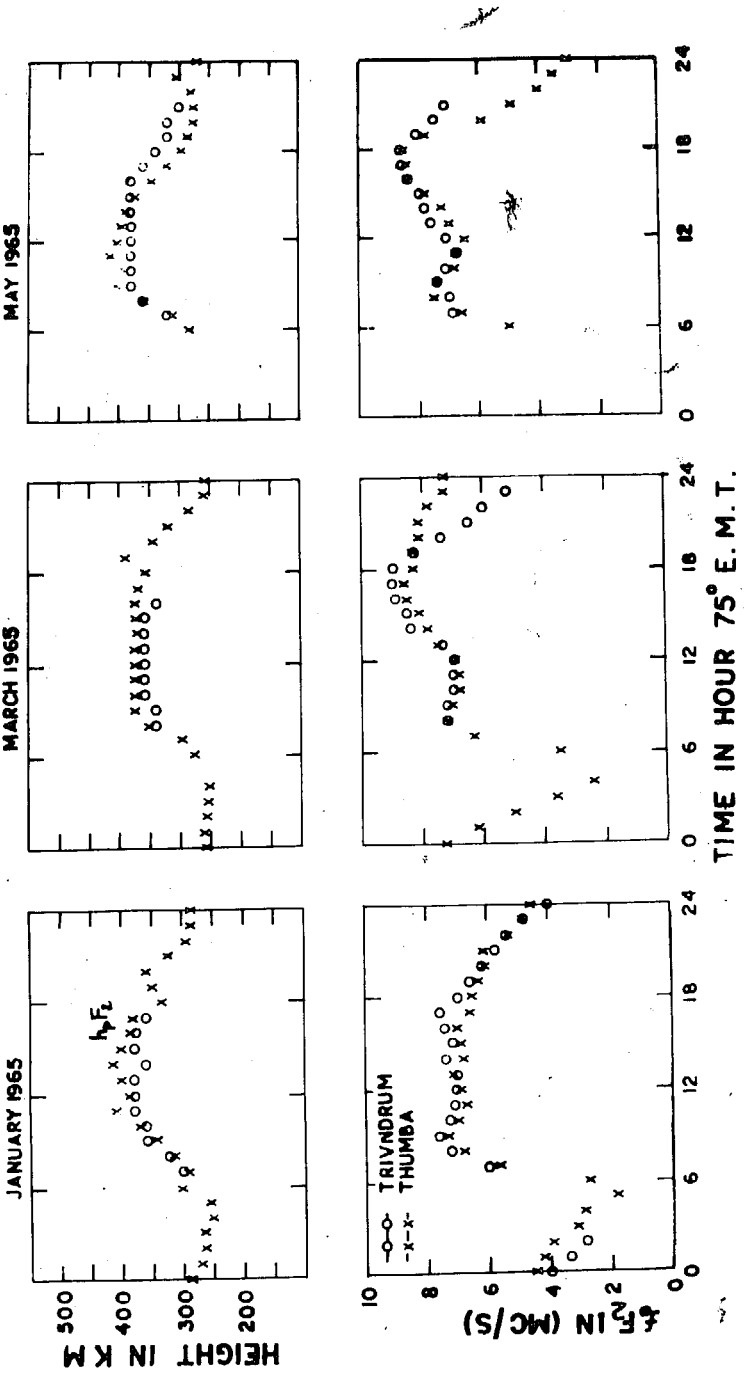

Fig. 1. Daily variations of foF_2 and h_pF_2 at Trivandrum and Thumba for the months of January, March and May 1965.

available for some of the months. The daytime value of f_oF2 are in general greater in Trivandrum than at Thumba and there seems to be large irregular differences in the f_oF_2 values at the two stations during the nighttime. These differences seem to be instrumental differences and are inherent in the comparison of an automatic photographically

recording instrument and a manually operated non-recording equipment. The difference are to be kept in consideration when the earlier data at Trivandrum are to be combined with the later data at Thumba during any analyses in future.

An automatic ionospheric recorder, model C2, has been in operation in Kodaikanal since May 1952; the coordinates of the station are Geog. lat. 10°14', Geog.long. 77° 29' Magnetic Dip. + 0.7°N. The instruments at Kodaikanal and Thumba are of similar type and so the differences between the data at the two stations may be considered as genuine spatial variation without any instrumental errors involved. The daily variations of f_oF_2, $h'F_2$ and $h'F$ at Kodaikanal and Thumba for different seasons of the I.G.S.Y. as well as averaged over the whole year are shown in Fig. 2 The yearly mean value for 1965 of f_oF_2, f_oF1, $h'F$ and $h'F_2$ at Kodaikanal (KOD) and Thumba (Thu) are given in Table 1.

It is seen that the annual average curve of h'F2 does not show any significant difference at the two stations. The daytime values of h'F are insignificantly higher at Thumba than at Kodaikanal.

The annual average value of f_oF_1 at the two stations are almost identical, the differences being less than the errors involved in the identification of f_oF1.

The annual average value of f_oF_2 are slightly higher at Kodaikanal than at Thumba during the daylight hours, while the case is reversed during the night hours. This is quite understandable because during the daytime hours of a low sunspot year the latitudinal variation of f_oF_2 shows a minimum over the magnetic equator while during the night hours, there is a slight maximum of f_oF_2 over the magnetic equator. The annual mean data of the (F_2) layer at Thumba are thus consistent with the location of the station.

Referring to the daily variations of $h'F_2$ and $h'F$ during individual seasons, it is difficult to note any significant differences between the two stations.

Referring to the f_oF_2 values it is seen that f_oF_2 during the night hours is smaller at Kodaikanal than at Thumba during any of the seasons confirming a hump of f_oF_2 over the magnetic equator during the night hours.

The day time values of f_oF_2 are almost identical at the two stations during the summer months. But during the winter months the f_oF_2 values are higher at Kodaikanal than at Thumba during the daylight hours. This is further clarified in Fig. 3 showing the individual simultaneous noon observations of f_oF_2 at Kodaikanal and Thumba. Most of the points are above the 45° line indicating the excess of f_oF_2 at Kodaikanal over the same at Thumba.

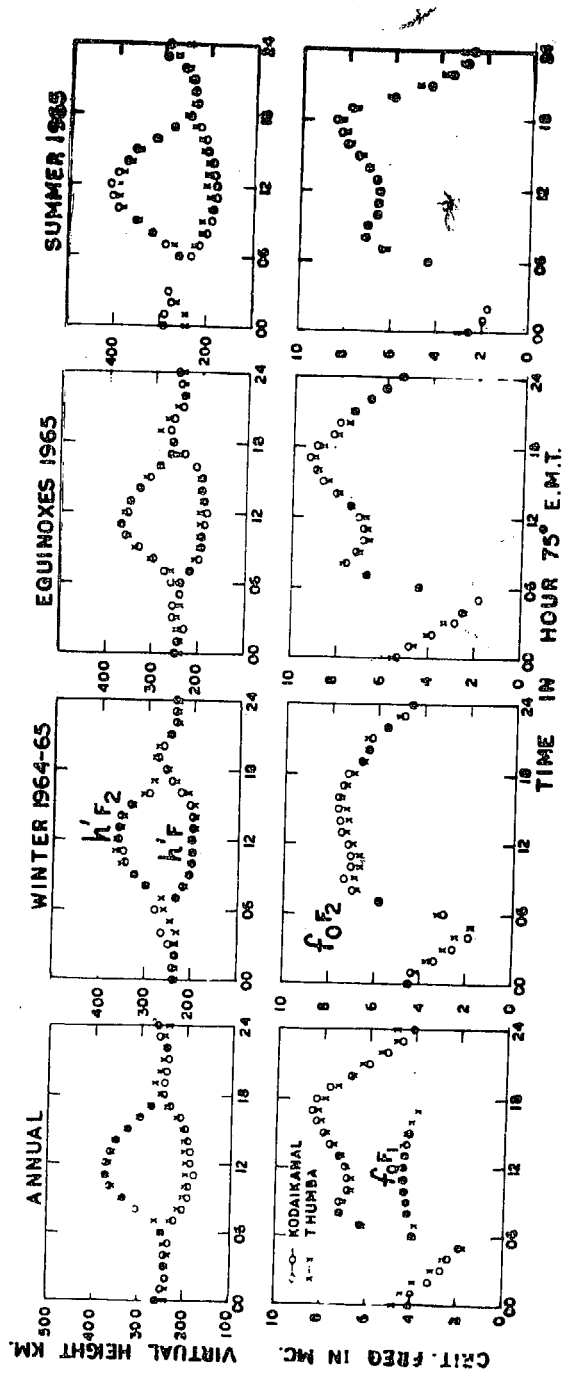

Fig. 2. Daily variations of $h'F_2$, $h'F$, f_oF_1 and f_oF_2 at Thumba and Kodaikanal during different seasons.

The article compares the Ionosonde observations at Thumba located near the magnetic equator (dip 0.6°S) with those of the neighbouring stations of Trivandrum (only a couple of Kilometers distance) and Kodaikanal (dip 0.7°N).

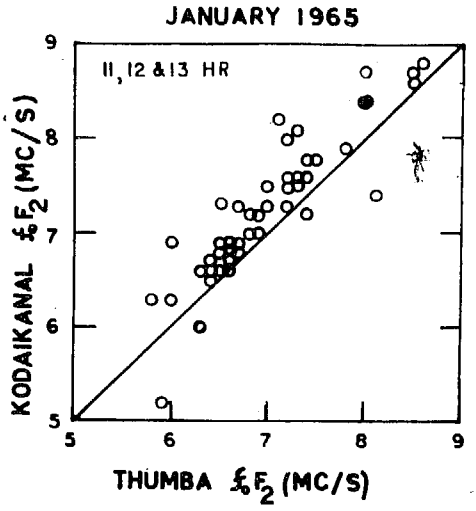

Fig. 3. Noon values of f_0F_2 Kodaikanal and Thumba for the month of Jan. 1965.

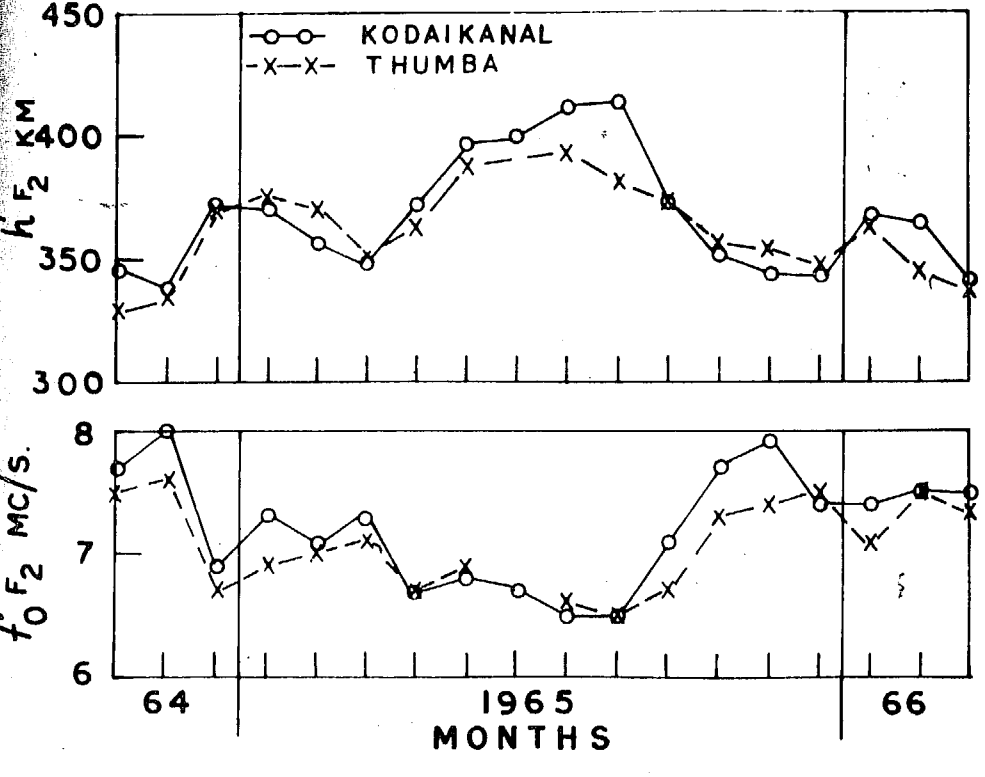

Fig. 4. Monthly variation of midday values of f_0F_2 and $h'F_2$ at kodaikanal and Thumba.

Table 1

YEARLY MEAN CHARACTERISTICS OF THE IONOSPHERE OVER THUMBA AND KODAIKANAL 1965.

Time	f_oF_2 Mc.		f_oF_1 Mc/s		h'F (km)		$h'F_2$(Km)	
	Thu.	Kod.	Thu.	Kod.	Thu.	Kod.	Thu.	Kod.
00	4.8	4.1			241	260		
01	4.4	4.0			240	249		
02	3.9	3.2			242	241		
03	3.1	2.7			240	252		
04	2.6	2.4			237	251		
05	1.7	1.9			245	237		
06	4.0	3.9			251	251		
07	6.2	6.2			228	222		
08	7.2	7.2	4.2	4.2	214	204	307	307
09	7.0	7.2	4.3	4.3	207	197	339	337
10	6.7	6.9	4.4	4.4	198	193	362	367
11	6.7	6.9	4.5	4.4	200	189	375	376
12	6.9	6.9	4.5	4.4	200	188	369	375
13	7.2	7.3	4.4	4.4	199	190	361	367
14	7.5	7.7	4.5	4.3	198	193	348	351
15	7.8	8.0	4.3	4.2	204	199	327	328
16	8.1	8.3	4.1	4.0	217	212	302	302
17	8.2	8.4	3.8		240	234	273	273
18	7.9	8.3			256	252		
19	7.3	7.7			271	251		
20	6.7	6.8			262	247		
21	6.3	6.0			250	241		
22	5.5	5.2			244	245		
23	4.8	4.6			249	259		

In Fig. 4 are shown the monthly variation of midday (11-12 and 13 hr. mean) value of f_0F_2 and $h'F_2$ at Kodaikanal and Thumba. The seasonal variation of f_0F_2 is similar at the two stations. The f_0F_2 values are significantly higher at Kodaikanal than at Thumba during the winter months, while it is slightly smaller at Kodaikanal than at Thumba during the summer months.

The values of $h'F_2$ are slightly higher at Kodaikanal than at Thumba during the summer months, while there is very little difference between $h'F_2$ of the two stations during the winter months.

CHAPTER - III.2 Electron density versus height distribution at Thumba

Chapter - III.2

III.2.1. Methods for determining the true height of reflection of radio-waves

(a) Model methods

(b) Integral equation methods

III.2.2. Method used for the present analysis

III.2.3. Calculations of layer parameters

III.2.4. Extrapolation of N(h) profiles above h_{max}.

III.2.5. Electron density distribution over Thumba.

Chapter - III.2. Electron density versus height distribution at Thumba

Introduction

Ionograms represent a graph of time delay (t) between the transmitted and the reflected pulse versus frequency (f) of the radio-waves. Assuming the speed of the radio-waves to be constant and equal to that in vacuum (c) this graph is equivalent to the virtual height (h') versus f where

$$h' = \tfrac{1}{2} ct \qquad (1)$$

Group velocity of the radio waves, that is the velocity with which a pulse of radio-waves moves in an ionized medium having a group retractive index μ' is given by

$$U = c/\mu' \qquad (2)$$

Therefore the time delay t is given by

$$t = 2\int_0^{h_r} \frac{dh}{U} \qquad (3)$$

where h_r is the true height of reflection. Combining equations 1, 2 and 3

$$h'(f) = \int_0^{h_r} \mu' \, dh \qquad (4)$$

Group refractive index μ' is a function of local

electron density N, frequency of the radio-waves f and the parameters of the earth's magnetic field.

II.2.1. Methods for determining true height of reflection of radio-waves

Calculations of real heights from the virtual heights are done by solving equation 4. Basically, there are two approaches for electron density distribution calculations. In the first known as the model method h'f curves are drawn for different known models of electron density distribution and the parameters of a particular ionogram are determined by comparing with the standard curves.

III.2.1(a). Model methods

According to the Chapman's theory of ionization (1931), the shape of electron density distribution near the level of maximum ionization density is shown to be parabolic in the form

$$N = No \quad 1 - \frac{(h - hm)^2}{4 H^2} \qquad (5)$$

Defining the semi-thickness of the parabola $Ym = 2H = hm - ho$ where ho is the lower boundary of the layer equation (5) can be written as

$$N = No \quad 1 - \frac{(h - hm)^2}{(Ym)^2} \qquad (6)$$

Appleton and Beynon (1940) have been shown that if f_c is the critical frequency of the layer than the virtual height h' for operating frequency f would be given by

$$h' = ho + \frac{Ym}{2} \frac{f}{fc} \log_e \frac{fc + f}{fc - f} \qquad (7)$$

The relation between h' and $\frac{1}{2} \frac{f}{fc} \log_e \frac{fc + f}{fc - f}$

is linear and slopes give ym and ho. Booker and Seaton (1940) tabulated the function $\frac{1}{2} \frac{f}{fc} \log_e \frac{fc + f}{fc - f}$ and made the calculations of the parameter more convenient. They have shown that the virtual height of reflection at a frequency .834 of fc is the height of maximum ionization in the equivalent parabolic layer, designated by hp and is used widely in the ionospheric data.

Thus a quick method for obtaining the main characteristics of ionization distribution is given by fitting a parabola to the shape of ionization distribution near the maximum electron density. Computed h'(f) curves for different values of hm, ym are compared with the observed pattern and parameters hm, ym can be identified from the curve of best fit. Ratcliffe (1951) gave an easy method of analysing h'(f) records assuming different models namely linear, square law and parabolic distributions of electron density with height. The method has been extended to include the

effect of earth's magnetic field by providing different families of curves for different ratios of gryo frequency.

III.2.1(b). Integral equation method

Usually N(h) profiles do not follow any definite mathematical model. An accurate method to find true heights is solving the integral in equation 4. Solution of this integral has been tried in two different ways.

(1) Direct inversion method

Appleton (1930) showed that if the effect of earth's magnetic field and of collisions are neglected, equation 4 reduces to an Abelian integral equation which can be directly inverted to give a solution.

Group refractive index μ' (f, N) in absence of collisions and magnetic field is given by

$$\mu = 1 - \frac{f_N^2}{f^2} \qquad (8)$$

where $f_N = \sqrt{\frac{Ne^2}{\varepsilon_o \pi m}}$ is the plasma frequency corresponding to electron density N, m being the mass of the electron and ε_o the permittivity of the medium.

Equation (4) can be inverted into the form

$$h'(f_N) = \frac{2}{\pi} \int_0^{f_N} \frac{h'(f)\, df}{\sqrt{f_N^2 - f^2}} . \qquad (9)$$

A simple method of analysing the records was

devised by Manning (1947). A substitution $f = f_N \sin\theta$ in equation (7) simplifies it to the form

$$h'(f_N) = \frac{2}{\pi} \int_0^{\pi/2} h'(f_N \sin\theta) \, d\theta \quad . \qquad (10)$$

The integration was done graphically with a planimeter.

Integration can be performed numerically by dividing the curve h' (fN sin θ) into a series of steps of equal width in θ . Kelso (1952) used Gaussion Christoffel Quadrants to evaluate the integral (10) numerically. To calculate height $h(f_N)$ at plasma frequency f_N, virtual heights h'(f) are read at different steps and average is taken.

Shinn (1954) has modified the coefficients to allow for the effect of earth's magnetic field, these rations are called Shinn-Kelso coefficients. Schemerling (1958) developed a method very close to the original Kelso method but modified to take into account the effect of earth's magnetic field automatically. Modified sampling frequencies are computed which depend on the gyro frequency and the dip angle of the station. Tables containing sampling ratios applicable to stations covering nearly all over the world have been calculated by Schemerling and Ventrice (1959).

(2) Lamination method

In the lamination method, an assumption is made only about the shape over a thin strip defined by a frequency interval of, rather than the shape of the whole layer. The integral in equation (4) is replaced by a discrete sum over a number of suitable frequency intervals. The coefficients of the equations are written in matrix form and inversion of matrix is done to solve the integral (Budden 1954).

Equation (4) can be transformed into a variable f_N as

$$h'(f) = \int_0^f \mu'(f, f_N) \frac{dh(f_N)}{df_N} \, df_N \qquad (11)$$

This transformation assumes that $h(f_N)$ is a monotonic function of f_N in the range $0 \leq f_N \leq f$. Assume that $h'(f)$ is given at equal intervals Δf of the frequency then denoting

$$\left.\begin{aligned} h'(k\,\Delta f) &= h'_k \\ h\,(k\,\Delta f) &= h_k \\ \text{and} \quad k\,\Delta f &= f_k \end{aligned}\right\} \qquad (12)$$

where k is an integer. The range of integration in equation (11) is divided into discrete intervals of Δf

so that for i^{th} interval $(i-1)\Delta f < f_N < i\Delta f$ where $i \leq k$.

It is assumed that in each interval $\frac{dh}{df_N}$ is constant, given by $\frac{dh}{df_N} = \frac{h_i - h_{i-1}}{\Delta f}$

On integration, equation (11) becomes

$$h'_k = \sum_{i=1}^{k} \frac{h_i - h_{i-1}}{\Delta f} \int_{(i-1)\Delta f}^{i\Delta f} \mu'(k\Delta f, f_N)\, df_N \qquad (13)$$

Let $M_{ki} = \frac{1}{\Delta f} \int_{(i-1)\Delta f}^{i\Delta f} \mu'(k\Delta f, f_N)\, df_N$ for $i \leq k$

$M_{ki} = 0$ for $i > k$ (14)

hence, from equation (13)

$$h'_k \approx \sum_{i=1}^{k} (h_i - h_{i-1})\, M_{ki} \qquad (15)$$

If ho is the height of the bottom of the layer from the ground, then $h'_k \approx h_o + \sum_{i=1}^{k} (h_i - h_{i-1})\, M_{ki}$. (16)

Representing equation (16) in the form of a triangular matrix, equation (13) can be written as

$$\begin{bmatrix} h_1 \\ h_2 \\ \vdots \\ h_k \end{bmatrix} = \begin{bmatrix} M_{11} & 0 \cdots\cdots 0 \\ M_{21} & M_{22} \cdots\cdots 0 \\ \vdots & \vdots \\ \end{bmatrix} \begin{bmatrix} 1 & 0 & 0 & \cdot \\ -1 & 1 & 0 & \cdot \\ 0 & -1 & 1 & \cdot \\ 0 & 0 & -1 & \cdot \\ \cdot & \cdot & \cdot & \cdot \\ \cdot & \cdot & \cdot & \cdot \\ \cdot & \cdot & \cdot & \cdot \\ \cdot & \cdot & \cdot & \cdot \end{bmatrix} \begin{bmatrix} h_1 \\ h_2 \\ \cdot \\ \cdot \\ \cdot \\ \cdot \\ \cdot \\ h_k \end{bmatrix} \qquad (17)$$

or $h' = M D h$ ... ... (18)

The product MD is also triangular matrix and is non-singular. It may be inverted to give

$$h = L h' \quad \text{... ... (19)}$$

where $L = (MD)^{-1}$ ... ... (20)

The method therefore involves three steps:

(a) evaluation of matrix elements . Mki

(b) inversion of matrix . MD

(c) evaluation of product - Lh'.

Operations, a and b are independent of observational data and need only be performed once forany one pair of values of the strength of magnetic field H and dip angle I of the station.

III.2.2. Method used for the present analysis

Lamination method of Budden (1954) has beem used for the present analysis which was modified by Sanatani (1966) to be worked out with the help of a smaller electronic computer I.B.M. 1620. From the Appleton Hartree formula, terms containing collission frequency (in F-region collision frequency is much less than the gyro frequency f_H) have been eliminated. Group refractive index is given by

$$\mu' = \mu + f\frac{\partial \mu}{\partial f} \qquad (21)$$

Substituting this in the equation (14) and performing the integration using 10 points Gauss numerical integration matrix element M_{ki} can be evaluated. True height is calculated successively from 1.2 Mc/s onward. Virtual height ho at 1.0 Mc/s is taken to be the base level height below which no ionisation is assumed. Hence, from equation (16), we have

$$h_k = h_{k-1} + \frac{1}{M_{kk}}\left[h'_k - h_o - \sum_{i=1}^{k-1}(h_i - h_{i-1})\, M_{ki}\right] \qquad (22)$$

III.2.3. Calculations of layer parameters

Along with the height distribution of electron density, some other parameters characterising the layer are calculated such as maximum electron density N_{max}, height of maximum electron density h_m, sub-peak electron content n_t and the semi-thickness of the layer y_m. N_{max} is calculated by the well-known equation relating the frequency of radio-waves and electron density of the reflecting level given by

$$N = 1.24 \times 10^4 \times (f)^2 \qquad (23)$$

where N is in El./c.c.

f is in Mc/s.

Hence, for the F-layer, $N_{max} = 1.24 \times 10^4 \times (f_oF_2)^2$ (24)

To calculate hm and Ym, a parabola is fitted near f_oF_2. Generally points at 80% and 90% of N_{max} are taken which correspond to $fr_1 = 0.95 \times f_oF_2$ and $fr_2 = 0.895 \times f_oF_2$. If hr_1 and hr_2 are the heights at these frequencies, then the points should satisfy the equation to a parobola.

$$h = hm\,ax. - Ym\sqrt{1 - \left(\frac{f}{fo}\right)^2} \qquad (25)$$

Substituting the points (fr_1, hr_1), (fr_2, hr_2) in the equation (25)

$$hr_1 = h_{max} - Ym\sqrt{1 - \left(\frac{fr_1}{fo}\right)^2} \qquad (26)$$

$$hr_2 = h_{max} - Ym\sqrt{1 - \left(\frac{fr_2}{fo}\right)^2} \qquad (27)$$

Solving equations (26), (27),

$$h_{max} = \frac{hr_2\sqrt{fo^2 - fr_1^2} - hr_1\sqrt{fo^2 - fr_2^2}}{\sqrt{fo^2 - fr_1^2} - \sqrt{fo^2 - fr_2^2}} \qquad (28)$$

and $$Ym = fo\,(hr_2 - hr_1) \Big/ \sqrt{fo^2 - fr_1^2} - \sqrt{fo^2 - fr_2^2} \qquad (29)$$

In case f_oF_2 is below 4.0 Mc/s, fr_1, fr_2 fall within the last strip. In such cases, fr_1, fr_2 are obtained by subtracting a fixed frequency interval from f_oF_2 i.e. -

when f_oF_2 is odd

$$fr_1 = f_oF_2 - 0.1$$

$$fr_2 = f_oF_2 - 0.3$$

when f_oF_2 is even

$$fr_1 = f_oF_2 - 0.2$$

$$fr_2 = f_oF_2 - 0.4.$$

In case fr_1 or fr_2 lie within a strip, height is calculated by linear interpolation. Thus if fr lies within a strip of frequencies f_r and f_{r+1} corresponding to heights h_k and h_{k+1}, then the height hr at a frequency fr is given by

$$hr = \frac{h_{k+1} - h_k}{f_{k+1} - f_k} \quad (fr - f_k) + h_k \qquad (30)$$

Sub-peak electron content n_t is calculated by integrating the electron density profile with respect to height.

$$n_t = \int_{ho}^{h_{max}} Ndh \qquad \ldots \qquad \ldots \qquad (31)$$

$$= 1.24 \int_{ho}^{h_{max}} f^2 \, dh \qquad \ldots \qquad (32)$$

$$= 1.24 \left[fo^2 \, h_{max} - 2 \int_{o}^{fo} f \, h(f) \, df \right] \qquad (33)$$

III.2.4. Extrapolation of N(h) profiles above h_{max}

Electron density distribution above the height of maximum electron density has been obtained using Bauer's (1962) model of the topside ionosphere. This model considers a Ternary ion mixture of O^+, He^+ and H^+ in an isothermal diffusive equilibrium. If subscripts 1, 2, 3 refer to O^+, He^+ and H^+ respectively, then expressing light ionic constituents in terms of relative concentration with respect to O^+, we can write

$$N = N_0 \left[\exp\left(-\frac{z'}{H_i}\right) \times \frac{\left(1 + \eta_{21} \exp\left(\frac{z'}{H_{12}}\right) + \eta_{31} \exp\left(\frac{z'}{H_{13}}\right)\right)}{1 + \eta_{21} + \eta_{31}} \right]^{1/2} \quad (34)$$

where $Z' = h' - ho'$ is a height parameter expressed in geopotential altitude $h' = \int_0^h (g/g_0)\, dh$ to account for the altitude variation of g. g_0 being acceleration due to gravity at earth's surface.

$$H_i = \frac{k T}{m_i g_0}$$

m_i = ionic mass

$$n_{ji} = \frac{n_{jo}}{n_{io}}$$

is the relative ion concentration at the reference level and

$$H_{ij} = \frac{kT}{(m_i - m_j)} g_o$$

equation (34) can be written in exponential form giving

$$N(Z') = No \exp\left[-\frac{1}{2}\left(\frac{Z'}{H_1}\right) - \ln\left(1+\eta_{21}\exp\left(\frac{Z'}{H_{12}}\right)+\eta_{31}\exp\left(\frac{Z'}{H_{13}}\right)\right) + \ln\left(1+\eta_{21}+\eta_{31}\right)\right] \quad (35)$$

In the present work $\eta_{21} = 4 \times 10^{-2}$ and $\eta_{31} = 7 \times 10^{-3}$ have been used. Gas temperature T have been derived using Bate's (1959) model atmosphere.

III.2.5. Electron density distribution over Thumba

Electron density distributions over Thumba have been computed for five international quiet days of the months, January, April and July for the years 1965 and 1967. Virtual heights at frequency interval of 0.2 Mc/s are read from 1.0 Mc/s onward upto the critical frequency. In case, the trace does not start from 1.0 Mc/s, extrapolation is done upto 1.0 Mc/s assuming the same height as at f_{min}. Thumba being at the centre of the electrojet region, the regular E-layer is not observed on the ionograms, being unidentified due to intense equatorial E_s-reflections. Extrapolation of E-layer trace has been made keeping f_bE_s as f_oE.

Electron density calculations have been made at steps of 10 km each. Extrapolation is made from h_{max} onwards upto 990 km. Averages from the individual days' profiles have been computed for each hour of the months under study.

The variation of electron density with the time of a day at fixed real heights is shown in Figure III.2.1.

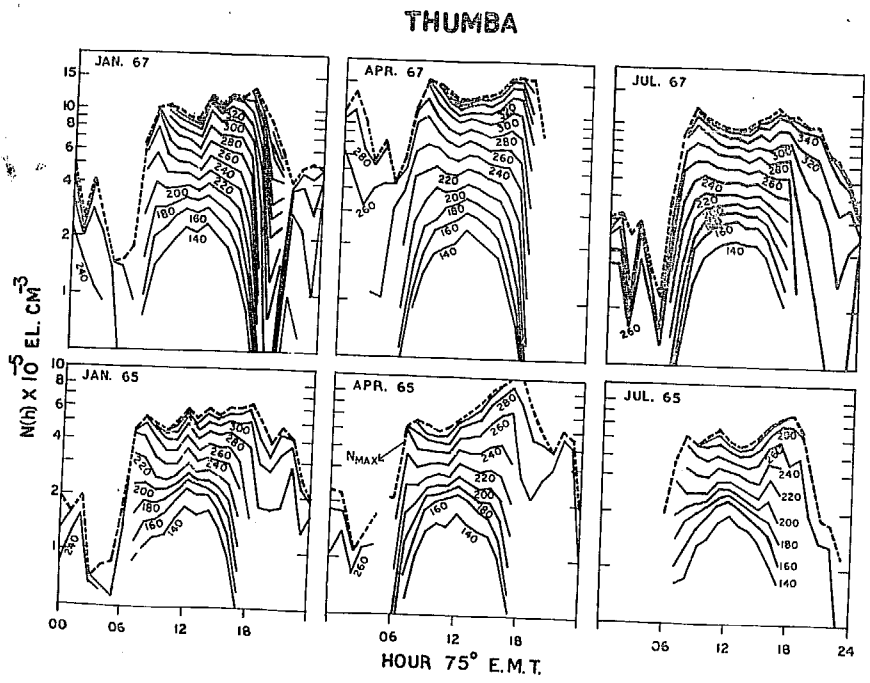

Fig. III.2.1.

Dashed line represents N_{max}. It should be noted that in the year 1965, early morning observations are smaller in number particularly during the month of July when not a single reflection was observed in the period 00 hr. to

05 hr., electron density being lower than the minimum value in the range of the instrument. Similarly in the month of April 1967 electron density profiles have not been attempted from 19 hr. to 23 hr., because of intense spread-F conditions prevailing in that period.

Referring to the Fig. III.2.1, so far as heights upto 180 km are concerned, daily variation of electron density shows symmetry about noon, in accordance with the Chapman's theory of ionisation. Divergence from this symmetry starts from about 200 km, forming a dip at midday also known as bite-out. This decrease of electron density at midday is a typical of equatorial F-region, giving rise to the well-known equatorial anomaly. If we look at the development of this midday dip from the noon maxima at lower heights, one finds two peaks around mid-day. As we go up to higher heights, the peaks shift away from each other, that is the forenoon peak shifts towards morning and the afternoon peak shifts towards evening.

Height distribution of electron density for the individual months in the year 1965 shows a prominent bite-out in the month of April with evening peak much higher than the morning one. For the month of July, bite-out is present with nearly equal peaks in the morning and evening. The bite-out is least observed for the month of January

when diurnal variation curves are rather flat in the daytime hours. Heights of maximum electron density are around 300 km for the month of July and April and about 320 km for the month of January.

In the year 1967, the nature of profiles is slightly different. Prominent evening peak which was observed in April 1965 is no longer present. Both morning and evening peaks are of equal magnitude for the months, April and July. Again in the month of January, bite-out is least observed.

In the year 1965, electron densities at lower heights are maximum for the month of July while at higher heights, they are maximum during April. In the year 1967, there is no difference in the magnitude of electron densities at lower heights, but at higher heights, one finds maximum electron densities during April and least during July. Comparing the results of 1965 and 1967, it is observed that during each month of study, electron densities at any heights are about 1.6 times higher in the year 1967.

Iso ionic charts for the periods, January 1965 and January 1967, are shown in Fig. III.2.2. Dashed line represents hmF_2 and the portion above this line is extrapolated using Bauer's model of topside ionosphere as described in the method. It can be seen that at any height

electron densities are higher in the year 1967. Close con-

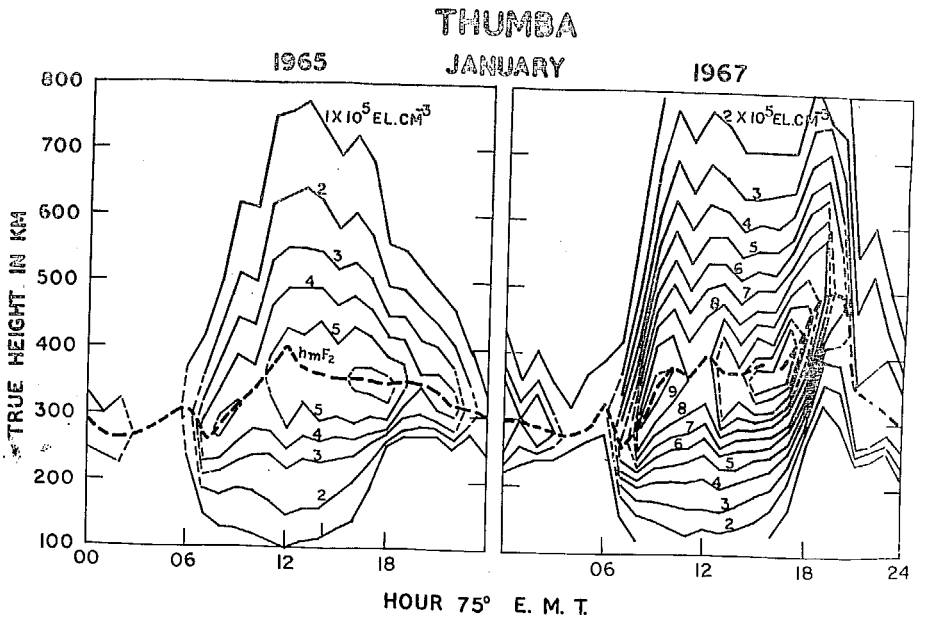

Fig. III.2.2.

tours representing maxima of electron densities are seen around 08 hr. in the morning and 17 hr. in the evening. The peaks for the period, January 1965, are 5 x 10^5 El./c.c. and 6 x 10^5 El.;c.c. respectively, which increase to 10 x 10^5 El./c.c. and 12 x 10^5 El./c.c. respectively in the year 1967.

Another important feature observed from this figure is a sharp lift of ionisation after sunset in the year 1967.

A height rise of about 100 km is observed between 18 hr. and 19 hr., which is followed by a rapid decrease from 20 hr. to 21 hr. The height remains more or less constant till morning hours, when small rise is observed at 06 hr. After sunrise, different layers as E, F_1 and F_2 are developed. The ionisations corresponding to E- and F-layers show a systematic decrease in heights with lowest heights occurring at noon, while opposite is the case for ionisations corresponding to F_2-layer, ionisation being lifted up after sunrise.

Figs. III.2.3 and III.2.4 show such charts for the

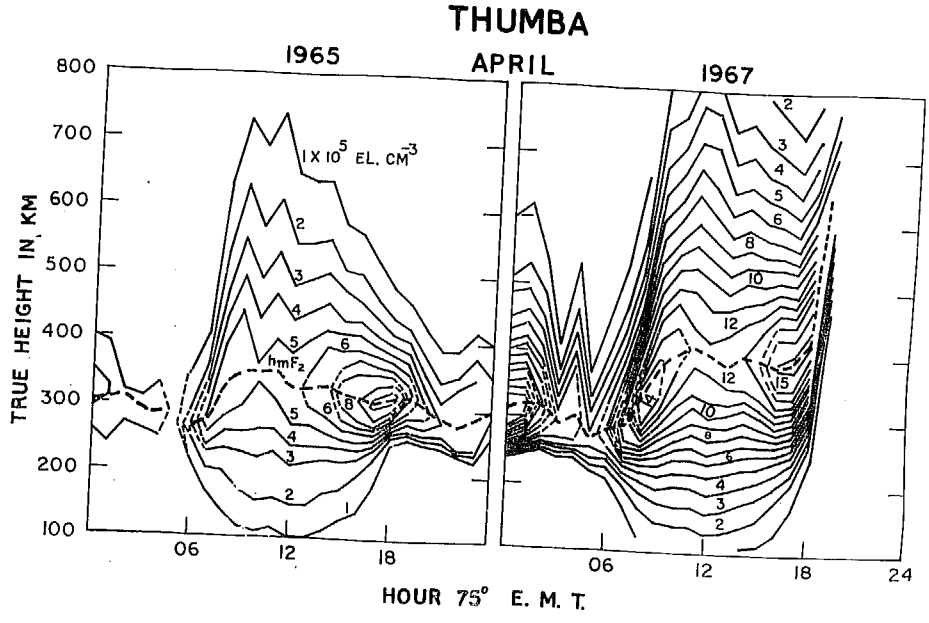

Fig. III.2.3.

months of April and July. The closed contours for the period, April 1965, are 5 x 10^5 El./c.c. in morning and 10 x 10^5 El./c.c. in the evening which increase to 14 x 10^5 El./c.c. and 16 x 10^5 El./c.c. respectively in the year 1967. A very sharp lift of ionisation from 18 hr. to 19 hr. is observed during April 1967. For the month July, much height variation is not observed for F_2 layer ionisation. Post sunset height rise is absent in the

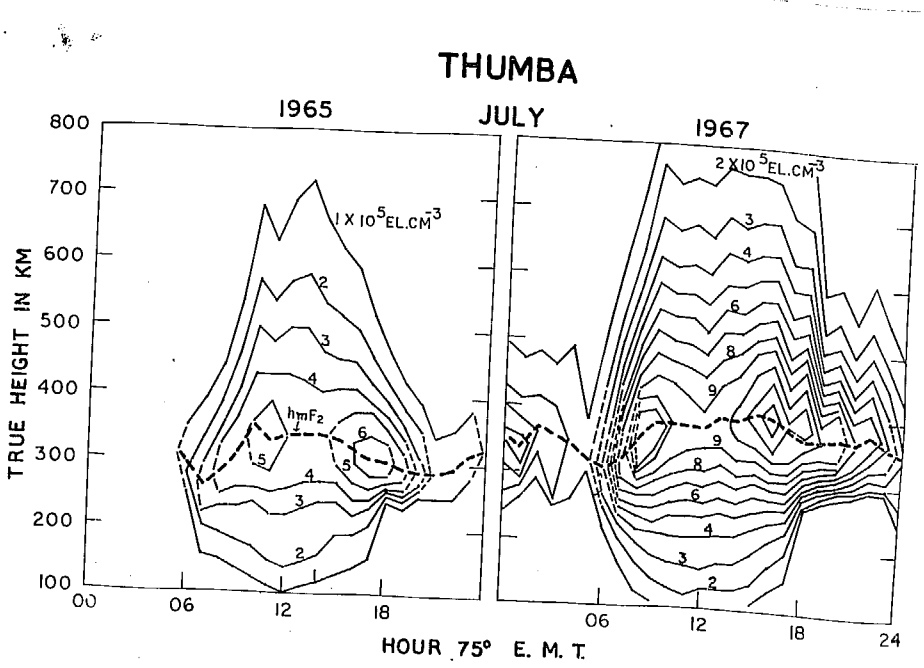

Fig. III.2.4.

month July of both the years. The closed contours are 5×10^5 El./c.c. and 6×10^5 El./c.c. in the year 1965 increasing to the values of 11×10^5 El./c.c. and 12×10^5 El./c.c. in the year 1967.

In general, from the contours of constant electron density, it can be noticed that while low ionisations show a reduction in height at noon, the ionisations of the F_2-layer lift up at noon. Another lift of the F_2-layer ionisation is seen in the post sunset period.

Diurnal variations of the quantities n_t and N_{max} are shown in Fig. III.2.5; curves for 1967 are shown by full lines and those for 1965 by dotted lines. Diurnal

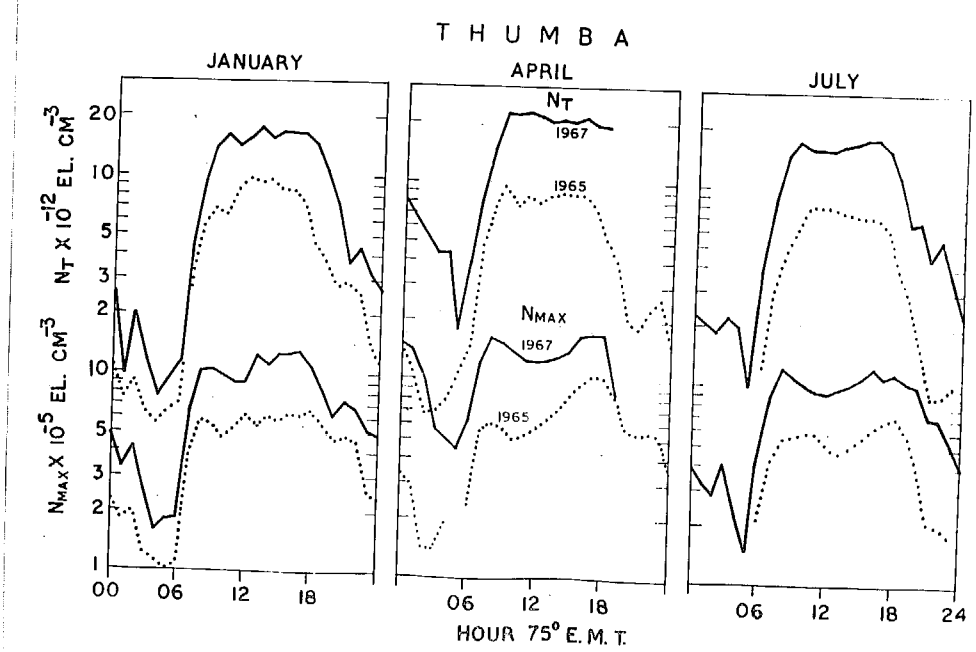

Fig. III.2.5.

variations of N_{max} for the month of January show flat curves during daytime hours. Bite-out is very clear in the month of April. Strong evening peak is observed in the year 1965, while two peaks are practically equal in the year 1967. The difference between two peaks is not marked one in the month July for both the years. On average, tendency of larger evening peak in 1965 is reduced in 1967. Studying the seasonal differences N_{max} is greatest for the month of April, being more than 10×10^5 El./c.c. compared to less than 7×10^5 El./c.c. during solstices (year 1965). Midnight ionisation is maximum during April and minimum during July. Another important feature is a rapid decrease in ionisation after sunset for the month of July. The occurrence of peaks seem to be earlier in the year 1967 than in 1965.

Bite-out is suppressed in case of sub-peak electron content n_t. That is the ionisation peak at noon at lower heights compensates the dip at higher heights to some extent.

A comparison of the real heights of maximum ionisation (h_{max}) is made with h_pF_2 values (virtual height at .834 of f_oF_2 is taken to be height of maximum ionisation in model methods; Booker and Seaton) and is shown

in Fig. III.2.6. A large difference, particularly during

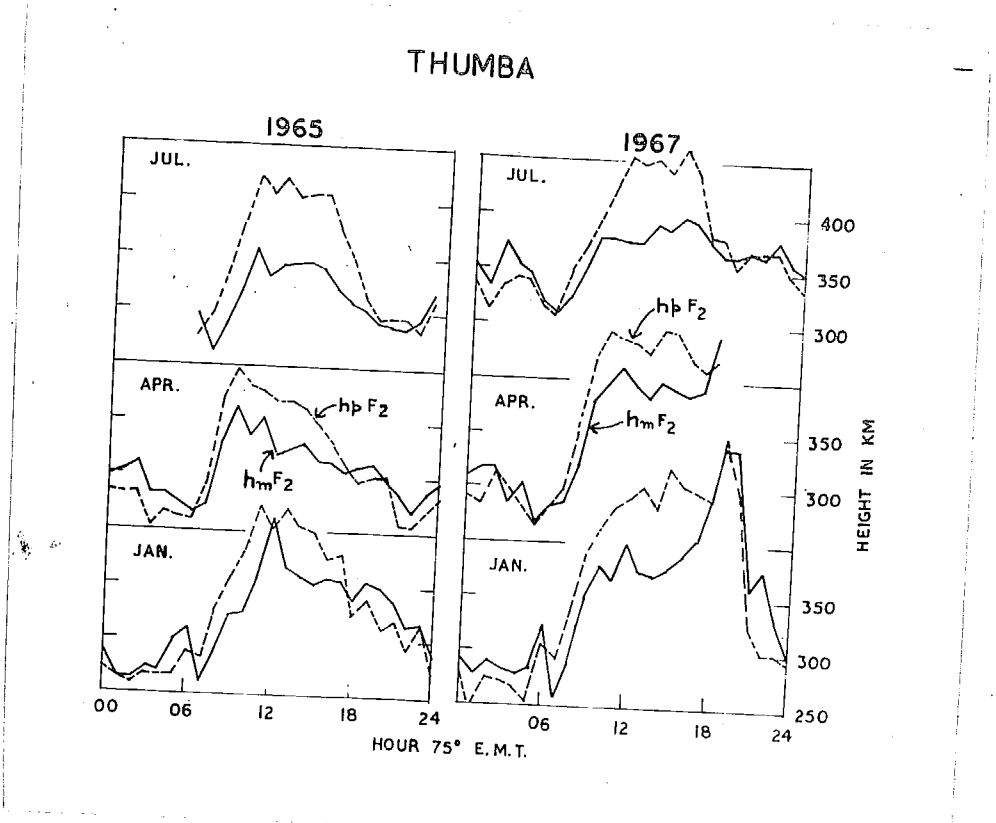

Fig. III.2.6.

daytime, is observed. Diurnal variation of h_{max} shows broad maxima at midday with slow decrease till evening and rapid height rise after sunset. In the year 1965, there is a height rise again at about 22 hr. followed by slow decrease till morning. In general, heights are increased in the year 1967. A marked rise in h_{max} after

sunset is observed for the month of January and April 1967, a characteristic of equatorial stations during high sunspot years. However for the month of July 1967, there is no height rise after sunset - an unusual feature. This post sunset height rise is closely related to the occurrence of spread-F, which will be discussed in the next two sub-chapters.

A study of the semi-thickness of the layer Ym was attempted which is shown in Fig. III.2.7. Strong diurnal

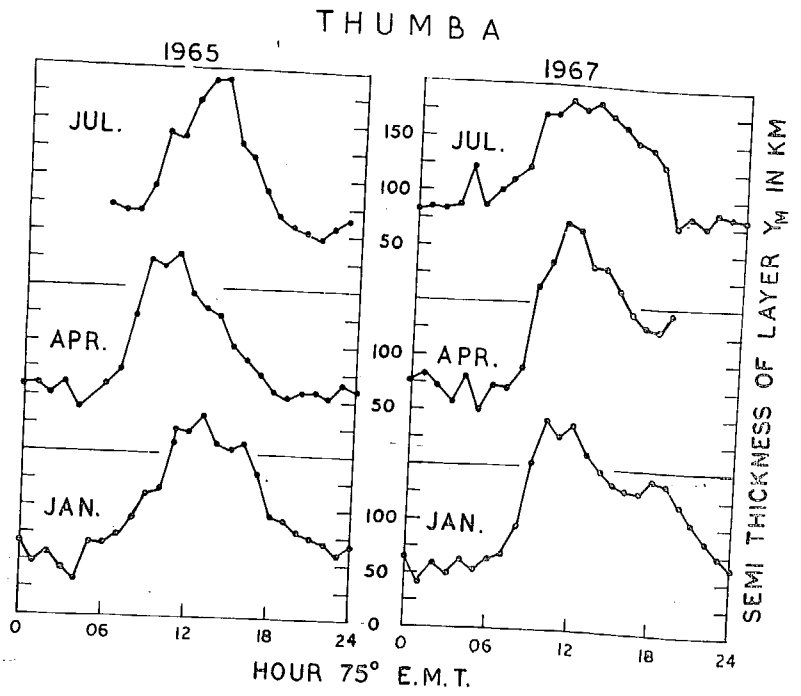

Fig. III.2.7.

variation in the parameter Ym is observed. Ym ranges from 50 km at nighttime to 175 km at midnoon. Slightly higher values are observed in the year 1967. Mean level during nighttime seems to be higher in the year 1967.

CHAPTER - III.3. SPREAD-F AT THUMBA DURING 1965-67

Chapter III.3.

CHAPTER - III.3 Spread-F at Thumba during 1965-67

III.3.1. Introduction

'Spread-F' is usually described in terms of the appearance of the conventional ionograms (h'F curves). Sometimes, the h'F curves become very diffuse, in contrast to the usual sharp traces. The echoes giving rise to this appearance have been named as 'spread echo', 'diffuse echo', 'scattered echo' etc. When this spreading or diffuseness occurs in the F-region echoes, this condition is called spread-F or F-scatter.

Scattered echoes were first observed by Mogel (1926) while monitoring the signals of a high power transmitter in Germany.

Eckersley (1929, 1932, 1937a, b, c) conducted a series of experiments and concluded that scattered echoes are produced by clouds in the E-layer by three modes of reflection:

(1) back-scattering from E-region

(2) scattering from irregularities in the E-region followed by regular oblique reflection via the F-region

(3) M-scattering.

Booker and Wells (1938) were the first to report spread-F at an equatorial station. They invoked mechanism involving Rayleigh scattering by irregularities in the

F-region.

Gipps, Gipps and Venton (1948) reported from a study at Brisbane that the broadening of the traces well below the critical frequency was due to the presence of several individual traces super-imposed on the normal trace which they referred as satellites. They concluded that the satellites arise from reflections coming from portions of ionosphere where the gradient of ionization was appreciably inclined to the horizontal. Bibl, Harnischmacher and Rawer (1954) reported that the direction of arrival of the satellite traces was always oblique. Extensive study of the satellite echoes was carried out at Brisbane by McNicol et al. (1956a, b) who showed that satellite traces were oblique echoes arriving at large angles to the vertical and also the angle of arrival changed as the satellite range varied.

Dieminger (1951) explained certain spread-F configurations on the basis of ground scattering. Radiowaves are reflected in the F-layer, scattered by irregularities on the ground, reflected again in the F-layer and return to the ionosonde. According to this mode of propagation ground scatter configuration should extend

from the first multiple on the ionogram. Applying the ray path calculations the lower edge of the configuration should be linear and is called caustic focus.

Singleton (1957) interpreted spread-F as due to scattering from clouds of enhanced ionization near the maximum of F_2-layer. Renau (1959a, 1959b, 1960) has considered a number of spread-F models as sharp ledges of ionization similar to those proposed by Whale (1951) to explain sporadic E, a scattering screen below the F-layer and aspect sensitive back-scattering by magnetic field aligned irregularities of ionization. However, these models are unable to explain the equatorial spread-F configurations as observed on ionograms.

Calvert and Cohen (1961) proposed a model based on the coherent scattering by thin magnetic field aligned irregularities, which is able to explain the equatorial spread-F configurations. It attributes most of the features of the spread-F configurations to refraction and retardation imposed on the radio-waves by the ionosphere as they travel to and from the position of scattering and scarsely involves the scattering process itself. Tracing of the ray paths between the ionosonde and position of scattering is done and corresponding delays are computed to form theoretical ionograms. Considering an irregularity the various paths

are (1) direct path to the irregularity and return (2) the path reflected to the irregularity by the overlying ionosphere and return and (3) the combination of these two - arriving by one and returning by another. In case irregularity is above the peak of layer only mode (1) is possible. Calculations of virtual heights were made considering the irregularity over head and those at the same height but located East or West of the ionosonde. Ionograms were predicted for individual scattering irregularities at various heights and at various ground distances from the ionosonde. Most of the features of equatorial spread-F were found in these theoretical ionograms.

III.3.2. Range and frequency spreading

McNicol, Webster and Bowman (1956) suggested a division of spread-F into two classes:

(a) If the diffuseness is pronounced along the section of the trace that sweeps upward, such that there is some ambiguity regarding the penetration of critical frequency, the spread is to be termed "frequency type".

(b) If the spread is more or less independent of frequency over a wide range of frequencies and the diffuseness is principally along the horizontal

part of the trace giving rise to ambiguity in virtual height, the spread effect is classed as 'range type'.

III.3.3. Degree of spread condition

As the degree of the spread condition may vary from a slight spread not obscuring the critical frequencies to a heavy spreading which may completely obscure the critical frequency, number of classifications have been made describing the degree of spreading observed on the ionograms. Such classifications are necessary for a detailed study or comparison study. Reber (1954a) described 'faint', 'moderate' and 'strong' spreading. Singleton (1957) considered degree of spreading by giving indices from 0 to 4 while Wright et al (1956) and Briggs (1958) have classified degree of spreading by indices 0 to 3 depending on the f_oF_2 tabulations, thus a tabulated value like 6.0 showing no spread is given an index of 0. Tabulation like 6.0 F indicates little spreading but accurate determination of f_oF_2 and is given an index of 1. Similarly tabulation like (6.0) F or U 6.0 F shows fairly high spreading with doubtful determination of the critical frequency and is given an index of 2, while complete spreading is tabulated like F- and represents the case when critical frequency cannot

be determined. This type of tabulation is given an index 3.

III.3.4. Examples of spread-F at Thumba

The appearance of the F-region as observed on the ionograms under spread-F conditions is quite variable. Fig. III.3.1. shows the typical examples of different spreading occurring at Thumba. The first example is a typical range spreading with clear trace in the top portion of layer, The second one shows a typical frequency spread with spreading confined to higher frequencies only. The third example is a complete spreading. The range type of spreading occurs generally in the initial states, while third type occurs around mid-night which finally gives rise to the frequency spreading in the later hours.

(Fig. III.3.1. is given in the next page)

Complete picture showing the development of the spread-F during a particular night is shown in Fig. III.3.2. There is no spread at 18 hr., virtual height of the layer being 250 km. The virtual height of the layer has increased to 280 km at 19 hr. and range spread starts appearing. Further rise of height follows at 20 hr., the virtual height being 310 km and complete spreading is observed. The layer height comes down afterwards and the complete spread remains upto 00 hr., the virtual height being 210 km at this hour. The spreading is seen to be

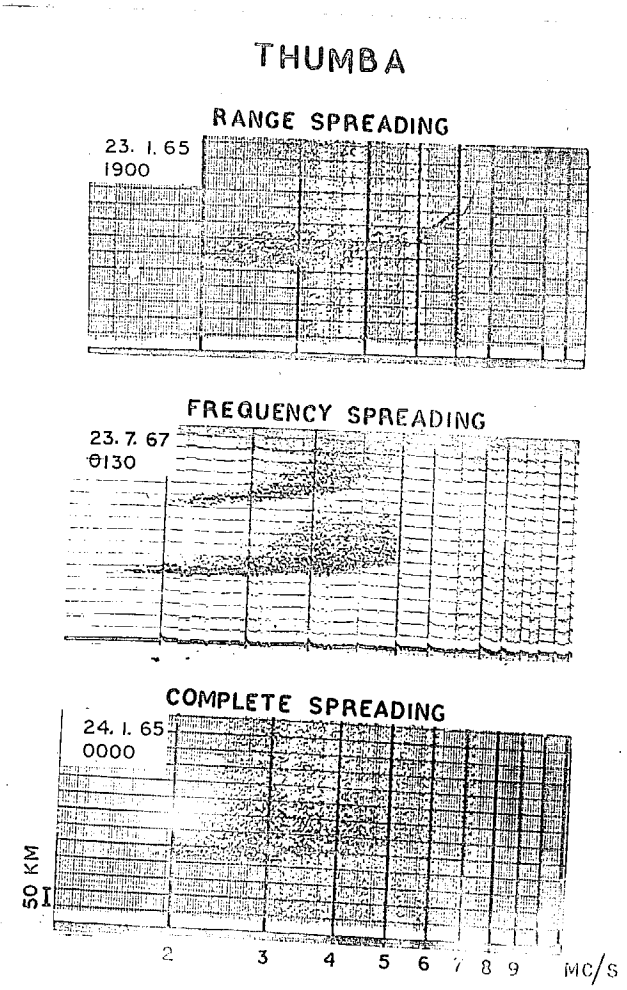
THUMBA
RANGE SPREADING
23. 1. 65
1900
FREQUENCY SPREADING
23. 7. 67
0130
COMPLETE SPREADING
24. 1. 65
0000
50 KM
2
3
4
5
6
7
8
9
MC/S

Fig. III.3.1.

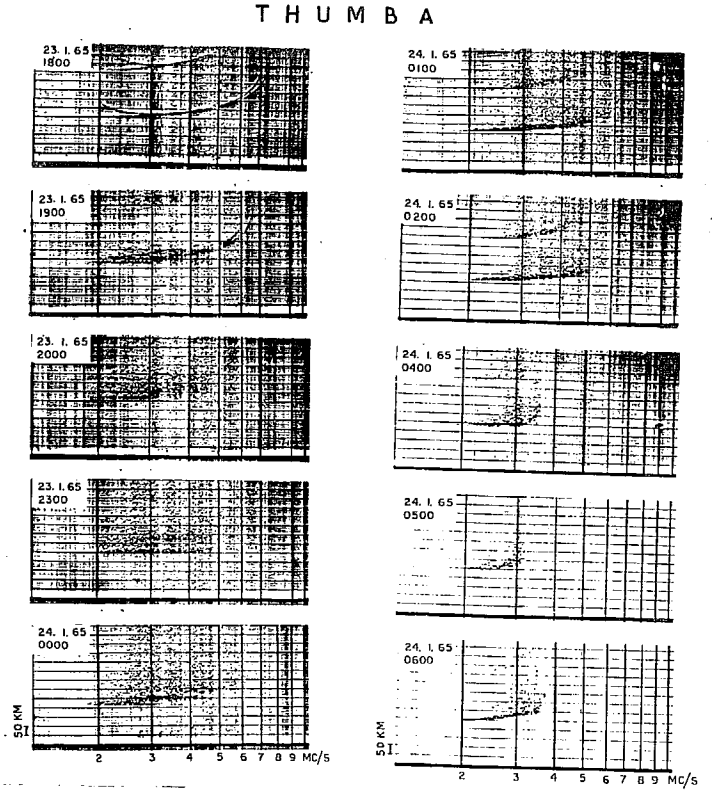

Fig. III.3.2.

reduced at 01 hr. which gives way to frequency spreading at later hours. The spreading remains till 06 hr. and vani-

shes at 07 hr. after the sunrise. Thus spreading starts from the bottom side of the layer when layer is moving up, attains heavy spreading around mid-night. After mid-night, the spreading at the bottom of layer vanishes while at the top is retained.

According to Martyn's theory, the under-surface of the layer is unstable when the layer is drifting upwards. Irregularities of electron density higher than the ambient density move slower hence into regions of lower surrounding density. Similarly irregularities of lower than the ambient density move upward through the region where electron density is higher. Thus the irregularities are enhanced at the under-surface. For a downward drifting layer irregularities are smoothed out at the under-surface but upper-surface becomes unstable. Irregularities of lower than ambient density above the maximum density of layer move downward through the layer and are considerably enhanced when reaching the height of maximum electron density of the layer.

The sequence of spread-F examples during a night in Fig. III.3.2 clearly shows that in the initial stages layer moves up and range spread is observed in the lower frequency range indicating presence of irregularities at the bottom of layer. With the subsequent height rise the spread shifts to higher frequencies, suggesting irre-

gularities moving upward through the layer. Examples after mid-night showing spread only near to the critical frequencies of the layer indicate irregularities confined to the upper surface of the layer after it has deifted downward.

In addition to these types of spread-F which occur during most of the nights, certain other types of spreadings are observed occasionally. Fig. III.3.3 shows examples of such records. Example 'a' shows the presence of a satellite below the main trace. Satellites occur occasionally before the start of the range spreading after the sunset. Generally, the satellites are observed above the main trace but sometimes they appear below the main trace also.

(Fig. III.3.3 is given in the next page)

Usually, high multiples are seen before the development of spread-F. Example 'c' shows such case of high multiple appearing even in the presence of spread-F condition. Example 'b' shows a clear trace with spreading just above it.

Some exaples of spreading which occur less frequently are shown as examples 'd', 'e' and 'f'. Example 'd' shows a clear trace with spreading occurring just at the end of trace. Such example has been described due to

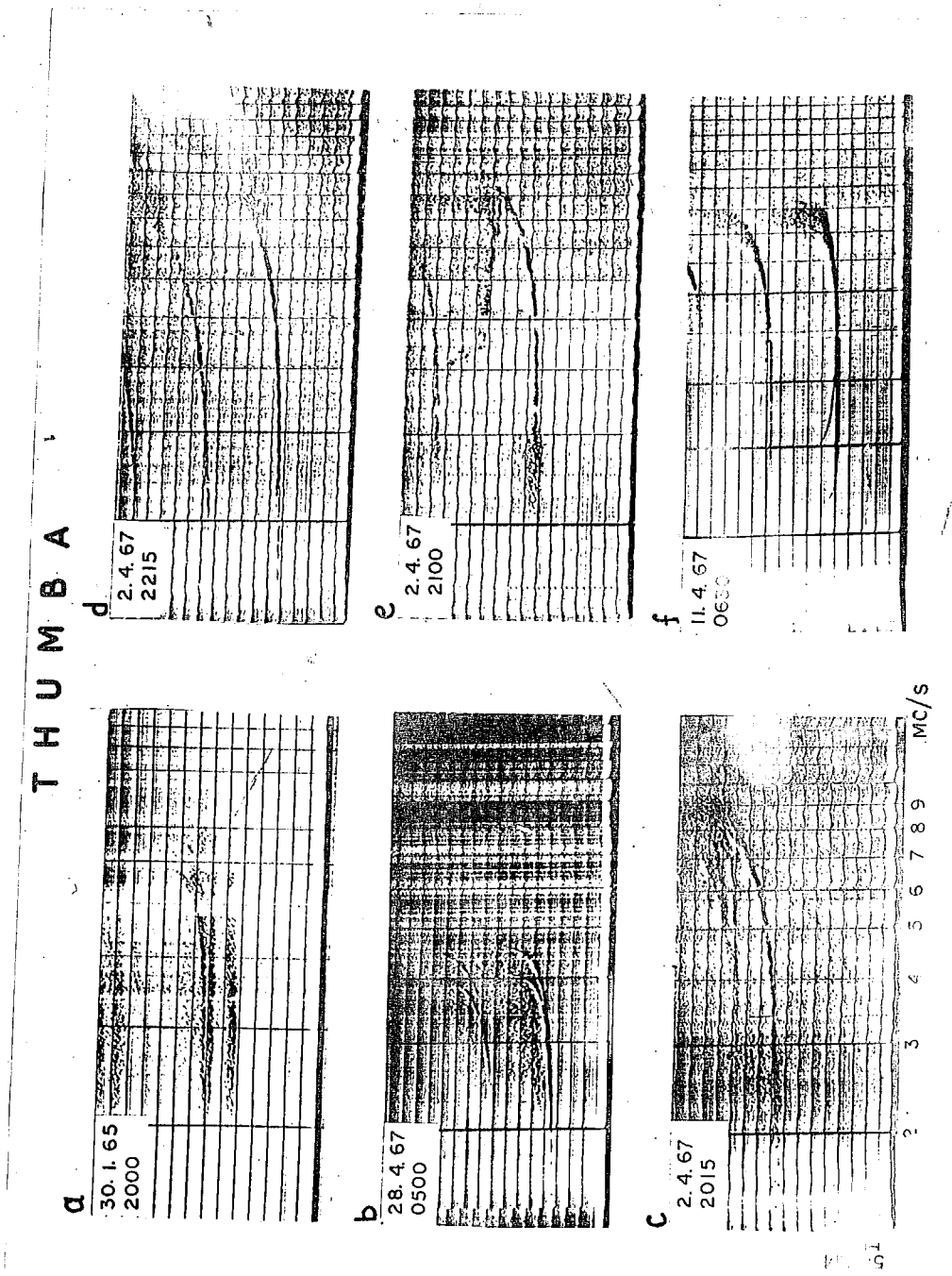
THUMBA
a
30. 1. 65
2000
b
28. 4. 67
0500
c
2. 4. 67
2015
d
2. 4. 67
2215
e
2. 4. 67
2100
f
11. 4. 67
0630
2
3
4
5
6
7
8
9
MC/S

Fig. III.3.3.

the presence of two different irregularities at different heights by Calvert. The last example is a spreading observed after sunrise.

III.3.5. Method of analysis used for the present study

Spread-F at Thumba has been studied for the period, 1965-67. Study is based on the estimation of the degree of spreading from the ionograms. Each ionogram in the night hours (18 - 06) of this period has been examined and given proper spread-F imdex. The convention for assigning the indices according to the degree of spreading is same as described by Wright et al (1956). However, records showing complete range spreading with clear critical frequency do not fall under their classification. Hence, an index of 1 is given for this type of spreading which occurs usually in the earlier part of the night.

The spread-F indices given according to degree of spreading are shown in Fig. III.3.4. The first record with a clear trace and no spreading is given an index of zero. The 2nd record shows spreading, but f_oF_2 can be clearly computed and such appearance is given an index of 1. A trace with fairly moderate spreading but a doubtful determination of f_oF_2 is given an index of 2. Last example shows

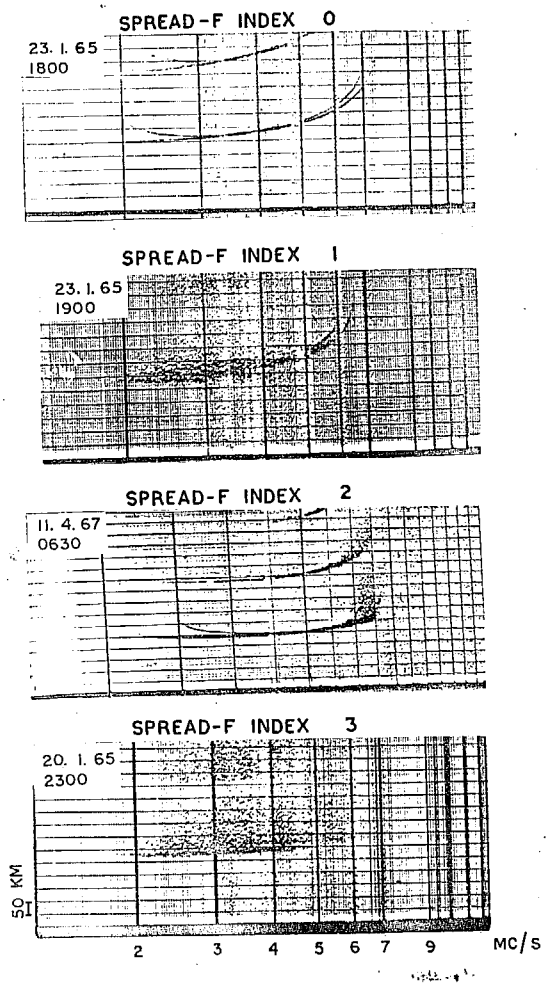
SPREAD-F INDEX 0
23. 1. 65
1800
SPREAD-F INDEX 1
23. 1. 65
1900
SPREAD-F INDEX 2
11. 4. 67
0630
SPREAD-F INDEX 3
20. 1. 65
2300
50 KM
2
3
4
5
6
7
9
MC/S

Fig. III.3.4.

a complete spreading where f_oF_2 cannot be estimated at all and is given an index 3. Spread-F indices for all nights of a month are averaged for each hour separately and the monthly mean spread-F indices at each hour are calculated.

III.3.6. Spread-F at Thumba during the period 1965-67

Fig. III.3.5 shows the monthly mean spread - F index for each month during the period, January 1965 to December 1967. For comparison, such indices have been calculated for the nearby station, Kodaikanal, from the published ionospheric data. The indices for Kodaikanal data have been assigned according to the classification described by Wright et al (1956) as explained earlier.

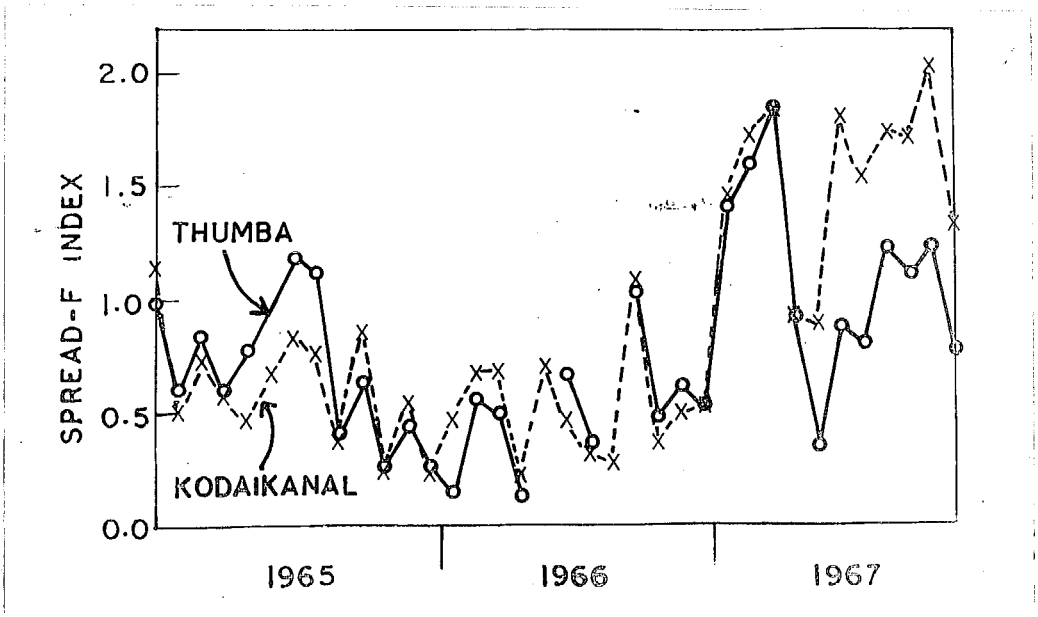

Fig. III.3.5.

No clear systematic seasonal variation can be inferred from the above plot. In the year 1965, spread-F seems to be higher during the summer (June solstice) months while in the year 1967, spread-F is much higher during the equinoctial months. Spread-F indices in the period, Winter 1965-66, seem to be lowest while a tendency of increase is seen in the year 1967. There is a sudden jump in the index value from January 1967 to February 1967, the index shooting from 0.5 to 1.5. The index remains high till April 1967 and then there is a sudden drop from April '67 to May-June 1967.

III.3.7. Nocturnal variations of spread-F index and F-layer height at Thumba

As the equatorial spread-F has been closely correlated with the height variations of F-layer, a study of the height variations has been made in each of the season in the period 1965-67 for both the stations, Thumba and Kodaikanal, and compared with the spread-F variations at these stations.

Lyon et al. (1961) have shown that under magnetically quiet and moderately disturbed conditions, the variations of h'F and hmF are similar. Further the N(h) profiles show that the rise of h'F does correspomd to a rise of the layer as a whole. Under very disturbed conditions hmF may

remain practically constant despite a small rise in h'F. However, in most cases h'F is a quite satisfactory index of the behaviour of the layer as a whole. Further, f_0E is very small at this time of the day, hence h'F should give a good indication of the true height of the layer. As the equatorial spread-F generally affects the base of the layer in the evening period, movement of h'F is as important as hmF. In the present comparison therefore h'F has been taken as the parameter representing the layer height and its vertical movements.

Fig. III.3.6 shows the nocturnal variations of the h'F and spread-F index during different seasons in the years 1965, 1966 and 1967. The seasons chosen are:

D-months - consisting of the months, January, February, November and December of a year,

E-months - consisting of the months, March, April, September and October of a year, and

J-months - consisting of the months, May, June, July and August of a year.

The nocturnal variation of spread-F index at Thumba show development of spread-F occurring after 18 hr. in each season of the period 1965-67. From an index value of 0 at 18 hr., it increases steadily reaching a maximum value around mid-night, and practically vanishes at 06 hr. The

peaks of spread-F index in the three years, 1965 to 1967, occur before mid-night in the seasons, winter and equinoxes, and after mid-night during summer season.

The nocturnal variations of the parameter h'F show a rapid post sunset rise in h'F values reaching maximum value and then slowly decreases till early morning. The peaks occur at about 19-20 hrs. during the seasons, winter and equinoxes, and around mid-night during summer.

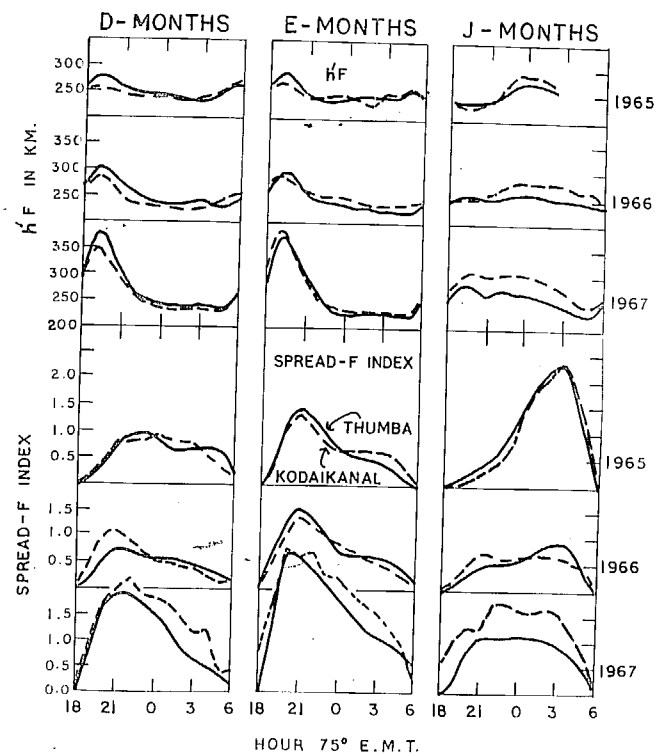

Fig. III.3.6.

Thus the spread-F index peaks are preceded by h'F peaks during each season in the entire period 1965-67. Seasonally, the peak spread-F index occurs earliest during equinoxes and latest during J-months. The height variation also shows the peak height occurring earliest during equinoxes and latest

during summer. In any of the seasons, the peak spread-F occurrence seems to occur earlier during the year 1967 than during 1965. This effect is more clearly observed during the J-months, the peak which occurs at 03 hr. in the year 1965 shifts to 00 hr. in the year 1967. Comparing the h'F variations, one finds the peak to occur around mid-night during J-months of the year 1965 and much earlier to it in the year 1967.

The nature of the nocturnal variation of the spread-F index as well as the magnitude of the spread-F index is closely related to the nature of the nocturnal variation of the h'F and post sunset height rise observed. During the D-months and E-months, there is sharp increase of the h'F around 19-20 hr. in the year 1967. Subsequently, one finds a remarkable increase in the spread-F index in the year 1967 for the two seasons. The height rise is nearly absent for the J-months in the year 1967 resulting in a small amount of spread-F observed for the same period.

The close association of spread-F with the h'F variations have been reported earlier by several workers. Booker and Wells (1938) reported height rise of about 100 km preceeding the onset of spread-F at Huancayo. Osborne (1951) reported close relation between h'F and spread-F variations

at Singapore. Martyn (1959) gave a theory to explain equatorial spread-F on the basis of the height changes in F-layer. Further work by Lyon et al (1960, 1961) and Rangaswamy and Kapasi (1963) confirmed the equatorial spread-F being associated with height variations of the F-layer. Rao and Rao (1961) reported close similarity between the nocturnal variations of h'F and spread-F except a delay between the two peaks (spread-F peak occurring later than the h'F peak).

III.3.8. Effect of magnetic activity on spread-F at Thumba

The spread-F at equatorial stations is found to be inhibited on magnetically disturbed days Wright et al (1956), Lyon et al (1958), Wright and Skinner (1959), Rangaswamy and Kapasi (1963). A study of the effect of the magnetic activity on spread-F at Thumba has been made in the period 1965-1967. Spread-F indices on five international quiet and five international disturbed days have been selected in this period and mean spread-F indices at each hour have been computed separately for the three seasons. All the three years have been combined together for better statistics. Fig. III.3.7 shows the nocturnal variations of the spread-F index on magnetically quiet and magnetically dis-

turbed days during different seasons and as a combined

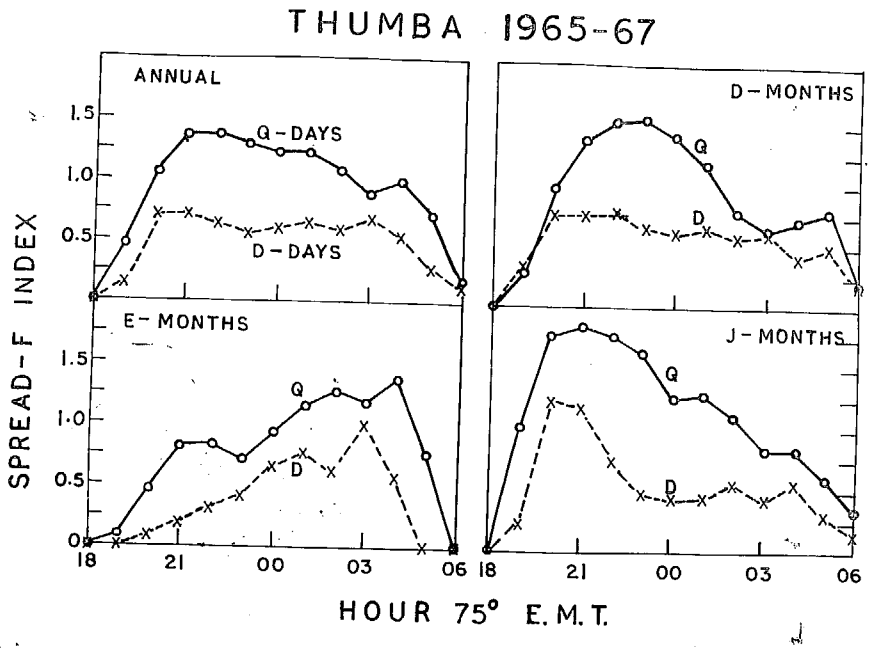

Fig. III.3.7.

picture of the period. A marked reduction in the spread-F index is seen on the disturbed days. The mean spread-F index in this period has maximum value of 1.35 on quiet days and about 0.70 on disturbed days. No seasonal difference is seen in the reduction of spread-F index on disturbed days.

Rangaswami and Kapasi (1963) have studied spread-F at the equatorial stations in the Indian zone for the IGY-

IGC period based on published ionospheric data bulletins. They obtained inhibition of spread-F occurrences at all equatorial station, Trivandrum, Kodaikanal, Tiruchirapalli and Madras, the inhibition being maximum for the equinoxes and minimum for the summer.

Wright et al (1956) have reported at Ibadan that during low sunspot years (1951-54) maximum occurrence of spread-F on quiet days is in summer and the maximum reduction due to magnetic disturbances in winter, while Lyon et al (1960) showed that during the years of high solar activity (1957-58) maximum occurrence of spread-F on quiet days and maximum reduction due to magnetic disturbances both occur in equinoxes.

Thus from the results obtained at Ibadan, it looks that seasonally the effect of magnetic disturbances is different in the different periods of solar activity. The present analysis at Thumba is for a period, 1965-67, which may be considered a period of intermediate solar activity, hence it may be possible that during this period due to change over of seasonal behaviour, one is not able to find any seasonal difference. However, more analysis, particularly during the low sunspot years, is needed to arrive at any definite conclusion regarding the seasonal difference in the effect of magnetic activity on spread-F.

III.3.9. Conclusions

(1) Development of spread-F at Thumba shows marked height rise in the F-layer, and pronounced range spread. Occasionally high multiples, satellites and sometimes stratifications in the layer structure are observed before the onset of range spread. After h'F has reached peak value, it comes down slowly and meantime spreading shifts to higher frequency side, finally giving rise to complete spreading from the start of echo to the end part of the trace. In the early morning hours, the spreading vanishes at the lower portion of layer and only frequency spread is observed just near the critical frequency.

(2) The spread-F in the period, 1965-67, shows a minimum in the period, Winter 1965-66, an increase is noticed in the year 1967. A maximum in the J-months is observed in the year, 1965, while equinoctial maxima are present in the year 1967. There is a sudden increase of spread-F index from January 1967 to February 1967 and sudden drop from April 1967 to May 1967. The h'F variations at Thumba as described in the Chapter III.1. show that there was a marked post sunset rise in h'F in the months of February-April 1967 which may be the reason for heavy spread-F conditions in this period.

(3) The nocturnal variations of spread-F index closely follow the nocturnal variations of h'F. Increase of spread-F during D-months and E-months of 1967 is related to the significant increase of h'F after sunset during these two seasons in the year 1967.

(4) The spread-F at Thumba is found to be markedly inhibited on magnetically disturbed days during any of the seasons in the period 1965-67.

CHAPTER - III.4 SEASONAL AND SOLAR CYCLE VARIATIONS OF SPREAD-F AT EQUATORIAL STATIONS

Chapter - III.4

CHAPTER - III.4 Seasonal and solar cycle variations of spread-F at equatorial stations

III.4.1. Introduction

The occurrence of spread-F during the nighttime at equatorial stations has been studied by many authors. Booker and Wells (1938) were the first to report the occurrence of diffuse traces after sunset at Huancayo and described these due to Rayleigh scattering by irregularities in the electron density distribution. Further, they observed that the onset of this phenomenon is closely correlated with a marked rise of 100 km or more in the height of the F-region between about 18 hr. and 20 hr. local time.

The occurrence of spread-F was later reported at other equatorial stations, namely Singapore (Osborne, 1951), Ibadan (Wright et al, 1956) and Kodaikanal (Bhargawa, 1958).

Singleton (1960) studied spread-F at various stations during IGY confining to two narrow strips of longitudes 75W $\pm$ 20° (American zone) and 120W $\pm$ 20° (Far East zone) and found that spread-F occurrence changes with latitude and that these changes have symmetry about the geomagnetic equator. He defined an equatorial region of high spread-F occurrence ranging from 20°N to 20°S latitudes.

Lyon et al (1960) investigated the spread-F occurrence during IGY at various stations dividing into longi-

tudinal regions, namely American, Afro-Asian and Far Eastern, and defined a narrow belt of equatorial spread-F region, having a very high incidence of spread-F occurrence; about 20^{o} wide in latitude centred at the dip equator.

A world wide study of spread-F was made by Shimazaki (1959) using IGY data and noted that at low latitudes spread-F occurrence is larger during local summer. Lyon et al (1960) also reported from IGY data analysis that in the equatorial spread-F belt, for all stations, spread-F was more common during local summer.

Wells (1954) reported that at Huancayo, spread-F is frequent during local summer and infrequent during local winter, from a study covering the years 1938-1943. Lyon et al (1961) have studied spread-F at Ibadan from 1952 to 1959 and showed that spread-F was maximum during local summer for each of the year. Spread-F at Kodaikanal was found more frequent during the equinoctial months in the period, September 1955 to September 1956 (Bhargawa, 1958), while Rangaswami and Kapasi (1963) have shown that during IGY-IGC, the peak spread-F occurrence was larger during equinoxes for quiet days and during the summer months for disturbed days. However, it may be seen from the diagram that average spread-F over the whole night is not significantly different during

the summer and equinoctial months.

The first attempt to investigate the solar cycle effect on spread-F occurrence at an equatorial station was made by Wells (1954) for Huancayo station during the period, 1938-45, and concluded that there is no clear relation of spread-F with solar activity.

Shimazaki (1959) compared spread-F occurrence during IGY to those during the year 1954 for a large number of stations and concluded that at low latitudes spread-F was more prominent during the year 1954.

Rangaswami and Kapasi (1963) computed spread-F incidence for Indian stations during the years, 1957 to 1962, and found that at Trivandrum and Kodaikanal, there is a positive relation of spread-F occurrence with solar activity.

At Ibadan, no clear relation between spread-F occurrence and sunspot number could be found in the period, 1952 to 1959, (Lyon et al). However, Lyon (1965) has shown that spread-F occurrence at Ibadan decreased linearly with sunspot numbers from 1959 to 1964.

In the present analysis, seasonal and solar cycle variations of spread-F at all equatorial stations within $\pm 5^{o}$ mag. lat. for which data are available are studied. The method of analysis is similar to that used by Wright et al

(1956) and Briggs (1958). That is spread-F indices are given to each tabulated value of f_oF_2 depending on the degree of spreading, and mean monthly spread-F index at each hour is calculated.

III.4.2. Solar cycle variations of spread-F at equatorial stations

To study the solar cycle variations of the spread-F at equatorial stations, data are analysed for the stations, Huancayo (1946-66), Ibadan (1955-66), Djibouti (1953-64) and Kodaikanal (1956-66), covering at least one solar cycle. The month to month variations of spread-F index at these stations are shown in Fig. III.4.1. For comparison, twelve

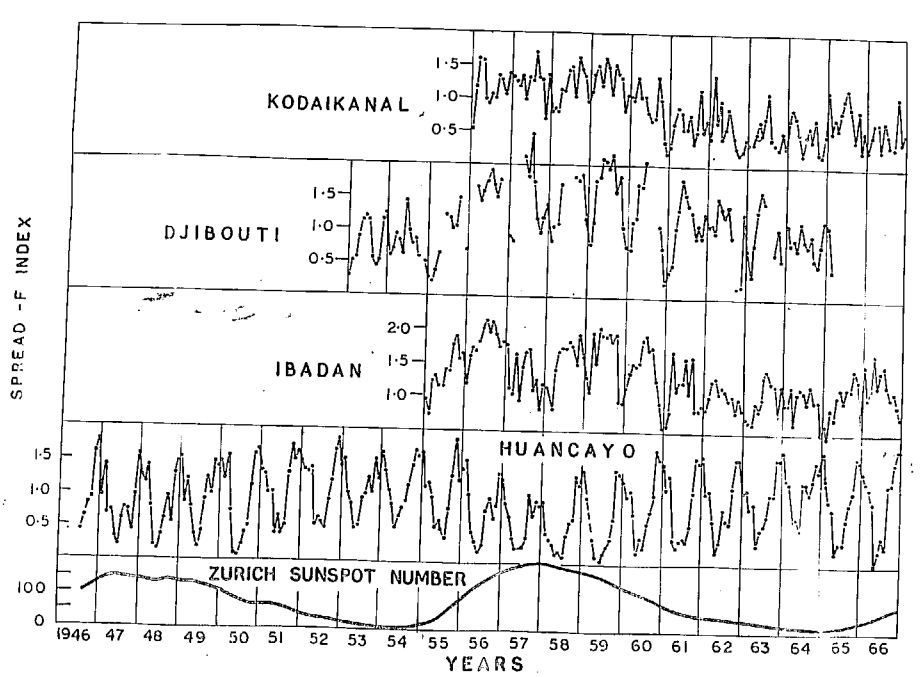

Fig. III.4.1

months running average Zurich sunspot number (R_z) for the period, 1946-66, are also shown in the Figure. A large seasonal variation of spread-F index is observed at Huancayo. The spread-F indices at Huancayo are significantly larger during the years 1953-54 and 1963-64 which are the minimum solar activity periods. Thus the spread-F is more frequent at Huancayo in the low solar activity period. For the station, Ibadan, except for the years, 1957-58, spread-F index shows direct relationship with Zurich sunspot number. Similarly, at Djibouti and Kodaikanal, there is direct relationship of spread-F with the Zurich sunspot number.

To show the effect of solar activity on spread-F, more explicitly spread-F indices for each season in the entire period of analysis are calculated and are plotted against mean sunspot number. Fig. III.4.2 shows the variation of spread-F index with sunspot number at each of the four stations during different seasons as well as annual one.

Referring to the annual variation, the spread-F index decreases linearly with the sunspot number at Huancayo while at other three stations, it increases with the sunspot number. Seasonally, at Huancayo decrease of spread-F

index with sunspot number is seen during any of the seasons, the decrease is nearly same as seen from the slopes of the straight lines which are the lines of bestfit drawn. At Ibadan and Djibouti, again the linear increase of spread-F is nearly same during any of the seasons, however, for Kodaikanal, the increase of spread-F with sunspots is much slower during D-months. Thus the present analysis shows that the spread-F at Huancayo varies inversely with sunspot number. Similar negative correlation between spread-F and sunspot number has been reported at another station in American zone, La Paz by Mejia (1965). The opposite solar cycle behaviours of spread-F at Huancayo and Kodaikanal indicate a significant longitudinal effect.

III.4.3. Seasonal variations of spread-F at equatorial stations

To study the seasonal variation of spread-F at the equatorial stations, monthly mean spread-F index was computed for each month during a period of high solar activity. This was supplemented by similar computations for a period of low activity. To clarify any longitudinal effect in the seasonal variation, spread-F at Natal during the period 1958-62, at Christmas island during the period 1945-46, and at Nha-Trang during 1951-52 and 1955 were also studied. Fig. III.4.3.

shows the seasonal variation at these stations. The period

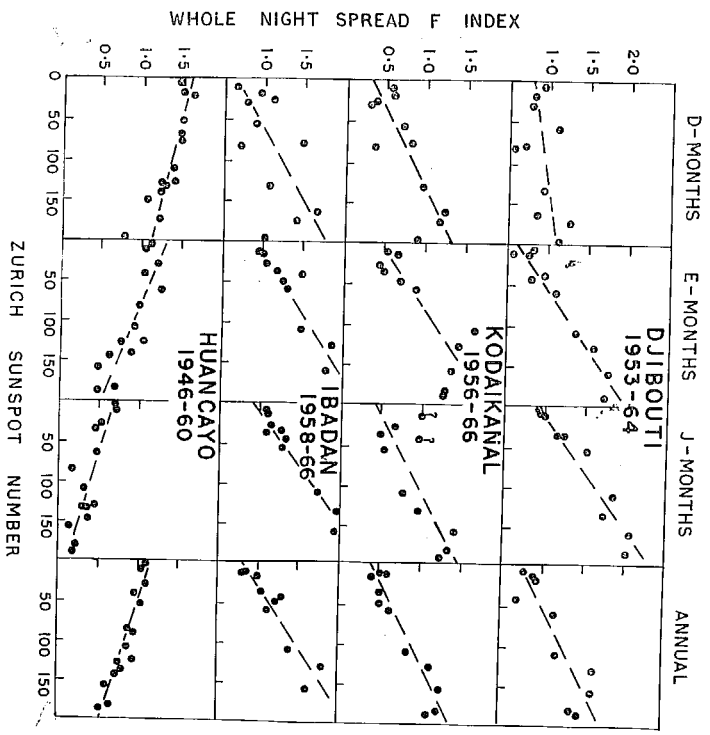

Fig. III.4.2.

of analysis is quoted in the figure. The geographic locations and the magnetic dips of the stations for which study has been done are quoted in Table.III.4.1.

(Fig. III.4.3 is given in the next page)

Spread-F index at Huancayo is maximum between November - January and minimum around June for any epoch of solar activity. This confirms the observations of Wells (1954). At Natal which is East of Huancayo, the behaviour is

similar except for a tendecy of secondary maximum during

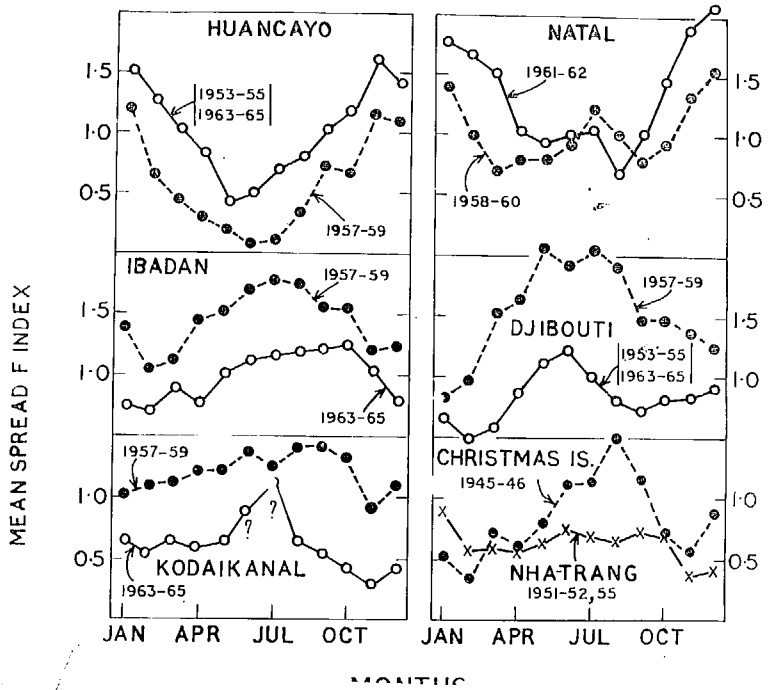

Fig. III.4.3.

the J-months. For both the stations, Huancayo and Natal, spread-F index is lower during the period of higher solar activity. Mejia (1965) have shown that spread-F at La-Paz was maximum during D-months and minimum during J-months.

At Ibadan and Djibouti, situated on the Western and Eastern part of Africa, spread-F index is maximum around J-months and minimum during D-months. The base level as well as the range of variation has come down in the period

of low solar activity.

Seasonal variation of spread-F index at Kodaikanal during 1957-59 shows very mild maximum around August - September, while during the low sunspot years, spread-F index has decreased and a maximum appears around July. However, it may be noted that during the summer months of low solar activity at Kodaikanal f_oF_2 drops to values less than the minimum range of the instrument for most part of the later half of the night and hence the points for June and July are not directly comparable to those of other months. It appears that the Indian stations have very small seasonal variation. The absence of seasonal variation is more clearly seen in the East Asian station Nha-Trang. The station, Christmas island in the Pacific zone, shows maximum during the J-months.

Thus a longitudinal effect is again observed in the seasonal variation of spread-F at equatorial stations. The seasonal variation is largest for American and almost insignificant for Asian stations.

(Table III.4.1 is given in the next page)

III.4.4. Spread-F equator

Reber (1956) defined a spread-F equator as the

TABLE - III.4.1

Geographic location of the stations with dip angles

Station	Geog. lat.	Geog. long.	Dip angle
Huancayo	12.0°S	75.3°W	2°N
Natal	5.3°S	35.1°W	6°S
Ibadan	7.4°N	3.9°E	6°S
Djibouti	11.5°N	43.0°E	6°N
Kodaikanal	10.2°N	77.5°E	4°N
Nha-Trang	12.2°N	102.2°E	8°N
Christmas Island	2.0°N	157.5°W	5°N

locus of places where spread-F is equal at solstices and probably less during equinoxes. From a world wide study of spread-F during a solar cycle, he concluded that spread-F equator is a great circle approximately parallel to the geomagnetic equator oscillating through an angle $\pm 25^{\circ}$ about an axis passing through Japan and Argentina with a period of 11 years.

Shimazaki (1959) studied spread-F all over the world using IGY data and found the result similar to Reber's findings. Singleton (1960) also made a survey of spread-F at different stations during IGY and concluded that apart from the magnetic control on spread-F occurrence, there is a solar control atleast in the equatorial region. This solar control gives rise to longitudinal effect in the equatorial region and Reber's findings were considered real and logical which arise because of solar and magnetic control on the frequency spreading.

Singleton (1963) explained the position of spread-F equator and its shift from a period of high solar activity to a period of low solar activity based on the theory of spread-F irregularities which are initiated by hydromagnetic waves and amplified according to the Martyn's theory (Singleton, 1962). Thus the formation of irregularities in the F-region depends not only on F-layer conditions, but

also on the hydromagnetic wave illumination of the upper ionosphere. The non-uniformity of this hydromagnetic wave illumination of the ionosphere determines the occurrence of spread-F at different locations on the basis of the latitude and the seasonal variation of hydromagnetic wave illumination. Singleton derived a hypothetical spread-F equator. He explained that shift of the observed spread-F equator at different solar activity periods to arise because of the changing F-layer conditions during the sunspot cycle.

According to the observed spread-F equators shown by Singleton (1963), the stations, Huancayo remains North of the equator during any epoch of the solar cycle, Kodaikanal remains South of the equator in both the epochs, but is nearer in the low sunspot years, however, a change over is seen for the station, Ibadan, being South of equator in period of high solar activity and North of equator in period of low solar activity.

Present analysis shows the results for Huancayo which are in agreement with the spread-F equators shown by Singleton. But results for Ibadan and Djibouti indicate similar seasonal variation during high and low solar activity periods indicating these stations to be South of equator in both the periods of solar activity. Similarly

a nearly equal amount of spread-F during winter and summer at Nha-Trang indicates the equator passing nearby that place. An analysis of spread-F at several low and middle latitude stations during years of different solar activity is necessary to define spread-F equator.

III.4.5. Spread-F and height variations at equatorial stations

The close relation between the spread-F occurrence and the height rise of F-layer preceding the onset of spread-F has been reported by many authors.(Booker and Wells, 1938, Osborne, 1951). Martyn (1959) gave a theory correlating these two phenomena. This height rise and its relation with spread-F variation at equatorial stations was further proved by several authors (Wright and Skinner, 1959; Lyon et al, 1960, 1961; Rao and Rao, 1961; Rangaswami and Kapasi, 1963). Singleton (1962) explained spread-F on the hydromagnetic wave illumination of the ionosphere which initiates the irregularities and the amplification of these irregularities due to vertical motion of the F-layer (Martyn, 1959).

An extensive analysis of the h'F variations and spread-F variations at equatorial stations covering different seasons and different solar activity periods has been done to examine the role of h'F variations on equatorial

spread-F.

Fig. III.4.4 shows nocturnal variations of h'F

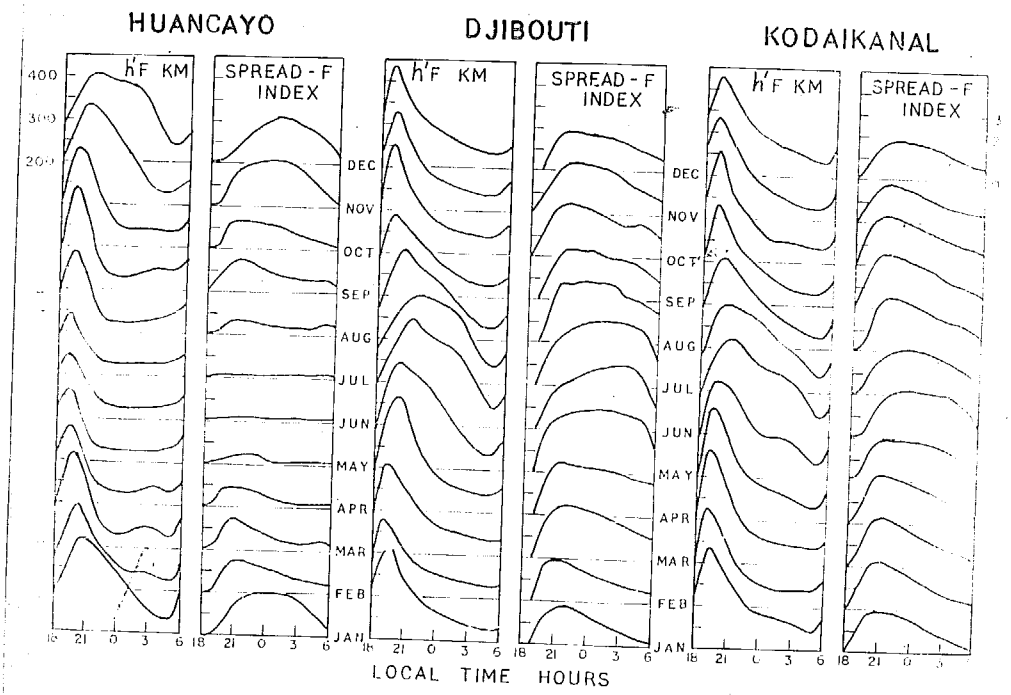

Fig. III.4.4.

and spread-F index in each month for the stations, Huancayo, Djibouti and Kodaikanal averaged over the years 1957-59. At Huancayo, the h'F peak occurs latest during D-months and earliest during J-months. The spread-F index peaks are also occurring latest during D-months and shift earlier towards the J-months; the spread-F peak occurring later than h'F peak. The height rise is maximum during D-months and h'F persists at higher level for a considerable time

while during J-months, there is a small height rise followed by rapid decrease in height. The consequence is immediately noted in the spread-F index variations. The spread-F index is largest during D-months and broad peak is observed while the index decreases steadily towards J-months. The broad maxima during D-months slowly changes into sharp maxima during equinoxes and practically no spread-F during J-months. Thus the seasonal and nocturnal variations of spread-F at Huancayo can be easily understood from the similar variations in h'F.

The situation at Djibouti is just reverse than that at Huancayo. The height rise and persistence at higher heights is observed during J-months which gives higher spread-F index as well as broad peak covering the whole night during the J-months. The smaller height rise and rapid decrease in height results in smaller spread-F index peak and immediate decrease of spread-F index during D-months. Further, the peak of h'F occurs earliest during D-months and latest during J-months which is reflected in the spread-F index variations also. The spread-F peak always occurring later than the h'F peak.

The behaviour at Kodaikanal is similar to that obtained at Djibouti. The spread-F peaks are always lagging h'F peaks. The shape of the nocturnal variation of spread-F index clearly depending on the h'F variation.

Thus the spread-F is found to be closely related with h'F variations at equatorial stations. The large height rise after the sunset and its long persistence gives rise to strong spread-F conditions lasting throughout the night, while rapid decrease of the height even after a sharp rise results in the immediate decline in the spread-F conditions. Further, peak spread-F occurs only after h'F has attained its peak. A delay in the h'F peak results in a delay of spread-F peak also.

The nocturnal variations of h'F and spread-F index during each of the seasons for the maximum sunspot years (1957-59) and minimum sunspot years are shown in Fig. III.4.5 for the stations, Huancayo, Ibadan, Djibouti and Kodaikanal.

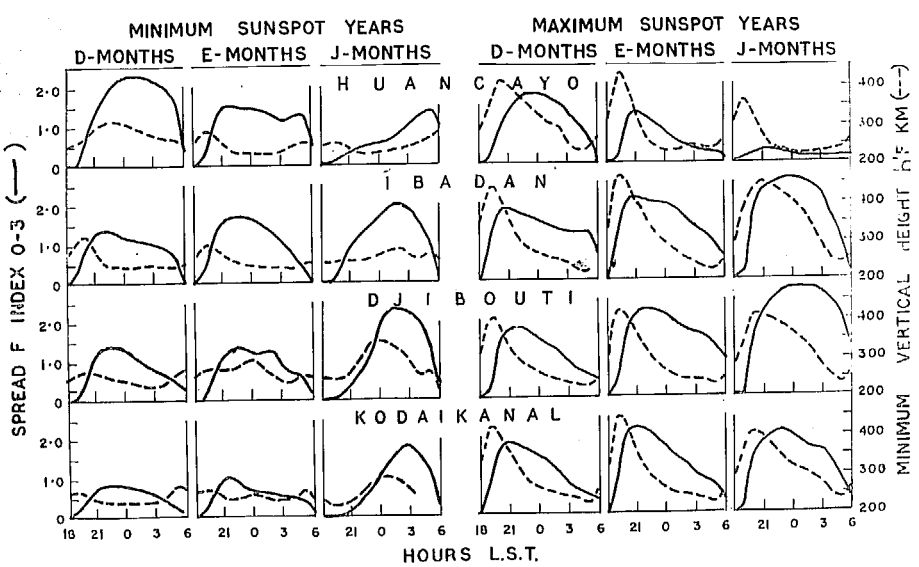

Fig. III.4.5.

During the high sunspot years at Huancayo, the spread-F index is maximum during D-months. The peak h'F is maximum for the E-months, but decreases to the normal value before midnight while during D-months the peak h'F is slightly lower, but h'f decrease slowly till the sunrise. Similarly at Ibadan, Djibouti and Kodaikanal spread-F is maximum during J-months where there is slow decrease of height after attaining the peak. There is a time lag of about 1 to 3 hours between the h'F and spread-F peak, the lag being more during D-months at Huancayo and during J-months at other stations.

The similar variations for low sunspot years show the h'F peak and spread-F index peak occurring slightly later than that for high sunspot years especially during the D-months at Huancayo and during J-months at other stations. The h'F values are considerably lower during low sunspot years while spread-F indices are lower except at Huancayo where there is an increase. The seasonal behaviour of spread-F index during low sunspot years is understood at all stations except at Huancayo where there is an increase of spread-F even though h'F values are lower as well as rise in h'F after sunset is much lower compared to values obtained during high sunspot years.

To study in more detail the h'F and spread-F varia-

tions at equatorial stations, similar analysis was done for each season of the entire analysis period. Fig. III.4.6 shows the nocturnal variations of spread-F index and h'F at these stations for high, medium and low sunspot years, shown at the top portion of the Fig., while the annual nocturnal variations of these quantities at each station are shown at the bottom half. For the stations, Ibadan, Djibouti and Kodaikanal, there is regular decrease in the h'F values which is reflected in the spread-F variations also. In contrast, the spread-F indices are higher for Huancayo from a high to low sunspot period regularly even though h'F values decrease. The peaks of spread-F index occur around 21 hr. during high and

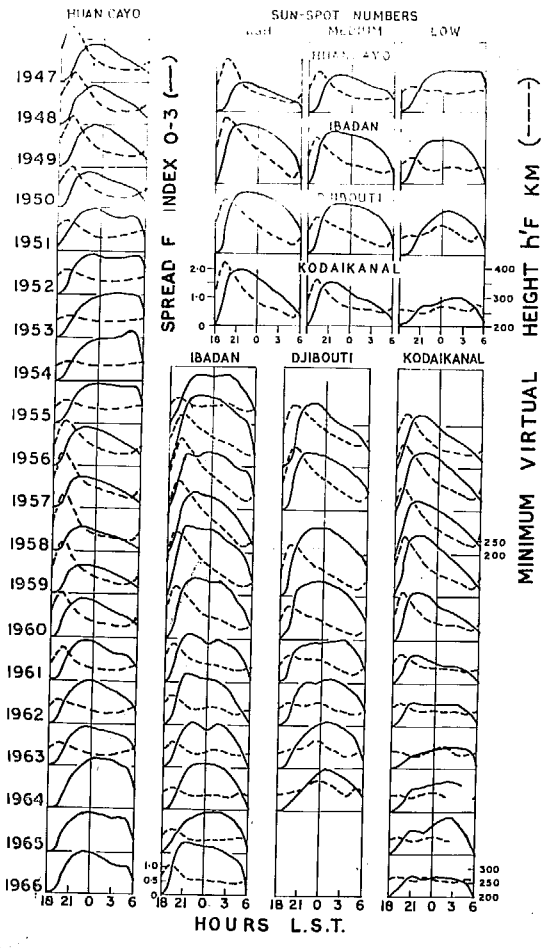

Fig. III.4.6.

medium sunspot period, but shift to around midnight during low sunspot periods.

The variations in the individual years show the h'F variations to be very small during low sunspot years and maximum at high sunspot years. The peaks of h'F variations remain to occur at about same time all the years but the peak spread-F index varies in a regular fashion, occurring in the pre-midnight period during high sunspot years and in the post midnight period during the low sunspot years. At Huancayo, there is inverse relation between h'F and spread-F index as seen from year to year variations of these two quantities, while at other stations, the spread-F index is directly depending on the h'F variations.

The nocturnal variations of h'F and spread-F index during each season for the station, Huancayo, are shown in Fig. III.4.7. During D-months, there is a sharp height rise in the high sunspot years, peak spread-F occurring at about 22 hr. while for low sunspot years, the h'F peak is around midnight and spread-F peak occurs at about 02 hr. There is a gradual change in the time of occurrence of this peak. During E-months, there is not much difference in the time of occurrence of h'F peak in different years, hence spread-F peak also occurs always at about 21 hr. The year to year changes are much more pronounced during the J-months

the spread-F peak occurs at about 21 hr, during the high sunspot years and shifts to about 05 hr. in the morning during low sunspot years. The h'F variations show a regular rise of h'F from 00 hr. to 06 hr. during [illegible] low sunspot years.

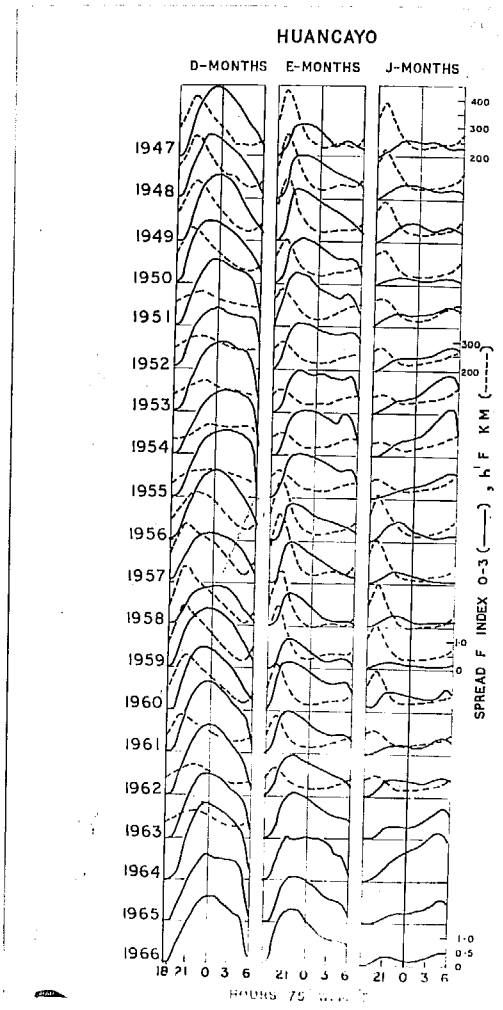

Fig. III.4.7.

The single spread-F index peak occurring during high sunspot years changes slowly to double peak curve during periods of medium sunspot activity which finally changes to a prominent morning peak in the low sunspot years. The h'F variation also shows from a single sharp peak after sunset during high sunspots to a double maxima curve during low sunspots with dip at about midnight.

Thus examining the h'F and spread-F variations at

Huancayo, the seasonal variations are directly related to the h'F variations, however, the year to year change is not understood which is in contrast to the expected result.

Fig. III.4.8 shows similar study for the station, Djibouti. During D-months, there is not much year to year variation of occurrence time of h'F peak or spread-F peak; the spread-F index depending on h'F values. For E-months and J-months, there is little shift in the peaks of h'F and spread-F index, peaks of the variation curves being shifted to early morning side during years of low sunspot activity.

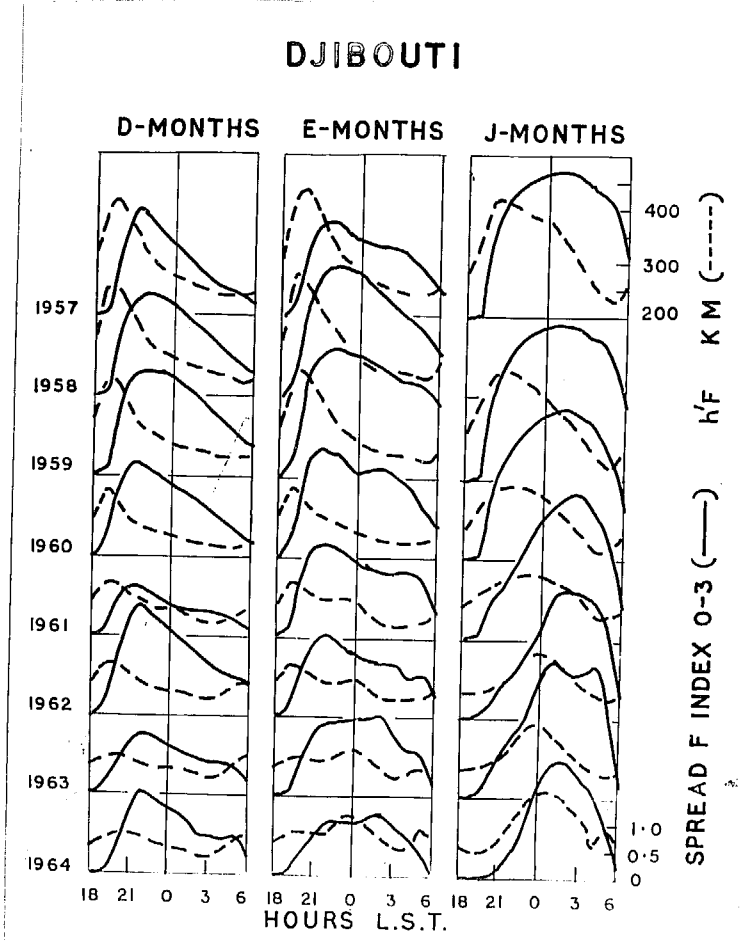

Fig. III.4.8.

The h'F values and spread-F indices show a regular decrease

from the year 1957 to 1964.

The year to year seasonal study of h'F and spread-F index at Ibadan is shown in Fig. III.4.9. Again one finds close correlation between the h'F variation and spread-F variation. The results for Kodaikanal are shown in Fig. III.4.10. The h'F peak and spread-F index peak are seen shifting each year from high sunspot years to low sunspot years, and regular decrease is observed in the h'F or spread-F index values. Marked change similar to that obtained at Huancayo is observed during J-months. The single peak observed during high sunspot years changes to double peak during medium sunspot

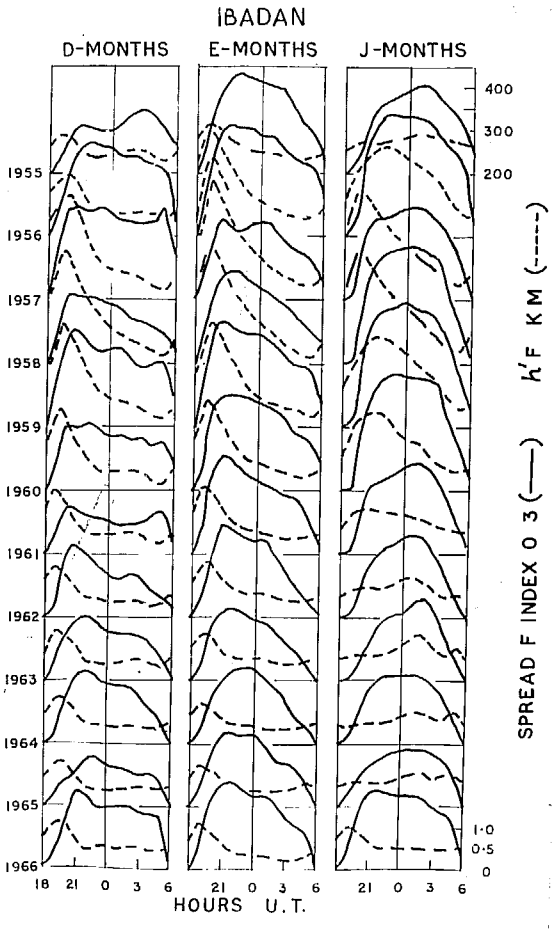

Fig. III.4.9.

years and to a morning peak during low sunspot years. The peak spread-F index occurs at about 21 hr. during high sunspot years and at about 03 hr. during low sunspot years. The magnitude of spread-F index during any season depending on the h'F variations.

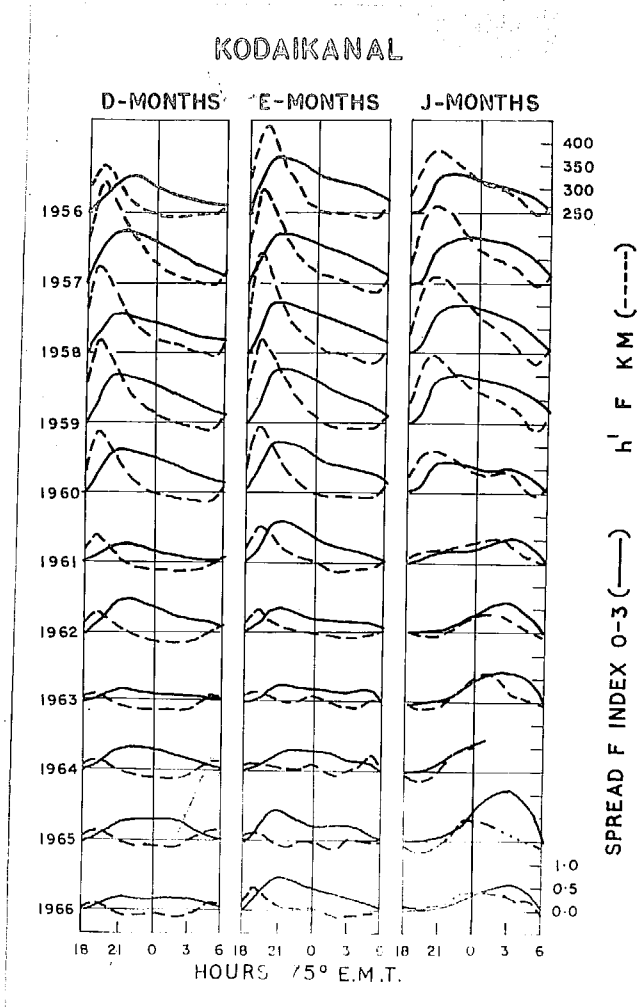

Fig. III.4.10.

Thus the stations, Kodaikanal, Djibouti and Ibadan show close relationship between h'F and spread-F index variations. All nocturnal, seasonal or solar cycle variations depending on the h'F variations. Bigger the height rise, higher is the spread-F index. For the station, Huancayo, the nature of variation of spread-F index during

any season depends on the nature of h'F variations, however there is decrease of spread-F index with the bigger h'F changes observed after sunset when comparing years of different solar activity. Thus for a particular year, the spread-F index is found to be correlated directly with h'F changes, but for different years, there is inverse relationship between h'F changes and spread-F index.

To find the effect of h'F on the spread-F index, data of Huancayo and Kodaikanal, were analysed for the IGY and a low sunspot period. Midnight values of h'F and spread-F index were computed for each month in these period and are plotted in Fig. III.4.11. Similarly maximum values of h'F

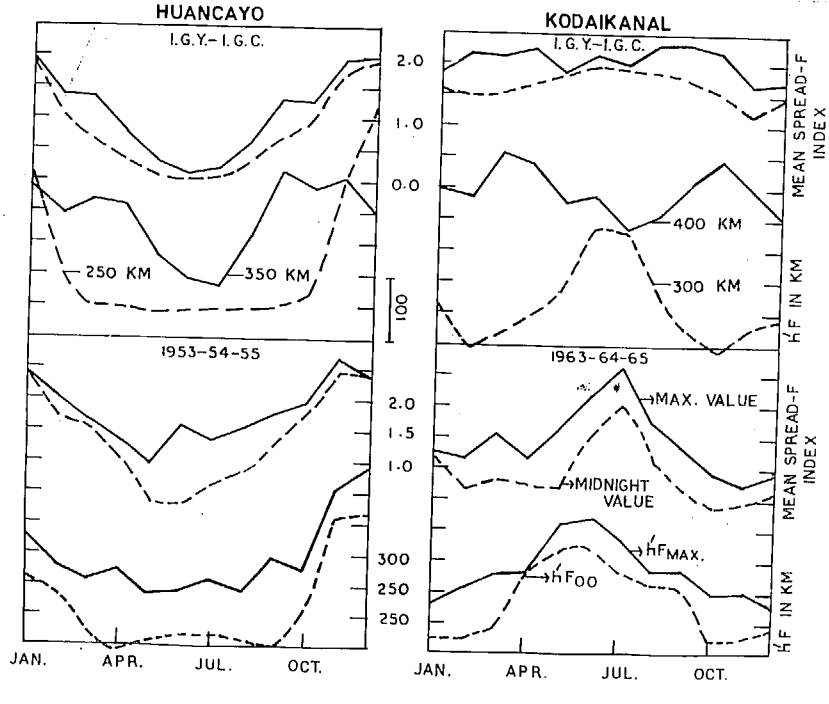

Fig. III.4.11.

and spread-F index for each month were computed in these two periods and are plotted in the same figure. The first one shows the effect of the height of the layer on spread-F while 2nd one shows the effect of the height rise of the layer on the peak spread-F obtained.

Referring to the IGY period, the maximum value of h'F and spread-F-index are closely related for the station, Huancayo. The maximum values are attained during D-months and minimum values during J-months. The mid-night h'F values are constant in the period, March to October, while midnight values of spread-F show a distinct minima during June-July. Thus spread-F index has much better correlation with the peak height attained rather than height at any instant. Similarly for Kodaikanal also, h'F max is more closely correlated with the peak spread-F index attained both showing equinoctial maxima.

Similarly during low sunspot years, the h'F max after sunset is closely correlated with the peak spread-F index obtained. Thus, both the stations, Huancayo and Kodaikanal, show a good correlation between the height rise, as determined by the maximum h'F attained after sunset, and maximum spread-F index.

III.4.6. Conclusions

(1) Spread-F at equatorial stations is found to have a

a pronounced solar cycle effect. There is a longitudinal effect on the solar cycle variation also. The station in American zone, Huancayo shows a negative relation with the sunspot numbers while there is direct relation of spread-F with sunspot numbers at the stations, Ibadan, Djibouti and Kodaikanal.

(2) The seasonal variation of spread-F at equatorial stations again shows a longitudinal effect. Stations in the American zone show a maxima during D-months and minima during J-months. An opposite behaviour is noticed at the African stations while practically insignificant seasonal variation is observed in the Asian zone.

(3) The nocturnal variation of spread-F at all the equatorial stations follow the nocturnal variation of h'F at these stations. The peak spread-F index lags behind the peak h'F value by about 1-3 hours. A rapid height rise followed by slow decrease of h'F gives rise to heavy spread-F which is sustained throughout the night period.

(4) The seasonal variations of the spread-F index during any epoch of solar activity are directly related to h'F changes.

(5) The height changes of h'F can explain the solar cycle variations of the spread-F index at the stations, Kodaikanal, Djibouti and Ibadan, where high rise of h'F during high sunspot years gives rise to more spread-F

compared to low sunspot years with low h'F rise and lower spread-F index. But it fails to explain the solar cycle change at Huancayo where there is bigger h'F rise in the years of high sunspots but still spread-F index is lower while in the years of low sunspot activity there is much smaller height rise but larger spread-F index. Thus the theory given by Singleton will fail to account for this discrepancy at Huancayo.

REFERENCES

Appleton E.V. and W.J.G. Beynon	1940	Proc. Phy. Soc., 52, 518.
Bates D.R.	1959	Proc. Roy. Soc., A253, 451.
Bauer S.J.	1962	N. Atmosph. Sci., 16, 276.
Bhargawa B.N.	1958	Ind. J. Meters. Geophys., 9, 35.
Bibl K., Harnismacher E. and Rawer K.	1955	Physics of the Ionosphere, Phys. Soc., 113.
Booker H.G. and Wells H.W.	1938	Terr. Magn. Atmosph. Electr., 43, 249.
Briggs B.H.	1958	J. Atmosph. Terr. Phys., 12, 89.
Booker H.G. and Seaton S.L.	1940	Phys. Rev., 57, 87.
Budden K.G.	1954	Ref. Cambridge Conf. Ionospheric Phys. (Phys. Soc., London), p. 332.
Calvert W. and Cohen R.	1961	J. Geophys. Res., 66, 3125.
Calvert W.	1962	N.B.S. Technical Note, 145.
Chapman S.	1931	Proc. Phys. Soc., 43, 26.
Dieminger W.	1951	Proc. Phys. Soc., B64, 142.
Eckersley T.L.	1929	J. Inst. Elect. Engrs., 67, 992.
Eckersley T.L.	1932	J. Inst. Elect. Engrs., 71, 405.
Eckersley T.L.	1937a	Nature, 140, 846.
Eckersley T.L.	1937b	Gesammelte Vortrage der Hauptvers der Lilienthal Gesellschaft, 307, 307.
Eckersley T.L.	1937c	Instn. Elect. Engrs., 80, 286.

Gipps G. Dev., Di. Gipps and Venton H.R.	1948	J. Coun. Sci. Industr. Res. Aust., 21, 215.
Glover F.N.	1960	N.B.S. Technical Note, 82.
Kelso J.M.	1952	J. Geophys. Res., 57, 357.
Kelso J.M.	1954	J. Atmosph. Terres. Phys., 5, 11.
Lyon A.J., Skinner N.J. and Wright R.W.H.	1958	Nature, 181, 1724.
Lyon A.J., Skinner N.J. and Wright R.W.H.	1960	J. Atmosph. Terres. Phys., 19, 149.
Lyon A.J., Skinner N.J. and Wright R.W.H.	1961	J. Atmosph. Terres. Phys., 21, 110.
Lyon A.J.	1965	Proc. 2nd Intern. Symp. on Eq. Aeronomy, ed. by F. de Mendonca, 239.
Martyn D.F.	1959	J. Geophys. Res., 64, 2178.
McNicol R.W.E., Webster H.C. and Bowman G.G.	1956a	Aust. J. Phys., 9, 247.
McNicol R.W.E., Webster H.C. and Bowman G.G.	1956b	Aust. J. Phys., 9, 272.
Mejia G.R.	1965	Proc. 2nd Intern. Symp. on Equatorial Aeronomy, ed. by F. de Mendonca, 233.
Mogel H.	1932	Telefunkenzeitung, 60, 29.
Olatunji E.O.	1966	Annles. de. Geophys., 22, 485.
Osborne B.W.	1951	J. Atmosph. Terres. Phys., 2, 66.
Piggott W.R. & K. Rawer	1961	U.R.S.I. Handbook of Ionogram interpretation and reduction, 29.
Rangaswamy S. & Kapasi K.B.	1963	J. Atmosph. Terres. Phys., 25, 721.
Rao M.S.V.G. & Rao B.R.	1961	J. Geophys. Res., 66, 2113.

Rastogi R.G. and Harish Chandra	1966	Proc. of IQSY Symp., New Delhi, p. 85.
Ratcliffe J.A.	1951	J. Geophys. Res., 56, 463.
Renau J.	1959	J. Geophys. Res., 64, 971.
Renau J.	1960	J. Geophys. Res., 65, 2269.
Satyanarayanmurthy Ch.	1962	Proc. of IGY Symp., New Delhi, CSIR, p. 48.
Sanatani S.	1966	Ph.D. Thesis.
Schemerling E.R.	1958	J. Atmosph. Terres. Phys., 12, 8.
Schemerling E.R. and Ventrice C.A.	1959	J. Atmosph. Terres. Phys., 14, 249.
Shimazaki T.	1959	J. Radio Research Labs., 6, 669.
Shinn D.H.	1953	J. Atmosph. Terres. Phys., 4, 240.
Singleton D.G.	1957	Aust. J. Phys., 10, 60
Singleton D.G.	1960	J. Geophys. Res., 65, 3615.
Singleton D.G.	1962	J. Atmosph. Terres. Phys., 24, 909.
Singleton D.G.	1963	J. Atmosph. Terres. Phys., 25, 121.
Thomas J.O. & M.D. Vickeres	1958	DSIR Radio Res. Space Rep., No. 28.
Wells H.W.	1954	J. Geophys. Res., 59, 273.
Whale H.A.	1951	J. Atmosph. Terres. Phys., 1, 233.
Wright R.W., Koster J.R. and Skinner N.J.	1956	J. Geophys. Res., 64, 2203.
Wright R.W. and Skinner N.J.	1959	J. Atmosph. Terres. Phys., 15, 121.

GALLEY No. C--84

J.A.T.P. 2374 Pergamon Press, Oxford
1st Proof MS pages 1–9 Galleys 1–3
The Universities Press, Belfast 3.12.69

1

Journal of Atmospheric and Terrestrial Physics 1960, Vol. 00, pp. 0000–0000. Pergamon Press. Printed in Northern Ireland

SHORT PAPER

Solar cycle and seasonal variation of spread-F near the magnetic equator*

H. CHANDRA and R. G. RASTOGI
Physical Research Laboratory, Ahmedabad 9, India

(*Received* 20 *May* 1969; *in revised form* 17 *July* 1969)

Abstract—Spread-F at equatorial stations, Ibadan, Djibouti and Kodaikanal is shown to increase with increasing solar activity. At Huancayo and other stations in the American zone there is least occurrence of spread-F in years of high solar activity. The seasonal variation of spread-F is greatest at stations in the American zone with a maximum in December and a minimum in June. At African stations a smaller seasonal variation is seen with maximum in June and minimum in December. At Asian stations the seasonal variation of spread-F is very small.

STUDIES of spread-F echoes during the night-time at equatorial stations have been reported for Huancayo (BOOKER and WELLS, 1938), Singapore (OSBORNE, 1951), Ibadan (WRIGHT *et al.*, 1956; LYON *et al.*, 1961) and at Kodaikanal (BHARGAVA, 1958). The existence of an equatorial belt of about $\pm 20°$ geomagnetic (or magnetic) latitude of high occurrence of spread-F was shown by SINGLETON (1960) and by LYON *et al.* (1960).

WELLS (1954) concluded that no clear relationship existed between spread-F at Huancayo and solar activity for the period 1938–45. LYON *et al.* (1961) showed that the incidence of spread-F at Ibadan on quiet days during 1952–59 was substantially greater in years of high sunspot activity, while for disturbed days no clear dependence of spread-F occurrence on solar activity could be detected. Later, LYON (1965) showed that during the period 1959–64 the spread-F occurrence at Ibadan systematically decreased with decreasing solar activity. RANGASWAMY and KAPASI (1963) showed that during the period 1958–62, the occurrence of spread-F at Trivandrum and Kodaikanal increases with sunspot number.

The present article describes the solar cycle and seasonal variations of spread-F at stations within $\pm 5°$ magnetic latitude and covering a period of at least one complete solar cycle. The Table 1 gives the coordinates of the stations whose data are discussed here.

The analysis is based on the monthly ionospheric data bulletins either published or supplied by the respective organisations. In order to take into account the magnitude of spread-F during any particular hour, the analysis is based on mean spread-F index rather than on the percentage occurrence of spread-F. An index 0 means a very clear ionogram without any spread and the index 3 means complete

* Presented at the 3rd International Symposium on Equatorial Aeronomy held at Ahmedabad during February 3–10, 1969.

Table 1. Geographic location of the stations with dip angles

Station	Geog. lat.	Geog. long.	Dip angle
Huancayo	12·0°S	75·3°W	2°N
Natal	5·3°S	35·1°W	6°S
Ibadan	7·4°N	3·9°E	6°S
Djibouti	11·5°N	43·0°E	6°N
Kodaikanal	10·2°N	77·5°E	4°N
Nha-Trang	12·2°N	102·2°E	8°N
Christmas Island	2·0°N	157·5°W	5°N

spreading such that no critical frequencies of the $F2$-region could be identified. The indices 1 and 2 indicate weak and moderate spread-F respectively. The indices are determined from hourly tabulation of f_0F2 in a similar way as described by earlier workers (WRIGHT *et al.*, 1956 and BRIGGS, 1958). Averages were determined from the monthly mean indices for individual hours between 18.00 and 06.00 hr and are discussed in the present analysis as monthly mean spread-F indices.

The month to month variations of spread-F index at Kodaikanal, Djibouti, Ibadan and Huancayo are shown in Fig. 1 for all the available periods of observation. The twelve months running average Zurich sunspot number (R_z) for the period 1946–66 is also shown for comparison. Even a cursory glance of the diagram shows a very

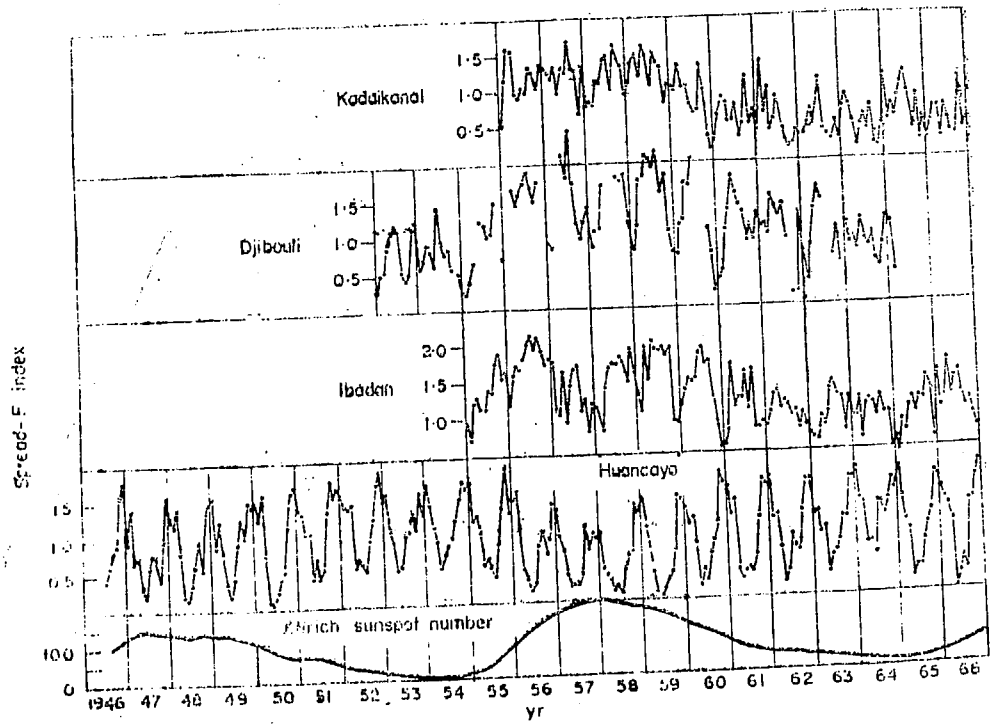

Fig. 1. Month to month variation of mean spread-F index at number of equatorial stations and of the Zurich sunspot number.

large seasonal variation of spread-F index at Huancayo. The spread-F indices at Huancayo are significantly larger during 1953–54 and 1963–64 which are minimum solar activity periods. The average spread-F index at Djibouti shows a distinct maximum during the high sunspot years 1957–58. For Ibadan except for the years 1957–58, the mean spread-F index shows clear direct relationship with Zurich sunspot number. At Kodaikanal, too, the spread-F index systematically decreases from 1957 to 1964.

To show the solar cycle variation more explicitly, the spread-F indices for each station are plotted against the mean sunspot number for each of the seasons, namely, J-months (May, June, July and August), E-months (March, April, September and October) and D-months (November, December, January and February). It is seen that for all seasons the spread-F index at Djibouti, Kodaikanal and Ibadan shows a linear increase with sunspot number. On the other hand, spread-F index at Huancayo decreases linearly with sunspot numbers for any of the seasons.

Thus, the present analysis shows beyond doubt that spread-F at Huancayo varies inversely with sunspot number. Similar negative correlation between spread-F and sunspot number has been reported at another station in American zone, La Paz by MEJIA (1965). The opposite solar cycle behaviours of spread-F at Huancayo and Kodaikanal indicate a significant longitudinal effect which may be associated with the large longitudinal variation of the magnetic field along the magnetic equator.

Seasonal variation of spread-F at these stations were calculated for a few years around the maximum and the minimum sunspot years. To clarify any longitudinal effect in the seasonal variation, spread-F at Natal during the period 1958–62, at Christmas Island during the period 1945–46 and at Nha-Trang during 1951–52 and 1955 were also studied. These curves are shown in Fig. 3.

It is seen that spread-F at Huancayo is maximum between November and January and minimum around June for any epoch of solar activity and confirms the observations of WELLS (1954). At Natal, which is east of Huancayo, the seasonal variation is again similar except for a tendency for a secondary maximum during the J-months. MEJIA (1965) has shown that spread-F at La Paz was maximum during D-months and minimum during J-months. At Ibadan and Djibouti, situated on the western and eastern part of Africa, spread-F is maximum around J-months and minimum during the D-months. Referring to the seasonal variation of spread-F at Kodaikanal during 1957–59 one finds a minor maximum around August–September while during the low sunspot years spread-F intensity has decreased and there appears to be maximum around July. However, it may be noted that during the Summer months of low solar activity at Kodaikanal f_0F2 drops to values less than the minimum range of the instrument for the most part of the later half of the night and thus the points for June and July are not directly comparable with those of other months. It is felt that spread-F at Indian stations has a very small seasonal variation. The absence of seasonal variation is more clearly seen in the East Asian station, Nha-Trang. The spread-F at Christmas Island situated in the Pacific zone shows a maximum during the northern Summer months.

Bhargava (1958) has reported that spread-F at Kodaikanal was most frequent during the equinoctial months in the period September 1955–September 1956. RANGASWAMI and KAPASI (1963) have shown that during IGY/IGC the peak

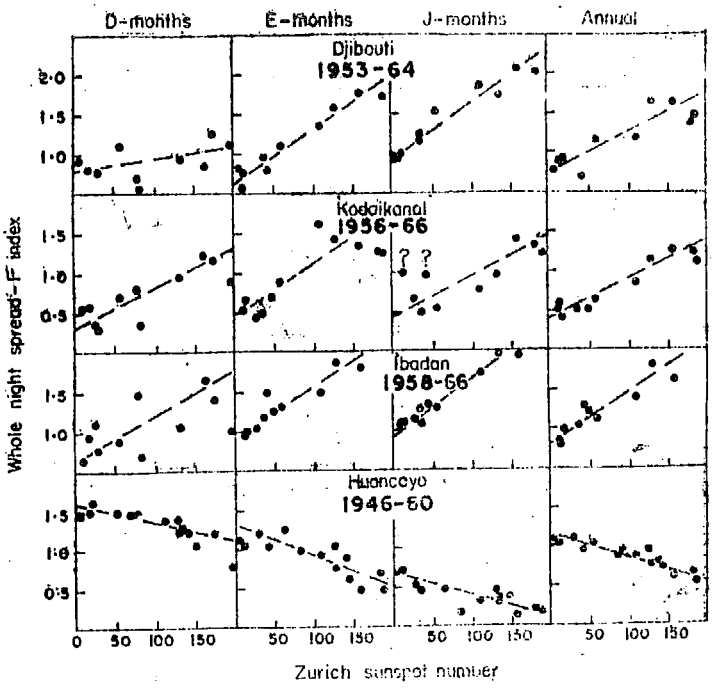

Fig. 2. Plots showing relations between spread-F index at number of equatorial stations and Zurich sunspot numbers for individual seasons.

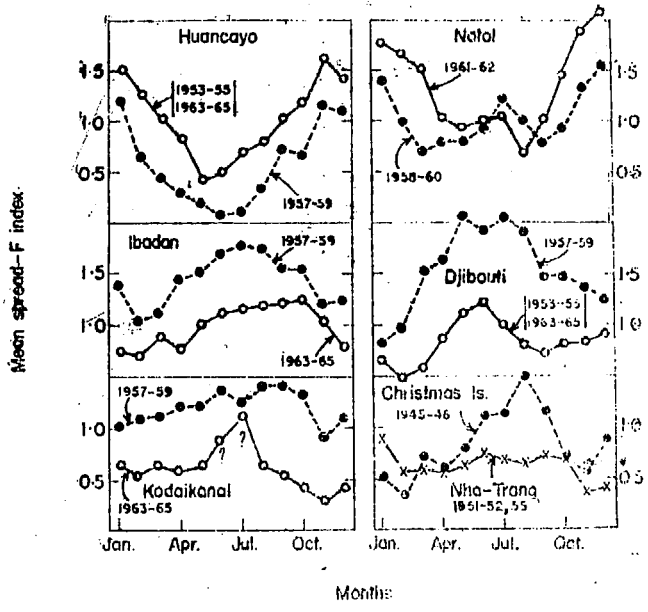

Fig. 3. Seasonal variation of the mean spread-F index at equatorial station during high and low solar activity periods.

spread-F occurrence was larger during equinoxes for quiet days and during the Summer months for disturbed days. It may be seen from the diagram that average spread-F over the whole night is not significantly different during the Summer and equinoctial months. LYON *et al.* (1961) studied spread-F at Ibadan from 1952 to 1959 and showed that spread-F was maximum during local Summer for each of the years. Thus, one finds again significant longitudinal effects in the seasonal variation of spread-F at equatorial stations.

REBER (1956) defined a spread-F equator as the locus of places where spread-F is equal at solstices and probably less during equinoxes. He found that this equator is nearly a great circle approximately parallel to the geomagnetic equator oscillating through an angle $\pm 25^\circ$ about an axis passing through Japan and Argentina, with a period of 11 yr. Further study of spread-F from the IGY data confirmed Reber's findings (SHIMAZAHI, 1959; SINGLETON, 1960).

SINGLETON (1963) discussed the position of spread-F equator under sunspot maximum and minimum conditions. According to him, Huancayo and Natal would be in the northern spread-F hemisphere during any of the epoch of solar activity. The equatorial stations in the Pacific and in the African zone would fall in different spread-F hemisphere during the maximum and minimum sunspot years.

Present analysis for the data for Ibadan and Djibouti do not show any change in the seasonal variation of spread-F with solar activity. The analysis of spread-F at more low and middle latitude stations during years of different solar activity is necessary to define spread-F equator. The analysis of spread-F on the top side of ionosphere would elucidate the synoptic study of spread-F.

Acknowledgement—Sincere thanks are due to Prediction Services of ITS, ESSA Laboratories, Boulder, USA, for supplying the ionospheric data of Huancayo and to GRI, Paris, France, for supplying the ionospheric data of Nha-Trang.

REFERENCES

BHARGAVA B. N.	1958	*Indian. J. met. Geophys.* **9**, 35.
BOOKER H. G. and WELLS H. W.	1938	*Terr. Magn. atmos. Elect.* **43**, 249.
BRIGGS B. H.	1958	*J. Atmosph. Terr. Phys.* **12**, 89.
LYON A. J., SKINNER N. J. and WRIGHT R. W. H.	1960	*J. Atmosph. Terr. Phys.* **21**, 100.
LYON A. J.	1965	*Proc. 2nd Int. Symp. Equatorial Aeronomy* (Edited by F. DE MENDONCA), pp. 239–241.
OSBORNE B. W.	1952	*J. Atmosph. Terr. Phys.* **2**, 66.
RANGASWAMY S. and KAPASI K. E.	1963	*J. Atmosph. Terr. Phys.* **25**, 721.
REBER G.	1956	*J. geophys. Res.* **61**, 157.
SHIMAZAKI T.	1959	*J. Radio Res. Labs. Japan* **6**, 669.
SINGLETON D. G.	1960	*J. geophys. Res.* **65**, 3615.
SINGLETON D. G.	1963	*J. Atmosph. Terr. Phys.* **25**, 121.
WELLS H. W.	1954	*J. geophys. Res.* **59**, 273.
WRIGHT R. W., KOSTER J. R. and SKINNER N. J.	1956	*J. Atmosph. Terr. Phys.* **8**, 240.